

https://dspace.org/

An experimental and thermodynamic study of iron catalyst activation and deactivation during Fischer Tropsch synthesis

Gorimbo, Joshua

2016

http://hdl.handle.net/10539/22998

Gorimbo, Joshua (2016) An experimental and thermodynamic study of iron catalyst activation and deactivation during Fischer Tropsch synthesis, University of the Witwatersrand, Johannesburg, <http://hdl.handle.net/10539/22998>

Downloaded from a DSpace repository. https://dspace.org/



AN EXPERIMENTAL AND THERMODYNAMIC STUDY OF IRON CATALYST ACTIVATION AND DEACTIVATION DURING FISCHER TROPSCH SYNTHESIS

JOSHUA GORIMBO

School of Chemical and Metallurgical Engineering, Faculty of Engineering and the Built Environment, University of the Witwatersrand, Johannesburg, South Africa

August, 2016

DECLARATION

I declare that this thesis is my own unaided work. It is being submitted for the Degree of Doctor of Philosophy to the University of the Witwatersrand, Johannesburg. It has not been submitted before for any degree or examination to any other University.

_____ on this ____ day of _____

(Candidate)

ABSTRACT

One gram amounts of a commercial iron based catalyst were loaded into three reactors and reduced with syngas, hydrogen and carbon monoxide respectively. Fischer Tropsch experiments on the three reactors in parallel with the same operating conditions, namely 60 mL(NTP)/min, 1 bar gauge and 250 °C, were then conducted for extended periods and the gaseous products analysed.

Initially (for about 150 hours) the three catalysts had quite different carbon monoxide conversions. After this until about 1000 hours the conversions were similar. However the distribution of products for the differently reduced catalyst was significantly different. This suggested that permanent changes had been done to the catalysts by the different reducing conditions.

To try to understand what the differences during the reduction process might be, a thermodynamic analysis of the solid phases after reduction was done. Unfortunately because all the thermodynamic data for the possible carbides was not available this analysis was of limited value. However it did suggest that hydrogen reduced catalyst might contain more oxides and the carbon monoxide reduced catalyst might contain more carbides. Some electron microscope and XRD experiments supported these ideas and might account for the different selectivities of the differently reduced catalysts.

Runs after about 5000 hours were done at different flowrates (60, 30 and 15 mL(NTP)/min) of syngas and again the big effects were on differences between the selectivities, the big effects being when going to the lowest flowrate.

After about 12000 hours regeneration of the catalysts was then done by oxidation and then the same syngas reduction on all the catalysts. Runs were then done at different pressures (1, 10 and 20 bar gauge) and again selectivities were the biggest effects that remained, clearly showing the initial reduction had made permanent changes.

In the final section some novel plots were used to try to make more sense of the results. It was shown that for all the catalysts the Olefin to Paraffin ratios were tied to each other under all conditions and that they were mainly a function of the conversions with much higher values at low conversions.

DEDICATION

To my mother **(U. Masukume)**

ACKNOWLEDGEMENTS

First, I would like to acknowledge the institutions that made my research possible: the University of the Witwatersrand for financial assistance through the Postgraduate Merit Award; and the Material and Process Synthesis (MaPS) group at the University of South Africa, which also provided financial support.

I also thank my supervisors, Professors David Glasser and Diane Hildebrandt, for their intellectual guidance, direction and motivation throughout my research work, both at the School of Chemical and Metallurgical Engineering at Wits University and at the MaPS unit. I appreciate administrative supervision by Dr Jean Mulopo at Wits. Dr Matinde and Dr Xiaojun Lu read the manuscript of this thesis, and provided constructive criticism. I also thank my fellow postgraduate students, especially those who participated in the Fischer-Tropsch Research Group with me. I also value the fruitful discussions I had with Dr Adolph Anga Muleja, Mr Bruce Mothibela and Mr Doctor Bense.

Mr Norman Blight contributed by ensuring that the thesis was clearly written in academic English.

I wish also to acknowledge my debt to my friends, Dr Gwiranai Danha, Dr Clayton Bhondai, Dr Ngonidzashe Chimwani, Dr Adolph Muleja, Mr Gladmore Rongai, Mr Roick Chikati, and Mr Sambulo Matema, who influenced and inspired me. In particular I am grateful to my family, Christopher, Trust, Washington and Rudo, to my daughter Tawananyasha, and most especially to my wife Sarudzai, a blessed gift from God, for her priceless and dimensionless support throughout.

All glory and honour and thanksgiving be to my God, forever, in Jesus' name.

PRESENTATIONS AND PUBLICATIONS

Parts of the data contained in this thesis are written in paper format for submission to peer reviewed journals as shown below. Some of the data were presented (poster and oral) and are outlined in this section.

Conference presentations

- J Gorimbo, D Glasser, D Hildebrandt and Y Yao. Pretreatment Studies with a Precipitated Iron Catalyst for Fischer-Tropsch Synthesis Under Different Reaction Conditions. Poster presentation, American Institute of Chemical Engineers (AIChE) annual meeting, 8-13 November 2015, Salt Lake City, USA.

- J Gorimbo, D Glasser, D Hildebrandt and J Mulopo, 2014, Effect of Reducing Agents (Syngas, H_2 and CO) on the Catalytic Performance of Iron Catalysts for Fischer-Tropsch Synthesis. Oral presentation, American Institute of Chemical Engineers (AIChE) annual meeting, 16-21 November 2014, Atlanta, USA.

- J Gorimbo, D. Glasser, D. Hildebrandt, J. Mulopo, A comparative study of Syngas, H_2 and CO as reducing gases in FT synthesis, Oral presentation, International Conference of Chemical Thermodynamics and the South African Institution of Chemical Engineers (ICCT/SAIChE) conference, 27 July to 1 August 2014, Durban, South Africa.

Manuscripts for Publications

- J Gorimbo, X Lu, D. Glasser, D. Hildebrandt, A comparative study on the effect of reducing iron catalyst with three different reducing gases. Ready for submission.

- J Gorimbo, X Lu. Glasser, D. Hildebrandt, Study of the response of gas phase Fischer Tropsch products of differently reduced catalysts to changes in operating conditions. Ready for submission.

- J Gorimbo, X Lu, D. Glasser, D. Hildebrandt, In situ regenerability of an Iron catalyst in Fischer-Tropsch synthesis. Ready for submission

TABLE OF CONTENTS

Section ***Page***

Declaration i

Abstract ii

Dedication iv

Acknowledgements v

Presentations and publications vi

Table of contents viii

List of figures xiv

List of tables xix

List of abbreviations, nomenclatures and symbols xx

CHAPTER 1 INTRODUCTION 1

1.1 Short background on Fischer Tropsch synthesis 1

1.2 Research problem statement 2

1.3 Research justification 3

1.4 Research objectives 5

1.5 Thesis outline 6

References 8

CHAPTER 2 LITERATURE REVIEW 10

2.1 Introduction 10

2.2 Conventional FT synthesis 11

2.3 Effects of operating conditions 12

2.3.1 Pressure in Fischer Tropsch synthesis 12

2.3.2 Effects of temperature on product selectivity 13

2.3.3 Flowrate effect on Fischer Tropsch synthesis 13

2.3.4 Time on stream 14

2.3.5 Fischer Tropsch catalyst 15

2.3.6 Water gas shift reaction 16
2.3.7 Effect of catalyst composition on the performance and selectivity of the catalyst 18
2.3.8 Effect of the nature of reducing gases during catalyst activation 19
2.3.9 Effect of CO reduction on FT catalyst 20
2.3.10 Effect of H_2 reduction on FT catalyst 21
2.3.11 Effect of syngas reduction on FT synthesis 22
2.4 Catalyst speciation products 23
2.5 Catalyst deactivation 24
2.6 Deactivation phenomena 25
2.7 Ways of catalyst regeneration 25
2.8 The effect of water on the stability of reduced catalyst 26
2.9 The effect of carbon dioxide formed and its formation pathways 27
2.10 Product distribution 28
2.10.1 Anderson – Schulz – Flory (ASF) model 28
2.11 Nature and type of FT reactors 29
References 32

CHAPTER 3 IN SITU STUDIES 56

3.1 Preview 56
3.2 The literature on *in situ* characterization 56
3.3 Thermodynamic predictions 58
3.4 Stability diagrams for iron catalyst during reduction 61
3.4.1 CO reduction prediction 62
3.4.2 H_2 Reduction prediction 65
3.5 Gaseous components in equilibrium with iron and its speciation products during reduction and reaction with syngas 68
3.5.1 Catalyst oxidation 69
References 72

CHAPTER 4 80

EXPERIMENTAL METHODOLOGY 80

4.1 Introduction 80
4.2 Experimental conditions 81
4.3 Gases used 81
4.4 Catalyst 83
4.5 Catalyst characterization 83
4.5.1 X-ray diffraction (XRD) 83
4.5.2 Brunauer-Emmet-Teller (BET) 84
4.5.3 High Resolution Transmission electron microscopy (HR-TEM) .. 84
4.6 FTS Reactors 84
4.7 Catalyst loading into the reactor 85
4.8 Experimental set-up 86
4.9 Experimental method 89
4.9.1 Catalyst reduction procedure 89
4.9.2 FT synthesis 89
4.9.3 Regeneration studies 91
4.9.4 Product separation and analysis 92
4.10 Product storage 96
4.11 Calculations 96
4.11.1 Olefin/paraffin ratio 98
4.11.2 Olefin/paraffin ratio 99
References 104

CHAPTER 5 106

A COMPARATIVE STUDY ON THE GAS PHASE FISHER TROPSCHS PRODUCTS OF REDUCING AN IRON CATALYST WITH THREE DIFFERENT REDUCING GASES 106

5.1 Introduction 107
5.2 Experimental 108
5.2.1 Catalyst and catalyst reduction 108

5.2.2 FT synthesis 109
5.3 Results 109
5.3.1 CO (gas) conversion 109
5.3.2 Effects of low pressure on reactant consumption rates 111
5.3.2.1 Reactant and FT rates at 1 bar gauge reactor pressure 111
5.3.2.2 Methane and carbon dioxide formation rates 115
5.3.2.3 Olefin formation rates 117
5.3.2.4 Paraffin formation rates 119
5.3.3 Product selectivity 123
5.3.4 Olefin to paraffin ratio 124
5.4 Discussion 126
5.5 Conclusion 129
References 130

CHAPTER 6 RESPONSE OF GAS PHASE FT PRODUCTS OF DIFFERENTLY REDUCED CATALYSTS TO CHANGES IN OPERATING CONDITIONS 135

6.1 Introduction 136
6.2 Experimental work 138
6.3 Results 140
6.3.1 Effect of flow rate on the CO conversion 140
6.3.2 Effect of flow rate on the selectivity to the products 144
6.3.3 Effect of flow rate on the olefin to paraffin ratios 149
6.3.4 Effect of pressure on the CO conversion 151
6.3.5 Effect of pressure on the selectivity to the products 156
6.3.6 Effect of pressure on the olefin to paraffin (O/P) ratio 159
6.3.7 Methane and CO_2 production 162
6.4 Discussion 164
6.5 Conclusion 165
References 167

CHAPTER 7 GAS PHASE PRODUCTS FROM FISCHER TROPSCH EXPERIMENTS AFTER OXIDATIVE REGENERATION OF IRON BASED CATALYSTS 172

7.1 Introduction 173
7.2 Materials and methods 176
7.3 Fischer Tropsch synthesis 178
7.4 Results and discussion 180
7.5 Discussion 192
7.6 Conclusion 194
References 196

CHAPTER 8 FURTHER ANALYSIS OF THE GAS PHASE FT EXPERIMENTAL DATA: P/O RATIOS, LU PLOTS AND YAO PLOTS 202

8.1 Introduction 203
8.2 Experimental work 208
8.3 Results 210
8.3.1 The olefin to paraffin ratio 210
8.4 Yao Plots 212
8.5 Lu Plots 216
8.6 The olefin to paraffin ratio as a function of CO conversion 225
8.7 Conclusion 227
References 229

CHAPTER 9 CONCLUSIONS AND RECOMMENDATIONS 233

9.1 Conclusions 233
9.1.1 Use of stability diagrams to predict catalyst speciation during activation 234
9.1.2 Low pressure FT runs 234
9.1.3 Effects of operating conditions 235
9.1.4 Oxidative regeneration of the almost deactivated catalyst 235

9.1.5 Use of plots to depict product distributions 236
9.2 Recommendations 237
References 239

LIST OF FIGURES

Figure	***Description***	***Page***
Figure 1.1:	Generic block diagram of the FT plant process including syngas product and FTS. Parts in red show areas for potential savings.	4
Figure 2.1:	Variation of the logarithm of equilibrium constant Log (kp) for the water-gas shift reaction with temperature (°C).	17
Figure 3.1:	Stability diagram of an iron based catalyst in equilibrium with PCO/PCO_2 during reduction at 1 atm.	62
Figure 3.2:	Gibbs free energy versus temperature for possible speciation pathways of the iron catalyst precursor under CO activation.	63
Figure 3.3:	Gibbs free energy versus temperature (^oC) for possible speciation pathways of the iron catalyst precursor under H_2 activation	65
Figure 3.4:	Stability diagram of an iron based catalyst in equilibrium with PH_2/PH_2O during reduction at 1 atm.	66
Figure 3.5:	Graph showing the ability of oxygen to oxidize Co, Fe and FeC	70
Figure 4.1:	Photograph of the disassembled reactor	84
Figure 4.2:	Representation of the FT reactor loaded with catalyst	85
Figure 4.3:	Flow scheme of the laboratory scale Fischer Tropsch rig with three fixed reactors in parallel	87
Figure 4.4:	Typical online analysis of the syngas (red line from TCD detector and blue line from that of FID).	95
Figure 4.5:	Typical online analysis of the calibration gas (red line from TCD detector and blue line from FID)	95
Figure 4.6:	Typical online analysis of the tailgas (red line from TCD detector and blue line from FID)	96
Figure 4.6:	Graphs of conversion again time on stream for the whole FT run periods considered in this thesis (a) Reac-Syn, (b) Reac-H_2 and (c) Reac-CO	103

Figure 5.1: Influence of reducing gases (syngas, hydrogen and carbon monoxide) on the catalyst stability (CO conversion) under the FT reaction conditions: 250 °C, 1 bar (gauge), 60 mL(NTP)/min and mass of the catalyst of 1 g. 111

Figure 5.2: Influence of reducing gases: CO consumption rate versus time on stream at 1 bar gauge and 250 °C. 112

Figure 5.3: Influence of reducing gases on FT rate ($\mathfrak{r}CO - \mathfrak{r}CO_2$): FT rate versus time on stream at 1 bar gauge and 250 °C. 113

Figure 5.4: Fischer Tropsch selectivity for the three differently reduced catalysts 114

Figure 5.5: Influence of reducing agents on methane production rate (at 250 °C, 1 bar gauge, 60 (NTP)mL/min and mcat = 1 g)..... 115

Figure 5.5: Influence of reducing agents on CO_2 production rate (at 250 °C, 1 bar gauge, 60 mL/min and mcat = 1 g) 116

Figure 5.7: Olefin production rate against time on stream under the following conditions: 250 °C, 1 bar gauge, 60 mL(NTP)/min and mass of catalyst 1 g..... 118

Figure 5.8: Paraffin production rate against time on stream under the following conditions: 250 °C, 1 bar gauge, 60 mL(NTP)/min and mass of catalyst 1 g..... 120

Figure 5.9: Effect of reducing agents (syngas, hydrogen and carbon monoxide) on the average steady state olefin production rate against carbon number for three differently reduced reactors (at 250 °C, 1 bar gauge, 60 (NTP)mL/min and mcat = 1 g)..... 121

Figure 5.10: Effect of reducing agents (syngas, hydrogen and carbon monoxide) on the average steady state paraffin formation rates as a function of carbon number under the following conditions: 250 °C, 1 bar gauge, 60 (NTP) mL/min and mass of catalyst 1 g 122

Figure 5.11: Effect of reducing agents (syngas, hydrogen and carbon monoxide) on the olefin to paraffin ratio as a function of time on stream: (a) for (O_2/P_2), (b) for (O_3/P_3), (c) for (O_4/P_4) and (d) for

(O_5/P_5) under the following conditions: 250°C, 1 bar gauge, 60 mL/min and mass of catalyst 1 g. O: olefin, P: paraffin and carbon number n: 2,3,4 and 5. 5. 125

Figure 6.1: Conversions of differently reduced reactors with changing flow rate: (a) for syngas reduced (Reac-Syn); (b) for hydrogen reduced (Reac-H_2) and (c) carbon monoxide reduced (Reac-CO). Reactor temperature was kept at 250 °C and reactor pressure at 1 bar gauge. 141

Figure 6.2: CO consumption rates of differently reduced reactors with changing flow rate: (a) for syngas reduced (Reac-Syn); (b) for hydrogen reduced (Reac-H_2) and (c) carbon monoxide reduced (Reac-CO). Reactor temperature was kept at 250 °C and reactor pressure at 1 bar gauge. 143

Figure 6.3: Selectivity to heavy hydrocarbons (C_{5+}) for (a) Reac-Syn (syngas reduced, (b) Reac-H_2 (hydrogen reduced), and (c) Reac-CO (Carbon monoxide reduced) under FT operating conditions: 250 °C, 1 bar gauge and various flow rates (15, 30 and 60 mL(NTP)/min) 146

Figure 6.4: Effect of flow rate on the selectivity to CO_2 and CH_4 under FT conditions of 250 ^oC, 1 bar gauge and various flow rate values of 15, 30 and 60 mL(NTP)/min 148

Figure 6.5: Effects of changing flow rates to olefin to paraffin ratio for (a) Reac-Syn, (b) for Reac-H_2, and (c) for Reac-CO under FT conditions of 250 ^oC, 1 bar gauge and various flow rate values 15, 30 and 60 mL(NTP)/min. 150

Figure 6.6: Effect of pressure on the CO conversion at various pressures: 1, 10 and 20 bar gauge while keeping the temperature at 250 ^oC, flow rate at 60 mL(NTP)/min, feed ratio $H_2/CO = 2$ and 1 g mass of the iron catalyst loaded in different reactors; (a) for Reac-Syn , (b) for Reac-H_2 and (c) for Reac-CO for TOS between 12000- 13 800 hours 153

Figure 6.7: Effect of pressure on the CO rates at various pressures: 1, 10 and 20 bar gauge while keeping the temperature at 250 ^{o}C, flow rate at 60 mL(NTP)/min, feed ratio H_2/CO = 2 and 1 g mass of the iron catalyst loaded in different reactors; (a) for Reac-Syn , (b) for Reac-H_2 and (c) for Reac-CO for TOS between 12000- 13 800 hours 155

Figure 6.8: Comparison of the selectivities to olefins and paraffins at different pressures 158

Figure 6.9: Variation of olefin to paraffin ratio with pressure for syngas reduced catalyst: (a) to (c) for the syngas, hydrogen and carbon monoxide reduced catalysts, respectively 161

Figure 6.10: The effect of pressure on CO_2 and CH_4 selectivity for (a) Reac-Syn (syngas reduced), (b) Reac-H_2 (hydrogen reduced) and (c) Reac-CO (carbon monoxide reduced) under FT conditions: 60 mL(NTP)/mL, 250 ^{o}C pressure from 1 to 10 bar gauge and 10 to 20 bar gauge 163

Figure 7.1: CO consumption rate before, during and after the regeneration under operating conditions: 250 ^{o}C, 60 mL(NTP)/min at 1 bar(gauge) for (a) Reac-Syn (syngas reduced), (b) Reac-H_2 (hydrogen reduced) and (c) Reac-CO (carbon monoxide reduced reactors). 182

Figure 7.2: CO conversion and FT selectivity before, during and after regeneration under operating conditions: 250 °C, 60 mL(NTP)/min at 1 bar gauge for (a) Reac-Syn, (b) Reac-H_2 and (c) Reac-CO reactors. Regeneration period is indicated by dotted lines 183

Figure 7.3: Selectivity to the light hydrocarbons before and after regeneration under operating conditions: 250 °C, 60 mL(NTP)/min at 1 bar gauge for average data (a) olefin, (b) paraffin for different reducing agents/reactors. 187

Figure 7.4: Selectivity to CO_2, CH_4 and C_{5+} before and after regeneration under operating conditions: 250 ^{o}C, 60 mL(NTP)/min at 1 bar gauge for average data (a) CO_2, (b) CH_4 and (c) C_{5+} for different reducing agents/reactors. 188

Figure 7.5: HRTEM image of (a) fresh catalyst (b) Reac-Syn spent catalyst (c) Reac-H_2 spent catalyst (d) Reac-CO spent catalyst..... 190

Figure 7.6: The corresponding electron diffractograms of the HRTEM images depicted in Figure 7.5 (a) fresh catalyst (b) Reac-Syn spent catalyst (c) Reac-H_2 spent catalyst (d) Reac-CO spent catalyst 191

Figure 7.6: XRD spectra of the fresh catalyst and the used ones from different reactors (After 14 000 hours TOS)..... 192

Figure 8.1: Typical ASF hydrocarbon product distribution plot (Bao, El-Halwagi, & Elbashir, 2010)..... 204

Figure 8.2: The plot of the ratio of $P_{(n+1)}/O_{(n+1)}$ as a function of the ratio of $P_{(n)}/O_{(n)}$ for Fischer-Tropsch synthesis..... 206

Figure 8.3: The Lu plot: A plot of the normalised mole fractions O_{n+1} versus O_n 207

Figure 8.4: The paraffin to olefin ratio $P_{(n+1)}/O_{(n+1)}$ as a function of P_n/O_n for FTS over iron based catalysts. Reac-Syn (reduced by syngas), Reac-H_2 (reduced by H_2) and Reac-CO (reduced by CO) and the reaction condition as shown in Table 8.1. 214

Figure 8.5: The paraffin to olefin ratio $P_{(n+1)}/O_{(n+1)}$ as a function of P_n/O_n for FTS over the iron based catalyst: (a) n = 2, (b) n = 3 and (c) n = 4 for differently reduced reactors (Reac-Syn, Reac-H_2 and Reac-CO) 215

Figure 8.9: Normalized mole fraction for C_2H_6, C_3H_6, and C_3H_8 for the three differently reduced reactors..... 222

Figure 8.10: Normalized mole fractions for C_3H_8, C_4H_8, and C_4H_{10} for the three differently reduced reactors..... 223

Figure 8.12: Olefin/Paraffin ratio as a function of conversion for all differently reduced reactors..... 226

LIST OF TABLES

Table	***Description***	***Page***
Table 3.1:	Variation of ΔG of reactions 3.6 and 3.7 with temperature	69
Table 4.1:	Component and mole percentage of the calibration gases used in the study	82
Table 4.2:	Initial reaction conditions for the FT synthesis	90
Table 4.3:	Summary of the online GC settings and columns used	94
Table 4.4:	Response factors for hydrocarbon products	98
Table 4.4:	Reaction and feed conditions for the FTS experiment. Note that 1 g of iron based catalyst was loaded into the reactor and this catalyst was not changed during the experiment.	100
Table 5.1:	Summary of experimental conditions for FTS for differently reduced iron based catalysts	109
Table 5.2:	Selectivity to FT products for different catalyst reducing agents	123
Table 6.1:	Operating conditions implemented at different time on streams (TOS) for three differently reduced reactors	139
Table 6.2:	Conversion averages for the three reactors at different flow rates	142
Table 6.3:	Component selectivities at different flow rates (a) Olefin Selectivity (b) Paraffin Selectivity (c) Olefin + Paraffin and C_{5+} Selectivity	145
Table 6.4:	Summary of averaged conversions for a given TOS range	152
Table 7.1:	BET results of the iron catalyst	177
Table 8.1:	Summary of the FT reaction conditions for the three reactors	209
Table 8.2:	Paraffin to Olefin ratios (P/O) at different conditions	211
Table 8.3:	Gradients obtained at different n values	215

LIST OF ABBREVIATIONS, NOMENCLATURES AND SYMBOLS

Abs	Absolute
Afrox	African Oxygen Limited
AIChE	American Institute of Chemical Engineers
ASF	Anderson–Schultz–Flory
bbl/day	barrels per day
BET	Brunauer–Emmett–Teller
BTL	Biomass to liquid
Co	Cobalt
CO	Carbon monoxide
CSTR	Continuous stirred-tank reactor
CTL	Coal to liquid
EDS	Energy dispersive X-ray spectroscopy
EXAFS	Extended X-ray absorption fine structure
FBR	Fixed bed reactor
Fe	Iron
FFD	Fixed fluidized bed reactor
FID	Flame ionisation detector
FR	Flow rate
FT	Fischer Tropsch
FTIR	Fourier transform infra-red
FTS	Fischer Tropsch synthesis
GC	Gas chromatograph
GTL	Gas to liquid
H_2	Hydrogen
HTFT	High temperature Fischer Tropsch
ICCT	International Conference on Chemical Thermodynamics
ID	Internal diameter
LPG	liquefied petroleum gas
mL/min	Millilitre per minute
mol/min	Mole per minute

N	Carbon number
N_2	Nitrogen
NMF	Normalised mole fractions
NTP	Normal temperature and pressure
OD	Outside diameter
P	Pressure
P&ID	Piping and instrumentation diagram
Reac-CO	Carbon monoxide reduced reactor
Reac-H_2	Hydrogen reduced reactor
Reac-Syn	Syngas reduced reactor
Syn	Syngas
SA	Surface area
SAIChE	South African Institution of Chemical Engineers
SASOL	South African Coal, Oil and Gas Corporation
SEM	Scanning electron microscopy
T	Temperature
TCD	Thermal conductivity detector
TEM	Transmission electron microscopy
TGA	Thermo gravimetric analysis
TOS	Time on stream
TPR	Temperature-programmed reduction
UHP	Ultra high purity
VLE	Vapour-liquid equilibrium
WGS	Water-gas shift
Wn	Mass fraction of the species with carbon number n
XPS	X-ray photoelectron spectroscopy
XRD	X-ray diffraction
A	Chain growth probability
B	Variation of the vapour pressure coefficient
µm	Micrometre

CHAPTER 1

INTRODUCTION

1.1 Short background on Fischer Tropsch synthesis

In the Fischer Tropsch synthesis (FTS) process, a mixture of predominantly CO and H_2 (synthesis gas/syngas) obtained from feedstocks such as natural gas, coal and biomass, is catalytically converted to hydrocarbons. Any carbon containing material can potentially be converted to syngas via a combination of gasification, reforming or partial oxidation. The FT process yields a wide spectrum of products, the most desirable ones being paraffins, olefins and oxygenates (De Klerk, 2011; Jalama, 2008; Ojeda & Rojas, 2012; Van de Loosdrecht et al., 2013). According to these researchers, the FT process requires a syngas with a H_2/CO ratio close to 2:1(Aasberg-Petersen et al., 2004; de Klerk, Li, & Zennaro, 2013; Kuo, 1984; Schijndel et al., 2011). The syngas is converted into hydrocarbons of various molecular weights according to the following reaction equations:

$$n\mathrm{CO} + (2n + 1)\mathrm{H_2} \rightarrow \mathrm{C_nH_{2n+2}} + n\mathrm{H_2O} \quad (1.1)$$

$$n\mathrm{CO} + 2n\mathrm{H_2} \rightarrow \mathrm{C_nH_{2n}} + n\mathrm{H_2O} \quad (1.2)$$

$$n\mathrm{CO} + 2n\mathrm{H_2} \rightarrow \mathrm{C_nH_{2n+2}O} + (n - 1)\mathrm{H_2O} \quad (1.3)$$

A variety of transition metals (Fe, Co, Ni and Ru) can be used as catalysts in FTS (Botes et al. 2013; Lee & Yoo, 2014; Tada & Iwasawa, 2009). Iron based catalysts have been widely used because of their low cost and lower methane selectivity (Kritzinger, 2002) and their ability to operate over a wide temperature range (220 to 350 ^{o}C) and at pressures from 10 to 60 bar (Huo et al. 2009).

Fischer Tropsch synthesis (FTS) has been identified as a pivotal unit in the coal to liquid (CTL), biomass to liquid (BTL) and gas to liquid (GTL) operations, whose performance defines the profitability of the whole process, and thus it has been

accorded more research attention in recent years. Surprisingly, the research into the operating conditions continues to be of critical importance on the acquisition of information that can help in understanding FT operations by running at low pressure. This is based on account of a widely held belief that FT operations are expensive to set up and the success correlates with the reactor capacity and operating pressure. It is also of importance to have smaller or mobile units using the same technology that can be used in remote areas.

1.2 Research problem statement

The increasing focus by Fischer Tropsch (FT) practitioners in the syngas conversion technology to minimize operation cost has created a strong impetus to re-examine and optimize the process. The FT is a downstream process of gasification whose performance is of paramount importance to economies of many countries (South Africa included), and as such research attention is justified. Surprisingly, the researches into the FT operating conditions process have been on the decline, and the publicly available information is inadequate to fully understand performance at all conditions.

FT operations are usually optimized to maximize the production of preferably higher molecular weight liquid hydrocarbon products. In the FT reactor, the primary components collected include waxes, hydrocarbon condensate, tail gas, and reaction water. A fundamental prerequisite to begin the design of FT is a determination of the operating conditions and the catalyst type. This, in turn, is a function of feed (its CO/H_2 ratio) noting that an iron catalyst tends to further alter this ratio via the water gas shift reaction. The determination of the catalyst to be used takes into account the price, nature of the feed, availability and estimation of time of operation (Chinchen, Logan & Spencer, 1984; Kuo, 1984; Lappas & Heracleous, 2010; Newsome David S., 1980; Rhodes, Hutchings & Ward, 1995).

The reduction of the catalyst precursor is an important stage during FT reaction, and reducing gases tend to influence the activity, the selectivity and the catalyst life span. During FT synthesis an iron catalyst precursor, in the form of hematite (α-Fe_2O_3), is introduced into the reactor and subjected to an activation treatment to

obtain the actual FT catalyst. The activation process involves passing through reducing agents such as H_2, CO and/or syngas over a catalyst precursor to yield an active catalytic state. The exact mechanism resulting in the differences in the selectivities of these catalysts is not clearly understood, but the effect is clearly recognizable after a long time on stream. Moreover, the need to understand the above phenomena has led to this research to ascertain how differently reduced catalysts respond to operation condition changes.

1.3 Research justification

Although major breakthroughs have been made towards commercializing the highly efficient FT process, the costs are still high compared to competing technologies. Major cost components are the FT reactors that can withstand high pressures and the additional hydrogen or carbon monoxide plants for catalyst reduction, and these parts are at the heart of the FT technology. Since the gasification process is normally done at ambient pressure, such as in biomass gasification, the operational cost could be reduced if the reaction is to be carried out at almost similar conditions of low pressure. Furthermore the use of the same syngas that will be used for the synthesis to reduce the catalyst will greatly reduce the capital costs as the hydrogen or CO plant will not be necessary (see mini-scale FT plant in **Figure 1.1**). As a result, the cost of the technology could perhaps be lowered below the conventional power generating systems despite the benefits of higher efficiency and cleaner environment.

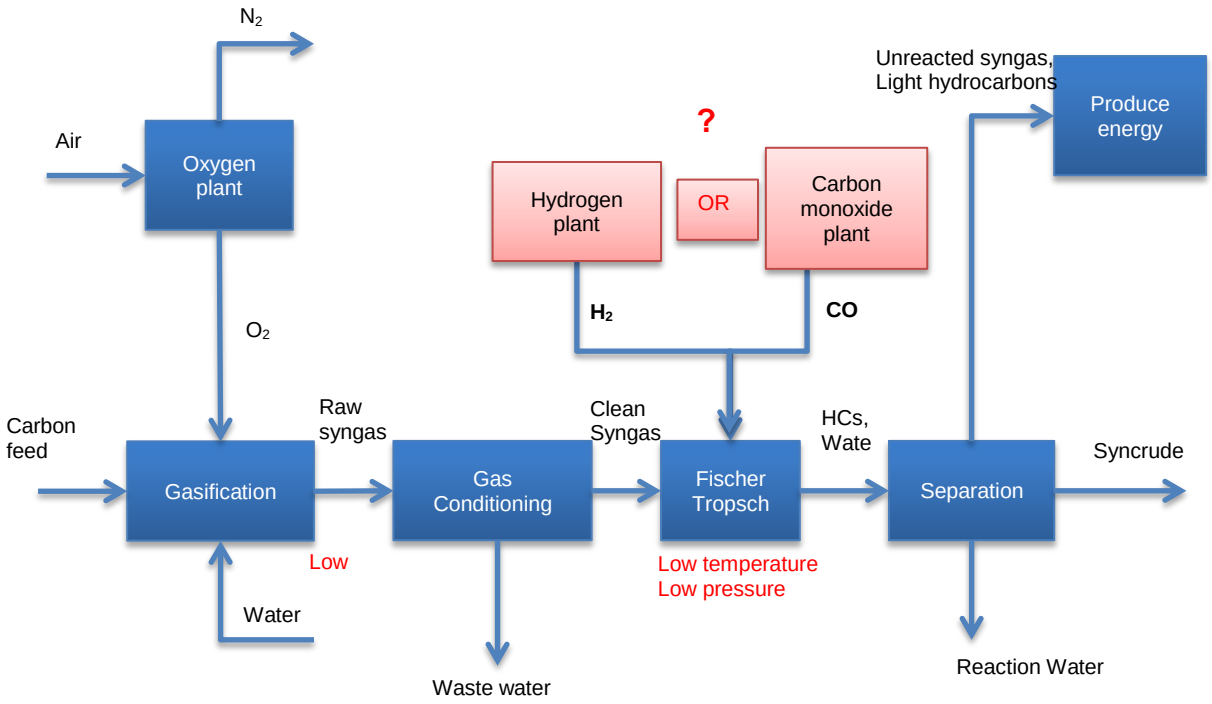

Figure 1.1: Generic block diagram of the FT plant process including syngas product and FTS. Parts in red show areas for potential savings.

The focus of this work is to experimentally explore the behaviour of the catalyst reduced with different gases (H_2, syngas and CO) at low pressure in FT synthesis. The low pressure conditions can be useful in process down-scaling and cost reduction, as the operation can be carried out at almost ambient pressure. Currently, no studies investigating simultaneously the effect of three reducing agents (syngas, H_2, and CO) at almost ambient pressure have been reported. In this study the FT synthesis was carried out at 1 bar gauge, a value which is far below the normal FT runs at 20–40 bars in an attempt to achieve a less expensive process.

Furthermore, significant funds and time are usually consumed during spent catalyst replacement in an FT operation plant. Such disturbances are inevitable during operation since the catalyst deactivates, and ways to maintain the yield at reasonable cost to enable the plant to run continuously for a long time may be required. The prolonged operation ensures that maximum achievable profit can be

obtained. A systematic control system can be used by altering the operating parameters to maintain the conversion (product formation). The choice of the right parameters, either individual or in combination, could maintain the yield, and the need to replace the catalyst can be delayed. Fortunately, it appears possible to reactivate the catalyst to approach the level (in terms of activity) of a freshly equilibrated catalyst by changing the parameters such as flowrate and pressure.

In this research, the FTS reaction was studied over a long period of time (more than 19 months), during which a number of operating condition changes were made and possible catalyst deactivation was observed. It was anticipated that differently reduced catalysts would yield different selectivities to products. In addition, the work is expected to contribute towards a better understanding of the conditions causing iron catalyst deactivation. The study found that these conditions could be tailored to yield a durable catalyst with excellent activity and better selectivity. And as such data were obtained, this research work provides a strong basis for further work on the durability of the catalyst and on the development of an appropriate reduction model that can be used, not only for the optimization of the overall reduction process but also for the investigation of the effect of reducing gases during the catalyst reduction process.

1.4 Research objectives

This thesis seeks to obtain clear and deeper understanding of the dynamic behaviour of differently reduced catalysts in a fixed bed reactor, and to transform the data obtained into valuable information that would aid FT operators in timely decision-making with regard to FT run time and performance.

This aim would be achieved via the following outlined activities and objectives:

- To study the effect of reducing gases, such as CO, $H_{2,}$ and syngas on the stability, activity and selectivity with Time-on-Stream (TOS) of impregnated iron catalyst in FT synthesis using a tubular fixed bed reactor.

- To gain an in-depth understanding of catalysts speciation during reduction by means of thermodynamics

- To study the effect of varying operating conditions of differently reduced catalyst.

- To study the regenerability of differently reduced catalyst after a long TOS.

- To use newly introduced plots to depict product distribution

The experimental work included constructing the FT rig, reducing the iron catalyst at atmospheric pressure, 250 ^{o}C, and flow of 60 mL(NTP)/min, with different reducing gases. The actual FTS was carried out mainly at similar operating conditions as those employed for the reduction of the catalyst.

1.5 Thesis outline

The work presented in this thesis is organised in nine chapters based on the nature of the investigations. The current chapter has presented the background, problem statement, research justification, research objectives and scope (outline) for the research work to follow.

Chapter 1 gives a short background on FTS, the research problem, the aims and objectives, and the scope and outline of the research.

Chapter 2 presents a review of the literature on Fischer Tropsch synthesis at various operating conditions and the progress made to date. The areas where information is still lacking are highlighted. Hence, this chapter provides a context for the research work to follow.

Chapter 3 starts with a brief overview of the literature on *in situ* characterization during catalyst reduction, some thermodynamic calculations to show the speciation pathway of the catalyst precursor during reduction, and the mechanism of reduction with different reducing agents.

Chapter 4 describes the experimental equipment and the measuring system components used in the work undertaken for the research as well as the programs involved and the methodology applied.

Chapter 5 presents results obtained at low pressure. Analysis of the data revealed some useful information that can be potentially utilized to reduce capital cost.

Chapter 6 dwells on the results obtained by alteration of operating conditions. This information can be potentially utilized for process control.

Chapter 7 is dedicated to the study of *in situ* catalyst regenerability using the feed gas (syngas). Fundamental information relating to the pathway of regeneration is formulated that might be useful in reactivating the catalyst that was showing reduced activity. But despite this progress, some challenges still remain with regard to the extension of the technique to an industrial setup.

Chapter 8 presents two types of plots (called Yao plots and Lu plots after the inventors) describing the data discussed in chapters 5–7. These two novel methods are proposed to describe product distributions in FT. Once accurately calibrated, the two plots could provide a simple means of estimating the product distribution.

Chapter 9 which completes the thesis, presents the main conclusions drawn from the work described in this thesis, and offers suggestions for future work.

This thesis thus provides invaluable information relating to low pressure FT and the manipulation of operation variables to tailor the product yields and plausible regeneration pathways. The usefulness of this is towards developing best strategies for effective FT runs and performance optimisation. Recommendations for future work are included in the same chapter. Lastly, the list of referenced material and appendices are given.

References

Aasberg-Petersen, K., Christensen, T. S., Dybkjaer, I., Sehested, J., Østberg, M., Coertzen, R. M., … Steynberg, A. P. (2004). Chapter 4 - Synthesis gas production for FT synthesis. In André Steynberg and Mark Dry (Ed.), *Studies in Surface Science and Catalysis* (Vol. Volume 152, pp. 258–405). Elsevier. Retrieved from http://www.sciencedirect.com/science/article/pii/S0167299104804610

Botes, F. G., Niemantsverdriet, J. W., & van de Loosdrecht, J. (2013). A comparison of cobalt and iron based slurry phase Fischer–Tropsch synthesis. *Catalysis and Synthetic Fuels: State of the Art and Outlook*, *215*, 112–120. http://doi.org/10.1016/j.cattod.2013.01.013

Chinchen, G. C., Logan, R. H., & Spencer, M. S. (1984). Water-gas shift reaction over an iron oxide/chromium oxide catalyst. II: Stability of activity. *Applied Catalysis*, *12*(1), 89–96. http://doi.org/10.1016/S0166-9834(00)81506-7

de Klerk, A. (2011). *Fischer-Tropsch Refining*. Retrieved from http://www.scopus.com/inward/record.url?eid=2-s2.0-84891567101&partnerID=40&md5=c2dd0acd8e9fa90a0a2b77156c7e1204

de Klerk, A., Li, Y.-W., & Zennaro, R. (2013). Fischer-Tropsch Technology. In *Greener Fischer-Tropsch Processes for Fuels and Feedstocks* (pp. 53–79). Retrieved from http://www.scopus.com/inward/record.url?eid=2-s2.0-84886342123&partnerID=40&md5=e93de2acaa5be7d6ad57d9bdfc0287d4

Jalama, K. (2008). *Fischer Tropsch synthesis over supported cobalt catalysts: effect of ethanol addition, precursors and gold doping*. Retrieved from http://wiredspace.wits.ac.za/handle/10539/4937

Kritzinger, J. A. (2002). The role of sulfur in commercial iron-based Fischer–Tropsch catalysis with focus on C2-product selectivity and yield. *Fischer-Tropsch Synthesis on the Eve of the XXI Century*, *71*(3–4), 307–318. http://doi.org/10.1016/S0920-5861(01)00457-6

Kuo, J. C. W. (1984). *GASIFICATION AND INDIRECT LIQUEFACTION.* Retrieved from http://www.scopus.com/inward/record.url?eid=2-s2.0-0021575919&partnerID=40&md5=925bc8f6f7abebac4068f5779baa51aa

Lappas, A., & Heracleous, E. (2010). Production of biofuels via Fischer-Tropsch synthesis: Biomass-to-liquids. In *Handbook of Biofuels Production: Processes and Technologies* (pp. 493–529). Retrieved from http://www.scopus.com/inward/record.url?eid=2-s2.0-84869086429&partnerID=40&md5=9647400344ea06fd2366cb787430e07e

Lee, D. W., & Yoo, B. R. (2014). Advanced metal oxide (supported) catalysts: Synthesis and applications. *Journal of Industrial and Engineering Chemistry*, *20*(6), 3947–3959. http://doi.org/10.1016/j.jiec.2014.08.004

Newsome David S. (1980). WATER-GAS SHIFT REACTION. *Catalysis Reviews Softcover Ed.*, *21*(2), 275–281.

Ojeda, M., & Rojas, S. (2012). *Biofuels from fischer-tropsch synthesis*. Retrieved from http://www.scopus.com/inward/record.url?eid=2-s2.0-84892804921&partnerID=40&md5=098cf9a8f9dc373ee2efd8a136416719

Rhodes, C., Hutchings, G. J., & Ward, A. M. (1995). Water-gas shift reaction: finding the mechanistic boundary. *Recent Advances in C1 Chemistry*, *23*(1), 43–58. http://doi.org/10.1016/0920-5861(94)00135-O

Schijndel, J. V., Thijssen, N., Baak, G., Avhale, A., Ellepola, J., & Grievink, J. (2011). *Development of a synthesis tool for Gas-To-Liquid complexes* (Vol. 29). Retrieved from https://www.scopus.com/inward/record.uri?eid=2-s2.0-79958831640&partnerID=40&md5=4a2eb863445c1cd315fa37d75a9ced12

Tada, M., & Iwasawa, Y. (2009). Advanced Design of Catalyst Surfaces with Metal Complexes for Selective Catalysis. In *Modern Surface Organometallic Chemistry* (pp. 375–415). Retrieved from http://www.scopus.com/inward/record.url?eid=2-s2.0-84890666754&partnerID=40&md5=6f4cd52314e4730d3163c063d7944df1

Van de Loosdrecht, J., Botes, F. G., Ciobica, I. M., Ferreira, A., Gibson, P., Moodley, D. J., … Niemantsverdriet, J. W. (2013). Fischer-Tropsch Synthesis: Catalysts and Chemistry. In *Comprehensive Inorganic Chemistry II (Second Edition): From Elements to Applications* (Vol. 7, pp. 525–557). Retrieved from http://www.scopus.com/inward/record.url?eid=2-s2.0-84902559789&partnerID=40&md5=bf301f4c6f75c09906975ae6e8ae11a9

CHAPTER 2

LITERATURE REVIEW

2.1 Introduction

The ultimate objective of this study is to investigate the effects of reducing Fischer Tropsch (FTS) iron catalyst with different reducing agents. In the FT process, catalyst reduction is of paramount importance as it transforms the catalyst precursor to the catalyst proper. Many researchers have studied and documented the effective use of H_2 as a reducing agent, whereas the use of CO and syngas has received less attention. These reducing agents effect phase changes to the catalyst precursor yielding active catalyst with fascinating properties. The speciates have different reactions to catalyze, and as such, the product distribution could then depend on the extent of reduction and the reducing gas used.

The main problems with any of the anything-to-liquids (XTL) technologies are that capital costs and the operational costs are extremely high. An XTL technology encompasses the conversion of gas-to-liquids (GTL), coal-to-liquids (CTL) and biomass-to-liquids (BTL) (Ojeda and Rojas 2012; Aasberg-Petersen et al. 2004; Dry and Steynberg 2004; van Steen and Claeys 2008; Rauch et al. 2013). As a result, securing a cheap feedstock supply can also reduce the capital costs of the whole hydrocarbon synthesis. Coal and biomass as solid feeds are converted to syngas in a gasifier, and natural gas is converted in a reformer, and typical examples are the partial oxidation, autothermal reforming or steam methane reforming. These and other technologies available for synthesis gas generation are discussed more extensively by Aasberg-Petersen et al. (2004).

The catalyst precursor, upon reduction, speciate to give different phases of varying stability depending on the reducing gas used. A thorough look into this speciation is given in chapter 3. This literature review includes information on speciation during reduction with different reducing agents. Reducing condition methods which

are in use are reviewed. A review of the reducing gases used is included. The factors affecting the reduction extent are examined. The discussion highlights a possible transformation mechanism to convert the precursor catalyst into the desired metallic iron or iron carbides. The literature review provides information that will help in elucidating a possible production route of the catalyst that is most effective.

2.2 Conventional FT synthesis

In the Fischer Tropsch process, a mixture of predominantly CO and H_2 (synthesis gas or syngas) obtained from feedstocks such as natural gas, coal and biomass, is catalytically converted to hydrocarbons (Lappas and Heracleous 2010; Van Ommen and Grievink 2014). In essence, any carbon-containing material can be potentially converted to syngas via a combination of gasification and reforming or partial oxidation (Bharadwaj and Schmidt 1995). The FT process yields a wide spectrum of products, the most desirable ones being paraffins, olefins and oxygenates, and large quantities of water are also produced as a by-product (De Smit and Weckhuysen 2008; De Smit et al. 2010)..

$$n\mathrm{CO} + (2n + 1)\mathrm{H_2} \rightarrow \mathrm{C_nH_{2n+2}} + n\mathrm{H_2O} \quad (2.1)$$

$$n\mathrm{CO} + 2n\mathrm{H_2} \rightarrow \mathrm{C_nH_{2n}} + n\mathrm{H_2O} \quad (2.2)$$

$$n\mathrm{CO} + 2n\mathrm{H_2} \rightarrow \mathrm{C_nH_{2n+2}O} + (n - 1)\mathrm{H_2O} \quad (2.3)$$

FT synthesis has been reviewed by several authors (Pretorius and de Klerk 2013; Van de Loosdrecht et al. 2013; Rauch, Kiennemann, and Sauciuc 2013; de Klerk, Li, and Zennaro 2013) revealing the diversity of the conventional Fischer Tropsch synthesis. Several publications also discuss the pros and cons of various operating conditions. The operating conditions usually employed in FT typically range from 220 to 250 °C and pressure of 20 to 60 bars (Hunpinyo et al. 2013; Y. Liu et al. 2007; Branislav Todic et al. 2016). In practice, the operating conditions are usually tailored depending on product distribution required, the catalyst used

and the reactor type (Hossein Atashi et al. 2015; Farias, Fernandes, and Sales 2010; Farias et al. 2007a).

2.3 Effects of operating conditions

Selectivity relates the yield of a particular product with respect to a particular reactant and this relation is mostly influenced by the process conditions (Soled et al. 1990). The influence of process conditions on the product selectivity has been investigated and well documented. Several review papers (Abelló and Montané 2011; Basha et al. 2015a; Sarkari, Fazlollahi, and Atashi 2012a; Mohanty et al. 2014) have been published highlighting the effects of changing flowrate, pressure, temperature and the catalyst on the product distribution. The effect of pressure, temperature, flowrate, time on stream and reduction of the catalyst are discussed briefly.

2.3.1 Pressure in Fischer Tropsch synthesis

In gas-to-liquids (GTL) plants, compromises must be made between product selectivities and yield, and the FT capital costs and operating conditions (Petersen et al. 2015; Sims et al. 2010). The economies of scale are used to justify the use of high operating pressures as this yields high conversions and helps control the heat removal (Kshetrimayum et al. 2015) and the possibility of recycling the tail gas in the FT reactors (Yao, 2011). In most cases, FT plants operate at high pressure, the maximum commissioned in 1987 was 45 bar by Sasol with Arge tubular fixed bed reactors (TFBR's) for LTFT synthesis (Espinoza et al. 1999a).

Increasing total pressure has in general the effect of increasing both the extent of conversion and the chain length of the products. Studies by Farias et al. (2008) showed that high pressures (25 to 30 atm) favoured the production of waxes, while greater direct selectivity towards diesel was favoured by low pressure (20 atm) when using iron based catalysts. In other pressure studies, by Todic et al. (2016a) using an iron based catalyst, increasing pressure resulted in the reduction of methane production and increase of C_{5+} products. Studies by Liu et al. (2007)

reported the same observation when an iron based catalyst promoted with manganese was used.

To date, an economical FT plant design which operates at low pressure and demands less operating expertise has not been developed for small plants. The emphasis on simplicity and minimized capital cost definitely affects the efficiency of the process.

2.3.2 Effects of temperature on product selectivity

The effect of temperature for iron based catalysed FTS reaction has been reported many times in the literature (Farias et al. 2007b; H. Atashi et al. 2015; Meshkani F. and Rezaei M. 2015; Espinoza et al. 1999b; Yuan et al. 2011). The consensus is that increasing temperature increases the rate of reaction but decreases the chain length of the products. Koeken, Ruitenbeek and De Jong (2011) reported a positive effect on the amount of light hydrocarbons produced whilst the heavy ones decreased. The current study will only be limited to the effect of pressure and flowrate, though temperature also plays a major role in FT production.

2.3.3 Flowrate effect on Fischer Tropsch synthesis

Gas flowrate affects the conversion and probably the product selectivities; that is, the higher the flowrate the lower the conversion, and the lower the flowrate the higher the conversion (Yaghobi 2013). The influence of flowrate on selectivity is still not well studied in the literature, and studies done thus far are not conclusive since the partial pressure of reactants is affected with this variation (Panahi and Skogestad 2011; Boyer et al. 2016); Hunpinyo et al. 2013).

The influence of the feed flowrate or residence time on product selectivity has been investigated and results are mostly depicted as a ratio of olefins and paraffins (Copperthwaite et al. 1987). Studies by Kuipers et al. (1996) showed an increase of the olefin to paraffin ratio with increasing space velocity (thus a decrease of the conversion) on a poly-crystalline cobalt foil. In another study, Iglesia, Reyes, and Madon (1991) reported an increase of the average molecular

weight of the products with decrease of the space velocity and also a decrease in the methane and olefin selectivities with a decrease of the space velocity, while the selectivity towards paraffins remains unchanged. The effect of the space velocity is mainly on the secondary reactions of olefins to paraffins (hence the significance of the ratio). The α-Olefins, which are primary Fischer Tropsch products, are known to participate in secondary reactions during the synthesis process (Novak, Madon, and Suhl 1982; Lu, Hildebrandt, and Glasser 2015). These conclusions suggest that readsorption and secondary reaction of the initially produced α-olefins is an important pathway leading to the formation of large molecular weight hydrocarbons during Fischer Tropsch synthesis. This is generally agreed upon by many researchers (Dwyer and Somorjai 1979; Iglesia, Reyes, and Madon 1991b; Snel and Espinoza 1989). The current work will explore how the differently reduced catalysts respond to changes in the feed flowrate.

2.3.4 **Time on stream**

Time on stream (TOS) in Fischer Tropsch is basically the period of time from when the reaction is started after catalyst reduction (initial period of synthesis) to the point the reaction is stopped (Sarup and Wojciechowski 1984; Karre et al. 2013; Vo, Nguyen, and Adesina 2010). It is well documented that catalyst deactivation happens with increase in TOS as many deactivating phenomena take place such as carbon deposition, sintering, poisoning and oxidation (Meng, Xu, and Gao 2007; C. Wang, Ma et al. 2015; Luo and Davis 2001; Raje et al. 1997). Studies have also been done to ascertain deactivation as a function of potassium promoter loading for precipitated iron catalyst (Pendyala et al. 2014).

The degree of deactivation varies with TOS and hence the product distribution varies accordingly. Very few researchers have reported the effects of time on stream on their product distribution though this parameter cannot be used alone explaining catalyst deactivation (Sarup and Wojciechowski 1984; Karre et al. 2013; Vo, Nguyen, and Adesina 2010). Donnelly and Satterfield (1989) reported that the average molecular weight of products from a commercial Ruhrchemie catalyst

decreased with time-on-stream and, at the same time, oxygenate production increased substantially after a period of 1300 hours' time on stream. In the same study, Donnelly and Satterfield (1989) observed that in contrast a precipitated iron catalyst with neither potassium nor silica showed stable selectivity but decreasing activity for 2000 hours-on-stream. The behaviour of the differently reduced catalyst after a long time on stream (about 14 000 hrs) under laboratory conditions has never been looked at to the best of our knowledge. This helps us have an insight into which reducing agent yields a catalyst with better stability for long TOS.

2.3.5 **Fischer Tropsch catalyst**

Fischer Tropsch catalysis is a growing area of research, as seen by an exponential increase in the publication activities on the topic. Iron and cobalt are the mostly used transition metals (de Klerk 2011; Mark E. Dry 1983a). Iron based catalysts have been widely used because of their low cost and availability; it is reported that iron is the most abundant element, by mass, in the Earth, constituting about 80% of the inner and outer cores of Earth (Frey and Reed 2012). The potential impact of other metal additives on these metals (Fe, Co) on their catalytic activity is gaining momentum. Pure components can be used as catalysts, but with continuing research multicomponent catalysts are studied and are now commonly used in FT technology to fulfil economic, and environmental demands. Several hybrid FT catalysts with additive metals are reported by a number of researchers (Ryu et al. 2015; B. Li et al. 2015; Qin et al. 2016; T. Lu et al. 2016a; Mosayebi and Haghtalab 2015; Mosayebi, Mehrpouya, and Abedini 2016). These hybrid catalysts tend to have selectivies towards a specific range of products; so, for instance, the hybrid catalysts of Cu-Zn-Al/Co-Hβ at low reaction temperature (290 °C) tend to yield C_3-C_5 hydrocarbons (T. Lu et al. 2016b). In the study by Wang et al. (2015), the catalytic conversion of syngas into hydrocarbons over hybrid catalysts consisting of a methanol synthesis catalyst and Pd modified zeolites (PdZSM-5, Pdβ, and PdY), promotes the formation of C_{4+} hydrocarbons supposedly due to the large pores and cavities of Pdβ and PdY. A process with Pt/ZSM-5 (Pt 2% (w)) catalyst to produce toluene and para-

xylene through the alkylation of benzene with syngas, was also reported by Zhong et al. (2016). The nature of these studies contributes significantly to the development of efficient catalysts for production of hydrocarbons from syngas.

2.3.6 **Water gas shift reaction**

The water-gas shift (WGS) reaction is a competitive process in FT synthesis in which carbon monoxide reacts with water produced during the FT reaction to produce carbon dioxide and hydrogen (Meshkani and Rezaei 2015a; Meshkani and Rezaei 2015b; Bukur et al. 2015; Martos, Dufour, and Ruiz 2009). According to Bukur et al. (2015) this reaction is essential to increase hydrogen production and to decrease the CO in the FT process. The water-gas shift (WGS) reaction is reversible and moderately exothermic, and it is thermodynamically limited at high temperatures (Newsome David S. 1980; Rhodes, Hutchings, and Ward 1995). **Figure 2.1** shows the variation of the log of equilibrium constant Log (k_p) for the water-gas shift reaction with temperature (°C). In general, low temperature FT of 190–250 °C favours greater equilibrium conversions to carbon dioxide (Rhodes, Hutchings, and Ward 1995). Consequently, in industrial plants, the WGS is usually carried out in two stages: a high-temperature stage (HTS) at 350–500 °C and a low-temperature stage (LTS) at 190–250 °C (Rhodes, Hutchings, and Ward 1995).

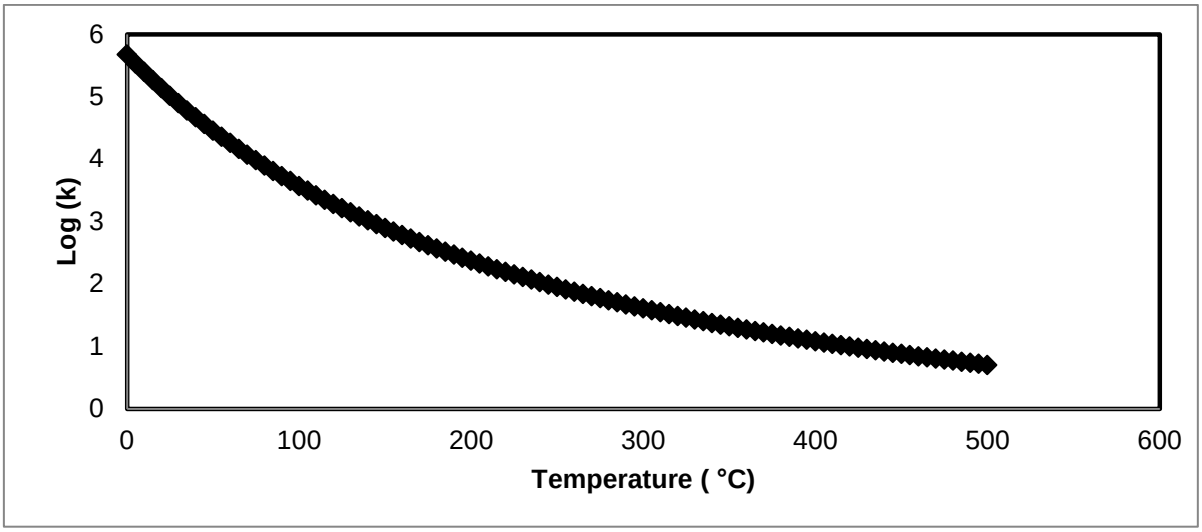

Figure 2.1: Variation of the logarithm of equilibrium constant Log (Kp) for the water-gas shift reaction with temperature (°C).

A measure of WGS activity is the amount of CO_2 formed in the reactor. The WGS reaction, which is known to be catalysed by magnetite (Newsome David 1980), can be presented as:

$$CO + H_2O \leftrightarrow CO_2 + H_2 \qquad (2.3)$$

Usage ratio (UR), defined by equation 2.4, is a useful property to look at when studying WGS (B. Todic et al. 2016b).

$$UR = \frac{moles\ of\ H_2\ consumed}{moles\ of\ CO\ consumed} \qquad (2.4)$$

The WGS reaction balances the H_2: CO ratio and this phenomenon is commonly observed in the case of coal-derived syngas, which has a H_2/CO ratio of less than 2. The stoichiometric ratio of the feed H_2/CO should preferably be about 2 to produce hydrocarbons according to equations 2.1, 2.2 and 2.3. In the absence of the WGS reaction, the usage ratio remains approximately 2. In the case of high WGS activity, where all water produced by FTS is consumed by the WGS reaction, the usage ratio would be less than 2 and the selectivity to CO_2 would be more than 50% assuming that CO is only consumed by the formation of hydrocarbons and WGS (D.B. Bukur, Todic, and Elbashir 2015).

In FT synthesis the catalyst precursor is mainly hematite (a-Fe_2O_3) which is reduced in situ to produce magnetite (Fe_3O_4) which is found to be the active phase (Chinchen, et al. 1984; Martos, et al. 2009). It is this magnetite that is known to catalyze the water gas shift reaction in Fischer Tropsch synthesis. So understanding the conditions that favour the formation of this phase in FT would be beneficial to FT practitioners.

2.3.7 Effect of catalyst composition on the performance and selectivity of the catalyst

Different oxides (ZnO, MnO, Al_2O_3), metals (Cu, Ru), and alkali (K, Na, Cs, Rb) metals have been used to increase the activity and the structural integrity of the FT catalysts (Wang and Spivey 2015; Jermwongratanachai et al. 2014; Jacobs et al. 2014a). Among them, copper and potassium are widely used, and these additives play an important role in determining the FTS product distribution and life span of the catalyst.

In addition, adding of promoters such as Cu and K to precipitated iron-based catalyst has been found to have significant influences on the crystallographic structure, morphological and physical properties of iron-based catalysts, as well as stability and selectivity performances during FT synthesis (Özkara-Aydinoğlu et al. 2012). Dopants such as ZnO, Cu, and K compounds have been reported to increase FTS rates on precipitated Fe_2O_3 precursors (Li et al. 2001).

Furthermore, studies by Das et al. (2013) indicate that increasing K loading decreases gaseous hydrocarbon formation and shifts selectivity to heavy hydrocarbons. Das et al. (2013) also observed that the K suppresses of the hydrogenation activity of the Fe-Cu/SiO_2 catalyst, leading to higher olefin yield in the products. Further studies by Ding et al. (2015) studied the impacts of K promoter on microstructures of a precipitated Cu-Fe based catalyst using N_2-physisorption (BET), X-ray photoelectron spectroscopy (XPS), X-ray diffractometer (XRD) and hydrogen temperature-programmed desorption/reduction (H_2-TPD/TPR). The study indicated that incorporation of K in the Cu-Fe based catalyst

reduced the surface area of the particles and promoted the migration of bulky iron species to surface layers and strengthened the interaction of surface Fe-Cu. In addition, the increase of K concentration facilitated the formation of heavy hydrocarbons (M. Ding et al. 2015).

Addition of both Cu and K to the catalysts showed a highly significant decrease of the catalyst deactivation rate and greatly enhanced the CO and H_2 conversion, 82% and 44% from 35% and 30% obtained with non-doped catalyst, respectively (Blanchard and Abatzoglou 2014). Similar conversion effects were observed by Pendyala et al. (2014). Increasing copper loading suppressed lower hydrocarbon (methane and C_2-C_4) selectivities and favoured higher hydrocarbon (C_{5+}) selectivity (Pendyala, Jacobs, et al. 2014).

Copper has traditionally been added to precipitated iron catalysts to aid reduction of Fe_2O_3 to metallic iron by lowering the reduction temperature (Cairns et al. 2006; Tang et al. 2009; O'Brien and Davis 2004). This lowering of reduction temperature is of particular importance when activating with hydrogen since the formed metallic iron is prone to sintering if the temperature is too high; however, it is not as critical when activating with carbon monoxide or syngas because iron carbides are formed and they are not as susceptible to sintering (O'Brien and Davis 2004). Cu and K compounds have been reported to favour the water-gas shift (WGS) activity, a reaction that occurs concurrently with FTS on Fe-based catalysts (Ma et al. 2014).

2.3.8 Effect of the nature of reducing gases during catalyst activation

The difference in pretreatment method causes the catalysts to exhibit significant differences in their catalytic activity for CO hydrogenation (Shroff et al. 1995a; D. B. Bukur et al. 1995). During FT synthesis hematite (α-Fe_2O_3), an iron catalyst precursor, is introduced into the reactor and subjected to an activation treatment to obtain the actual Fischer Tropsch catalyst. The activation process involves passing through gases such as H_2, CO or syngas over a catalyst precursor to give highly active catalytic state. During the reduction stage the catalyst precursor

hematite (α-Fe_2O_3) is known to be converted to magnetite (Fe_3O_4) regardless of the activation gas used for pretreatment (Herranz et al. 2006). The fate of the intermediate magnetite will then be determined by the nature of the reducing agent, temperature and pressure.

In the FTS reaction, the CO-activated catalyst is reported to give comparatively higher initial activity than the H_2 and syngas-reduced catalysts, and the trend remained unchanged in the activity following the transformation of iron carbides to Fe_3O_4 (M. Ding et al. 2011). The nature of the reducing gases determines the initial phase of the catalyst after reduction stage. These phase differences are well explained in section 2.6.2.1 for CO reduction, section 2.6.2.2 for H_2 reduction and section 2.6.2.3 for syngas reduction.

The literature suggests that magnetite has negligible catalytic activity for FT synthesis (van der Laan and Beenackers 2000) whereas carbide formation is necessary before the catalyst becomes active (Park et al. 2015). The extent of transformation into carbide correlates well with catalyst activity during the activation step (Shroff et al. 1995b).

The degree of reduction depends on several factors, including iron catalyst precursor, support material and its pretreatment; pore diameter, pore volume and available total surface area; method of impregnation or deposition; drying and calcination conditions; and reduction conditions (Lee and Yoo 2014; Porosoff, Yan, and Chen 2016; Iglesia 1997; Jacobs, Ma, and Davis 2014b; Boellaard, Van der Kraan, and Geus 2002). This in turn affects the number of active sites on the catalyst.

2.3.9 **Effect of CO reduction on FT catalyst**

Reduction has been reported to occur in four steps, with iron carbides being the ultimate phase. The reduction kinetics of the first step ($Fe_2O_3 \rightarrow Fe_3O_4$) is reported to be faster whilst the reduction kinetics of $Fe_3O_4 \rightarrow FeO$ is reported to be the rate-limiting step (Zhu et al. 2015)

$Fe_2O_3 \rightarrow Fe_3O_4 \rightarrow FeO \rightarrow Fe \rightarrow Fe_yC_x$

$$3Fe_2O_3 + CO \longrightarrow 2Fe_3O_4 + CO_2 \qquad \Delta G_{250} = -69.45\ kJ \qquad (2.4)$$

$$Fe_3O_4 + CO \longrightarrow 3FeO + CO_2 \qquad \Delta G_{250} = +8.76\ kJ \qquad (2.5)$$

$$FeO + CO \longrightarrow Fe + CO_2 \qquad \Delta G_{250} = -7.29\ kJ \qquad (2.6)$$

$$6Fe + 2CO \longrightarrow 2Fe_3C + O_2 \qquad \Delta G_{250} = +344.15\ kJ \qquad (2.7)$$

Summing these reactions gives the reduction of hematite to iron carbides

$$1.5Fe_2O_3 + 6.5CO \longrightarrow 2Fe_3C + 5.5CO_2 \qquad \Delta G_{250} = -113.20kJ \qquad (2.8)$$

Wüstite is meta-stable at temperatures below 570 °C, so this reduction will appear as if its 3 stages with magnetite reducing directly to metallic iron without first being converted to wustite (Ferdous and Demirel 2010). Equation (8) reportedly takes place readily at typical FT reaction temperature because of the low apparent activation energy of this reaction (Ferdous and Demirel 2010).

The use of CO as a reducing agent has received attention from the researchers though at varying conditions. For instance activating with CO was tested at 270 ˚C for 24 hours at a gas pressure of 1.3 MPa and this was shown to yield active Fe_5C_2 (Pendyala et al. 2010), and this activation gas is reported to give high active and stable catalyst (O'Brien et al. 1996). CO activation has been reported to form large amounts of iron carbides (χ-$Fe_{2.5}$) and carbonaceous species on the surface of magnetite (Ding et al. 2011; Pham et al. 2014).

2.3.10 **Effect of H_2 reduction on FT catalyst**

Reduction with H_2 is similar to the one with CO and has been reported to go via 3 steps $Fe_2O_3 \rightarrow Fe_3O_4 \rightarrow FeO \rightarrow Fe$ (Masina et al. 2015; Lin, Chen, and Li 2003).

Hydrogen is the most used reducing agent in the literature, with researcher varying conditions according to the TPR results of the catalyst used (de Smit et al. 2009; (D. B. Bukur et al. 1995; H. Wang et al. 2009; Shimokawabe, Furuichi, and Ishii 1979; Dİlmaç, Yörük, and Gülaboğlu 2015).The reduction reaction occurs in three steps from hematite with iron carbides as the ultimate phase. Carbide formation is most unlikely in hydrogen reduction (in terms of mass balance.

$$3Fe_2O_3 + H_2 \longrightarrow 2Fe_3O_4 + H_2O \qquad \Delta G_{250} = -49.93\ kJ \qquad (2.8)$$

$$Fe_3O_4 + H_2 \longrightarrow 3FeO + H_2O \qquad \Delta G_{250} = +28.28\ kJ \qquad (2.9)$$

$$FeO + H_2 \longrightarrow Fe + H_2O \qquad \Delta G_{250} = +12.23\ kJ \qquad (2.10)$$

Summing these reactions gives the reduction of hematite to metallic iron. A fully reduced iron metal catalyst shows no activity for Fischer Tropsch synthesis, but becomes active along with its conversion into carbides

$$Fe_2O_3 + 3H_2 \longrightarrow 2Fe + 3H_2O \quad \Delta G_{250} = +26.68\ kJ \qquad (2.11)$$

From a delta G viewpoint, CO reduction is generally better than hydrogen.

2.3.11 **Effect of syngas reduction on FT synthesis**

Often a mixture of CO and H_2 is used as a reducing gas with the ratio of CO/H_2 varying dependent on source of the syngas available. Studies by Shroff et al. (1995) demonstrated that the partial pressure of hydrogen in the activating gas has a significant effect on the performance of the catalyst.

The catalyst reduction pathway proceeds in two steps that involve reduction of hematite into magnetite and magnetite carbidisation into iron carbides. Syngas has been used in different ratios: H_2/CO = 0.7/1.0 mixture (Shroff et al. 1995).

Hydrogen has a superior diffusion coefficient and adsorption capacity hence the H_2 improves the reduction rate (Yoshioka et al. 2008). There are other factors

influencing reduction, such as catalyst particle size, porosity, reducing pressure and temperature (Rytter et al. 2007; Azzam et al. 2014; Zamaniyan et al. 2013; Merino et al. 2016). Chernavskii et al. (2015) reported that the reduction of hematite to magnetite proceeds with similar rates in syngas and pure carbon monoxide, while magnetite can be carbidized more rapidly in carbon monoxide. Chernavskii et al. (2015) also observed that the concentration of iron carbide was approximately three times higher in CO activated relative to syngas activation.

When syngas with low partial pressure of H_2 or CO is used as a pretreatment gas, iron carbides are produced (Mingyue Ding et al. 2014; Dragomir B. Bukur et al. 1995).The nature of the resulting Fe phase formed during pretreatment depends on the duration of exposure to the reactant feed, the feed makeup (composition of the feed), the reactor system and the activation conditions (temperature and pressure) as stated by Shroff et al. (1995).

2.4 Catalyst speciation products

Insight into the speciation of the iron catalyst precursor during reduction has been obtained using in situ techniques. Analyses have been made of catalyst phases that exist during catalyst reduction by several authors to identify the most-persistent catalyst phase (Zhang and Schrader 1985; van der Kraan, Boellaard, and Crajé 1993; Rochet et al. 2011; Saib et al. 2006). These phases were measured using improved in situ methods. Supporting evidence for iron catalyst speciation during synthesis was found in tight correlations between activity (more carbides) and catalyst deactivation (more iron oxides) (Moodley et al. 2009a; Bartholomew 1984; Butt 1984). Metallic iron has previously been recognized during catalyst activation although the thermodynamics of its formation says otherwise (see Chapter 3). There is a need for more information on the importance and behaviour of catalysts during FT synthesis. Chapter 3 dwells more on the thermodynamics of these speciations and gives a brief review on the topic.

2.5 Catalyst deactivation

FT catalyst deactivation can be defined as the loss over time of the catalytic activity or selectivity (Polinski, Rao, and Stencel 1984; Bartholomew 1984; Istadi et al. 2011). This is a problem of great concern to FT practitioners. The costs to industry for process shutdown to replace the catalyst are high.

The catalyst stability is an important factor though it has received comparatively less attention than catalyst activity and selectivity. There two types of deactivation during reaction, mostly due to the physical degradation and/or chemical or phase change (Bartholomew 2001; Van Berge et al. 2000; De Smit and Weckhuysen 2008). Catalyst deactivation during the conversion of syngas to liquid fuels is an inevitable problem of great and continuing concern, and models and mechanisms of deactivation have been developed (Moodley et al. 2009a; Argyle, Frost, and Bartholomew 2014; van de Loosdrecht et al. 2007; Sadeqzadeh et al. 2013).

Phenomena such as product selectivity and catalyst deactivation are known to be highly dependent on reaction conditions, thus temperature and pressure. Under FT working conditions, the iron based catalyst is known to speciate to iron oxides and iron carbides (Bartholomew 1984; Moodley et al. 2009a). The activities of these speciation products in FT synthesis remain controversial. The majority of the available literature has suggested that iron carbides are perhaps the active phases in iron Catalysed FT reactions (Gnanamani et al. 2013; Herranz et al. 2006; Mingyue Ding et al. 2014; Shroff et al. 1995) whereas the iron oxides are regarded as catalytically inactive (De Smit et al. 2010). The commonly reported carbides formed during FTS are ɛ́-$Fe_{2.2}C$, ε-Fe_3C, Θ-Fe_3C, χ-Fe_5C_2, and Fe_7C_3 (De Smit and Weckhuysen, 2008**).** Shroff et al. (1995) observed a correlation between the carbide content and the Fischer Tropsch activity, while Herranz et al. (2006) observed the formation of Cementite (Θ- Fe_3C) and Hagg (χ- $Fe_{2.5}C$) after CO and syngas pretreatment, respectively, and further stated that the cementite species are less active during FT synthesis, and under FT reaction conditions they tend to evolve into the more active Hagg carbide. Nevertheless, the exact role of each carbide phase in the catalytic reaction remains unclear.

2.6 Deactivation phenomena

Catalyst deactivation has been defined as the loss over time of catalytic activity or selectivity (Bartholomew 2001). According to Bartholomew 2001, the major deactivating mechanisms of catalysts have been reported as due to poisoning, fouling, and oxidation. Catalyst poisoning refers to the partial or total deactivation of a catalyst caused by exposure to a range of chemical compounds, and in FT synthesis, iron and cobalt are mainly poisoned by H_2S, COS, As, NH_3 and metal carbonyls (Bartholomew 2001; Sparks et al. 2013; Zhao-Tie, Jing-Lai, and Bi-Jiang 1994). Basically, fouling is the physical deposition of species from the fluid phase onto the catalyst surface, which results in activity loss due to blockage of sites altering pore geometry and affects how a chemical process proceeds (Mann, El-Kady, and Marzin 1985). In the advanced stages of FT synthesis, deposits of carbon and coke in the pores of the catalyst also render the catalyst inactive and plugging of the reactor voids. The coke formed may vary from primarily carbons such as graphite to high molecular weight hydrocarbons (Moodley et al. 2009b; Saib et al. 2010).

The oxidation of supported Fischer Tropsch catalysts by means of water has also been studied in detail. In general, water is one of the Fischer Tropsch reaction products, and can probably cause oxidation and deactivation of a reduced catalyst (van Berge et al. 2000).

2.7 Ways of catalyst regeneration

The loss of catalytic activity with increasing TOS in FT synthesis is inevitable. When the activity has declined to a critical level, the activity of the catalyst will need to be restored. Deactivation of FT catalysts is a problem that causes loss of catalytic activity with time and coking is one of the main deactivating mechanisms (Argyle and Bartholomew 2015a). Carbon can be deposited on the catalyst or the reactor tube (Figueiredo 1982) and this carbon exists in different morphologies: carbon whiskers, well ordered graphitic deposits, and non-oriented deposits (Figueiredo and Pereira 2012; Tsou et al. 2003; Samant et al. 2004; Ermakova et

al. 2001). Studies in the literature have already looked at some restoration pathways (Pretorius and de Klerk 2013; Argyle and Bartholomew 2015b; Jacobs, Ma, and Davis 2014c; Van De Loosdrecht et al. 2016). Regeneration allows reaction of FT catalysts and results in less downtime during catalyst replacement by re-using the catalyst that is already in the reactor. In-situ regeneration has been studied by some authors and oxidative regeneration of catalyst was the main chemistry of reactivation.

This oxidative regeneration of carbon deactivated catalyst involves removing coke by burning it off, thereby generating CO and CO_2 as by-products which are purged out of the reactors by the pressure gradient (Yoshimura and Furimsky 1986). The oxidation also converts metal carbides to corresponding metal oxides, which are their inactive form.

Catalysts undergo chemical and physical changes during FT synthesis processes, and hence require periodic chemical treatments to maintain and/or restore their catalytic performance. In fact, FT catalysts lose their activity with time, and their relatively high costs drive FT practitioners to regenerate them to restore their activity, which has been done ex situ (Marafi, Stanislaus, and Furimsky 2010; Butt 1984). System downtime is of great concern during ex situ regeneration. Ex situ regeneration is generally quite time-consuming as the process involves dismantling the reactor. In addition, the catalyst may be exposed to contamination due to handling. However, in situ regeneration has proved to give good activity recovery, almost close to the initial activity as in the current study (80% activation); this percentage regeneration tends to vary with the nature of the initial reducing agent and can also be affected by factors such as uneven gas flow. Moreover, portions of the catalyst bed remain unregenerated, while other parts are subjected to excessive regeneration.

2.8 The effect of water on the stability of reduced catalyst

Water is produced during the Fischer Tropsch synthesis and tends to be present in varying quantities during synthesis, depending on the reactor system and the

nature of the catalyst (Fischer et al. 2015; Meshkani and Rezaei 2015a; Sadeqzadeh et al. 2013; Bezemer et al. 2010). The effect of water on FT depends on the type of support (pore size and type), metal nature, loading (dispersion and cluster size), additives and preparation procedures (Botes 2007). Water is a main product of the Fischer Tropsch synthesis and the concentration increases with increasing conversion, and the partial pressure of water in the reactor determines the state of the catalyst (Pendyala et al. 2010).

Iron catalysts suffer from product inhibition due to the product water produced in the pathways, shown by equations 2.1, 2.2 and 2.3, which makes the gas phase more oxidizing. Studies have shown that FT reaction rates decrease with an increase in the partial pressure of water (Thüne et al. 2012). A reversible decrease of the catalyst activity has been observed by Satterfield et al. (1986) after addition of 12 and 27 mol % water to the feed gas. In the same study the author (Satterfield et al. 1986) studied the effect of added H_2O on both the product distribution and the catalyst through the use of Mossbauer spectroscopy, and observed an increase in olefin to paraffin ratio and decrease of reaction rate after addition of water. Iron based catalyst tends to get re-oxidized at high partial pressure of water, and this is dependent on the ratio of hydrogen and water partial pressure in the reactor. Pendyala et al. (2010) studied the effect of water on the performance of potassium promoted iron catalyst during FT synthesis and observed a decrease in CO conversation and deactivation of the catalyst.

2.9 The effect of carbon dioxide formed and its formation pathways

Carbon dioxide (CO_2) is another undesirable FT synthesis by-product which can limit carbon utilization efficiency (Istadi et al. 2011). As for water formation, the removal of adsorbed oxygen formed in CO dissociation steps includes reaction with adsorbed hydrogen to form H_2O and with adsorbed CO to form CO_2. Another pathway is a water-gas shift (WGS) reaction which is comparatively more pronounced on iron-based catalysts than cobalt-based catalysts, due to high WGF activity for iron catalysts. Yao et al. (2011) studied the effect of CO_2 on an iron-based catalyst during low-temperature FTS and observed that CO_2 may be

converted to hydrocarbons only when the composition of the co-feed CO_2 has a value higher than that set by the equilibrium constraints. The CO_2 addition to synthesis gas does not influence CO_2 forward rates, as explained by Visconti et al. (2016) but rather increases the rate of their reverse steps in the manner predicted by kinetic analyses of reversible reactions using non-equilibrium thermodynamic treatments.

$$CO_{(gauge)} + H_2O_{(gauge)} \rightarrow CO_{2(gauge)} + H_{2\,(gauge)} \qquad \Delta H = -9.374\ \text{cal/K} \qquad (2.12)$$

The Gibbs free energy for the WGS reaction is negative under FT temperatures. The ΔH value decreases as the temperature is increased.

2.10 Product distribution

2.10.1 Anderson – Schulz – Flory (ASF) model

FTS follows a polymerization type mechanism with the products described by the Anderson–Schulz–Flory (ASF) model (Liu et al. 2011; Van Santen et al. 2014; Dieter et al., 2015). This model is able to describe lighter products of carbon number less than 10, while the higher carbon number products can deviate from linearity (Donnelly et al. 1988; Liu et al. 2011). The majority of the reported ASF plots showed a nearly straight line only in the C_4–C_{12} region (Tavakoli et al. 2008). A number of authors have determined the growth factor from the straight-line portion of the ASF plot. This made the experimental determination of the alpha (α) value somehow arbitrary (Puskas and Hurlbut 2003).

An analytical extension of the classical ideal Anderson–Schulz–Flory (ASF) distribution for the products of Fischer Tropsch reactions was reported by Förtsch, Dieter, et al. (2015). This model was capable of describing real distributions with the known deviations from the ideal ASF distribution for C_1 and C_2 components. The extended ASF model's wide range of applicability is reported to have allowed simple and direct extraction of the relevant parameters from experimental data (Förtsch, Pabst et al. 2015).

The chain-length-dependent desorption model for the iron-based low-temperature Fischer Tropsch (Fe-LTFT) synthesis was proposed by Botes (2007). The model could successfully describe the olefin and paraffin distributions in the C_{3+} range, and the total C_2 formation rate was predicted almost perfectly, though the methane formation rate was described adequately. In an attempt to provide a better descriptive model, Lu plots and Yali plots were developed. These plots have also been used to describe product distribution in FT with success (Muleja et al. 2016; X. Lu et al. 2012; Yao et al. 2012).

2.11 Nature and type of FT reactors

In Fischer Tropsch synthesis (FTS), the reactor plays an important role. The nature of the reactor used is governed by the operating conditions and the products desired. For instance, researchers aiming to produce lighter cuts such as gasoline and diesel opt for higher temperature Fischer Tropsch (HTFT) processes. Several reviews provide an overview of recent and past research activities in the field of catalyst development and reactor design (Basha et al. 2015b; Sarkari et al. 2012c; Hulet et al. 2009; Babita 2011; Saeidi et al. 2014b; Kolb 2013; T. Wang et al. 2007).

For many years there have been studies and improvements on different operating conditions to make the existing reactors more efficient. Recent studies have seen the use of new configurations such as a dual-type membrane reactor and a coupling configurations reactor, which improved the performances of the FT process (Saeidi et al. 2014b). The use of the slurry reactor has been reported with advantages of simple construction, excellent heat transfer performance, online catalyst addition and withdrawal, and a reasonable interphase mass transfer rate with low energy input, which make it very suitable for gas-to-liquid processes (Wang et al. 2007). Several reviews have also surveyed the use of fixed bed reactors with plug flow hydrodynamics (Fleisch et al. 2002; Khodakov et al. 2007; Sarkari et al. 2012b). For example, Shell, who happens to be a major player in this field, uses a tubular fixed bed reactor (Fleisch,et al. 2002). These three main types

of reactors used for FT reaction (Davis 2002; Sie and Krishna 1999) are briefly described below.

a) Fixed bed reactors which are used by Sasol (Pvt) Ltd to produce high value linear waxes at low temperatures (225 °C) (Espinoza et al. 1999b; Mark E. Dry 1983b). The catalyst is loaded in 5 cm internal diameter tubes. Heat removal is achieved by converting water circulating outside of the tubes into steam (Jalama 2008; A. Steynberg 2004; A. P. Steynberg 2004).

b) Fluidised bed reactors with either a fixed or a circulating bed. The main difference between the two types of reactors is that in the fixed fluidised bed reactor (FFD) the catalyst bed remains stationary and the gases pass upward through the bed, while in the circulating fluidised bed reactor (CFB) the catalyst is entrained in the fast moving stream (Sie and Krishna 1999; Jalama 2008).

c) Slurry bed reactors in which gas is bubbled through a suspension of finely divided catalyst in a liquid which has a low vapour pressure at the temperature of operation (Dry and Steynberg 2004; Jalama 2008).

Typical industrial FTS processes with fixed-bed reactors normally produce complex mixtures consisting of hydrocarbons ranging from methane to wax. In fixed-bed reactors, pressure drop has been reported, and facilitated heat removal; catalyst particles of a few millimetres in size are generally used in fixed-bed reactors (Gadalla, Vallee, and Jia 2013; Yakovenko et al. 2015), contributing to the existence of intra-particle pore-diffusion limitations (Sie and Krishna 1999). In a study by Gadalla et al. (2012), the catalyst was crushed and sieved, retaining particles ranging in size from 75 to 125 μm.

Additional theoretical details and practical aspects often used in selecting and designing FT reactors can be found in the literature (Steynberg and Vogel 2006; Martelli et al. 2012; Stelmachowski and Nowicki 2003; Deckwer et al. 1980; Martínez, Prieto, and Rollán 2009; Yamin and Fatemi 2005). Furthermore, the Material and Process Synthesis Group of UNISA has also conducted a considerable amount of research using fixed bed and continuously stirred tank

reactors (Yao 2011; Muleja et al. 2016; X. Lu et al. 2011; Jalama 2008). In situ regeneration studies in fixed-bed reactors are therefore of significant importance.

References

Aasberg-Petersen, K., T.S. Christensen, I. Dybkjaer, J. Sehested, M. Østberg, R.M. Coertzen, M.J. Keyser, and A.P. Steynberg. 2004. “Chapter 4 - Synthesis Gas Production for FT Synthesis.” In *Studies in Surface Science and Catalysis*, edited by André Steynberg and Mark Dry, Volume 152:258–405. Elsevier. http://www.sciencedirect.com/science/article/pii/S0167299104804610.

Abelló, S., and D. Montané. 2011. “Exploring Iron-Based Multifunctional Catalysts for Fischer-Tropsch Synthesis: A Review.” *ChemSusChem* 4 (11): 1538–56. doi:10.1002/cssc.201100189.

Argyle, M.D., and C.H. Bartholomew. 2015a. “Heterogeneous Catalyst Deactivation and Regeneration: A Review.” *Catalysts* 5 (1): 145–269. doi:10.3390/catal5010145.

———. 2015b. “Heterogeneous Catalyst Deactivation and Regeneration: A Review.” *Catalysts* 5 (1): 145–269. doi:10.3390/catal5010145.

Argyle, M.D., T.S. Frost, and C.H. Bartholomew. 2014. “Cobalt Fischer-Tropsch Catalyst Deactivation Modeled Using Generalized Power Law Expressions.” *Topics in Catalysis* 57 (6-9): 415–29. doi:10.1007/s11244-013-0197-9.

Atashi, Hossein, Sam Razmjooei, Mahdi Khorashadizadeh, Mehdi Shiva, Farshad Farshchi Tabrizi, and Seyed Amir Hossein Seyed Mousavi. 2015. “Effects of Operating Conditions on Selectivity of Fe–Co–Mn/MgO at High Temperature CO Hydrogenation.” *Journal of the Taiwan Institute of Chemical Engineers* 54 (September): 83–90. doi:10.1016/j.jtice.2015.03.017.

Atashi, H., S. Razmjooei, M. Khorashadizadeh, M. Shiva, F.F. Tabrizi, and S.A.H.S. Mousavi. 2015. “Effects of Operating Conditions on Selectivity of Fe-Co-Mn/MgO at High Temperature CO Hydrogenation.” *Journal of the Taiwan Institute of Chemical Engineers* 54: 83–90. doi:10.1016/j.jtice.2015.03.017.

Azzam, K., G. Jacobs, W. Ma, and B.H. Davis. 2014. “Effect of Cobalt Particle Size on the Catalyst Intrinsic Activity for Fischer-Tropsch Synthesis.” *Catalysis Letters* 144 (3): 389–94. doi:10.1007/s10562-013-1172-6.

Babita, K., S. Sridhar, and K.V. Raghavan. 2011. “Membrane Reactors for Fuel Cell Quality Hydrogen through WGSR - Review of Their Status, Challenges and Opportunities.” *International Journal of Hydrogen Energy* 36 (11): 6671–88. doi:10.1016/j.ijhydene.2011.02.107.

Bartholomew, Calvin H. 1984. “Catalyst deactivation.” *Chemical Engineering (New York)* 91 (23): 96–112.

Bartholomew, Calvin H. 2001. “Mechanisms of Catalyst Deactivation.” *Catalyst Deactivation* 212 (1–2): 17–60. doi:10.1016/S0926-860X(00)00843-7.

Basha, O.M., L. Sehabiague, A. Abdel-Wahab, and B.I. Morsi. 2015a. “Fischer-Tropsch Synthesis in Slurry Bubble Column Reactors: Experimental Investigations and Modeling - A Review.” *International Journal of Chemical Reactor Engineering* 13 (3): 201–88. doi:10.1515/ijcre-2014-0146.

———. 2015b. “Fischer-Tropsch Synthesis in Slurry Bubble Column Reactors: Experimental Investigations and Modeling - A Review.” *International Journal of Chemical Reactor Engineering* 13 (3): 201–88. doi:10.1515/ijcre-2014-0146.

Bezemer, G.L., T.J. Remans, A.P. Van Bavel, and A.I. Dugulan. 2010. “Direct Evidence of Water-Assisted Sintering of Cobalt on Carbon Nanofiber Catalysts during Simulated Fischer-Tropsch Conditions Revealed with in Situ Mössbauer Spectroscopy.” *Journal of the American Chemical Society* 132 (25): 8540–41. doi:10.1021/ja103002k.

Bharadwaj, S.S., and L.D. Schmidt. 1995. “Trends in Natural Gas UtilisationCatalytic Partial Oxidation of Natural Gas to Syngas.” *Fuel Processing Technology* 42 (2): 109–27. doi:10.1016/0378-3820(94)00098-E.

Blanchard, J., and N. Abatzoglou. 2014. “Nano-Iron Carbide Synthesized by Plasma as Catalyst for Fischer-Tropsch Synthesis in Slurry Reactors: The Role of Iron Loading and K, Cu Promoters.” *Catalysis Today* 237: 150–56. doi:10.1016/j.cattod.2013.12.027.

Boellaard, E., A.M. Van der Kraan, and J.W. Geus. 2002. “Preparation, Reduction and CO Chemisorption Properties of Cyanide-Derived NixFe/Al2O3 Catalysts.” *Applied Catalysis A: General* 224 (1-2): 1–20. doi:10.1016/S0926-860X(01)00670-6.

Botes, F.G. 2007. “Proposal of a New Product Characterization Model for the Iron-Based Low-Temperature Fischer-Tropsch Synthesis.” *Energy and Fuels* 21 (3): 1379–89. doi:10.1021/ef060483d.

Boyer, C., J. Gazarian, V. Lecocq, S. Maury, A. Forret, J.M. Schweitzer, and V. Souchon. 2016. “Development of the Fischer-Tropsch Process: From the Reaction Concept to the Process Book.” *Oil and Gas Science and Technology* 71 (3). doi:10.2516/ogst/2015032.

Bukur, D. B., K. Okabe, M. P. Rosynek, C. P. Li, D. J. Wang, K. R. P. M. Rao, and G. P. Huffman. 1995. “Activation Studies with a Precipitated Iron Catalyst for Fischer-Tropsch Synthesis: I. Characterization Studies.” *Journal of Catalysis* 155 (2): 353–65. doi:10.1006/jcat.1995.1217.

Bukur, D.B., B. Todic, and N. Elbashir. 2015. “Role of Water-Gas-Shift Reaction in Fischer-Tropsch Synthesis on Iron Catalysts: A Review.” Article in Press. Scopus. http://www.scopus.com/inward/record.url?eid=2-s2.0-84950154201&partnerID=40&md5=13000f65afe4cd61988d0a3a96792834.

Bukur, Dragomir B., Manoj Koranne, Xiaosu Lang, K. R. P. M. Rao, and Gerald P. Huffman. 1995. “Pretreatment Effect Studies with a Precipitated Iron Fischer-Tropsch Catalyst.” *Applied Catalysis A: General* 126 (1): 85–113. doi:10.1016/0926-860X(95)00020-8.

Butt, John B. 1984. *Catalyst deactivation and regeneration.* Vol. 6. Catalysis: Science and Technology. http://www.scopus.com/inward/record.url?eid=2-s2.0-0021595034&partnerID=40&md5=66178b1d44bb6108e18744ec38eec899.

Cairns, P., M.E. Dry, E. Van Steen, and M. Claeys. 2006. “Copper, a Selectivity Promoter in Iron Based Fischer-Tropsch Synthesis?” In . http://www.scopus.com/inward/record.url?eid=2-s2.0-34748904737&partnerID=40&md5=792387e84b2e37bee6d3d2d8712e3753.

Chernavskii, P.A., V.O. Kazak, G.V. Pankina, V.V. Ordomsky, and A.Y. Khodakov. 2015. “Mechanistic Aspects of the Activation of Silica-Supported Iron Catalysts for Fischer-Tropsch Synthesis in Carbon Monoxide and Syngas.” Article in Press. Scopus. http://www.scopus.com/inward/record.url?eid=2-s2.0-84948159415&partnerID=40&md5=e12ddedbebbf1731ef48e0c12906c82b.

Chinchen, G.C., R.H. Logan, and M.S. Spencer. 1984. “Water-Gas Shift Reaction over an Iron Oxide/chromium Oxide Catalyst. II: Stability of Activity.” *Applied Catalysis* 12 (1): 89–96. doi:10.1016/S0166-9834(00)81506-7.

Copperthwaite, Richard G., Graham J. Hutchings, Mark van der Riet, and Jeremy Woodhouse. 1987. “Cabon monoxide hydrogenation using manganese oxide based catalyst: Effect of operating conditions on alkene selectivity.” *Industrial and Engineering Chemistry Research* 26 (5): 869–74.

Das, S.K., P. Mohanty, S. Majhi, and K.K. Pant. 2013. “CO-Hydrogenation over Silica Supported Iron Based Catalysts: Influence of Potassium Loading.” *Applied Energy* 111: 267–76. doi:10.1016/j.apenergy.2013.04.070.

Davis, B.H. 2002. “Overview of Reactors for Liquid Phase Fischer-Tropsch Synthesis.” *Catalysis Today* 71 (3-4): 249–300. doi:10.1016/S0920-5861(01)00455-2.

Deckwer, Wolf Dieter, Youssef Louisi, Ahmed Zaldi, and Milos Ralek. 1980. “Hydrodynamic properties of the fischer tropsch slurry process.” *Industrial & Engineering Chemistry, Process Design and Development* 19 (4): 699–708.

de Klerk, A. 2011. *Fischer-Tropsch Refining*. Fischer-Tropsch Refining. https://www.scopus.com/inward/record.uri?eid=2-s2.0-84891567101&partnerID=40&md5=c2dd0acd8e9fa90a0a2b77156c7e1204.

de Klerk, A., Y.-W. Li, and R. Zennaro. 2013. “Fischer-Tropsch Technology.” In *Greener Fischer-Tropsch Processes for Fuels and Feedstocks*, 53–79. http://www.scopus.com/inward/record.url?eid=2-s2.0-84886342123&partnerID=40&md5=e93de2acaa5be7d6ad57d9bdfc0287d4.

De Smit, E., F. Cinquini, A.M. Beale, O.V. Safonova, W. Van Beek, P. Sautet, and B.M. Weckhuysen. 2010. “Stability and Reactivity of ε-X-θ Iron Carbide Catalyst Phases in Fischer-Tropsch Synthesis: Controlling μc.” *Journal of*

the American Chemical Society 132 (42): 14928–41. doi:10.1021/ja105853q.

de Smit, Emiel, Andrew M. Beale, Sergey Nikitenko, and Bert M. Weckhuysen. 2009. “Local and Long Range Order in Promoted Iron-Based Fischer–Tropsch Catalysts: A Combined in Situ X-Ray Absorption Spectroscopy/wide Angle X-Ray Scattering Study.” *Journal of Catalysis* 262 (2): 244–56. doi:10.1016/j.jcat.2008.12.021.

De Smit, E., and B.M. Weckhuysen. 2008. “The Renaissance of Iron-Based Fischer-Tropsch Synthesis: On the Multifaceted Catalyst Deactivation Behaviour.” *Chemical Society Reviews* 37 (12): 2758–81. doi:10.1039/b805427d.

Dİlmaç, N., S. Yörük, and Ş.M. Gülaboğlu. 2015. “Investigation of Direct Reduction Mechanism of Attepe Iron Ore by Hydrogen in a Fluidized Bed.” *Metallurgical and Materials Transactions B: Process Metallurgy and Materials Processing Science* 46 (5): 2278–87. doi:10.1007/s11663-015-0409-8.

Ding, Mingyue, Yong Yang, Baoshan Wu, Yongwang Li, Tiejun Wang, and Longlong Ma. 2014. “Study on Reduction and Carburization Behaviors of Iron-Based Fischer-Tropsch Synthesis Catalyst.” *Energy Procedia*, International Conference on Applied Energy, ICAE2014, 61: 2267–70. doi:10.1016/j.egypro.2014.12.444.

Ding, M., J. Tu, M. Qiu, T. Wang, L. Ma, and Y. Li. 2015. “Impact of Potassium Promoter on Cu-Fe Based Mixed Alcohols Synthesis Catalyst.” *Applied Energy* 138: 584–89. doi:10.1016/j.apenergy.2014.01.010.

Ding, M., Y. Yang, B. Wu, T. Wang, H. Xiang, and Y. Li. 2011. “Effect of Reducing Agents on Microstructure and Catalytic Performance of Precipitated Iron-Manganese Catalyst for Fischer-Tropsch Synthesis.” *Fuel Processing Technology* 92 (12): 2353–59. doi:10.1016/j.fuproc.2011.08.011.

Donnelly, T.J., and C.N. Satterfield. 1989. “Product Distributions of the Fischer-Tropsch Synthesis on Precipitated Iron Catalysts.” *Applied Catalysis* 52 (1): 93–114. doi:10.1016/S0166-9834(00)83375-8.

Donnelly, T.J., I.C. Yates, and C.N. Satterfield. 1988. “Analysis and Prediction of Product Distributions of the Fischer-Tropsch Synthesis.” *Energy & Fuels* 2 (6): 734–39.

Dry, Mark E. 1983a. *SASOL Fischer trospch processes.* Vol. 2. Appl Ind Catal. https://www.scopus.com/inward/record.uri?eid=2-s2.0-0020863666&partnerID=40&md5=48a768eaada5ef6e07f30b9ea0e66687.

———. 1983b. *SASOL Fischer tropsch processes.* Vol. 2. Appl Ind Catal. http://www.scopus.com/inward/record.url?eid=2-s2.0-0020863666&partnerID=40&md5=48a768eaada5ef6e07f30b9ea0e66687.

Dry, M.E., and A.P. Steynberg. 2004. *Commercial FT Process Applications*. Vol. 152. Studies in Surface Science and Catalysis. https://www.scopus.com/inward/record.uri?eid=2-s2.0-9644268209&partnerID=40&md5=30d695056e7c08362b94a3eeca0a7a52.

Dwyer, D.J., and G.A. Somorjai. 1979. “The Role of Readsorption in Determining the Product Distribution during CO Hydrogenation over Fe Single Crystals.” *Journal of Catalysis* 56 (2): 249–57. doi:10.1016/0021-9517(79)90111-8.

Ermakova, M.A., D.Yu. Ermakov, A.L. Chuvilin, and G.G. Kuvshinov. 2001. “Decomposition of Methane over Iron Catalysts at the Range of Moderate Temperatures: The Influence of Structure of the Catalytic Systems and the Reaction Conditions on the Yield of Carbon and Morphology of Carbon Filaments.” *Journal of Catalysis* 201 (2): 183–97. doi:10.1006/jcat.2001.3243.

Espinoza, R.L., A.P. Steynberg, B. Jager, and A.C. Vosloo. 1999a. “Low Temperature Fischer–Tropsch Synthesis from a Sasol Perspective.” *Applied Catalysis A: General* 186 (1–2): 13–26. doi:10.1016/S0926-860X(99)00161-1.

Espinoza, R. L., A. P. Steynberg, B. Jager, and A. C. Vosloo. 1999b. “Low Temperature Fischer–Tropsch Synthesis from a Sasol Perspective.” *Applied Catalysis A: General* 186 (1–2): 13–26. doi:10.1016/S0926-860X(99)00161-1.

Farias, F. E. M., F. a. N. Fernandes, and F. G. Sales. 2010. “Effect of Operating Conditions on Fischer-Tropsch Liquid Products Produced by Unpromoted

and Potassium-Promoted Iron Catalyst." *Latin American Applied Research* 40 (2): 161–66.

Farias, F.E.M., F.G. Sales, and F.A.N. Fernandes. 2008. "Effect of Operating Conditions and Potassium Content on Fischer-Tropsch Liquid Products Produced by Potassium-Promoted Iron Catalysts." *Journal of Natural Gas Chemistry* 17 (2): 175–78. doi:10.1016/S1003-9953(08)60047-X.

Farias, F.E.M., F.R.C. Silva, S.J.M. Cartaxo, F.A.N. Fernandes, and F.G. Sales. 2007a. "Effect of Operating Conditions on Fischer-Tropsch Liquid Products." *Latin American Applied Research* 37 (4): 283–87.

Farias, F. E. M., F. R. C. Silva, S. J. M. Cartaxo, F. a. N. Fernandes, and F. G. Sales. 2007b. "Effect of Operating Conditions on Fischer-Tropsch Liquid Products." *Latin American Applied Research* 37 (4): 283–87.

Figueiredo, J.L., and M.F.R. Pereira. 2012. "Porous Texture Versus Surface Chemistry in Applications of Adsorption by Carbons." In *Novel Carbon Adsorbents*, 471–98. http://www.scopus.com/inward/record.url?eid=2-s2.0-84882688429&partnerID=40&md5=e170afedf1ce52880f3ed3d9c6373088.

Figueiredo, Jose Luis. 1982. "Carbon formation and gasification on Nickel." In , 45–63. http://www.scopus.com/inward/record.url?eid=2-s2.0-0020256412&partnerID=40&md5=44b98efb76a8ecca3784e6d56f87be65.

Fischer, N., B. Clapham, T. Feltes, and M. Claeys. 2015. "Cobalt-Based Fischer-Tropsch Activity and Selectivity as a Function of Crystallite Size and Water Partial Pressure." *ACS Catalysis* 5 (1): 113–21. doi:10.1021/cs500936t.

Fleisch, T.H., R.A. Sills, and M.D. Briscoe. 2002. "2002 - Emergence of the Gas-to-Liquids Industry: A Review of Global GTL Developments." *Journal of Natural Gas Chemistry* 11 (1-2): 1–14.

Förtsch, Dieter, Kyra Pabst, and Edwin Groß-Hardt. 2015. "The Product Distribution in Fischer–Tropsch Synthesis: An Extension of the ASF Model to Describe Common Deviations." *Chemical Engineering Science* 138 (December): 333–46. doi:10.1016/j.ces.2015.07.005.

Förtsch, D., K. Pabst, and E. Groß-Hardt. 2015. "The Product Distribution in Fischer-Tropsch Synthesis: An Extension of the ASF Model to Describe Common Deviations." *Chemical Engineering Science* 138: 333–46. doi:10.1016/j.ces.2015.07.005.

Frey, P.A., and G.H. Reed. 2012. “The Ubiquity of Iron.” *ACS Chemical Biology* 7 (9): 1477–81. doi:10.1021/cb300323q.

Gadalla, H., Z. Jia, S.J. Vallee, B.H. Davis, and D. Sparks. 2012. “Comparing the Performance of Compact Heat Exchange Reactor to CSTR for Fischer Tropsch Synthesis.” In . https://www.scopus.com/inward/record.uri?eid=2-s2.0-84861427777&partnerID=40&md5=6c0deb8ac294cfdfb29b585b62fc7995.

Gadalla, H., S.J. Vallee, and Z. Jia. 2013. “Compact Heat Exchange Reactors in Pilot Plants for Fischer-Tropsch Synthesis and Mixed Alcohol Production.” In . https://www.scopus.com/inward/record.uri?eid=2-s2.0-84883116243&partnerID=40&md5=3fcd6bccb246516fd9fdb9e8938a7e52.

Gnanamani, M.K., H.H. Hamdeh, W.D. Shafer, D.E. Sparks, and B.H. Davis. 2013. “Fischer-Tropsch Synthesis: Effect of Potassium on Activity and Selectivity for Oxide and Carbide Fe Catalysts.” *Catalysis Letters* 143 (11): 1123–31. doi:10.1007/s10562-013-1110-7.

Herranz, T., S. Rojas, F.J. Pérez-Alonso, M. Ojeda, P. Terreros, and J.L.G. Fierro. 2006. “Genesis of Iron Carbides and Their Role in the Synthesis of Hydrocarbons from Synthesis Gas.” *Journal of Catalysis* 243 (1): 199–211. doi:10.1016/j.jcat.2006.07.012.

Hulet, C., P. Clement, P. Tochon, D. Schweich, N. Dromard, and J. Anfray. 2009. “Literature Review on Heat Transfer in Two and Three-Phase Bubble Columns.” *International Journal of Chemical Reactor Engineering* 7. https://www.scopus.com/inward/record.uri?eid=2-s2.0-62649144710&partnerID=40&md5=019099b2434aee43e8bcfc723992a042.

Hunpinyo, P., P. Narataruksa, K. Pana-Suppamassadu, S. Tungkamani, N. Chollacoop, and H. Sukkathanyawat. 2013. *Effect of Reaction Conditions on the Catalytic Performance of Ruthenium Supported Alumina Catalyst for Fischer-Tropsch Synthesis*. Vol. 22. Smart Innovation, Systems and Technologies. https://www.scopus.com/inward/record.uri?eid=2-s2.0-84879432221&partnerID=40&md5=3961dd7ac987611c4b12b2ed08bbacb1.

Iglesia, E. 1997. “Design, Synthesis, and Use of Cobalt-Based Fischer-Tropsch Synthesis Catalysts.” *Applied Catalysis A: General* 161 (1-2): 59–78.

Iglesia, E., S.C. Reyes, and R.J. Madon. 1991a. “Transport-Enhanced α-Olefin Readsorption Pathways in Ru-Catalysed Hydrocarbon Synthesis.” *Journal of Catalysis* 129 (1): 238–56. doi:10.1016/0021-9517(91)90027-2.

———. 1991b. “Transport-Enhanced α-Olefin Readsorption Pathways in Ru-Catalysed Hydrocarbon Synthesis.” *Journal of Catalysis* 129 (1): 238–56. doi:10.1016/0021-9517(91)90027-2.

Istadi, I., D.D. Anggoro, N.A.S. Amin, and D.H.W. Ling. 2011. “Catalyst Deactivation Simulation through Carbon Deposition in Carbon Dioxide Reforming over Ni/cao-Al 2o 3 Catalyst.” *Bulletin of Chemical Reaction Engineering and Catalysis* 6 (2): 129–36.

Jacobs, G., W. Ma, and B.H. Davis. 2014a. “Influence of Reduction Promoters on Stability of Cobalt/γ-Alumina Fischer-Tropsch Synthesis Catalysts.” *Catalysts* 4 (1): 49–76. doi:10.3390/catal4010049.

———. 2014b. “Influence of Reduction Promoters on Stability of Cobalt/γ-Alumina Fischer-Tropsch Synthesis Catalysts.” *Catalysts* 4 (1): 49–76. doi:10.3390/catal4010049.

———. 2014c. “Influence of Reduction Promoters on Stability of Cobalt/γ-Alumina Fischer-Tropsch Synthesis Catalysts.” *Catalysts* 4 (1): 49–76. doi:10.3390/catal4010049.

Jalama, Kalala. 2008. “Fischer Tropsch Synthesis over Supported Cobalt Catalysts: Effect of Ethanol Addition, Precursors and Gold Doping.” http://wiredspace.wits.ac.za/handle/10539/4937.

Jermwongratanachai, T., G. Jacobs, W.D. Shafer, V.R.R. Pendyala, W. Ma, M.K. Gnanamani, S. Hopps, et al. 2014. “Fischer-Tropsch Synthesis: TPR and XANES Analysis of the Impact of Simulated Regeneration Cycles on the Reducibility of Co/alumina Catalysts with Different Promoters (Pt, Ru, Re, Ag, Au, Rh, Ir).” *Catalysis Today* 228: 15–21. doi:10.1016/j.cattod.2013.10.057.

Karre, A.V., A. Kababji, E.L. Kugler, and D.B. Dadyburjor. 2013. “Effect of Time on Stream and Temperature on Upgraded Products from Fischer-Tropsch Synthesis When Zeolite Is Added to Iron-Based Activated-Carbon-Supported Catalyst.” *Catalysis Today* 214: 82–89. doi:10.1016/j.cattod.2013.04.010.

Khodakov, A.Y., W. Chu, and P. Fongarland. 2007. “Advances in the Development of Novel Cobalt Fischer-Tropsch Catalysts for Synthesis of Long-Chain Hydrocarbons and Clean Fuels.” *Chemical Reviews* 107 (5): 1692–1744. doi:10.1021/cr050972v.

Koeken, A.C.J., M. Ruitenbeek, and K.P. De Jong. 2011. “Effects of Process Parameters on Carbon Deposition during Iron Catalysed Fischer-Tropsch Synthesis Studied with a Tapered Element Oscillating Microbalance.” In . https://www.scopus.com/inward/record.uri?eid=2-s2.0-84860750529&partnerID=40&md5=7c839dae0610d8b488fb36f28425a0fe.

Kolb, G. 2013. “Review: Microstructured Reactors for Distributed and Renewable Production of Fuels and Electrical Energy.” *Chemical Engineering and Processing: Process Intensification* 65: 1–44. doi:10.1016/j.cep.2012.10.015.

Kshetrimayum, Krishnadash S., Park Seongho, Jong Ikhwan, Na Jonggeol, and Han Chonghun. 2015. “Simulation Study of Heat Transfer Enhancement due to Wall Boiling Condition in a Microchannel Reactor Block for Fischer-Tropsch Synthesis.” In *Computer Aided Chemical Engineering*, edited by Jakob K. Huusom and Rafiqul Gani Krist V. Gernaey, Volume 37:1355–60. Elsevier. http://www.sciencedirect.com/science/article/pii/B9780444635778500711.

Kuipers, E.W., C. Scheper, J.H. Wilson, I.H. Vinkenburg, and H. Oosterbeek. 1996. “Non-ASF Product Distributions due to Secondary Reactions during Fischer-Tropsch Synthesis.” *Journal of Catalysis* 158 (1): 288–300. doi:10.1006/jcat.1996.0028.

Lappas, A., and E. Heracleous. 2010. “Production of Biofuels via Fischer-Tropsch Synthesis: Biomass-to-Liquids.” In *Handbook of Biofuels Production: Processes and Technologies*, 493–529. http://www.scopus.com/inward/record.url?eid=2-s2.0-84869086429&partnerID=40&md5=9647400344ea06fd2366cb787430e07e.

Lee, D.W., and B.R. Yoo. 2014. “Advanced Metal Oxide (supported) Catalysts: Synthesis and Applications.” *Journal of Industrial and Engineering Chemistry* 20 (6): 3947–59. doi:10.1016/j.jiec.2014.08.004.

Li, B., X. Luo, Y. Zhu, and X. Wang. 2015. “Immobilization of Cu(II) in KIT-6 Supported Co_3O_4 and Catalytic Performance for Epoxidation of Styrene.” *Applied Surface Science* 359: 609–20. doi:10.1016/j.apsusc.2015.10.131.

Lin, Hsin-Yu, Yu-Wen Chen, and Chiuping Li. 2003. “The Mechanism of Reduction of Iron Oxide by Hydrogen.” *Thermochimica Acta* 400 (1–2): 61–67. doi:10.1016/S0040-6031(02)00478-1.

Li, S., A. Li, S. Krishnamoorthy, and E. Iglesia. 2001. “Effects of Zn, Cu, and K Promoters on the Structure and on the Reduction, Carburization, and Catalytic Behavior of Iron-Based Fischer-Tropsch Synthesis Catalysts.” *Catalysis Letters* 77 (4): 197–205. doi:10.1023/A:1013284217689.

Liu, X., A. Hamasaki, T. Honma, and M. Tokunaga. 2011. “Anti-ASF Distribution in Fischer-Tropsch Synthesis over Unsupported Cobalt Catalysts in a Batch Slurry Phase Reactor.” *Catalysis Today* 175 (1): 494–503. doi:10.1016/j.cattod.2011.03.030.

Liu, Y., B.-T. Teng, X.-H. Guo, Y. Li, J. Chang, L. Tian, X. Hao, et al. 2007. “Effect of Reaction Conditions on the Catalytic Performance of Fe-Mn Catalyst for Fischer-Tropsch Synthesis.” *Journal of Molecular Catalysis A: Chemical* 272 (1-2): 182–90. doi:10.1016/j.molcata.2007.03.046.

Luo, M., and B.H. Davis. 2001. *Deactivation and Regeneration of Alkali Metal Promoted Iron Fischer-Tropsch Synthesis Catalysts*. Vol. 139. Studies in Surface Science and Catalysis. http://www.scopus.com/inward/record.url?eid=2-s2.0-0035787112&partnerID=40&md5=a978d52be51c1648e776cd816d156e26.

Lu, T., W. Wu, M. Yang, X. Yang, L. Zhou, and Y. Su. 2016a. “Promotion Effect of Co on Cu-Zn-Al/Hβ Catalyst for Light Hydrocarbons (C3-C5) Synthesis from Syngas.” *Fuel Processing Technology* 148: 372–79. doi:10.1016/j.fuproc.2016.03.023.

———. 2016b. “Promotion Effect of Co on Cu-Zn-Al/Hβ Catalyst for Light Hydrocarbons (C3-C5) Synthesis from Syngas.” *Fuel Processing Technology* 148: 372–79. doi:10.1016/j.fuproc.2016.03.023.

Lu, X., D. Hildebrandt, and D. Glasser. 2015. “Distribution between C2 and C3 in Low Temperature Fischer-Tropsch Synthesis over a TiO2-Supported Cobalt

Catalyst." *Applied Catalysis A: General* 506: 67–76. doi:10.1016/j.apcata.2015.08.038.

Lu, X., D. Hildebrandt, X. Liu, and D. Glasser. 2012. "A Thermodynamic Approach to Olefin Product Distribution in Fischer-Tropsch Synthesis." *Industrial and Engineering Chemistry Research* 51 (51): 16544–51. doi:10.1021/ie3000453.

Lu, X., X. Zhu, D. Hildebrandt, X. Liu, and D. Glasser. 2011. "A New Way to Look at Fischer-Tropsch Synthesis Using Flushing Experiments." *Industrial and Engineering Chemistry Research* 50 (8): 4359–65. doi:10.1021/ie102095c.

Mann, R., F.Y.A. El-Kady, and R. Marzin. 1985. "Catalyst Deactivation by Fouling: A Wedge-Layering Analysis of the Consecutive Reaction." *Chemical Engineering Science* 40 (2): 249–57. doi:10.1016/0009-2509(85)80064-6.

Marafi, Meena, Antony Stanislaus, and Edward Furimsky. 2010. "Chapter 6 - Regeneration." In *Handbook of Spent Hydroprocessing Catalysts*, 121–90. Amsterdam: Elsevier. http://www.sciencedirect.com/science/article/pii/B9780444535566000069.

Martelli, E., T.G. Kreutz, M. Gatti, P. Chiesa, and S. Consonni. 2012. "Design Criteria and Optimization of Heat Recovery Steam Cycles for High-Efficiency, Coal-Fired, Fischer-Tropsch Plants." In , 3:363–73. doi:10.1115/GT2012-69661.

Martínez, A., G. Prieto, and J. Rollán. 2009. "Nanofibrous γ-Al_2O_3 as Support for Co-Based Fischer-Tropsch Catalysts: Pondering the Relevance of Diffusional and Dispersion Effects on Catalytic Performance." *Journal of Catalysis* 263 (2): 292–305. doi:10.1016/j.jcat.2009.02.021.

Martos, C., J. Dufour, and A. Ruiz. 2009. "Synthesis of Fe_3O_4-Based Catalysts for the High-Temperature Water Gas Shift Reaction." *International Journal of Hydrogen Energy* 34 (10): 4475–81. doi:10.1016/j.ijhydene.2008.08.042.

Masina, C.J., J.H. Neethling, E.J. Olivier, E. Ferg, S. Manzini, L. Lodya, P. Mohlala, and M.W. Ngobeni. 2015. "Mechanism of Reduction in Hydrogen Atmosphere and Thermal Transformation of Synthetic Ferrihydrite Nanoparticles." *Thermochimica Acta* 599: 73–83. doi:10.1016/j.tca.2014.11.018.

Ma, W., G. Jacobs, U.M. Graham, and B.H. Davis. 2014. “Fischer-Tropsch Synthesis: Effect of K Loading on the Water-Gas Shift Reaction and Liquid Hydrocarbon Formation Rate over Precipitated Iron Catalysts.” *Topics in Catalysis* 57 (6-9): 561–71. doi:10.1007/s11244-013-0212-1.

Meng, X., C. Xu, and J. Gao. 2007. “Coking Behavior and Catalyst Deactivation for Catalytic Pyrolysis of Heavy Oil.” *Fuel* 86 (12-13): 1720–26. doi:10.1016/j.fuel.2006.12.023.

Merino, D., I. Pérez-Miqueo, O. Sanz, and M. Montes. 2016. “On the Way to a More Open Porous Network of a Co-Re/Al_2O_3 Catalyst for Fischer-Tropsch Synthesis: Pore Size and Particle Size Effects on Its Performance.” *Topics in Catalysis* 59 (2-4): 207–18. doi:10.1007/s11244-015-0436-3.

Meshkani, F., and M. Rezaei. 2015a. “Comparison of Preparation Methods of Iron-Based Catalysts for High-Temperature Water-Gas Shift Reaction.” *Chemical Engineering and Technology* 38 (8): 1460–68. doi:10.1002/ceat.201400693.

Meshkani F., and Rezaei M. 2015. “High-Temperature Water-Gas Shift Reaction over Nanostructured Cr-Free $Fe_2O_3Al_2O_3$CuOMO (M: Ba, Ca, Mg and Sr) Catalysts for Hydrogen Production.” *Journal of Industrial and Engineering Chemistry* 30: 353–58. doi:10.1016/j.jiec.2015.05.039.

Meshkani, F., and M. Rezaei. 2015b. “Hydrogen Production by High Temperature Water Gas Shift Reaction over Highly Active and Stable Chromium Free Fe-Al-Ni Catalysts.” *International Journal of Hydrogen Energy* 40 (34): 10867–75. doi:10.1016/j.ijhydene.2015.06.170.

Mohanty, P., K.K. Pant, S.N. Naik, J. Parikh, A. Hornung, and J.N. Sahu. 2014. “Synthesis of Green Fuels from Biogenic Waste through Thermochemical Route - The Role of Heterogeneous Catalyst: A Review.” *Renewable and Sustainable Energy Reviews* 38: 131–53. doi:10.1016/j.rser.2014.05.011.

Moodley, D.J., J. van de Loosdrecht, A.M. Saib, M.J. Overett, A.K. Datye, and J.W. Niemantsverdriet. 2009a. “Carbon Deposition as a Deactivation Mechanism of Cobalt-Based Fischer-Tropsch Synthesis Catalysts under Realistic Conditions.” *Applied Catalysis A: General* 354 (1-2): 102–10. doi:10.1016/j.apcata.2008.11.015.

———. 2009b. “Carbon Deposition as a Deactivation Mechanism of Cobalt-Based Fischer–Tropsch Synthesis Catalysts under Realistic Conditions.” *Applied Catalysis A: General* 354 (1–2): 102–10. doi:10.1016/j.apcata.2008.11.015.

Mosayebi, A., and A. Haghtalab. 2015. “The Comprehensive Kinetic Modeling of the Fischer-Tropsch Synthesis over Co at Ru/γ-Al_2O_3 Core-Shell Structure Catalyst.” *Chemical Engineering Journal* 259: 191–204. doi:10.1016/j.cej.2014.07.040.

Mosayebi, A., M.A. Mehrpouya, and R. Abedini. 2016. “The Development of New Comprehensive Kinetic Modeling for Fischer-Tropsch Synthesis Process over Co-Ru/γ-Al_2O_3 Nano-Catalyst in a Fixed-Bed Reactor.” *Chemical Engineering Journal* 286: 416–26. doi:10.1016/j.cej.2015.10.087.

Muleja, A.A., Y. Yao, D. Glasser, and D. Hildebrandt. 2016. “A Study of Fischer-Tropsch Synthesis: Product Distribution of the Light Hydrocarbons.” *Applied Catalysis A: General* 517: 217–26. doi:10.1016/j.apcata.2016.03.015.

Newsome David S. 1980. “Water gas shift reaction.” *Catalysis Reviews Softcover Ed.* 21 (2): 275–81.

Novak, S., R.J. Madon, and H. Suhl. 1982. “Secondary Effects in the Fischer-Tropsch Synthesis.” *Journal of Catalysis* 77 (1): 141–51. doi:10.1016/0021-9517(82)90154-3.

O’Brien, R.J., and B.H. Davis. 2004. “Impact of Copper on an Alkali Promoted Iron Fischer-Tropsch Catalyst.” *Catalysis Letters* 94 (1-2): 1–6.

Ojeda, M., and S. Rojas. 2012. *Biofuels from Fischer-Tropsch Synthesis*. Biofuels from Fischer-Tropsch Synthesis. http://www.scopus.com/inward/record.url?eid=2-s2.0-84892804921&partnerID=40&md5=098cf9a8f9dc373ee2efd8a136416719.

Özkara-Aydinoğlu, Ş., Ö. Ataç, Ö.F. Gül, Ş. Kinayyiğit, S. Şal, M. Baranak, and T. Boz. 2012. “α-Olefin Selectivity of Fe-Cu-K Catalysts in Fischer-Tropsch Synthesis: Effects of Catalyst Composition and Process Conditions.” *Chemical Engineering Journal* 181-182: 581–89. doi:10.1016/j.cej.2011.11.094.

Panahi, M., and S. Skogestad. 2011. “Controlled Variables Selection for a Gas-to-Liquids Process.” In . https://www.scopus.com/inward/record.uri?eid=2-

s2.0-84857224149&partnerID=40&md5=b5e75d38ec29744c748ba20f652e2850.

Park, H., D.H. Youn, J.Y. Kim, W.Y. Kim, Y.H. Choi, Y.H. Lee, S.H. Choi, and J.S. Lee. 2015. “Selective Formation of Hägg Iron Carbide with G-C_3N_4 as a Sacrificial Support for Highly Active Fischer-Tropsch Synthesis.” *ChemCatChem* 7 (21): 3488–94. doi:10.1002/cctc.201500794.

Pendyala, V.R.R., U.M. Graham, G. Jacobs, H.H. Hamdeh, and B.H. Davis. 2014. “Fischer-Tropsch Synthesis: Deactivation as a Function of Potassium Promoter Loading for Precipitated Iron Catalyst.” Article in Press. Scopus. https://www.scopus.com/inward/record.uri?eid=2-s2.0-84906202522&partnerID=40&md5=0c356d56e9ecd0be7d44d8f5570edf4d.

Pendyala, V.R.R., G. Jacobs, H.H. Hamdeh, W.D. Shafer, D.E. Sparks, S. Hopps, and B.H. Davis. 2014. “Fischer-Tropsch Synthesis: Effect of Activation Gas after Varying Cu Promoter Loading over K-Promoted Fe-Based Catalyst.” *Catalysis Letters* 144 (9): 1624–35. doi:10.1007/s10562-014-1302-9.

Pendyala, V.R.R., G. Jacobs, J.C. Mohandas, M. Luo, H.H. Hamdeh, Y. Ji, M.C. Ribeiro, and B.H. Davis. 2010. “Fischer-Tropsch Synthesis: Effect of Water over Iron-Based Catalysts.” *Catalysis Letters* 140 (3-4): 98–105. doi:10.1007/s10562-010-0452-7.

Petersen, Abdul M., Somayeh Farzad, and Johann F. Görgens. 2015. “Techno-Economic Assessment of Integrating Methanol or Fischer–Tropsch Synthesis in a South African Sugar Mill.” *Bioresource Technology* 183 (May): 141–52. doi:10.1016/j.biortech.2015.02.007.

Pham, T.H., X. Duan, G. Qian, X. Zhou, and D. Chen. 2014. “CO Activation Pathways of Fischer-Tropsch Synthesis on χ-Fe 5C2 (510): Direct versus Hydrogen-Assisted CO Dissociation.” *Journal of Physical Chemistry C* 118 (19): 10170–76. doi:10.1021/jp502225r.

Polinski, Leon M., V.Udaya S. Rao, and John M. Stencel. 1984. *Catalysis and catalytic deactivation.* Sci and Technol of Coal and Coal Util.

Porosoff, M.D., B. Yan, and J.G. Chen. 2016. “Catalytic Reduction of CO_2 by H_2 for Synthesis of CO, Methanol and Hydrocarbons: Challenges and Opportunities.” *Energy and Environmental Science* 9 (1): 62–73. doi:10.1039/c5ee02657a.

Pretorius, J., and A. de Klerk. 2013. “Fischer-Tropsch Catalyst Life Cycle.” In *Greener Fischer-Tropsch Processes for Fuels and Feedstocks*, 267–79. https://www.scopus.com/inward/record.uri?eid=2-s2.0-84886340914&partnerID=40&md5=003ba469ac3d8efea100724fee775ff3.

Puskas, I., and R.S. Hurlbut. 2003. “Comments about the Causes of Deviations from the Anderson-Schulz-Flory Distribution of the Fischer-Tropsch Reaction Products.” *Catalysis Today* 84 (1-2): 99–109. doi:10.1016/S0920-5861(03)00305-5.

Qin, H., S. Kang, Y. Wang, H. Liu, Z. Ni, Y. Huang, Y. Li, and X. Li. 2016. “Lignin-Based Fabrication of Co@C Core-Shell Nanoparticles as Efficient Catalyst for Selective Fischer-Tropsch Synthesis of C_{5+} Compounds.” *ACS Sustainable Chemistry and Engineering* 4 (3): 1240–47. doi:10.1021/acssuschemeng.5b01269.

Raje, A.P., R.J. O’Brien, L. Xu, and B.H. Davis. 1997. *Deactivation of Iron-Based Catalysts for Slurry Phase Fischer-Tropsch Synthesis*. Vol. 111. Studies in Surface Science and Catalysis. http://www.scopus.com/inward/record.url?eid=2-s2.0-37849185752&partnerID=40&md5=10b705486c4a634526e3208e5e395b13.

Rauch, R., A. Kiennemann, and A. Sauciuc. 2013. “Fischer-Tropsch Synthesis to Biofuels (BtL Process).” In *The Role of Catalysis for the Sustainable Production of Bio-Fuels and Bio-Chemicals*, 397–443. http://www.scopus.com/inward/record.url?eid=2-s2.0-84926448805&partnerID=40&md5=6295e204b170e53d9a691dbaa5e2d70c.

Rhodes, C., G.J. Hutchings, and A.M. Ward. 1995. “Water-Gas Shift Reaction: Finding the Mechanistic Boundary.” *Recent Advances in C1 Chemistry* 23 (1): 43–58. doi:10.1016/0920-5861(94)00135-O.

Rochet, A., V. Moizan, C. Pichon, F. Diehl, A. Berliet, and V. Briois. 2011. “In Situ and Operando Structural Characterisation of a Fischer-Tropsch Supported Cobalt Catalyst.” *Catalysis Today* 171 (1): 186–91. doi:10.1016/j.cattod.2011.03.079.

Rytter, E., S. Eri, T.H. Skagseth, D. Schanke, E. Bergene, R. Myrstad, and A. Lindvåg. 2007. “Catalyst Particle Size of Cobalt/rhenium on Porous Alumina and the Effect on Fischer - Tropsch Catalytic Performance.” *Industrial and Engineering Chemistry Research* 46 (26): 9032–36. doi:10.1021/ie071136+.

Ryu, J.-H., S.-H. Kang, J.-H. Kim, Y.-J. Lee, and K.-W. Jun. 2015. “Fischer-Tropsch Synthesis on Co-Al<inf>2</inf>O<inf>3</inf>-(promoter)/ZSM5 Hybrid Catalysts for the Production of Gasoline Range Hydrocarbons.” *Korean Journal of Chemical Engineering* 32 (10): 1993–98. doi:10.1007/s11814-015-0046-6.

Sadeqzadeh, M., S. Chambrey, S. Piché, P. Fongarland, F. Luck, D. Curulla-Ferré, D. Schweich, J. Bousquet, and A.Y. Khodakov. 2013. “Deactivation of a Co/Al_2O_3 Fischer-Tropsch Catalyst by Water-Induced Sintering in Slurry Reactor: Modeling and Experimental Investigations.” *Catalysis Today* 215: 52–59. doi:10.1016/j.cattod.2013.03.022.

Saeidi, S., M.T. Amiri, N.A.S. Amin, and M.R. Rahimpour. 2014a. “Progress in Reactors for Higherature Fischer-Tropsch Process: Determination Place of Intensifier Reactor Perspective.” *International Journal of Chemical Reactor Engineering* 12 (1). doi:10.1515/ijcre-2014-0045.

———. 2014b. “Progress in Reactors for Higherature Fischer-Tropsch Process: Determination Place of Intensifier Reactor Perspective.” *International Journal of Chemical Reactor Engineering* 12 (1). doi:10.1515/ijcre-2014-0045.

Saib, A.M., A. Borgna, J. Van De Loosdrecht, P.J. Van Berge, and J.W. Niemantsverdriet. 2006. “In Situ Surface Oxidation Study of a Planar Co/SiO2/Si(100) Model Catalyst with Nanosized Cobalt Crystallites under Model Fischer-Tropsch Synthesis Conditions.” *Journal of Physical Chemistry B* 110 (17): 8657–64. doi:10.1021/jp0573700.

Saib, A.M., D.J. Moodley, I.M. Ciobîcă, M.M. Hauman, B.H. Sigwebela, C.J. Weststrate, J.W. Niemantsverdriet, and J. van de Loosdrecht. 2010. “Fundamental Understanding of Deactivation and Regeneration of Cobalt Fischer–Tropsch Synthesis Catalysts.” *Eleventh International Symposium on Catalyst Deactivation , Delft(The Netherlands,) October 25-28, 2009.* 154 (3–4): 271–82. doi:10.1016/j.cattod.2010.02.008.

Samant, P.V., F. Gonçalves, M.M.A. Freitas, M.F.R. Pereira, and J.L. Figueiredo. 2004. “Surface Activation of a Polymer Based Carbon.” *Carbon* 42 (7): 1315–19. doi:10.1016/j.carbon.2004.01.034.

Sarkari, M., F. Fazlollahi, and H. Atashi. 2012a. “Fischer Tropsch Synthesis: The Promoter Effects, Operating Conditions, and Reactor Synthesis.” *International Journal of Chemical Reactor Engineering* 10 (1). doi:10.1515/1542-6580.2843.

———. 2012b. “Fischer Tropsch Synthesis: The Promoter Effects, Operating Conditions, and Reactor Synthesis.” *International Journal of Chemical Reactor Engineering* 10 (1). doi:10.1515/1542-6580.2843.

———. 2012c. “Fischer Tropsch Synthesis: The Promoter Effects, Operating Conditions, and Reactor Synthesis.” *International Journal of Chemical Reactor Engineering* 10 (1). doi:10.1515/1542-6580.2843.

Sarup, B., and B.W. Wojciechowski. 1984. “Effect of time on stream and feed composition on the selectivity of a Cobalt Fischer tropsch catalyst” *Canadian Journal of Chemical Engineering* 62 (2): 249–56.

Shimokawabe, M., R. Furuichi, and T. Ishii. 1979. “Influence of the Preparation History of α-Fe2O3 on Its Reactivity for Hydrogen Reduction.” *Thermochimica Acta* 28 (2): 287–305. doi:10.1016/0040-6031(79)85133-3.

Shroff, M.D., D.S. Kalakkad, K.E. Coulter, S.D. Kohler, M.S. Harrington, N.B. Jackson, A.G. Sault, and A.K. Datye. 1995a. “Activation of Precipitated Iron Fischer-Tropsch Synthesis Catalysts.” *Journal of Catalysis* 156 (2): 185–207. doi:10.1006/jcat.1995.1247.

———. 1995b. “Activation of Precipitated Iron Fischer-Tropsch Synthesis Catalysts.” *Journal of Catalysis* 156 (2): 185–207. doi:10.1006/jcat.1995.1247.

Sie, S.T., and R. Krishna. 1999. “Fundamentals and Selection of Advanced Fischer–Tropsch Reactors.” *Applied Catalysis A: General* 186 (1–2): 55–70. doi:10.1016/S0926-860X(99)00164-7.

Sims, R.E.H., W. Mabee, J.N. Saddler, and M. Taylor. 2010. “An Overview of Second Generation Biofuel Technologies.” *Bioresource Technology* 101 (6): 1570–80. doi:10.1016/j.biortech.2009.11.046.

Snel, R., and R.L. Espinoza. 1989. “Secondary Reactions of Primary Products of the Fischer-Tropsch Synthesis. Part II. the Role of Propene.” *Journal of Molecular Catalysis* 54 (1): 103–17. doi:10.1016/0304-5102(89)80143-9.

Soled, S., E. Iglesia, and R.A. Fiato. 1990. “Activity and Selectivity Control in Iron Catalysed Fischer-Tropsch Synthesis - The Influence of Iron Catalyst Phase on Slurry Fischer-Tropsch Reaction Pathways; Selective Synthesis of Alpha-Olefins.” *Catalysis Letters* 7 (1-4): 271–80. doi:10.1007/BF00764508.

Sparks, Dennis E., Gary Jacobs, Muthu Kumaran Gnanamani, Venkat Ramana Rao Pendyala, Wenping Ma, Jungshik Kang, Wilson D. Shafer, et al. 2013. “Poisoning of Cobalt Catalyst Used for Fischer–Tropsch Synthesis.” *Catalysis and Synthetic Fuels: State of the Art and Outlook* 215 (October): 67–72. doi:10.1016/j.cattod.2013.01.011.

Stelmachowski, M., and L. Nowicki. 2003. “Fuel from the Synthesis Gas-the Role of Process Engineering.” *Applied Energy* 74 (1-2): 85–93. doi:10.1016/S0306-2619(02)00134-4.

Steynberg, A. 2004. *Fischer-Tropsch Technology: Preface*. Vol. 152. Studies in Surface Science and Catalysis. https://www.scopus.com/inward/record.uri?eid=2-s2.0-9644294231&partnerID=40&md5=714960bb6f422bbd8ca0c56d453705ce.

Steynberg, A.P. 2004. *Introduction to Fischer-Tropsch Technology*. Vol. 152. Studies in Surface Science and Catalysis. https://www.scopus.com/inward/record.uri?eid=2-s2.0-9644260538&partnerID=40&md5=2908b7b2c74a326c21913ae8e1edf6fd.

Steynberg, A.P., and A.P. Vogel. 2006. “Challenging the Limits for the Design and Scale-up of Catalytic Fluid Bed Reactors.” In . Vol. 231. https://www.scopus.com/inward/record.uri?eid=2-s2.0-33745257608&partnerID=40&md5=d28923bb3885912cfe88d569f4971f7f.

Tang, Q., X. Guo, C. Wang, S. Fan, L. Bo, and Y. Wang. 2009. “Effect of Potassium and Copper Additive on Iron-Ruthenium Composite Catalyst for Fischer-Tropsch Synthesis.” In , 2:1840–47. http://www.scopus.com/inward/record.url?eid=2-s2.0-84877659653&partnerID=40&md5=79e554a3db57049768becc4fac5e0222.

Tavakoli, Akram, Morteza Sohrabi, and Ali Kargari. 2008. “Application of Anderson–Schulz–Flory (ASF) Equation in the Product Distribution of Slurry Phase FT Synthesis with Nanosized Iron Catalysts.” *Chemical Engineering Journal* 136 (2–3): 358–63. doi:10.1016/j.cej.2007.04.017.

Todic, B., L. Nowicki, N. Nikacevic, and D.B. Bukur. 2016a. “Fischer-Tropsch Synthesis Product Selectivity over an Industrial Iron-Based Catalyst: Effect of Process Conditions.” *Catalysis Today* 261: 28–39. doi:10.1016/j.cattod.2015.09.005.

———. 2016b. “Fischer-Tropsch Synthesis Product Selectivity over an Industrial Iron-Based Catalyst: Effect of Process Conditions.” *Catalysis Today* 261: 28–39. doi:10.1016/j.cattod.2015.09.005.

Todic, Branislav, Lech Nowicki, Nikola Nikacevic, and Dragomir B. Bukur. 2016. “Fischer–Tropsch Synthesis Product Selectivity over an Industrial Iron-Based Catalyst: Effect of Process Conditions.” *Recent Advances in F-T Synthesis and Fuel Processing Catalysis* 261 (March): 28–39. doi:10.1016/j.cattod.2015.09.005.

Tsou, J., P. Magnoux, M. Guisnet, J.J.M. Órfao, and J.L. Figueiredo. 2003. “Oscillations in the Oxidation of MIBK over a Pt/HFAU Catalyst: Role of Coke Combustion.” *Catalysis Communications* 4 (12): 651–56. doi:10.1016/j.catcom.2003.10.009.

Van Berge, P.J., J. Van De Loosdrecht, S. Barradas, and A.M. Van Der Kraan. 2000. “Oxidation of Cobalt Based Fischer-Tropsch Catalysts as a Deactivation Mechanism.” *Catalysis Today* 58 (4): 321–34. doi:10.1016/S0920-5861(00)00265-0.

van Berge, P.J, J van de Loosdrecht, S Barradas, and A.M van der Kraan. 2000. “Oxidation of Cobalt Based Fischer–Tropsch Catalysts as a Deactivation Mechanism.” *Catalysis Today* 58 (4): 321–34. doi:10.1016/S0920-5861(00)00265-0.

van de Loosdrecht, J., B. Balzhinimaev, J.-A. Dalmon, J.W. Niemantsverdriet, S.V. Tsybulya, A.M. Saib, P.J. van Berge, and J.L. Visagie. 2007. “Cobalt Fischer-Tropsch Synthesis: Deactivation by Oxidation?” *Catalysis Today* 123 (1-4): 293–302. doi:10.1016/j.cattod.2007.02.032.

Van de Loosdrecht, J., F.G. Botes, I.M. Ciobica, A. Ferreira, P. Gibson, D.J. Moodley, A.M. Saib, J.L. Visagie, C.J. Weststrate, and J.W. Niemantsverdriet. 2013. “Fischer-Tropsch Synthesis: Catalysts and Chemistry.” In *Comprehensive Inorganic Chemistry II (Second Edition): From Elements to Applications*, 7:525–57. http://www.scopus.com/inward/record.url?eid=2-s2.0-84902559789&partnerID=40&md5=bf301f4c6f75c09906975ae6e8ae11a9.

Van De Loosdrecht, J., I.M. Ciobîca, P. Gibson, N.S. Govender, D.J. Moodley, A.M. Saib, C.J. Weststrate, and J.W. Niemantsverdriet. 2016. “Providing Fundamental and Applied Insights into Fischer-Tropsch Catalysis: Sasol-Eindhoven University of Technology Collaboration.” *ACS Catalysis* 6 (6): 3840–55. doi:10.1021/acscatal.6b00595.

van der Kraan, A.M., E. Boellaard, and M.W.J. Crajé. 1993. “Characterization of Catalysts by Mossbauer Spectroscopy: An Application to the Study of Fischer-Tropsch, Hydrotreating and Super Claus Catalysts.” *Nuclear Inst. and Methods in Physics Research, B* 76 (1-4): 6–12. doi:10.1016/0168-583X(93)95112-I.

van der Laan, Gerard P., and Antonie A.C.M. Beenackers. 2000. “Intrinsic Kinetics of the Gas–solid Fischer–Tropsch and Water Gas Shift Reactions over a Precipitated Iron Catalyst.” *Applied Catalysis A: General* 193 (1–2): 39–53. doi:10.1016/S0926-860X(99)00412-3.

Van Ommen, J.R., and J. Grievink. 2014. “Synthesis Gas Utilization for Transportation Fuel Production.” In *Biomass as a Sustainable Energy Source for the Future: Fundamentals of Conversion Processes*, 525–46. http://www.scopus.com/inward/record.url?eid=2-s2.0-84926397752&partnerID=40&md5=bb1c612e3f077d1cdc74d932564e946a.

Van Santen, R.A., M.M. Ghouri, A.J. Markvoort, and E.J.M. Hensen. 2014. “The Molecular Kinetics of the Fischer-Tropsch Reaction.” In *Bridging Heterogeneous and Homogeneous Catalysis: Concepts, Strategies, and Applications*, 553–606. https://www.scopus.com/inward/record.uri?eid=2-s2.0-84927075939&partnerID=40&md5=beb988c65d4cef624a7a6c821c9fa4d2.

van Steen, E., and M. Claeys. 2008. “Fischer-Tropsch Catalysts for the Biomass-to-Liquid Process.” *Chemical Engineering and Technology* 31 (5): 655–66. doi:10.1002/ceat.200800067.

Visconti, Carlo Giorgio, Michela Martinelli, Leonardo Falbo, Laura Fratalocchi, and Luca Lietti. n.d. “CO_2 Hydrogenation to Hydrocarbons over Co and Fe-Based Fischer-Tropsch Catalysts.” *Catalysis Today*. doi:10.1016/j.cattod.2016.04.010.

Vo, D.-V.N., T.-H. Nguyen, and A.A. Adesina. 2010. “Fischer-Tropsch Synthesis over Promoted Mo Carbide Catalysts: Time-on-Stream Behaviour.” In . https://www.scopus.com/inward/record.uri?eid=2-s2.0-79951489521&partnerID=40&md5=b3918eb47e8ee19158ce384f3964f33a.

Wang, C., X. Ma, Q. Ge, and H. Xu. 2015. “A Comparative Study of PdZSM-5, Pdβ, and PdY in Hybrid Catalysts for Syngas to Hydrocarbon Conversion.” *Catalysis Science and Technology* 5 (3): 1847–53. doi:10.1039/c4cy01494d.

Wang, C., N. Sun, N. Zhao, W. Wei, Y. Sun, C. Sun, H. Liu, and C.E. Snape. 2015. “Coking and Deactivation of a Mesoporous Ni-CaO-ZrO_2 Catalyst in Dry Reforming of Methane: A Study under Different Feeding Compositions.” *Fuel* 143: 527–35. doi:10.1016/j.fuel.2014.11.097.

Wang, H., Y. Yang, B.-S. Wu, J. Xu, M.-Y. Ding, H.-L. Wang, W.-H. Fan, H.-W. Xiang, and Y.-W. Li. 2009. “Hydrogen Reduction Kinetics Modeling of a Precipitated Iron Fischer-Tropsch Catalyst.” *Journal of Molecular Catalysis A: Chemical* 308 (1-2): 96–107. doi:10.1016/j.molcata.2009.03.030.

Wang, T., J. Wang, and Y. Jin. 2007. “Slurry Reactors for Gas-to-Liquid Processes: A Review.” *Industrial and Engineering Chemistry Research* 46 (18): 5824–47. doi:10.1021/ie070330t.

Wang, Z., and J.J. Spivey. 2015. “Effect of ZrO_2, Al_2O_3 and La_2O_3 on Cobalt-Copper Catalysts for Higher Alcohols Synthesis.” *Applied Catalysis A: General* 507: 75–81. doi:10.1016/j.apcata.2015.09.032.

Yaghobi, Nakisa. 2013. “The Role of Gas Hourly Space Velocity and Feed Composition for Catalytic Oxidative Coupling of Methane: Experimental Study.” *Journal of King Saud University - Engineering Sciences* 25 (1): 1–10. doi:10.1016/j.jksues.2011.06.007.

Yakovenko, R.E., G.B. Narochnyi, A.P. Savost'Yanov, and V.A. Kirsanov. 2015. "Feasibility of Using a Tube Reactor in High-Intensity Fischer-Tropsch Synthesis." *Chemical and Petroleum Engineering* 51 (3): 159–63. doi:10.1007/s10556-015-0017-0.

Yamin, P., and S. Fatemi. 2005. "Neural Networks for Modeling of Chemical Reaction Data: A Step by Step Methodology, Support for Reactor Design and Simulation." In . Vol. 2005. https://www.scopus.com/inward/record.uri?eid=2-s2.0-33646721381&partnerID=40&md5=3261ccdc87bb2afe8981216f2e2a9c0d.

Yao, Yali. 2011. "Fischer tropsch synthesis using CO_2-containing syngas mixtures over Cobalt and Iron based catalysts." University of the Witwatersrand, Johannesburg. http://mobile.wiredspace.wits.ac.za/handle/10539/11292.

Yao, Yali, Xinying Liu, Diane Hildebrandt, and David Glasser. 2012. "Fischer–Tropsch Synthesis Using $H_2/CO/CO_2$ Syngas Mixtures: A Comparison of Paraffin to Olefin Ratios for Iron and Cobalt Based Catalysts." *Applied Catalysis A: General* 433–434 (August): 58–68. doi:10.1016/j.apcata.2012.04.041.

Yoshimura, Y., and E. Furimsky. 1986. "Oxidative Regeneration of Hydrotreating Catalysts." *Applied Catalysis* 23 (1): 157–71. doi:10.1016/S0166-9834(00)81459-1.

Yoshioka, H., M. Ota, Y. Sato, H. Inomata, R.L. Smith, and C.J. Peters. 2008. "Analysis of H_2-Clathrate Hydrate Formation Kinetics with a Phase Diffusion Model." In . http://www.scopus.com/inward/record.url?eid=2-s2.0-79952207928&partnerID=40&md5=5509fdcef031ea40d77e514fdd2ae7fc.

Yuan, W., G.C. Vaughan, C.B. Roberts, and M.R. Eden. 2011. *Modeling and Optimization of Supercritical Phase Fischer-Tropsch Synthesis*. Vol. 29. Computer Aided Chemical Engineering. http://www.scopus.com/inward/record.url?eid=2-s2.0-79958796160&partnerID=40&md5=1796711ed1165648aedaf238e0692c64.

Zamaniyan, Akbar, Yadollah Mortazavi, Abbas Ali Khodadadi, and Ali Nakhaei Pour. 2013. "Effect of Mass Transfer Limitations on Catalyst Performance during Reduction and Carburization of Iron Based Fischer-Tropsch

Synthesis Catalysts." *Journal of Energy Chemistry* 22 (5): 795–803. doi:10.1016/S2095-4956(13)60106-0.

Zhang, H.-b., and G.L. Schrader. 1985. "Characterization of a Fused Iron Catalyst for Fischer-Tropsch Synthesis by in Situ Laser Raman Spectroscopy." *Journal of Catalysis* 95 (1): 325–32. doi:10.1016/0021-9517(85)90038-7.

Zhao-Tie, Liu, Zhou Jing-Lai, and Zhang Bi-Jiang. 1994. "Poisoning of Iron Catalyst by COS in Syngas for Fischer—Tropsch Synthesis." *Journal of Molecular Catalysis* 94 (2): 255–61. doi:10.1016/0304-5102(94)87035-7.

Zhong, J., X. Liu, F. Yang, and X. Zhu. 2016. "Study on Alkylation of Benzene and Syngas over Pt/zsm-5 Catalyst and Process Conditions." *Petroleum Processing and Petrochemicals* 47 (5): 62–66.

Zhu, J., W. Wang, X.N. Hua, F. Wang, Z. Xia, and Z. Deng. 2015. "Phase Distribution and Stepwise Kinetics of Iron Oxides Reduction during Chemical Looping Hydrogen Generation in a Packed Bed Reactor." *International Journal of Hydrogen Energy* 40 (36): 12097–107. doi:10.1016/j.ijhydene.2015.07.028.

CHAPTER 3

IN SITU STUDIES

3.1 Preview

In this chapter the researcher interrogates the literature on *in situ* characterization during catalyst reduction. From *in situ* studies conducted so far, it is agreed that during activation, the catalyst precursor hematite is converted to magnetite regardless of the activation gas used for the pretreatment. The use of CO gas is reported to yield iron carbides, while the use of H_2 gas yields metallic iron. The *in situ* characterization of syngas reduction is scarce in the literature; no prior research on this topic was available.

The researcher also conducted some thermodynamic calculations to show the speciation pathway of the catalyst precursor during reduction. The formation of iron carbides is thermodynamically feasible when CO gas is used. When H_2 gas is used, the hematite to magnetite is thermodynamically feasible, while the formation of metallic iron is thermodynamically disfavored. The formation of metallic iron observed from thermodynamic calculations is or could be attributed to high H_2/H_2O ratios. The speciation of the catalyst precursor when syngas is used is governed by the CO/H_2 ratio, and assuming the ideal conditions a mixture of iron carbides and metallic iron are presumed to be present.

3.2 The literature on *in situ* characterization

The last three decades have seen a dramatic rise in the number of applications of spectroscopy for Fischer Tropsch (FT) catalysis research. This useful technology is now being applied to understand the catalyst precursor speciation pathways during reduction and FT synthesis. Spectroscopy has been successfully used and investigated in the past to understand FT catalyst activation pathways (Dumesic and Topsøe 1977). Various papers have been published on this aspect (Raupp and

Delgass 1979; van der Kraan, Boellaard, and Crajé 1993; Niemantsverdriet et al. 1980a; Jacobs et al. 2013). Despite all the work that has been done, studies to establish the changes in phase (in operando) with time on stream of the catalyst still require more attention. This will shed light on the mode of catalyst activation, deactivation and regeneration in the FT process.

In situ characterization refers to the study of the catalytic material in its reaction vessel under real working conditions, owing to which it enjoys a number of advantages over *ex situ* techniques which are prone to sample handling complications (Tada and Iwasawa 2009a; Tada and Iwasawa 2009b). Real time sample analysis, increased accuracy, real operating conditions and avoidance of air oxidation and handling contamination are a few advantages that the *in situ* characterization technique offers in FT studies. Heterogeneous catalysis is a multiphase system, and an understanding of the predominant phases at different conditions and the interplay between the phases is important. Therefore, it is important to explore the applicability of spectroscopy, itself an area that needs considerable attention, to expand the domain of spectroscopy especially *in-situ* characterization.

From *in situ* studies conducted so far, it is agreed that during activation, the catalyst precursor hematite (α-Fe_2O_3) is converted to magnetite (Fe_3O_4) regardless of the activation gas used for pretreatment (Yaming Jin and Datye 2000a; Hao et al. 2008; Zhang et al. 2004). The fate of the intermediate magnetite is determined by parameters such as the nature of the reducing agent, temperature and pressure (De Smit and Weckhuysen 2008). If H_2 gas is used, metallic iron Fe will be formed, while iron carbides are formed when CO gas or syngas is used. Wang et al. (2009) used *in situ* Mossbauer effect spectroscopy to study catalyst phase changes and reported that reduction of precipitated iron based catalyst with H_2 gas proceeds via the magnetite intermediate and then to metallic iron**.** Amelse et al. (1978) examined the iron catalyst by Mössbauer spectroscopy at various stages of calcination and reduction, and after use as a synthesis catalyst. The results supported Wang's (2009) findings that the iron in the initial oxide (α-Fe_2O_3) was reduced to α-Fe in H_2 gas. Subjected to the FT reaction conditions, the catalyst was carburized within 90 min to

the extent that no metallic iron could be detected in the Mössbauer spectra (Amelse, Butt, and Schwartz 1978). The two-stage reduction of hematite, (α-$Fe_2O_3 \rightarrow Fe_3O_4 \rightarrow Fe$) has been postulated at reduction temperatures less than 570 °C, whereas the three-stage reduction mechanism ($3Fe_2O_3 \rightarrow 2Fe_3O_4 \rightarrow 6FeO \rightarrow 6Fe$) was observed at temperatures higher than 570 °C (Lin, Chen, and Li 2003a; Mondal et al. 2004; Dİlmaç et al. 2015; Jozwiak et al. 2007b). Datye (2000) used high resolution transmission electron microscopy (HRTEM) and X-ray diffraction (XRD) methods to study the CO reduction of iron catalyst, and reported two stages of phase transformation, from hematite to magnetite and magnetite to iron carbide. In the second stage, some carbon deposition accompanying further carburization was reported (Dayte 2000). In addition, Luo, Hamdeh, and Davis (2009) also studied the CO reduction of iron catalyst using Mossbauer analysis, and reported the same pathway of reduction.

Yaming Jin and Datye (2000b) used temperature-programmed reduction of an iron catalyst using both carbon monoxide (CO-TPR) and hydrogen (H_2-TPR) to study the phase transformations in iron catalysts. The products of reduction, analysed using a high-resolution transmission electron microscopy (HRTEM) and X-ray diffraction (XRD) methods, confirmed the three stages of phase transformation of the catalysts during the temperature-programmed reaction. Mauro et al, (2010) made use of an In-Situ TPR-EXAFS/XANES technique to investigation of the Influence of group I alkali promoters on the local atomic and electronic structure of carburized Iron/Silica catalysts in FT synthesis. The results enabled them to measure the relative composition of the different compounds as a function of the carburization time, temperature, and atomic number of the group 1 promoter.

3.3 Thermodynamic predictions

Thermodynamic data on FT catalysis play an important role in the prediction of the phase changes during reduction and the subsequent reaction being catalysed, and also to corroborate the spectroscopic observation. The importance of understanding the thermodynamics of these phase changes is emphasized in this chapter. The chapter also contains a useful appendix on Gibbs energy of reaction data of the

catalyst phases of interest. However, the amount of data available at this time is limited as different carbides are yet to be assigned their catalytic duties in FT synthesis. A review by De Smit and Weckhuysen (2008) reported the formation of Fe_7C_3 , χ-Fe_5C_2 , Θ-Fe_3C and ἐ-$Fe_{2.2}C$ phases, their crystallographic data, and their synthesis pathways during FT synthesis.

Thermodynamic information is of paramount importance when one needs to optimize product yields by tailoring the conditions to favour the stability of desired catalytic phases.

Mössbauer spectroscopy studies of an iron based catalyst were examined at various stages of calcination and reduction and after use as a synthesis catalyst (Amelse, Butt, and Schwartz 1978). The authors observed that about 90% of the iron in the initial oxide (α-Fe_2O_3) was reduced to α-Fe metal during 24 h reduction in H_2 at 425 °C. When subjected to the reaction conditions, the catalyst was carburized within 90 min to form iron carbides, to such an extent that no metallic iron could be detected in the Mössbauer spectra.

Iron carbides have been synthesized and tested for FT catalysis, for example, the synthesis pathway for Hägg carbide (χ-Fe_5C_2) as given by Park et al. (2015a). De Smit et al. (2010) observed that a catalyst containing mainly crystalline χ -Fe_5C_2 was highly susceptible to oxidation during FT synthesis, while the catalyst containing θ-Fe_3C and amorphous carbide phases showed a lower activity and selectivity. Detailed discussion of the various iron carbide phases has been given by many authors (Du Plessis, De Villiers, and Kruger 2007**;** Henriksson, Sandberg, and Wallenius 2008; Moodley et al. 2009; Leineweber et al. 2012). These authors made use of *ab initio* calculations, diffraction experiments and Rietveld refinement, to determine crystal structure for different carbides. Based on the formation energy (E_f) of iron carbides calculated by Henriksson, Sandberg, and Wallenius (2008), the order of stability from the lowest to highest stable is given as follows :

Fe_7C_3 < χ-Fe_5C_2 < Θ-Fe_3C.

This ordering of stability for the iron carbides is consistent with the experimental findings by Eckstrom and Adcock (1950) that the Fe_5C_2 occurs as a precursor to Fe_3C. In recent years, there had been growing interest in these types of carbides, mainly because of the role they may play in the FT catalytic process (Park et al. 2015b; Pham et al. 2015; Herranz et al. 2006; Xu et al. 2014). Under reaction conditions in FT catalysis, the catalyst composition is generally represented as Fe_xC_y and researchers seek the variation of x and y with time-on-stream (TOS). Such TOS data are particularly important as they affect the product distribution. For instance, studies by de Smit et al. (2009) reveal that catalyst containing χ-Fe_5C_2 is catalytically more active whereas the Θ-Fe_3C is found in deactivating catalyst. Cementite (Θ-Fe_3C) phase was also reported by Herranz et al. (2006b) to be less active in the Fischer Tropsch synthesis. The use of e-Iron carbide (ɛ́-$Fe_{2.2}C$ and ε-Fe_2C) was reported to be effective at low-temperature Fischer Tropsch synthesis (LTFTS) at 443 K (Xu et al. 2014).

Despite the large amount of work and the assortment of technologies employed to examine catalyst speciation during reaction and reduction, the exact definition of the role of the carbide phases is still controversial. It is probably fair to say that nowhere in these examples has it been established without query that iron carbide, in any of its many forms, provides directly an active site for the synthesis that can be associated with the formation of a particular product or class of products.

During synthesis, the catalyst itself is in equilibrium with the FT reactants and products that surrounds it (Karimi, Rahmani, and Moqadam 2012). Therefore, the catalyst changes phases based on the gas composition and pressure, indicative of an equilibrium response (Marano and Holder 1997; Quan et al. 2014; Kun et al. 2009). The catalyst remains active, but the activity changes depending on temperature, pressure, the ratios of P_{H2}/P_{H2O} and P_{CO}/P_{CO2}, and other deactivating factors (Po¨hlmann et al. 2013; Borg et al. 2006). An active FT iron catalyst rarely exists as a pure substance, and this is because it is usually diluted with precursors such as hematite, magnetite and wüstite (Niemantsverdriet et al. 1980; Kazak et al. 2015; De Smit and Weckhuysen 2008). This dilution reduces the effect of the catalyst on carbon monoxide (CO) conversion as the active catalyst phase speciate to non-

catalytic phases. According to Cairns and Tevebaugh (1964), the equilibrium theory is able to determine the stable phases of a catalyst that are in equilibrium with a gas of a P_{H2}/P_{H2O} or P_{CO}/P_{CO2} composition during reduction.

3.4 Stability diagrams for iron catalyst during reduction

The systems of Fe –CO $–CO_2$ and Fe $–H_2$ $–H_2O$ can be of high technical importance in explaining catalyst reduction or activation. *In situ* catalyst activation has been done using H_2, CO and syngas (Luo, Hamdeh, and Davis 2007; Chernavskii et al. 2016; Bukur et al. 1995; Shroff et al. 1995). Preliminary calculations based on the Gibbs free energy of reaction supports that iron carbides are the most probable species to be formed during activation with syngas or carbon monoxide. All of these observations demonstrate that equilibration in the gas phase is key for iron catalysts speciation. It must be emphasized at this point that the analyses that follow while useful in describing what might happen, are not complete as the thermodynamic data for all the different carbides that are postulated to be present and be active for FT catalysis are not available. However the results as mentioned above do have some limited value and also suggest that it would be useful to try to obtain these values or at least estimates of them.

The phase stability diagrams given in **Figures 3.1 and 3.2** (generated by HSC 6 software. The name of the program is based on the fact that calculation modules automatically utilize the same extensive thermochemical database which contains enthalpy (H), entropy (S) and heat capacity (Cp) data) gives us an estimation of prevailing phases at given partial pressures of gases based on the assumption that solids are immiscible. In these diagrams, the stability areas of different catalyst phases under theoretical conditions help us tailor the conditions that favour the formation of certain phases. A precise measurement of gaseous components and the corresponding catalyst composition help us understand the conditions necessary for catalyst reduction. Reducing gases give different initial catalyst phases that will further change as the syngas is introduced for FT synthesis. For instance, *in situ* catalyst reduction with hydrogen yields metallic iron, and this is supported by the stability diagram shown in **Figure 3.3**. As shown in **Figure 3.1**, catalyst activation

with CO gas or syngas with low H_2 partial pressure at FT conditions yields mainly iron carbides, which are active catalysts.

3.4.1 CO reduction prediction

The thermodynamics of reduction can be of interest over the entire composition range for the various P_{H2}/P_{H2O} and P_{CO}/P_{CO2} ratios of reduction. The approach of reducing the catalyst at atmospheric pressure and running the reaction at almost atmospheric pressure requires knowledge of catalyst thermodynamics at low temperatures and low pressures. Under these conditions, carbonaceous deposits sometimes occur due to the boudouard reaction shown in Reaction 3.3, and the presence is detrimental to catalyst effectiveness (Düdder et al. 2014; Jahangiri et al. 2014). As a result, knowledge of the conditions under which carbon deposits can form is therefore important.

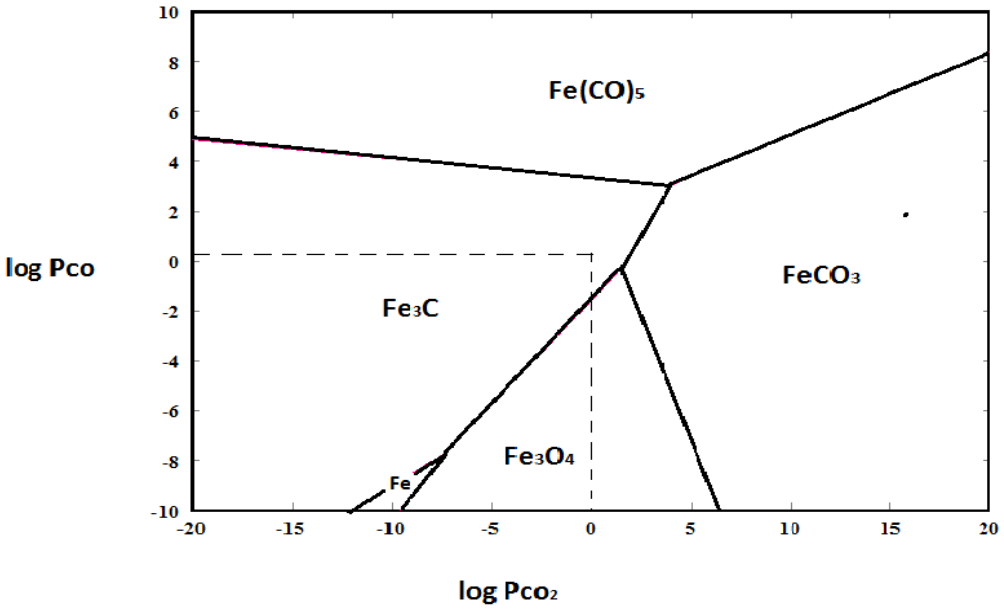

Figure 3.1: Stability diagram of an iron based catalyst in equilibrium with PCO/PCO_2 during reduction at 1 atm.

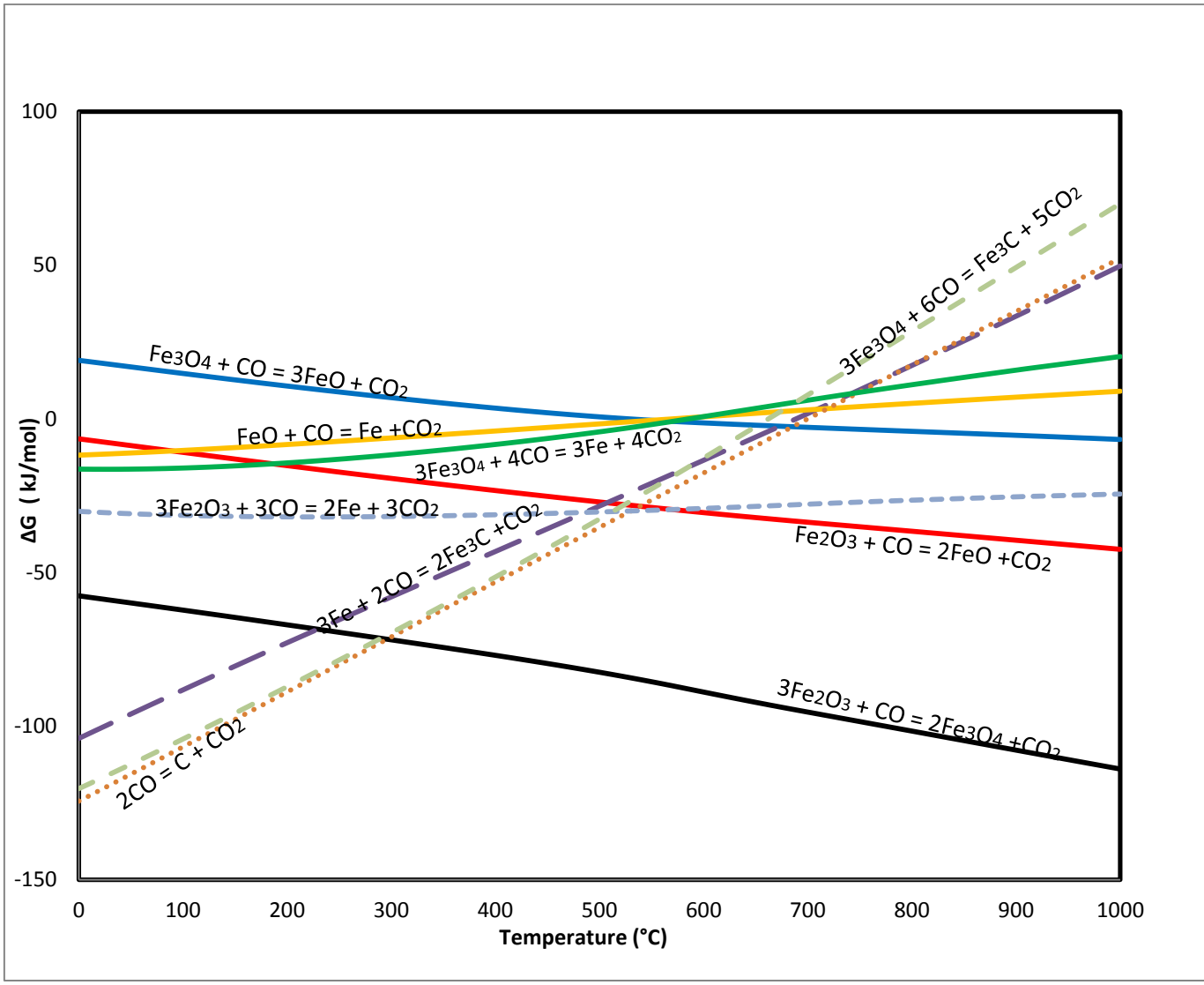

Figure 3.2: Gibbs free energy versus temperature for possible speciation pathways of the iron catalyst precursor under CO activation.

The researcher has expounded all the possible pathways that hematite may take during reduction and reaction (see **Figure 3.2**). In addition, plausible pathways for hematite to magnetite and magnetite to iron carbide were reported in the literature (O'Brien et al. 1996; O'Brien et al. 1996; Niemantsverdriet et al. 1980b; Jozwiak et al. 2007c; De Smit E. and Weckhuysen B.M. 2008). As shown in **Figure 3.2**, the likelihood of reaction 3.1 increases with temperature, while reaction 4.2 only has a negative Gibbs Free Energy in the temperature range of up to 660 °C. The formation of iron carbides happens at any CO/CO_2 ratio.

$$3Fe_2O_3 + CO \rightarrow 2Fe_3O_4 + CO_2 \quad (3.1)$$

During CO reduction the Fe_3O_4 formed may be converted directly to iron carbides without further formation of FeO and Fe.

$$3Fe_3O_4 + 6CO \rightarrow Fe_3C + 5CO_2 \quad (3.2)$$

The Boudouard reaction that forms carbon dioxide and carbon from the disproportionation of carbon monoxide tends to occur at temperatures lower than 695 °C. The formation of carbon is called sooting or coking, and this can cause serious and irreversible damage to catalysts and catalyst beds (Düdder et al. 2014; Jahangiri et al. 2014). The boudouard reaction is known to be influenced by the presence of alkali metals (Y. K. Rao and Adjorlolo 1984; Van Niekerk, Dippenaar, and Kotze 1986; Kaczorowski, Lindstad, and Syvertsen 2007). The Boudouard reaction has the stoichiometric equation.

$$2CO \rightarrow C + CO_2 \quad (3.3)$$

Carbon monoxide disintegration and carbidization are expected to occur simultaneously (Sawai, Iguchi, and Hayashi 1998; Ding et al. 2014) as evidenced by almost the same standard enthalpies of formation.

3.4.2 H_2 Reduction prediction

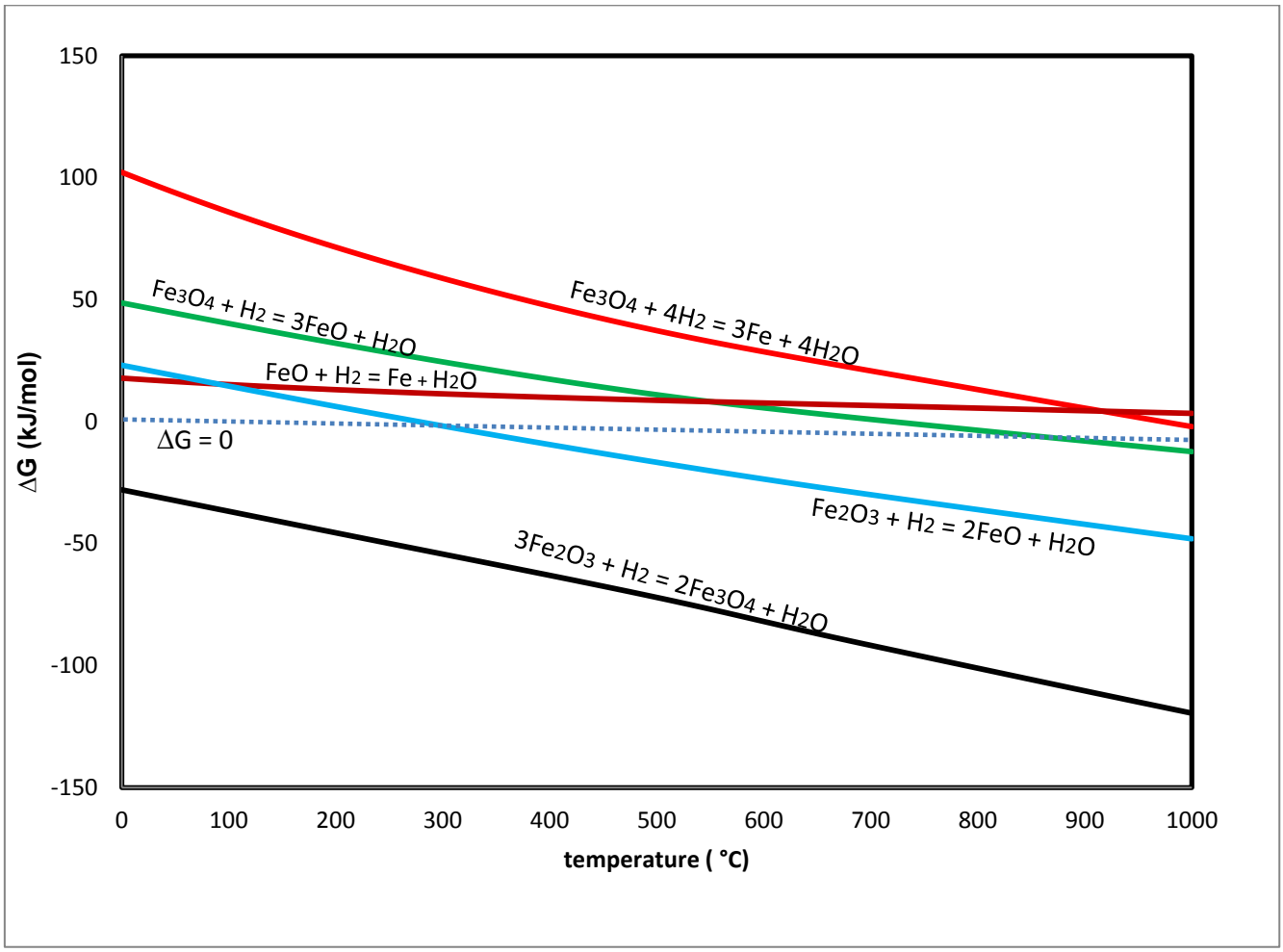

Figure 3.3: Gibbs free energy versus temperature (^{o}C) for possible speciation pathways of the iron catalyst precursor under H_2 activation

Figure 3.3 shows that the reduction of hematite using H_2 yields magnetite as the final product of reduction. The formation of metallic iron is thermodynamically unfavored at FT temperatures of 200–350 °C as shown in Figure 4.3. This observation is not in line with what is in the common literature (Wang et al. 2009a; Van der Kraan, Boellaard, and Crajé 1993; Raupp and Delgass 1979; K. R. P. M. Rao et al. 1996; Yaming Jin and Datye 2000b; Jozwiak et al. 2007b). For example, activation of Fe_2O_3 with H_2 is known to take a two stage reduction step with metallic iron as the final

product (Shimokawabe, Furuichi, and Ishii 1979; Colombo, Gazzarrini, and Lanzavecchia 1967). The conversion of hematite to magnetite is favoured as shown with the delta ΔG values in **Figure 3.3**, whereas the formation of metallic Fe from magnetite only happens when a certain H_2/H_2O ratio is reached as shown from the plotted stability diagram **Figure 3.4**. For each mole of hydrogen consumed a mole of H_2O is produced, so the formation of metallic Fe is a function of the H_2/ H_2O ratio.

$$3Fe_2O_3 + H_2 \rightarrow 2Fe_3O_4 + H_2O \quad (3.4)$$

$$Fe_3O_4 + 4H_2 \rightarrow 3\,Fe + 4H_2O \quad (3.5)$$

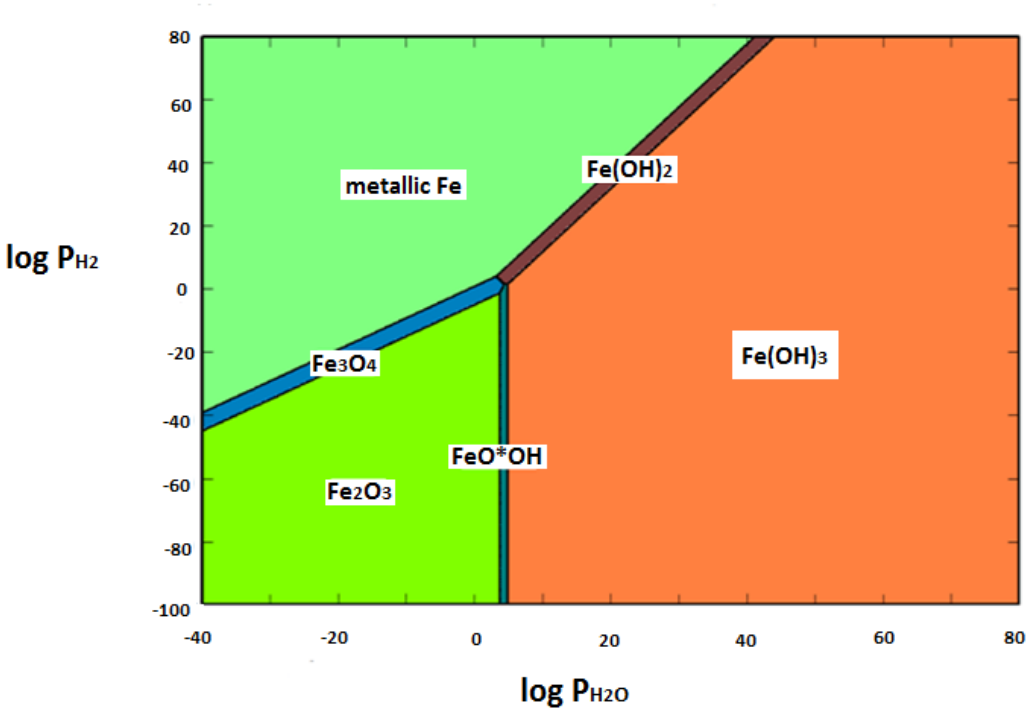

Figure 3.4: Stability diagram of an iron based catalyst in equilibrium with P_{H_2}/P_{H_2O} during reduction at 1 atm.

In situ studies prove the existence of metallic iron after reduction with H_2 (Luo, Hamdeh, and Davis 2009; Wang et al. 2009; Jin and Datye 2000; Jozwiak et al. 2007a), but the observations by these authors are at variance with thermodynamic calculations carried out in this study. (Figure 3.3 G > 0). Tiernan, Barnes, and Parkes (2001) came to the conclusion that reduction of hematite to magnetite happens via a

phase boundary, while that of magnetite to free iron was via random nucleation. Other researchers such as Lin, Chen, and Li (2003b) and Pineau, Kanari, and Gaballah (2006) came to the same conclusion.

The rapid reduction of hematite to magnetite reported by Wang et al. (2009) is in agreement with the negative ΔG values of reduction for both CO and H_2. Jozwiak et al. (2007) reported the appearance of wustite (FeO) phase as an intermediate of hematite reduction in hydrogen only above 570 °C using the *in situ* XRD method. The observation made by Jozwiak et al. (2007) agrees with thermodynamic calculations shown in Figure 3.2.

The reduction profile in hydrogen is reported to be a two stage process of α-Fe_2O_3 through Fe_3O_4 to metallic iron (Leith and Howden 1988 ; Ding et al. 2014). Meshkani and Rezaei (2015**)** observed the same pattern and assigned the two peaks to reduction of α-Fe_2O_3 to Fe_3O_4 and the broad peak to Fe_3O_4 to FeO and metallic iron.

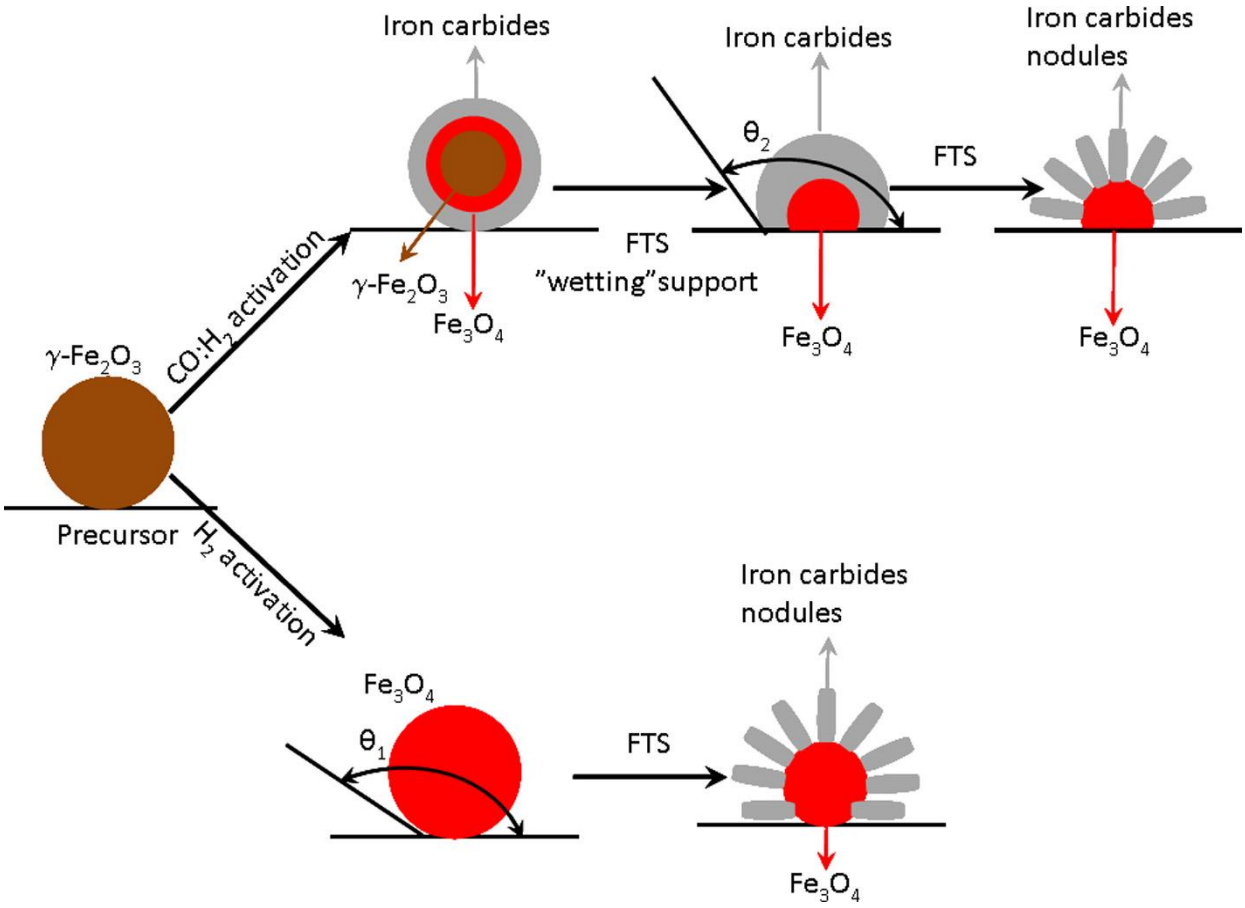

The above schematic representation depicts the sequential phase modifications from precursor up to active catalysts depending on the activation gas used (Pérez De Berti et al. 2016).

3.5 Gaseous components in equilibrium with iron and its speciation products during reduction and reaction with syngas

To better understand iron catalyst speciation during reduction with syngas and synthesis of hydrocarbon, thermodynamic equilibria involving gaseous and solid system were evaluated.

Thermodynamic calculations have to take into account the gaseous components in equilibrium with different speciation products. The species O_2, CO, CO_2, H_2, H_2O, CH_4 and other low hydrocarbons are produced in equilibrium with solid phases, Fe_3C, Fe_2C and Fe_3O_4.

Thermodynamics dictates that as the partial pressure of CO_2 and H_2O increases, the environment becomes more oxidizing, resulting in the formation of iron oxides. The stability diagrams depict that iron catalysts are a mixture of magnetite and iron carbides. For increased concentration of H_2O, carbides are converted to iron oxide.

Oxidation of the catalyst by H_2O is favoured and not favoured thermodynamically by CO_2.

$$Fe_3C + 6H_2O \rightarrow Fe_3O_4 + CO_2 + 6H_2 \quad (3.6)$$

$$Fe_3C + 5CO_2 \rightarrow Fe_3O_4 + 6CO \quad (3.7)$$

Table 3.1: Variation of ∆G of reactions 3.6 and 3.7 with temperature

Temperature (˚C)	∆G for rxn 3.6 (Kcal)	∆G for rxn 3.7 (Kcal)
150	-10.755	22.883
200	-9.955	20.832
250	-9.240	18.756
300	-8.623	16.642
350	-8.100	14.491
400	-7.671	12.301

3.5.1 Catalyst oxidation

During catalyst activation or FT synthesis the interaction of reducing agents or syngas with Fe-based catalyst results in the formation of several gaseous components (e.g. CO, H_2, CO_2, H_2O, CH_4). The partial pressure of each gaseous component determines the predominant state of the catalyst. Catalyst speciation happens due to different partial pressures of the gaseous components, hence the stable iron phases formed during FT synthesis are those that are in equilibrium with the gas composition. Gaseous H_2 and CO are reducing whereas H_2O and CO_2 are oxidizing. The ratio of P_{H2}/P_{H2O} and P_{CO}/P_{CO2} or the partial pressure of water and carbon dioxide does not have an appreciable deactivating effect (by oxidation) on the FT reaction rate over Co catalysts, while for iron based catalysts it deactivates by oxidation (see **Figure 3.5**). These calculations are also in agreement with the work done by Espinoza et al. (1999).

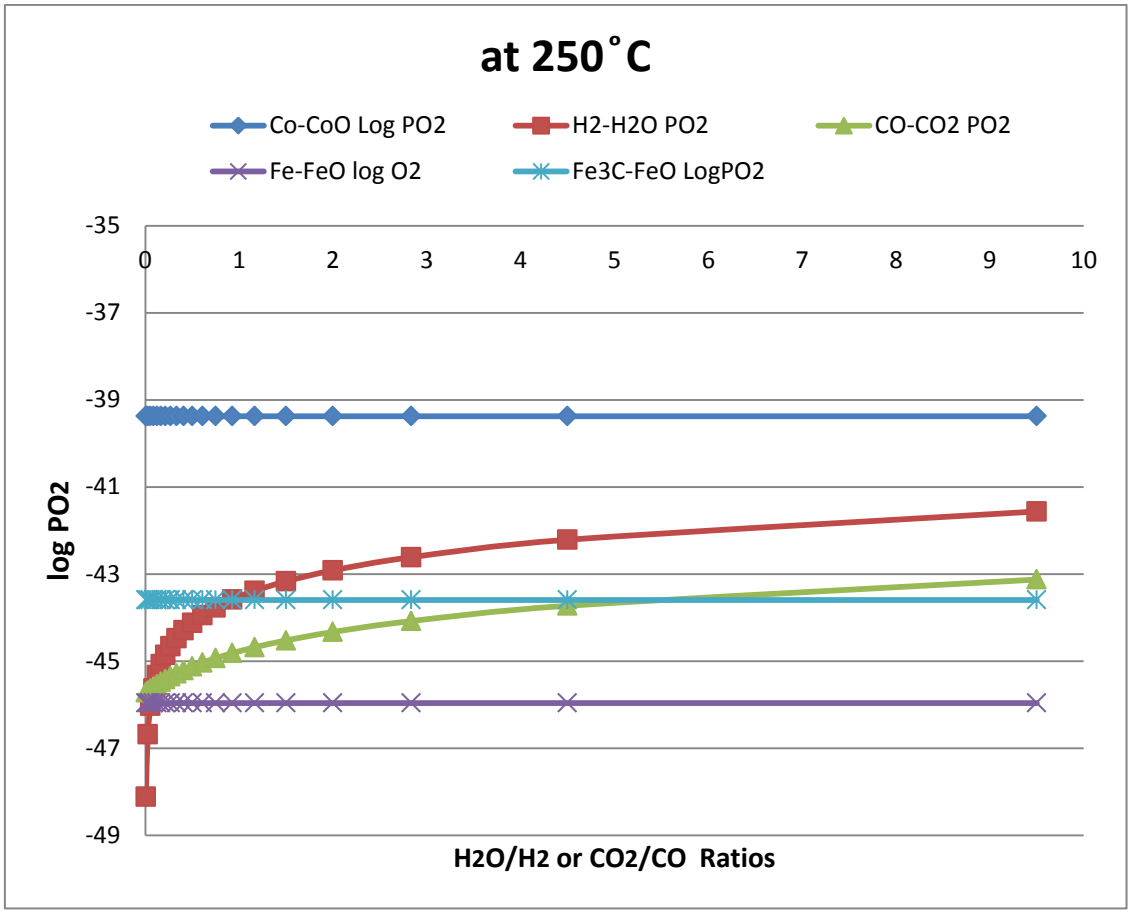

Figure 3.5: Graph showing the ability of oxygen to oxidize Co, Fe and FeC

The maximum allowable oxygen partial pressure during catalyst activation according to the diagram above is 10^ $^{-45}$ bar according to thermodynamics of the FT system. Iron oxidation by H_2O and CO_2 is known to be dependent on the PH_2/PH_2O and PCO/PCO_2 ratio. The oxygen producing Fe –CO $-CO_2$ and Fe $-H_2$ $-H_2O$ reactions such as

$$Fe + \frac{1}{2}O_2 \rightarrow FeO \qquad (3.8)$$

The oxygen concentration can be given by Log PO_2 = -log K(T).

$$CO + \frac{1}{2}O_2 \rightarrow CO_2 \qquad (3.9)$$

The oxygen concentration can be given by Log $\boldsymbol{P}O_2 = 2\log(\boldsymbol{P}_{CO_2}/\boldsymbol{P}_{CO}) - \log K_{co}$.

$$H_2 + \frac{1}{2} O_2 \rightarrow H_2O \qquad (3.10)$$

The oxygen concentration can be given by Log PO_2 = 2log ($\boldsymbol{P}H_2/\boldsymbol{P}H_2O$) + log K_{H2} .

NB: the oxygen partial pressure is therefore dependent on the $\boldsymbol{P}H_2/\boldsymbol{P}H_2O$, $\boldsymbol{P}CO_2/\boldsymbol{P}CO$ ratios and the equilibrium constants. Plots of O_2 partial pressure against H_2, CO and CO_2 partial pressure predict the stability of different species.

References

Amelse, J.A., J.B. Butt, and L.H. Schwartz. 1978. “Carburization of Supported Iron Synthesis Catalysts.” *Journal of Physical Chemistry* 82 (5): 558–63.

Borg, Ø., S. Storsæter, S. Eri, H. Wigum, E. Rytter, and A. Holmen. 2006. “The Effect of Water on the Activity and Selectivity for γ-Alumina Supported Cobalt Fischer-Tropsch Catalysts with Different Pore Sizes.” *Catalysis Letters* 107 (1-2): 95–102. doi:10.1007/s10562-005-9736-8.

Bukur, D. B., K. Okabe, M. P. Rosynek, C. P. Li, D. J. Wang, K. R. P. M. Rao, and G. P. Huffman. 1995. “Activation Studies with a Precipitated Iron Catalyst for Fischer-Tropsch Synthesis: I. Characterization Studies.” *Journal of Catalysis* 155 (2): 353–65. doi:10.1006/jcat.1995.1217.

Cairns, E.J., and A.D. Tevebaugh. 1964. “CHO Gas Phase Compositions in Equilibrium with Carbon, and Carbon Deposition Boundaries at One Atmosphere.” *Journal of Chemical and Engineering Data* 9 (3): 453–62.

Chernavskii, P.A., V.O. Kazak, G.V. Pankina, V.V. Ordomsky, and A.Y. Khodakov. 2016. “Mechanistic Aspects of the Activation of Silica-Supported Iron Catalysts for Fischer-Tropsch Synthesis in Carbon Monoxide and Syngas.” *ChemCatChem* 8 (2): 390–95. doi:10.1002/cctc.201500811.

Colombo, U, F Gazzarrini, and G Lanzavecchia. 1967. “Mechanisms of Iron Oxides Reduction at Temperatures below 400°C.” *Materials Science and Engineering* 2 (3): 125–35. doi:10.1016/0025-5416(67)90030-4.

De Smit, E., F. Cinquini, A.M. Beale, O.V. Safonova, W. Van Beek, P. Sautet, and B.M. Weckhuysen. 2010. “Stability and Reactivity of ε-X-θ Iron Carbide Catalyst Phases in Fischer-Tropsch Synthesis: Controlling μc.” *Journal of the American Chemical Society* 132 (42): 14928–41. doi:10.1021/ja105853q.

de Smit, Emiel, Andrew M. Beale, Sergey Nikitenko, and Bert M. Weckhuysen. 2009. “Local and Long Range Order in Promoted Iron-Based Fischer–Tropsch Catalysts: A Combined in Situ X-Ray Absorption Spectroscopy/wide Angle X-Ray Scattering Study.” *Journal of Catalysis* 262 (2): 244–56. doi:10.1016/j.jcat.2008.12.021.

De Smit, E., and B.M. Weckhuysen. 2008. “The Renaissance of Iron-Based Fischer-Tropsch Synthesis: On the Multifaceted Catalyst Deactivation Behaviour.” *Chemical Society Reviews* 37 (12): 2758–81. doi:10.1039/b805427d.

De Smit E., and Weckhuysen B.M. 2008. “The Renaissance of Iron-Based Fischer-Tropsch Synthesis: On the Multifaceted Catalyst Deactivation Behaviour.” *Chemical Society Reviews* 37 (12): 2758–81. doi:10.1039/b805427d.

Dİlmaç, N., S. Yörük, and Ş.M. Gülaboğlu. 2015. “Investigation of Direct Reduction Mechanism of Attepe Iron Ore by Hydrogen in a Fluidized Bed.” *Metallurgical and Materials Transactions B: Process Metallurgy and Materials Processing Science* 46 (5): 2278–87. doi:10.1007/s11663-015-0409-8.

Ding, Mingyue, Yong Yang, Baoshan Wu, Yongwang Li, Tiejun Wang, and Longlong Ma. 2014. “Study on Reduction and Carburization Behaviors of Iron-Based Fischer-Tropsch Synthesis Catalyst.” *Energy Procedia*, International Conference on Applied Energy, ICAE2014, 61: 2267–70. doi:10.1016/j.egypro.2014.12.444.

Düdder, H., K. Kähler, B. Krause, K. Mette, S. Kühl, M. Behrens, V. Scherer, and M. Muhler. 2014. “The Role of Carbonaceous Deposits in the Activity and Stability of Ni-Based Catalysts Applied in the Dry Reforming of Methane.” *Catalysis Science and Technology* 4 (9): 3317–28. doi:10.1039/c4cy00409d.

Dumesic, J.A., and H. Topsøe. 1977. *Mössbauer Spectroscopy Applications to Heterogeneous Catalysis*. Vol. 26. Advances in Catalysis. http://www.scopus.com/inward/record.url?eid=2-s2.0-0001279329&partnerID=40&md5=febb6d1a2d0644b67e3bedffc9d8dab5.

Du Plessis, H.E., J.P.R. De Villiers, and G.J. Kruger. 2007. “Re-Determination of the Crystal Structure of χ-Fe5C 2 Hägg Carbide.” *Zeitschrift Fur Kristallographie* 222 (5): 211–17. doi:10.1524/zkri.2007.222.5.211.

Espinoza, R.L., A.P. Steynberg, B. Jager, and A.C. Vosloo. 1999. “Low Temperature Fischer–Tropsch Synthesis from a Sasol Perspective.” *Applied Catalysis A: General* 186 (1–2): 13–26. doi:10.1016/S0926-860X(99)00161-1.

Hao, Q., L. Bai, H. Xiang, and Y. Li. 2008. “Phase Transformations of a Spray-Dried Iron Catalyst for Slurry Fischer-Tropsch Synthesis during Activation and Reaction.” *Fuel Processing Technology* 89 (12): 1358–64. doi:10.1016/j.fuproc.2008.06.005.

Henriksson, K.O.E., N. Sandberg, and J. Wallenius. 2008. “Carbides in Stainless Steels: Results from Ab Initio Investigations.” *Applied Physics Letters* 93 (19). doi:10.1063/1.3026175.

Herranz, T., S. Rojas, F.J. Pérez-Alonso, M. Ojeda, P. Terreros, and J.L.G. Fierro. 2006a. “Genesis of Iron Carbides and Their Role in the Synthesis of Hydrocarbons from Synthesis Gas.” *Journal of Catalysis* 243 (1): 199–211. doi:10.1016/j.jcat.2006.07.012.

———. 2006b. “Genesis of Iron Carbides and Their Role in the Synthesis of Hydrocarbons from Synthesis Gas.” *Journal of Catalysis* 243 (1): 199–211. doi:10.1016/j.jcat.2006.07.012.

Jacobs, G., W. Ma, P. Gao, B. Todic, T. Bhatelia, D.B. Bukur, and B.H. Davis. 2013. “The Application of Synchrotron Methods in Characterizing Iron and Cobalt Fischer-Tropsch Synthesis Catalysts.” *Catalysis Today* 214: 100–139. doi:10.1016/j.cattod.2013.05.011.

Jahangiri, H., J. Bennett, P. Mahjoubi, K. Wilson, and S. Gu. 2014. “A Review of Advanced Catalyst Development for Fischer-Tropsch Synthesis of Hydrocarbons from Biomass Derived Syn-Gas.” *Catalysis Science and Technology* 4 (8): 2210–29. doi:10.1039/c4cy00327f.

Jin, Yaming, and Abhaya K. Datye. 2000a. “Phase Transformations in Iron Fischer–Tropsch Catalysts during Temperature-Programmed Reduction.” *Journal of Catalysis* 196 (1): 8–17. doi:10.1006/jcat.2000.3024.

———. 2000b. “Phase Transformations in Iron Fischer–Tropsch Catalysts during Temperature-Programmed Reduction.” *Journal of Catalysis* 196 (1): 8–17. doi:10.1006/jcat.2000.3024.

Jin, Y., and A.K. Datye. 2000. “Phase Transformations in Iron Fischer-Tropsch Catalysts during Temperature-Programmed Reduction.” *Journal of Catalysis* 196 (1): 8–17. doi:10.1006/jcat.2000.3024.

Jozwiak, W.K., E. Kaczmarek, T.P. Maniecki, W. Ignaczak, and W. Maniukiewicz. 2007a. “Reduction Behavior of Iron Oxides in Hydrogen and Carbon Monoxide Atmospheres.” *Applied Catalysis A: General* 326 (1): 17–27. doi:10.1016/j.apcata.2007.03.021.

———. 2007b. “Reduction Behavior of Iron Oxides in Hydrogen and Carbon Monoxide Atmospheres.” *Applied Catalysis A: General* 326 (1): 17–27. doi:10.1016/j.apcata.2007.03.021.

———. 2007c. “Reduction Behavior of Iron Oxides in Hydrogen and Carbon Monoxide Atmospheres.” *Applied Catalysis A: General* 326 (1): 17–27. doi:10.1016/j.apcata.2007.03.021.

Kaczorowski, J., T. Lindstad, and M. Syvertsen. 2007. “The Influence of Potassium on the Boudouard Reaction in Manganese Production.” *ISIJ International* 47 (11): 1599–1604. doi:10.2355/isijinternational.47.1599.

Karimi, Z., M. Rahmani, and M. Moqadam. 2012. “A Study on Vapour-Liquid Equilibria in Fischer-Tropsch Synthesis.” *CHISA 2012* 42: 25–33. doi:10.1016/j.proeng.2012.07.391.

Kazak, V.O., P.A. Chernavskii, G.V. Pankina, A.Y. Khodakov, and V.V. Ordomsky. 2015. “Effect of a Carrier’s Nature on the Activation of Supported Iron Catalysts.” *Russian Journal of Physical Chemistry A* 89 (11): 2032–35. doi:10.1134/S0036024415110060.

Kun, C., C. Zhen-hua, Y. Zhen, L. Yan, and H. Zhi-ming. 2009. “Prediction of Vapor-Liquid Equilibrium at High Pressure Using a New Excess Free Energy Mixing Rule Coupled with the Original UNIFAC Method and the SRK Equation of State.” *Industrial and Engineering Chemistry Research* 48 (14): 6836–45. doi:10.1021/ie900111h.

Leineweber, A., S. Shang, Z.-K. Liu, M. Widenmeyer, and R. Niewa. 2012. “Crystal Structure Determination of Hägg Carbide, χ-Fe 5C 2 by First-Principles Calculations and Rietveld Refinement.” *Zeitschrift Fur Kristallographie* 227 (4): 207–20. doi:10.1524/zkri.2012.1490.

Leith, I. R., and M. G. Howden. 1988. “Temperature-Programmed Reduction of Mixed Iron—manganese Oxide Catalysts in Hydrogen and Carbon Monoxide.” *Applied Catalysis* 37: 75–92. doi:10.1016/S0166-9834(00)80752-6.

Lin, Hsin-Yu, Yu-Wen Chen, and Chiuping Li. 2003a. “The Mechanism of Reduction of Iron Oxide by Hydrogen.” *Thermochimica Acta* 400 (1–2): 61–67. doi:10.1016/S0040-6031(02)00478-1.

———. 2003b. “The Mechanism of Reduction of Iron Oxide by Hydrogen.” *Thermochimica Acta* 400 (1–2): 61–67. doi:10.1016/S0040-6031(02)00478-1.

Luo, M., H. Hamdeh, and B.H. Davis. 2007. “Potassium Promoted Iron Fischer-Tropsch Synthesis Catalyst Activation Study with Mössbauer Spectroscopy.” In . http://www.scopus.com/inward/record.url?eid=2-s2.0-37349104946&partnerID=40&md5=2c450f576563c6bac8b03e5aa0ed51fc.

———. 2009. “Fischer-Tropsch Synthesis. Catalyst Activation of Low Alpha Iron Catalyst.” *Catalysis Today* 140 (3-4): 127–34. doi:10.1016/j.cattod.2008.10.004.

Marano, J.J., and G.D. Holder. 1997. “Characterization of Fischer-Tropsch Liquids for Vapor-Liquid Equilibria Calculations.” *Fluid Phase Equilibria* 138 (1-2): 1–21.

Mauro et al. Fischer−Tropsch Synthesis: An In-Situ TPR-EXAFS/XANES Investigation of the Influence of Group I Alkali Promoters on the Local Atomic and Electronic Structure of Carburized Iron/Silica Catalysts, *J. Phys. Chem. C*, **2010**, *114* (17), pp 7895–7903

Meshkani, F., and M. Rezaei. 2015. “The Effect of Preparation Factors on the Structural and Catalytic Properties of Mesoporous Nanocrystalline Iron-Based Catalysts for High Temperature Water Gas Shift Reaction.” Scopus.

Mondal, K., H. Lorethova, E. Hippo, T. Wiltowski, and S.B. Lalvani. 2004. “Reduction of Iron Oxide in Carbon Monoxide Atmosphere—reaction Controlled Kinetics.” *Fuel Processing Technology* 86 (1): 33–47. doi:10.1016/j.fuproc.2003.12.009.

Niemantsverdriet, J.W., A.M. Van Der Kraan, W.L. Van Dijk, and H.S. Van Der Baan. 1980a. “Behavior of Metallic Iron Catalysts during Fischer-Tropsch Synthesis Studied with Mössbauer Spectroscopy, X-Ray Diffraction, Carbon Content Determination, and Reaction Kinetic Measurements.” *Journal of Physical Chemistry* 84 (25): 3363–70.

———. 1980b. “Behavior of Metallic Iron Catalysts during Fischer-Tropsch Synthesis Studied with Mössbauer Spectroscopy, X-Ray Diffraction, Carbon Content Determination, and Reaction Kinetic Measurements.” *Journal of Physical Chemistry* 84 (25): 3363–70.

O’Brien, R.J., L. Xu, R.L. Spicer, and B.H. Davis. 1996. “Activation Study of Precipitated Iron Fischer-Tropsch Catalysts.” *Energy and Fuels* 10 (4): 921–26.

Park, H., D.H. Youn, J.Y. Kim, W.Y. Kim, Y.H. Choi, Y.H. Lee, S.H. Choi, and J.S. Lee. 2015a. “Selective Formation of Hägg Iron Carbide with G-C3N4 as a

Sacrificial Support for Highly Active Fischer-Tropsch Synthesis." *ChemCatChem* 7 (21): 3488–94. doi:10.1002/cctc.201500794.

———. 2015b. "Selective Formation of Hägg Iron Carbide with G-C3N4 as a Sacrificial Support for Highly Active Fischer-Tropsch Synthesis." *ChemCatChem* 7 (21): 3488–94. doi:10.1002/cctc.201500794.

Pham, T.H., Y. Qi, J. Yang, X. Duan, G. Qian, X. Zhou, D. Chen, and W. Yuan. 2015. "Insights into Hägg Iron-Carbide-Catalysed Fischer-Tropsch Synthesis: Suppression of CH4 Formation and Enhancement of C-C Coupling on χ-Fe5C2 (510)." *ACS Catalysis* 5 (4): 2203–8. doi:10.1021/cs501668g.

Pineau, A., N. Kanari, and I. Gaballah. 2006. "Kinetics of Reduction of Iron Oxides by H2: Part I: Low Temperature Reduction of Hematite." *Thermochimica Acta* 447 (1): 89–100. doi:10.1016/j.tca.2005.10.004.

Po¨hlmann, F., P. Kaiser, C. Kern, and A. Jess. 2013. "Effect of CO2 and H2O Content in Syngas on Activity and Selectivity of a Cobalt Based Fischer-Tropsch Synthesis Catalyst." In , 2013:155–61. http://www.scopus.com/inward/record.url?eid=2-s2.0-84907274653&partnerID=40&md5=4e3ccc681b4a997cedb4aaea92fe4f82.

Quan, G.-Y., X.-J. Tang, and Z.-Z. Zhang. 2014. "Research Progress in Vapor-Liquid Equilibrium of Fischer-Tropsch Synthesis System." *Guocheng Gongcheng Xuebao/The Chinese Journal of Process Engineering* 14 (6): 1063–71.

Rao, K.R.P.M., F.E. Huggins, G.P. Huffman, R.J. Gormley, R.J. O'Brien, and B.H. Davis. 1996. "Mössbauer Study of Iron Fischer-Tropsch Catalysts during Activation and Synthesis." *Energy and Fuels* 10 (3): 546–51.

Rao, Y.K., and A.A. Adjorlolo. 1984. "CATALYSIS OF THE BOUDOUARD REACTION." *High Temperature Science* 19 (1): 51–77.

Raupp, G.B., and W.N. Delgass. 1979. "Mössbauer Investigation of Supported Fe Catalysts. III. In Situ Kinetics and Spectroscopy during Fischer-Tropsch Synthesis." *Journal of Catalysis* 58 (3): 361–69. doi:10.1016/0021-9517(79)90275-6.

Sawai, Satoshi, Yoshiaki Iguchi, and Shoji Hayashi. 1998. "Iron carbide formation with CO gas and CO-H2 gas mixture under low sulfur potential using the two-step process of metallization and carbidization." *Tetsu-To-Hagane/Journal of the Iron and Steel Institute of Japan* 84 (12): 844–49.

Shimokawabe, M., R. Furuichi, and T. Ishii. 1979. “Influence of the Preparation History of α-Fe2O3 on Its Reactivity for Hydrogen Reduction.” *Thermochimica Acta* 28 (2): 287–305. doi:10.1016/0040-6031(79)85133-3.

Shroff, M.D., D.S. Kalakkad, K.E. Coulter, S.D. Kohler, M.S. Harrington, N.B. Jackson, A.G. Sault, and A.K. Datye. 1995. “Activation of Precipitated Iron Fischer-Tropsch Synthesis Catalysts.” *Journal of Catalysis* 156 (2): 185–207. doi:10.1006/jcat.1995.1247.

Tada, M., and Y. Iwasawa. 2009a. “Active Ensemble Structures for Selective Oxidation Catalyses at Surfaces.” In *Modern Heterogeneous Oxidation Catalysis: Design, Reactions and Characterization*, 43–76. http://www.scopus.com/inward/record.url?eid=2-s2.0-84891330202&partnerID=40&md5=b46332f10915821a47a2f2b8d029ed24.

———. 2009b. “Advanced Design of Catalyst Surfaces with Metal Complexes for Selective Catalysis.” In *Modern Surface Organometallic Chemistry*, 375–415. http://www.scopus.com/inward/record.url?eid=2-s2.0-84890666754&partnerID=40&md5=6f4cd52314e4730d3163c063d7944df1.

Tiernan, M.J., P.A. Barnes, and G.M.B. Parkes. 2001. “Reduction of Iron Oxide Catalysts: The Investigation of Kinetic Parameters Using Rate Perturbation and Linear Heating Thermoanalytical Techniques.” *Journal of Physical Chemistry B* 105 (1): 220–28.

van der Kraan, A.M., E. Boellaard, and M.W.J. Crajé. 1993. “Characterization of Catalysts by Mossbauer Spectroscopy: An Application to the Study of Fischer-Tropsch, Hydrotreating and Super Claus Catalysts.” *Nuclear Inst. and Methods in Physics Research, B* 76 (1-4): 6–12. doi:10.1016/0168-583X(93)95112-I.

Van Niekerk, W.H., R.J. Dippenaar, and D.A. Kotze. 1986. “Influence of potassium on the reactivity and strength of coke, with special reference to the role of coke ash.” *Journal of The South African Institute of Mining and Metallurgy* 86 (1): 25–29.

Wang, Hong, Yong Yang, Bao-Shan Wu, Jian Xu, Ming-Yue Ding, Hu-Lin Wang, Wen-Hao Fan, Hong-Wei Xiang, and Yong-Wang Li. 2009. “Hydrogen Reduction Kinetics Modeling of a Precipitated Iron Fischer–Tropsch Catalyst.”

Journal of Molecular Catalysis A: Chemical 308 (1–2): 96–107. doi:10.1016/j.molcata.2009.03.030.

Wang, H., Y. Yang, B.-S. Wu, J. Xu, M.-Y. Ding, H.-L. Wang, W.-H. Fan, H.-W. Xiang, and Y.-W. Li. 2009a. “Hydrogen Reduction Kinetics Modeling of a Precipitated Iron Fischer-Tropsch Catalyst.” *Journal of Molecular Catalysis A: Chemical* 308 (1-2): 96–107. doi:10.1016/j.molcata.2009.03.030.

———. 2009b. “Hydrogen Reduction Kinetics Modeling of a Precipitated Iron Fischer-Tropsch Catalyst.” *Journal of Molecular Catalysis A: Chemical* 308 (1-2): 96–107. doi:10.1016/j.molcata.2009.03.030.

Xu, K., B. Sun, J. Lin, W. Wen, Y. Pei, S. Yan, M. Qiao, X. Zhang, and B. Zong. 2014. “ε -Iron Carbide as a Low-Temperature Fischer-Tropsch Synthesis Catalyst.” *Nature Communications* 5. doi:10.1038/ncomms6783.

Zhang, R., L. Bai, Y. Yang, H. Xiang, Y. Li, and J. Zhou. 2004. “Phase Change of Precipitated Iron Catalyst during Reaction Process of Fischer-Tropsch Synthesis.” *Chinese Journal of Catalysis* 25 (5): 409–12.

CHAPTER 4

EXPERIMENTAL METHODOLOGY

4.1 Introduction

In this chapter, the writer sets out a detailed description of the experimental procedures followed in order to obtain the laboratory-scale results that form the basis of discussion in the subsequent chapters. The first part of this description comprises a brief overview of the experimental conditions, the gases used, the catalyst, and the reactors selected for this investigation. The second part explains how the researcher set up the rig, and provides a diagram of the process and the instrumentation, to aid readers to follow the sequence that connects the experimental units. Lastly, the author outlines the procedures required to run the Fischer Tropsch (FT) system, collect the data, and analyse them with gas chromatography instruments.

4.2 Experimental conditions

For his FTS experiments, the researcher opted for mild operating conditions, that is, a low running pressure (1 bar gauge) after reducing the catalyst at atmospheric pressure. The FT process temperature was also set at a relatively low 250 ^{o}C. The reasons for this choice were to simplify the whole FT process, to reduce the eventual capital cost of applying this research industrially, and to prolong the lifespan of the catalyst if possible.

The three gases selected were hydrogen, carbon monoxide and synthesis gas. This enabled the author to investigate and compare the effects of reducing gases in FTS. He conducted a series of long-term (about 14 000 hours) FTS runs, starting with a low pressure (1 bar gauge), and altering both the pressures from 1 to 10 and 20 bar gauge and the flow rates from 15 mL(NTP)/min to 30 mL(NTP)/min and 60 mL(NTP)/min. The aim was to test the responses of the catalyst to different reduction conditions. The results were meant to identify the best reducing agent in terms of activity, stability and resistance to deactivation.

The general steps involved in this FT synthesis work were: (i) rig building, ii) catalyst characterization, iii) loading the catalyst into the reactors, iv) reducing the catalyst, (v) performing FT reactions at different conditions and vi) regeneration of the catalyst.

4.3 Gases used

The gases required for FT synthesis, which were supplied by African Oxygen (AFROX Ltd), in standard gas cylinders (40 Kg) for use in the laboratory, included the carrier gases and the auxiliaries (argon, helium, hydrogen and air) used for gas chromatography (GC) operations, which required ultra-high purity (UHP) grades (> 99.9997%). Three kinds of catalyst reducing gases were used for the catalyst activation: (1) UHP H_2; (2) UHP CO; (3) syngas, which is a mixture of H_2/CO/N_2. The same syngas was also used for the FT reactions. The researcher calibrated the online GC by means of a gas mixture comprising H_2, CO, CO_2, N_2,

CH_4, C_2H_4, and C_2H_6. The components of the syngas and calibration gases are given in **Table 4.1.**

Table 4.1: Component and mole percentage of the calibration gases used in the study

Component	Mole percentage (% mol)	
	Syngas (mole %)	**Calibration gas (mole %)**
H_2	60	53.2
CO	30	28.8
N_2	10	9.8
CO_2		5.0
CH_4		2.5
C_2H_4		0.2
C_2H_6		0.5

The author used UHP He and Ar (baseline) gases to calibrate the thermal conductivity detector (TCD), and Air Instrument Grade (AIG zero), H_2 (UHP) and the carrier gas Ar (baseline) for the flame ionization detector (FID) used during the sample analysis with the GC. The cylinders were fitted with pressure regulators, and the gases were sent to the FT rig via high pressure lines. Nitrogen gas was used for various purposes, including leak testing and purging the system.

4.4 Catalyst

An iron-based FT catalyst ($FeCuKSiO_2$) manufactured and commercially supplied was used throughout the FT experiments.

4.5 Catalyst characterization

Characterization, which involves the investigation and measurement of a material in terms of its structure and properties, is critical to understanding the nature of the catalyst that is to be used in the experiments. The properties, which include its chemical composition, surface area, pore volume and morphology, are in turn responsible for the catalyst's selectivity, and hence affect the distribution of the FT product (Niemantsverdriet et al. 1980; Reymond, Mériaudeau, and Teichner 1982). The researcher used various characterization techniques to determine the structural and chemical characteristics of the chosen iron catalyst. For example, powder X-Ray diffraction (XRD) was employed to assess the crystallinity of the iron loaded, and to verify the phases of iron in the catalyst; whereas electron microscopy was used to determine the particle morphology and iron crystallite size. The physicochemical characteristics of catalysts were determined by means of the Brunauer-Emmett-Teller (BET) and X-ray diffraction (XRD) analysis methods. The characterization techniques used in this study were similar to those reported other researchers.

4.5.1 X-ray diffraction (XRD)

X-ray diffraction (XRD) measurements were performed to obtain information concerning the phase composition and the crystallite size distribution. Prior to the analysis, samples were loaded into the holder. The tube voltage and current of the instrument were set at 40 kV and 30 mA respectively. The XRD instrument, which operated on a rhodium tube, had a K-beta filter mounted on it. The samples were run in a Rigaku XRD instrument equipped with a scintillation counter detector. The powder samples were scanned in the 0°–75° 2θ range at the rate of 0.2^o/min.

4.5.2 Brunauer-Emmet-Teller (BET)

The BET analysis, which measures the specific surface area and the pore volume of the iron catalyst, required a preliminary procedure. The sample was out-gassed under vacuum overnight, at 80–100 ^{o}C to drive away any moisture in the samples. The surface area and porosity of the sample were measured with a Micromeritics TriStar II - Surface Area and Porosity analyser.

4.5.3 High Resolution Transmission electron microscopy (HTEM)

A technique referred to as High Resolution transmission electron microscopy (HRTEM) was used to study the structure of the iron catalyst.

Samples were prepared by drop-coating one drop of specimen solution onto a holey carbon coated nickel grid. This was then dried under a Xenon lamp for about 10 minutes, where after the sample coated grids were analysed under the microscope. Transmission electron micrographs were collected using an FEI Tecnai G2 20 field-emission gun (FEG) TEM, operated in bright field mode at an accelerating voltage of 200 kV. Energy dispersive x-ray spectra were collected using an EDAX liquid nitrogen cooled Lithium doped Silicon detector.

4.6 FTS Reactors

The reactor system and specification have been detailed in a previous report [Yao (2011)]. A brief description is provided below. Three fixed bed reactors were used in this study. **Figure 4.1** shows the disassembled reactor with screwed end fittings. The reactor is made of a stainless steel tube (A) with dimensions tube length 204 mm and internal diameter of 8 mm, with screwed end fittings (B and C).

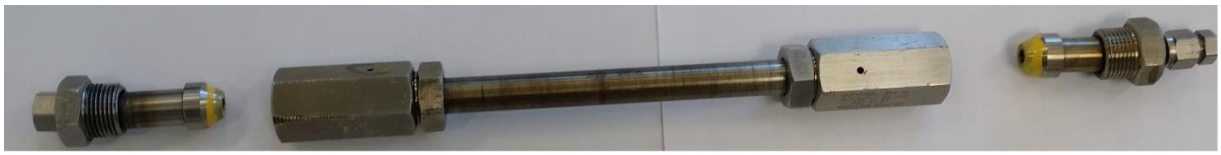

Figure 4.1: Photograph of the disassembled reactor.

4.7 Catalyst loading into the reactor

Prior to the catalyst loading, the FT rig was tested with nitrogen gas for any possible leaks. Once all the fitting joints and lines were tight, the reactor was detached from the rig. Each of the reactors was then disassembled in order to load the catalyst. **Figure 4.2** depicts a schematic representation of a loaded FT reactor with steel balls, iron catalyst and a thin layer of quartz wool. Measurements were done to locate the middle part of the reactor, then stainless steel balls were added to the middle of the reactor, and the thin layer of quartz wool was then pushed down the reactor shaft 6.35 mm (¼ inch). Thereafter one gram of catalyst was loaded followed by another thin layer of quartz wool. Additional stainless steel balls were inserted in the reactor tube to occupy the remaining volume, and then a final layer of quartz wool.

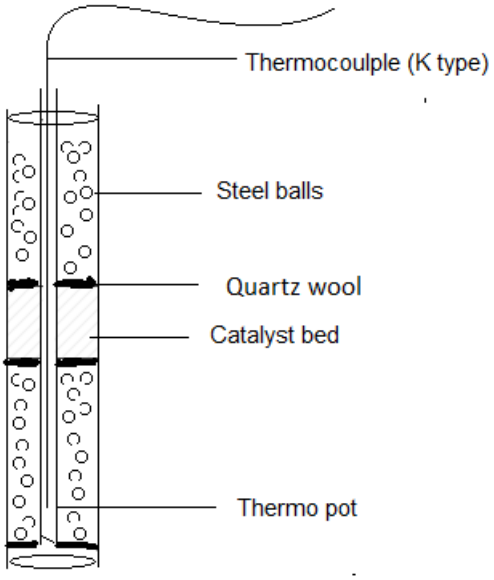

Figure 4.2: Representation of the FT reactor loaded with catalyst

Steel balls were used to keep the catalyst bed in position (in the middle of the reactor) and enhancing the gas distribution and flow patterns inside the reactor; the steel balls also preheated the syngas to the required experimental temperature, and they occupied all the tube length not taken up by catalyst. This also contributed to maintaining isothermal conditions along the entire length of the

reactors. Quartz wool was positioned at the catalyst–balls interfaces above and below the catalyst bed to prevent the catalyst from being blown out of the reactor tube. The temperature along the reactor tube was measured by a moveable thermocouple (K type of 1/16” OD thermocouple which was placed centrally in an axial position within the thermopot (1/8” OD thermopot). The temperature profile along the reactor before and during reaction was then measured. After loading the catalyst, all three reactors were mounted back to the FT rig. Then, leakage testing was conducted again for the three reactors to make sure there was no leakage for the entire reactor system. The reactors were then insulated with a thermal blanket to prevent heat loss. The middle part of each reactor was heated with heating coils which were placed around the reactor and the top and bottom parts, forming the heating sheath. Temperature controllers were used to enable the setting of desired temperatures. These three zones (top, middle and bottom of the reactor) were monitored by the same kind of temperature controllers.

4.8 Experimental set-up

The experimental set-up (**Figure 4.3**) was designed and built with three fixed bed reactors in a parallel configuration to achieve the aim of this study. An important aspect of the parallel concept is the possibility to share the same feed cylinder, nitrogen and analysis equipment, thereby reducing the possibilities of errors.

The same feed (synthesis gas) was distributed to the three reactors using the Brooks mass flow controllers (Brooks Instrument 5850). A non-return valve was mounted after each mass flow control (MFC) channel to prevent the products from flowing back to the MFC. Besides feeding the system with syngas, other channels were available to supply other gases such as nitrogen and reducing gases to the reactors. Back pressure regulators were manually controlled to keep the reactor pressure at desired set point. All the experiments were conducted in a laboratory scale fixed bed reactor set-up, as shown in **Figure 4.3**.

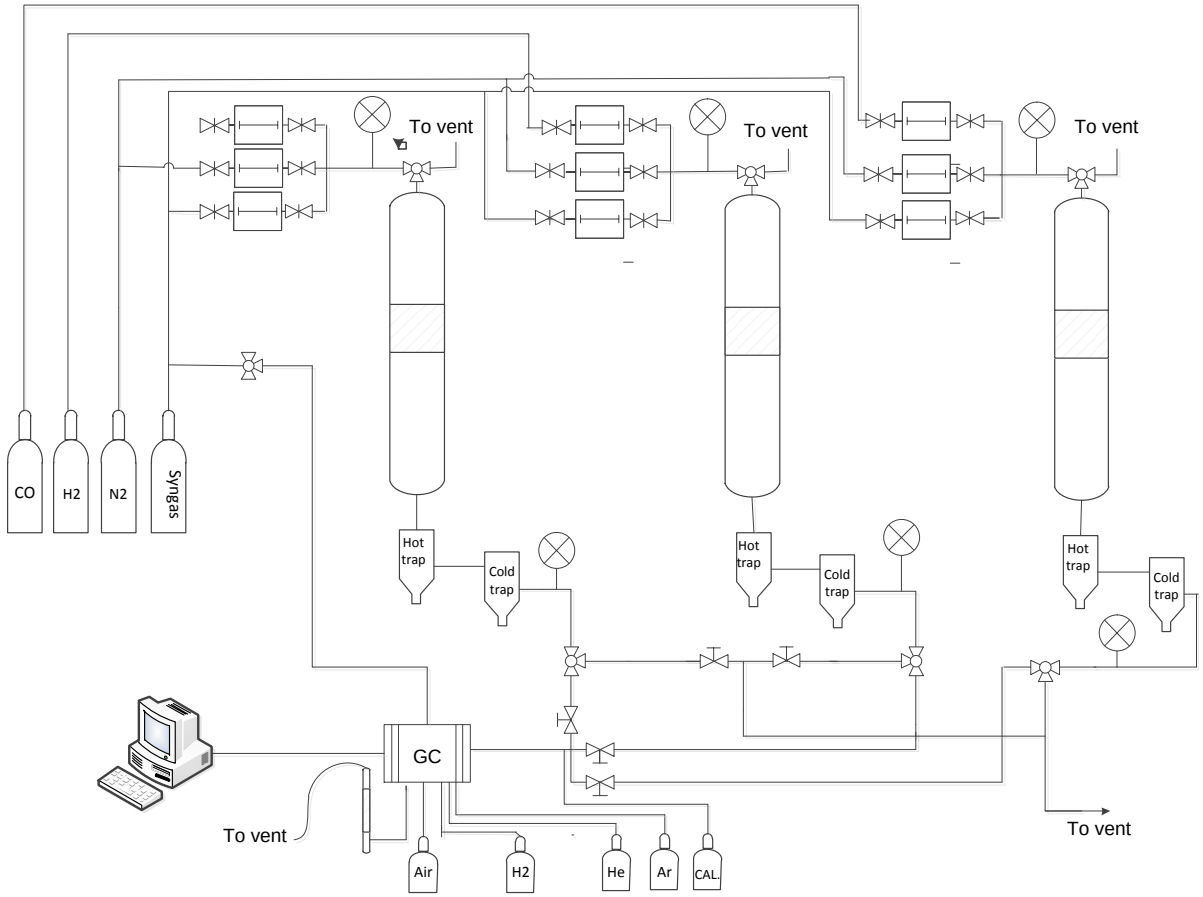

Figure 4.3: Flow scheme of the laboratory scale Fischer Tropsch rig with three fixed reactors in parallel



Fixed bed reactor

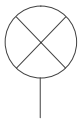

Back pressure regulator



Knock out pots



Three way valve



Non return valve



Two way valve

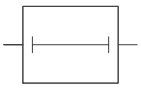

Mass flow controller

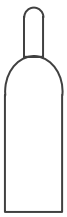

Gas Cylinder

4.9 Experimental method

4.9.1 Catalyst reduction procedure

One gram of the iron based catalyst was loaded in each of the three reactors. Three kinds of reducing agents (H_2, CO and syngas) were used for the catalyst reduction in these three reactors, respectively: syngas for the catalyst reduction of reactor 1 (Reac-Syn), H_2 for that of reactor 2 Reac-H_2 and CO for that of reactor 3 (Reac-CO).

Before catalyst reduction, the catalyst in each of the reactors was dried under the flow of nitrogen at 60 mL(NTP)/min, at the temperature of 120 °C, and at atmospheric pressure, for 2 hours, to get rid of the moisture which might have accumulated during catalyst loading.

After the drying, the same catalyst reduction procedure was performed on the three reactors. The only difference was the reducing agents: the catalyst in reactor 1 (Reac-Syn) was reduced with syngas, the catalyst in reactor 2 (Reac-H_2) was reduced with hydrogen and the catalyst in reactor 3 (Reac-CO) was reduced with carbon monoxide. The three kinds of reducing gases were introduced into the three reactors, respectively, at a flow of 60 mL(NTP)/min, at atmospheric pressure, and the temperature was increased from 120 (drying temperature) to 250 °C (reduction temperature) at a heating rate of 1 °C/min. The system was left at 250 ^{o}C in the atmosphere of reducing agents for 48 hours prior to running the FT reaction.

4.9.2 FT synthesis

After reduction, Reac-Syn (syngas reduced) was maintained at the same temperature and flow rate but the pressure was increased from atmosphere to 1 bar gauge for FT synthesis (FTS) run. The temperature of Reac-H_2 and Reac-CO (reduced by hydrogen and carbon monoxide respectively) was reduced to 100 °C before introducing syngas feed so as to avoid any temperature runaways once the FTS reaction was initiated. Similarly, the pressure of Reac-H_2 and Reac-CO was

increased from atmospheric to 1 bar gauge (2 bar absolute) and the temperature was raised gradually from 100 ^{o}C to 250 °C. The FTS experiments were carried out under the reaction conditions (**Table 4.2**) for 1000 hours of time on stream (TOS) without changing the operating conditions for all three reactors. The results obtained from these FTS runs are presented and discussed in Chapter 5. A summary of the operating conditions used during our FT experiments is shown in **Table 4.2.** The FT experiments continued and operating conditions, specifically the reactor pressure and flow rate, were varied for the rest of the FT reactions. The effects of varying the operating conditions for the FT reactions appeared different and depended on the reducing agents. The results from these investigations are detailed and discussed in Chapter 6.

The syngas feed composition was 60% H_2, 30% CO and 10% N_2 for all the reactors, and this corresponded to partial pressures of P_{H2} = 1.2, P_{CO} = 0.6 and P_{N2} = 0.2 bar within the reactor. The syngas flow rate was set at 60 mL(NTP)/min and at this flow rate, the space velocity at normal temperature and pressure was 60 mL(NTP)/min/g Fe.

Table 4.2: Initial reaction conditions for the FT synthesis

	Reac-Syn	**Reac-H_2**	**Reac-CO**
Reducing gas	Syngas	Hydrogen	Carbon monoxide
Catalyst weight (gauge)	1	1	1
Temperature (°C)	250	250	250
Flowrate mL(NTP)/min	60	60	60
Pressure (bar gauge)	1	1	1

4.9.3 **Regeneration studies**

The catalytic activity decreased noticeably with TOS but also due to unplanned power supply outages to the FT rig. The researcher therefore devised a way of regenerating the catalyst step by step, as described below. This is an oxido-reduction process. The same regeneration steps were conducted for all the three reactors starting with Reac-Syn, followed by Reac-CO and finally Reac-H_2.

- The flow of syngas to the reactor was stopped, which was set at 60 mL(NTP)/min, whilst nitrogen was introduced into the system at the same flowrate.

- The back pressure regulator was fully opened and the system was run at atmospheric pressure.

- The temperature was increased from 250 to 270 °C at a rate of 1 °C/min.

- The reactor was then left under the flow of nitrogen at 60 mL(NTP)/min, at atmospheric pressure and at 270 °C, overnight.

- Then the temperature was decreased from 270 to 100 °C and a mixture gas of 4.9 % O_2 in 94.1 % helium was introduced to the reactor at a flowrate of 30 mL(NTP)/min whilst the flow of N_2 60 mL(NTP)/min) was kept passing through the reactor overnight.

- After that, the reactor temperature was increased to 180 °C at a rate of 20 °C in 10 mins and maintained there for one hour, then increased another 20 °C in 10 mins until it reached 200 °C.

- While at 200 °C the flow of N_2 was stopped and the flow of O_2/He remained at 30 mL(NTP)/min overnight.

- N_2 was then re-introduced at 60 mL(NTP)/min whilst the flow of O_2/He was slowly reduced to zero, resulting in the end of catalyst oxygenation.

The catalyst oxidation process was then followed by the reduction pathway where the temperature was reduced to 120 °C and kept there for 2 hours. This was followed by the reduction of the catalyst under the same conditions (250 °C, 60 mL(NTP)/min at atmospheric pressure for 48 hours) as done previously, but this time syngas was used as the reducing agent for all the reactors. This was the end of regeneration. After regeneration, the researcher reverted to normal FT runs where the reactor pressure was increased to 1 bar gauge and the flow rate was maintained at 60 mL(NTP)/min and the temperature at 250 °C. The data obtained from the regeneration investigation are reported and discussed in Chapter 7.

4.9.4 **Product separation and analysis**

FT main products exiting the reactor are usually grouped into three categories: gases, liquids and solids. This classification is based on the length of the carbon chain. The solid products (waxes) were collected in the hot trap kept at 150 °C. The liquid products were trapped further down in the cold trap kept at room temperature. The gaseous components went to the GC for analysis and/or vented.

Product analysis was attained through three detectors. The tail gas from each of the reactors was analysed by an online GC which was equipped with two Thermal Conductivity Detectors (TCDs) and both used argon as the reference gas. The integrated peaks areas from these chromatograms were used to monitor the conversion levels of the reactants (hydrogen and carbon monoxide). The GC was also equipped with Flame Ionization Detector (FID) which detected and separated organic compounds from C_1 to C_5. Samples from the gaseous stream were taken every 83 min via sample valves from the sampling loop and analysed by the online GC, and the excess gas from the sampling loop passed through a bubble meter to the vent. It was not an obstacle to analyze samples from the three reactor configurations of this experimental set-up. This was because products from the three reactors were analysed in a cyclic manner (reactor 1- 2-3:1-2-3 cycles).

The gaseous inorganic compounds CO, H_2, N_2, CO_2, and hydrocarbons C_1-C_5 were analysed using an online DANI 1000 GC instrument equipped with both FID

and TCD. The GC used in this study was similar to the one reported by Yao (2011). The GC was equipped with three multiple sampling valves which were heated at 150 °C and the detectors at 220 °C. The mechanism of sampling of the GC is reported in the Yao thesis (2011). Details about the GC settings and columns in the present research are summarized in **Table 4.3** below. The inorganic components (H_2, CO, CO_2, and N_2) were separated on a Teknokroma Porapack Q column and the hydrocarbon products were separated on a Varian capillary column.

To properly quantify the product amounts, calibration was done using a premixed gas with known molar fractions. The percentage composition of the calibration cylinder is given in **Table 4.1**. The amounts of the products will then be given by determining the relationship between the size of a peak for a known amount of analyte in a standard against the amount of that analyte in a sample of unknown concentration. The quantities of C_1 and C_2 hydrocarbons were determined directly and the remaining hydrocarbons in the gas phase were calculated using the calibration for C_2 and the corresponding response factors (**Table 4.4**).

Table 4.3: Summary of the online GC settings and columns used

On-line GC	**DANI GC 1000**
Oven temperature programme	50 °C - 8 °C /min - 200 °C
Detector 1	FID, T - 220 ^{o}C
Column 1	Varian capillary column (Cp-Poraplot Q-HT), 12.5m*0.53mm* 20µm
Sample valve temperature	150 °C
Carrier gas	UHP Ar with flow rate of 30 mL (NTP)/min
Product analysis	C1- C5
Detector 2	TCD - A, T = 220 °C
Column 2	Teknokroma, porapack Q (Tmax: 250 °C), 80/100 mesh, 2m*1/8''*2.1mm
Column 3	Teknokroma, molecular sieve 13X (Tmax: 400 °C), 80/100 mesh, 2m*1/8''
Sample valve temperature	150 °C
Carrier gas	UHP Ar with flow rate of 30 mL(NTP)/min
Oven temperature programme	Hold at 50 °C for 8 min, heat to 200 °C at 8 °C /min, hold at 200 °C for 45 min
Product analysis	CH_4, CO_2, N_2, CO
Detector 3	TCD_B, T=220 °C
Column 4	Teknokroma, molecular sieve 5A (Tmax: 400 °C), 80/100 mesh, 1.5m*1/8''
Sample valve temperature	150 °C
Flame gas	Air with flow rate of 20 mL(NTP)/min and UHP H_2 with flow rate of 200 mL (NTP)/min
Carrier gas	UHP He, 30 mL (NTP)/min
Oven temperature programme	Hold at 50 °C for 8 min, heat to 200 °C at 8 °C /min, hold at 200 °C for 45 min
Product analysis	H_2

Products from the two hot and cold traps were collected and sent to the Offline gas chromatography for analysis. Typical chromatograms from the TCDs and FID are given in **Figures 4.4** to **4.6**, respectively.

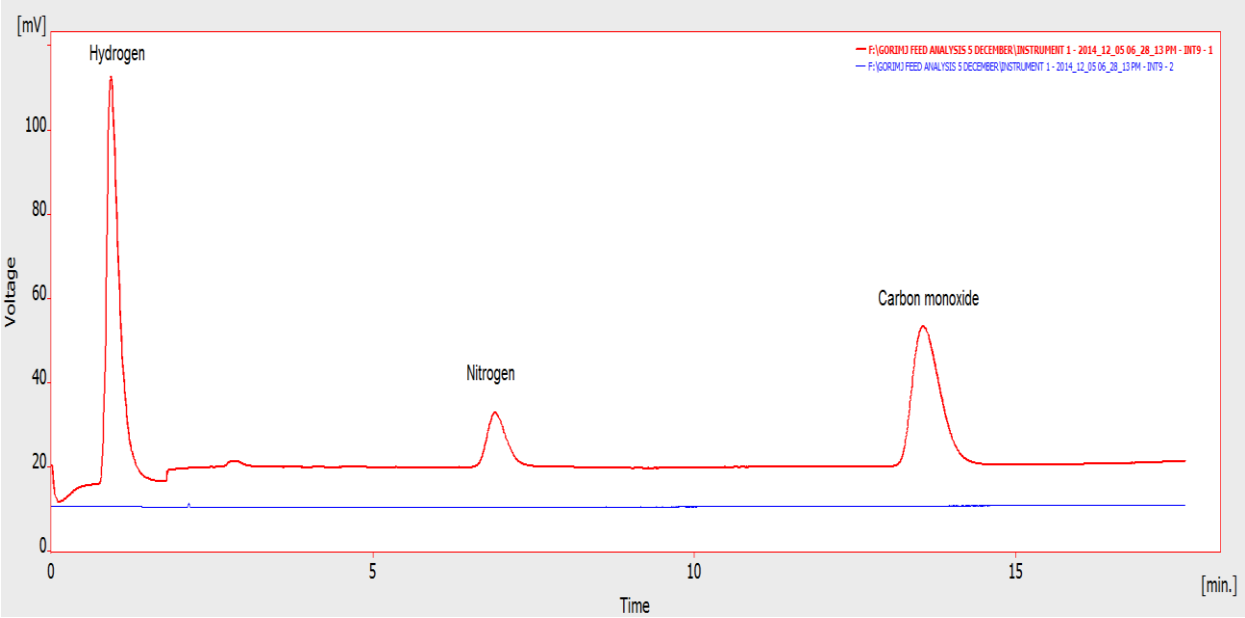

Figure 4.4: Typical online analysis of the syngas (red line from TCD detector and blue line from that of FID).

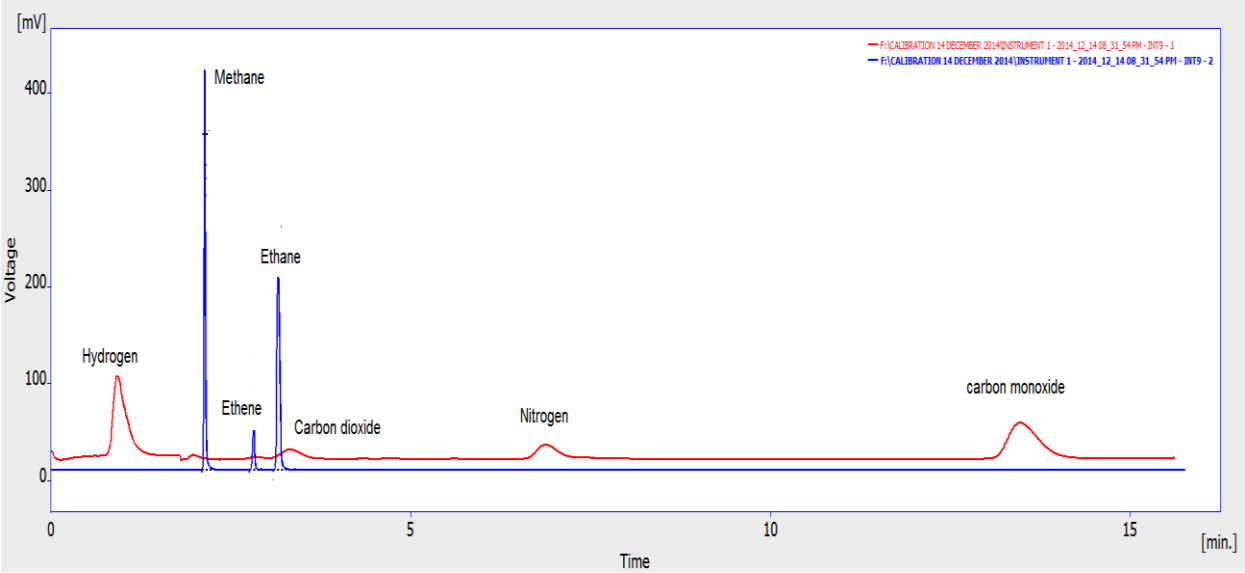

Figure 4.5: Typical online analysis of the calibration gas (red line from TCD detector and blue line from FID)

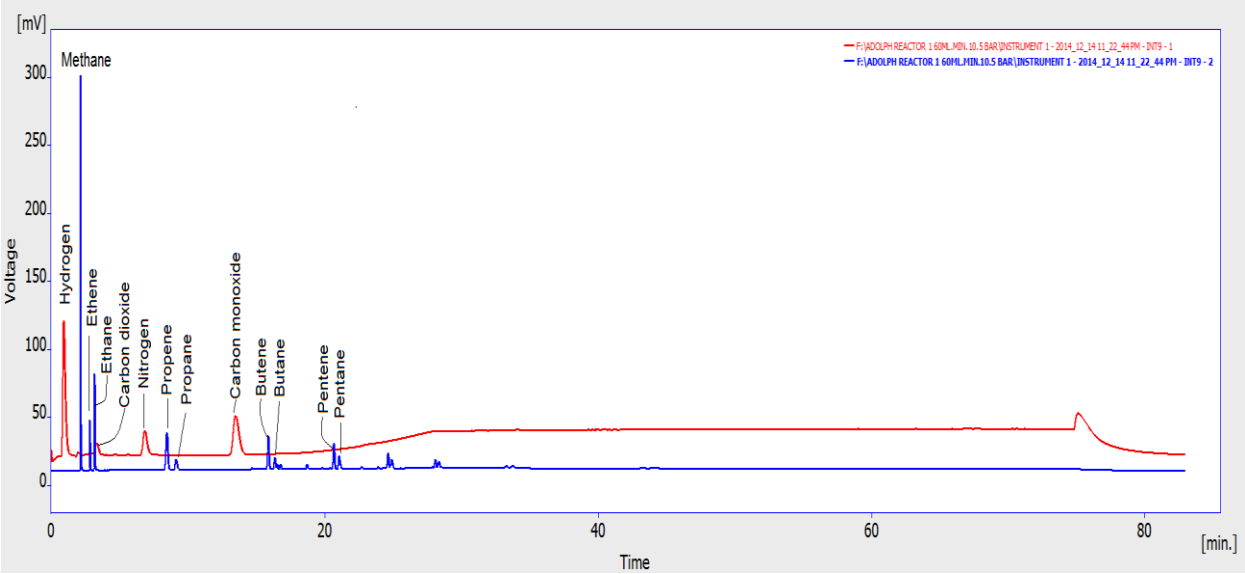

Figure 4.6: Typical online analysis of the tailgas (red line from TCD detector and blue line from FID)

4.10 Product storage

The solid and liquid products were collected in glass vials sealed with paraffin paper, labelled with stickers and stored in a refrigerator awaiting analysis.

4.11 Calculations

The data collected from the on-line were quantitatively processed. Nitrogen (10 vol % of N_2) contained in syngas feed of FT experiments was used as the internal standard for the measurements of TCD data. Once the molar flow rates of the various reactants and products had been determined, further calculations were then performed. Mass balance calculations including the conversion of reactants CO and H_2 were determined using the equations below. These calculation are similar to those used by the previous researchers (Bahome 2007; Mokoena 2005; Yao 2011; Lu 2012; Jalama 2008; Yao 2011; Lu 2012). The experimental procedure used dates back to decades (Duvenhage, 1994).

$$\%\ CO = \frac{F_{in}X_{co,in} - F_{out}X_{co,out}}{F_{in}X_{co,in}} \quad (4.3)$$

Where:

$X_{co,in}$ is the molar fraction of CO in the reactor inlet gas feed;

and $X_{co,out}$ is the molar fraction of CO in the reactor outlet gas stream.

The CO consumption rate is calculated as follows:

$$r_{co} = \frac{F_{out}X_{co,out} - F_{in}X_{co,in}}{m_{cat}} \quad (4.4)$$

where:

r_{co} is the rate of CO consumption, mol/(min.gcat)

m_{cat} is the mass of the catalyst used in this reaction, in grams.

The formation rate of gas a product θ_i, mol/(min.gcat) is given by:

$$r_{\theta_i} = \frac{F_{out}X_{\theta_{i,out}}}{m_{cat}} \quad (4.5)$$

Where:

$X_{\theta_{i,out}}$ is the molar fraction of θ_i in the reactor outlet gas stream.

The product selectivity was calculated on the moles of carbon basis, as follows:

$$Sel\ (\theta) = \frac{[nC]_\theta}{-r_{co} \times t \times m_{cat}} \quad (4.6)$$

where:

$Sel\ (\theta)$ represents the selectivity of product θ and $[nC]_\theta$ represents the moles of carbon contained in the product θ.

The response factors as reported by (Dietz 1967) were used to correct hydrocarbons based on the known areas of C_2H_4 (olefin) and C_2H_6 (paraffin) in the calibration.

Table 4.4: Response factors for hydrocarbon products

Carbon number	Olefin	Paraffin
2	1	1
3	0.7	0.74
4	0.55	0.55
5	0.47	0.47
6	0.4	0.4
7	0.35	0.35
8	0.32	0.32
9	0.28	0.28
10	0.24	0.24
11	0.21	0.21
12	0.19	0.19
13	0.18	0.18
14	0.17	0.17
15	0.15	0.15

4.11.1 Olefin/paraffin ratio

Olefin/paraffin (O/P) ratio was calculated as follows, considering the relative molar amount for the same carbon number in the outlet stream:

$$O_n/P_n = N_{C_nH_{2n}}/N_{C_nH_{2n+2}} \quad (4.7)$$

4.11.2 **Olefin/paraffin ratio**

Olefin/olefin (O_n/O_{n-1}) ratio looked at the relative molar amount for the immediate neighbouring olefins in the outlet stream, which was calculated as follows:

$$O_n/O_{n-1} = N_{C_nH_{2n}}/N_{C_{n-1}H_{2(n-1)}} \quad (4.8)$$

It is important to note the time scales for the whole FT run for all the different reactors and **Table 4.5** presents the events for the whole duration of the study. Detailed accounts of the actual work performed to evaluate FTS are presented in the respective sections that follow. The focus of the thesis was on light hydrocarbons monitored by the online GC only, though liquid and solid (wax) hydrocarbons were obtained. It is worth noting that the hydrogen conversion is not reported due to analysis limitations. The graphs plotted **in Figure 4.7** depict the conversion against the time on stream presented in the thesis.

Table 4.4: Reaction and feed conditions for the FTS experiment. Note that 1 g of iron based catalyst was loaded into the reactor and this catalyst was not changed during the experiment.

Time on Stream in Hours (TOS)	Experimental Conditions	Activity
0-1000	FT Synthesis 60 mL(NTP)/min, 250°C, 1 bar	The results obtained are presented in chapter 5
1000-5000	Nitrogen flowing 60 mL(NTP)/min, 250°C, 1 bar	Shortage of syngas. Results not presented in this thesis
5000-7000	FT Synthesis, Effect of flow rate investigated from 60, 30 and 15mL(NTP)/min. At 1 bar, 250°C	These results are presented in chapter 6
7000-11800	Nitrogen flow 60mL(NTP)/min, 1 bar	Shortage of syngas
11800-13000	Ft synthesis 60mL(NTP)/min, 250 °C, 1 bar	Regeneration studies. Results presented in chapter 7
13000-14600	FT synthesis Effect of pressure investigated from 1,10 and 20 bar. At 60mL(NTP)/min, 250 °C	Results presented in chapter 6

The time run recorded was from 0 to about 14500 hours' time on stream as highlighted in Table 4.5. The graphs in Figure 4.7 only show the section reported in the thesis. The idea was to report section with minimal or no interruptions such as shortages of syngas and power outages.

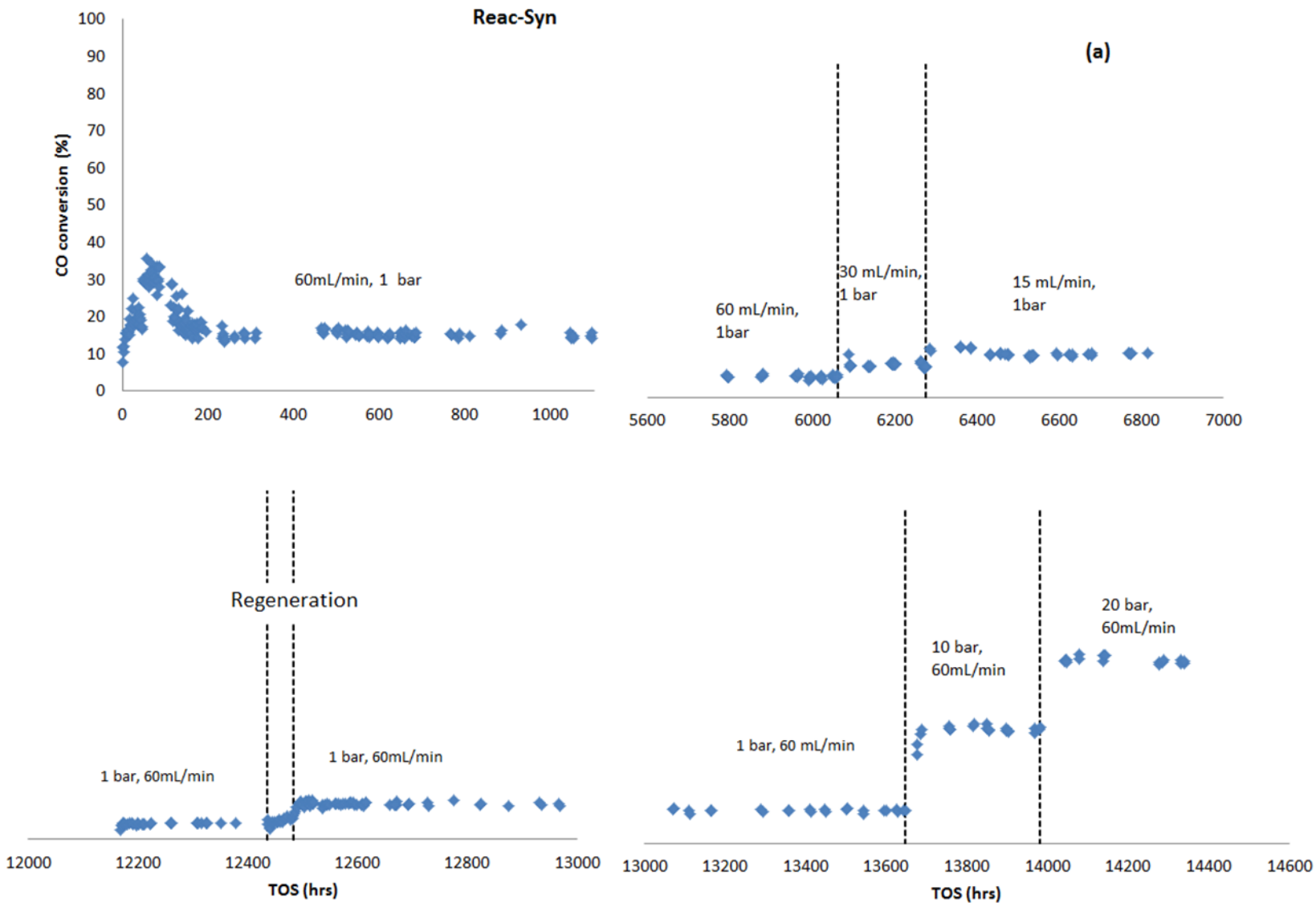
Reac-Syn
(a)
CO conversion (%)
60mL/min, 1 bar
60 mL/min, 1bar
30 mL/min, 1 bar
15 mL/min, 1bar
Regeneration
1 bar, 60mL/min
1 bar, 60mL/min
1 bar, 60 mL/min
10 bar, 60mL/min
20 bar, 60mL/min
TOS (hrs)
TOS (hrs)

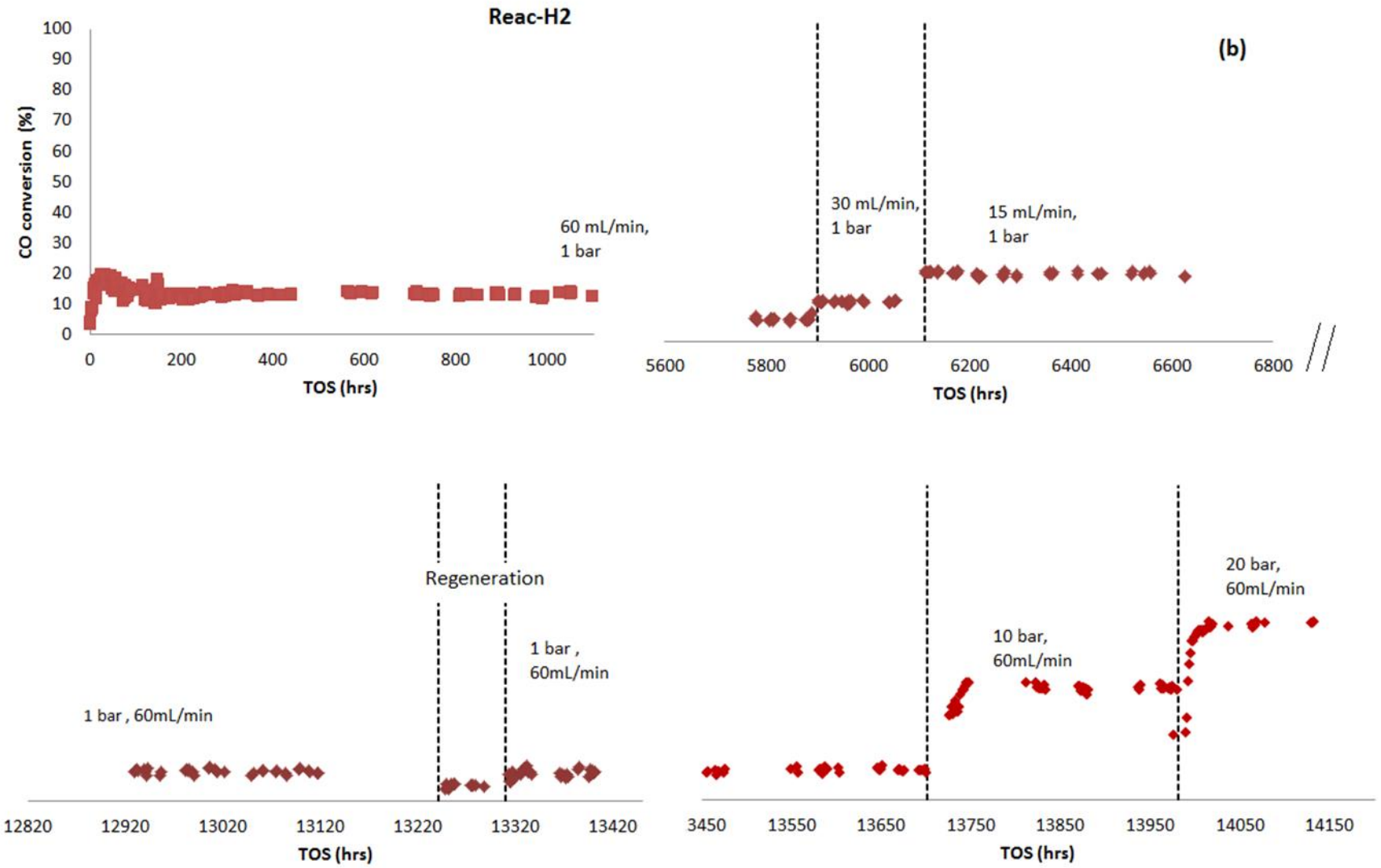
Reac-H2
CO conversion (%)
100
90
80
70
60
50
40
30
20
10
0
0
200
400
600
800
1000
TOS (hrs)
60 mL/min,
1 bar
(b)
30 mL/min,
1 bar
15 mL/min,
1 bar
5600
5800
6000
6200
6400
6600
6800
TOS (hrs)
1 bar , 60mL/min
Regeneration
1 bar ,
60mL/min
12820
12920
13020
13120
13220
13320
13420
TOS (hrs)
10 bar,
60mL/min
20 bar,
60mL/min
3450
13550
13650
13750
13850
13950
14050
14150
TOS (hrs)

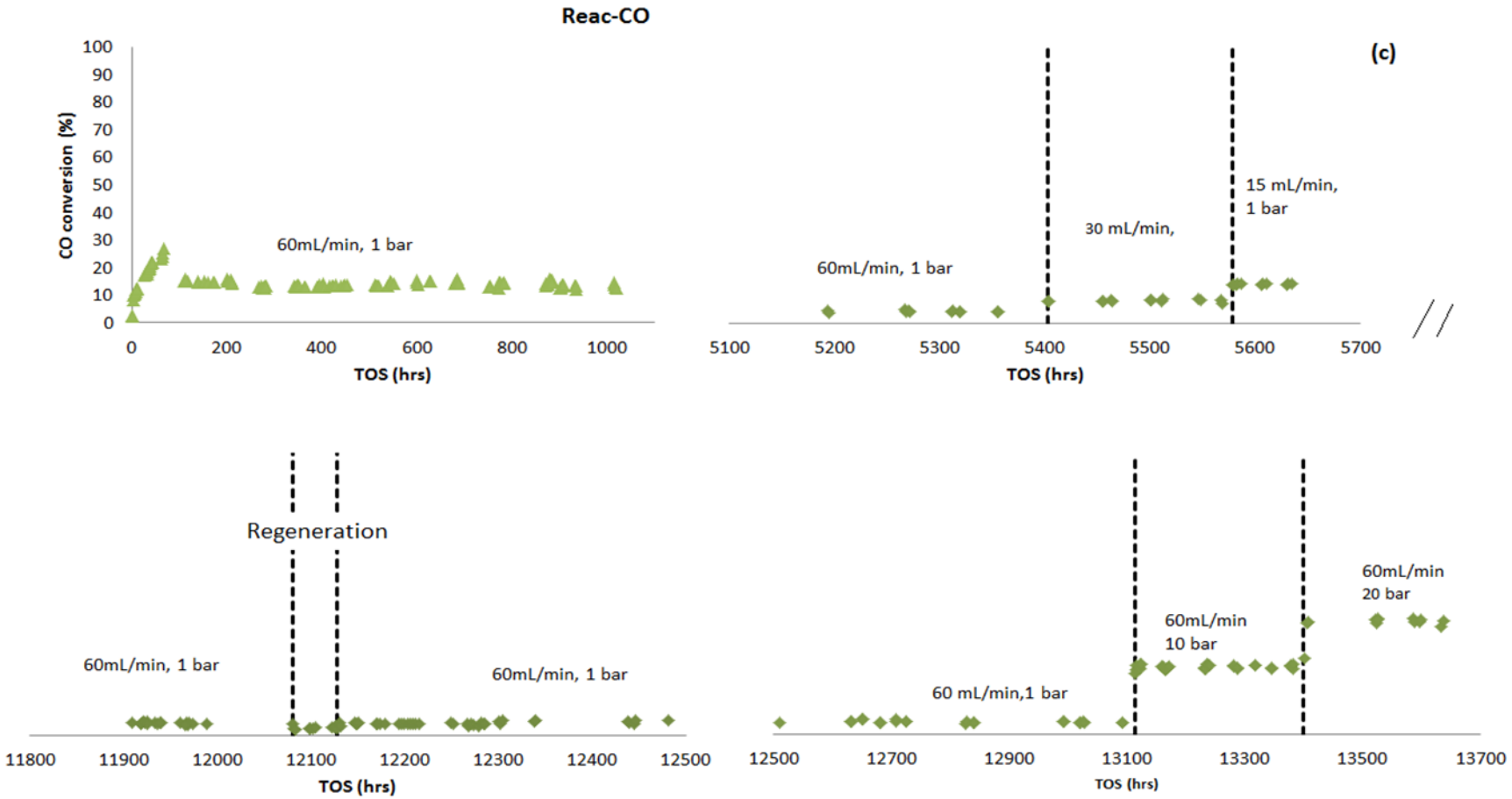

Figure 4.6: Graphs of conversion again time on stream for the whole FT run periods considered in this thesis (a) Reac-Syn, (b) Reac-H_2 and (c) Reac-CO

References

Bahome, Munga Christian. 2007. “Synthesis and Use of Carbon Nanotubes as a Support for the Fischer-Tropsch Synthesis.” Faculty of Engineering and the Built Environment, University of the Witwatersrand, Johannesburg. http://mobile.wiredspace.wits.ac.za/handle/10539/4502.

Dietz, W. A. 1967. “Response Factors for Gas Chromatographic Analyses.” *Journal of Chromatographic Science* 5 (2): 68–71. doi:10.1093/chromsci/5.2.68.

Duvenhage, D. J. 1994. The Preparation, Characterization and Evaluation of Titania Supported Fe:Co Bimetallic Catalysts for Hydrogenation of CO, PhD Thesis, University of the Witwatersrand, Johannesburg.

Jalama, Kalala. 2008. “Fischer Tropsch Synthesis over Supported Cobalt Catalysts: Effect of Ethanol Addition, Precursors and Gold Doping.” http://wiredspace.wits.ac.za/handle/10539/4937.

Lu, Xiaojun. 2012. “Fischer-Tropsch Synthesis: Towards Understanding.” http://mobile.wiredspace.wits.ac.za/handle/10539/11175.

Mokoena, Emma Magdeline. 2005. “Synthesis and Use of Silica Materials as Supports for the Fischer-Tropsch Reaction.” Faculty of Science, University of the Witwatersrand, Johannesburg. http://146.141.12.21/handle/10539/1848.

Niemantsverdriet, J.W., A.M. Van Der Kraan, W.L. Van Dijk, and H.S. Van Der Baan. 1980. “Behavior of Metallic Iron Catalysts during Fischer-Tropsch Synthesis Studied with Mössbauer Spectroscopy, X-Ray Diffraction, Carbon Content Determination, and Reaction Kinetic Measurements.” *Journal of Physical Chemistry* 84 (25): 3363–70.

Reymond, J.P., P. Mériaudeau, and S.J. Teichner. 1982. “Changes in the Surface Structure and Composition of an Iron Catalyst of Reduced or Unreduced Fe2O3 during the Reaction of Carbon Monoxide and Hydrogen.” *Journal of Catalysis* 75 (1): 39–48. doi:10.1016/0021-9517(82)90119-1.

Yao, Yali. 2011. “Fischer- tropsch synthesis usingCO2-containing syngas mixtures over Cobalt and Iron based catalysts.” University of the Witwatersrand, Johannesburg. http://mobile.wiredspace.wits.ac.za/handle/10539/11292.

CHAPTER 5

A COMPARATIVE STUDY ON THE GAS PHASE FISCHER TROPSCHS PRODUCTS OF REDUCING AN IRON CATALYST WITH THREE DIFFERENT REDUCING GASES

The material in this chapter has been written in a paper format and is ready for submission. Some of the data were accepted for a poster presentation at AIChE annual meeting 2015.

Abstract

In this chapter, the effect of running the FT synthesis process, at a pressure of 1 bar gauge, using an iron catalyst that has been reduced by three different reducing gases was investigated. In order to achieve this task, the three reactors were set up in parallel and each of them loaded with the same quantity of the iron catalyst ($FeCuKSiO_2$). After loading, the catalyst in the first reactor was reduced with synthesis gas (a combination of carbon monoxide and hydrogen). The catalyst in the second reactor was reduced using hydrogen (H_2) gas, while that in the third reactor was reduced with carbon monoxide (CO) gas. A typical FT reaction experiment was conducted for a total of 1000 hours in all the three reactors, under the same operating conditions such as flow rate, pressure and temperature. In this study only the gas-phase products leaving the reactors were analysed and compared.

5.1 Introduction

The dependency of Fischer Tropsch synthesis (FTS) product distribution on operating conditions has been studied (Patel and Lang 1990; Donnelly and Satterfield 1989). The process conditions are reported to have an effect on the overall product selectivity of FTS (Todic et al., 2016). The interplay between the kinetics and thermodynamics of various parallel reactions, under different process conditions, determines the overall selectivity to FTS products. It is further reported that total pressure has a positive effect on the FTS reaction rate (Dinse et al., 2012). Research done by Dinse et al (2012), showed that increasing pressure results in a decrease in methane production, and an increase in the C_{5+} for a Mn promoted Co/SiO_2 catalyst. Furthermore, studies on iron catalyst have shown that pressure has a negligible effect on FTS selectivity (Botes et al. 2013; Dry 2004).

Generally in the case of an FT process, the catalyst is reduced in situ with hydrogen, CO or syngas to yield an active catalyst. Several studies have been done to ascertain the effect of pressure during reduction. For example, Hao et al. (2009) observed that catalyst activity decreases with an increase in reduction pressure, and this was attributed to the decrease in the iron carbide content as activation pressure increased. After the catalyst has been reduced, it is introduced to the new environment where syngas is added and it undergoes further speciation. The complexity of iron catalyst speciation during the FT catalyst reduction process has been investigated by many authors using spectroscopic studies (Bukur et al., 1995; O'Brien et al., 1996; Farias et al., 2010; Zamaniyan et al., 2013; Braconnier et al., 2013; Pineau et al., 2006; Colombo et al., 1967; Rao et al., 1996; Bukur et al., 1995; Jozwiak et al., 2007; Ding et al., 2014; Lin et al., 2003). Nevertheless, the literature on low pressure FT synthesis is scarce. However, based on Hao et al. (2009) reduction studies with syngas, low pressure FT runs may presumably increase the catalyst life span.

FT might be expensive when conducted at high pressures. For example, current commercial FT processes operate at 20-40 bars and this makes the process highly complex and expensive to run (Liu et al. 2013; Choi et al. 1997). As a result,

the possibility of lowering the reaction pressure might simplify the process, especially in a small to medium scale Biomass to Liquid process. The kinetics of low operation pressure predict lower CO conversion, and hence lower yields, and this may not be a viable move from an industrial point of view (Ma et al. 2014). The main objective of this work was to experimentally explore the behaviour of low pressure on catalyst reduced with different gases in FT synthesis. This can be useful in process down-scaling and cost reduction as the operation will be at almost ambient pressure. Currently, no studies investigating simultaneously the influence of three reducing agents (syngas, H_2 and CO) at almost ambient pressure have been reported. The current study performed FT synthesis at 1 bar gauge, a value which is far below the normal FT runs at 20–40 bars in an attempt to achieve a less expensive process.

5.2 Experimental

5.2.1 Catalyst and catalyst reduction

FTS experiments were performed with three differently reduced catalysts in three different fixed bed reactors. One gram of the iron based catalyst was loaded in each of the three reactors. Three kinds of reducing agents (Syngas, H_2, and CO) were used for the catalyst reduction in these three reactors, respectively: syngas for the catalyst reduction of reactor 1 (Reac -Syn), H_2 for that of reactor 2 (Reac - H_2) and CO for that of reactor 3 (Reac – CO).

Before catalyst reduction, the catalyst in each of the reactors was dried under the flow of nitrogen at 60 mL(NTP)/min, at the temperature of 120 °C, and at atmospheric pressure, for 2 hours, to get rid of the moisture which might have accumulated during catalyst loading.

The temperature was increased from 120 (drying temperature) to 250 °C (reduction temperature) at a heating rate of 1 °C/min. All the reactors were left at 250 ^{o}C in the atmosphere of reducing agents for 48 hours prior to running the FT reaction.

5.2.2 FT synthesis

After reduction, Reac-syn (syngas reduced) was maintained at the same temperature and flow rate but the pressure was increased from atmosphere to 1 bar gauge for FT synthesis (FTS) run. The temperature of Reac-H_2 and Reac-CO (reduced by hydrogen and carbon monoxide respectively) was reduced to 100 °C before introducing syngas feed so as to avoid any temperature runaways once the FTS reaction was initiated. Similarly, the pressure of Reac-H_2 and Reac-CO was increased from atmospheric to 1 bar gauge (2 bar absolute) and the temperature was raised gradually from 100 ^{o}C to 250 °C. The FTS experiments were carried out under the reaction conditions for 1000 hours of time on stream (TOS) without changing the operating conditions for all three reactors. A summary of the operating conditions used during our FT experiments is shown in the **Table 5.1**.

Table 5.1: Summary of experimental conditions for FTS for differently reduced iron based catalysts

	Reac-Syn	**Reac-H_2**	**Reac-CO**
Reducing gas	Syngas	Hydrogen	Carbon monoxide
Catalyst weight (gauge)	1	1	1
Temperature (°C)	250	250	250
Flowrate mL(NTP)/min	60	60	60
Pressure (bar gauge)	1	1	1

5.3 Results

5.3.1 CO (gas) conversion

The CO (gas) conversions of the FT reactions for the three differently reduced reactors (Reac-Syn, Reac-H_2 and Reac-CO) were measured against the TOS for

1000 hours. The results from the effects of reducing gases were compared in Figure 1. The Reac-syn showed a sharp initial increase in the CO conversion, whereas the magnitude of this spike was not that pronounced in the Reac-H_2 and Reac-CO tests. This initial sharp increase can be attributed to the increase in the reactant partial pressures as the reactor pressure was increased from ambient to 1 bar gauge during transition from the reduction to reaction period, and probably due to the saturation of the active sites as the liquid products are still building up in the catalyst pores. As a result, the reaction at this stage was probably not diffusion controlled through the liquid, as reported by Rytter and Lualdi ((Rytter et al. (2007); (Lualdi et al. 2011a)), through the liquid. The difference in the catalyst activity shown in **Figure 5.1** was only apparent at the initial stages of 150 hours after the syngas was introduced to Reac-H_2 and Reac-CO, as opposed to Reac-syn where the syngas was kept flowing through the catalyst from the reduction process. In this case, the steady state was then reached after about 150 hours of time on stream (TOS) when all the reactors in the system have reached a period having the same reaction rate.

It is evident from **Figure 5.1** that the long term CO conversion from the differently reduced catalysts attained the same value of about 14.5% (14.5% is the steady state conversion) under the reaction conditions investigated for 1000 hours TOS. The Reac-Syn does seem slightly higher but this difference is small enough not to be sure that it is a real effect.

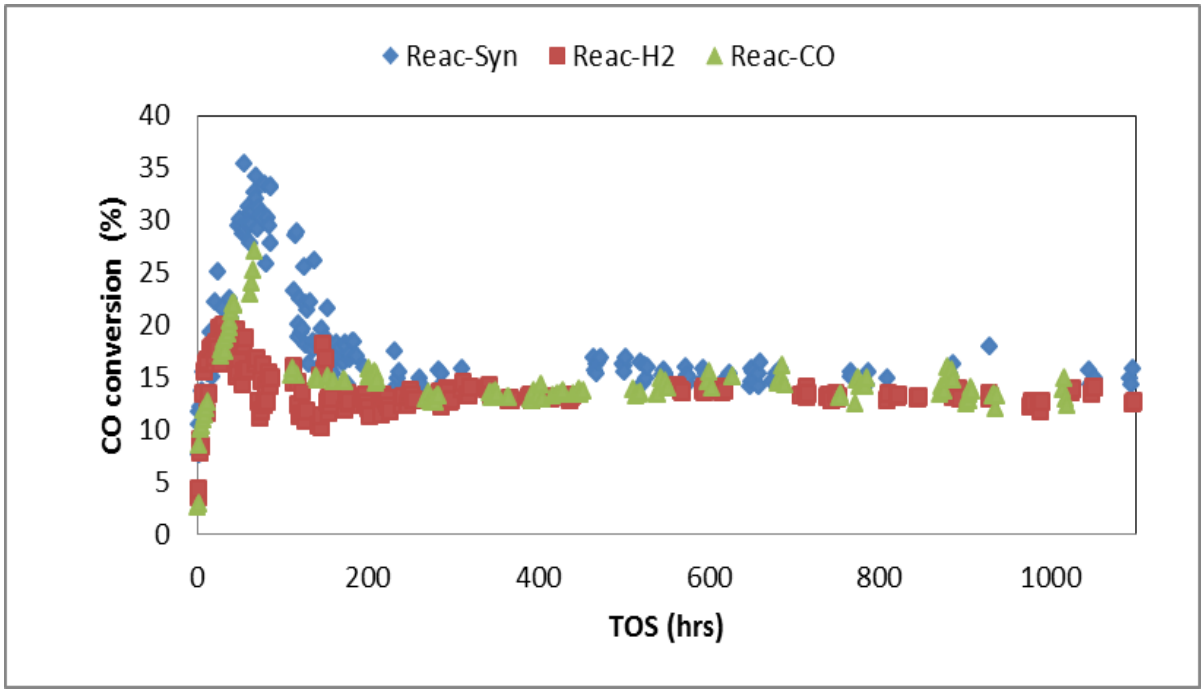

Figure 5.1: Influence of reducing gases (syngas, hydrogen and carbon monoxide) on the catalyst stability (CO conversion) under the FT reaction conditions: 250 ᴰC, 1 bar (gauge), 60 mL(NTP)/min and mass of the catalyst of 1 g.

5.3.2 Effects of low pressure on reactant consumption rates

5.3.2.1 Reactant and FT rates at 1 bar gauge reactor pressure

The effect of reducing gases (syngas, hydrogen and carbon monoxide) on the activity of the Fe catalyst during FT synthesis was determined for the period of 1000 hours TOS. The results for the CO consumption rates were compared and are presented in **Figure 5.2**.

The Reac-syn displayed an initial increase in terms of the reaction rate at the beginning of the FT reaction for about 150 hours from exposure to the synthesis gas, reaching a CO consumption rate of 2.64×10^{-4} mol/min/.gcat. On the other hand, the Reac-H_2 and Reac-CO reduced showed an increase but with a lesser magnitude, followed by a gradual decrease in activity. The initial increase in the rate may be attributed to a high initial activity of the catalyst when the catalyst

surfaces are still fresh, while the steady state rate of 1.173×10^{-4} mol/min/.gcat was attained after approximately 150 hours. This observed phenomenon signifies that, irrespective of the reducing agent used, effectively the same overall reaction rate is eventually achieved.

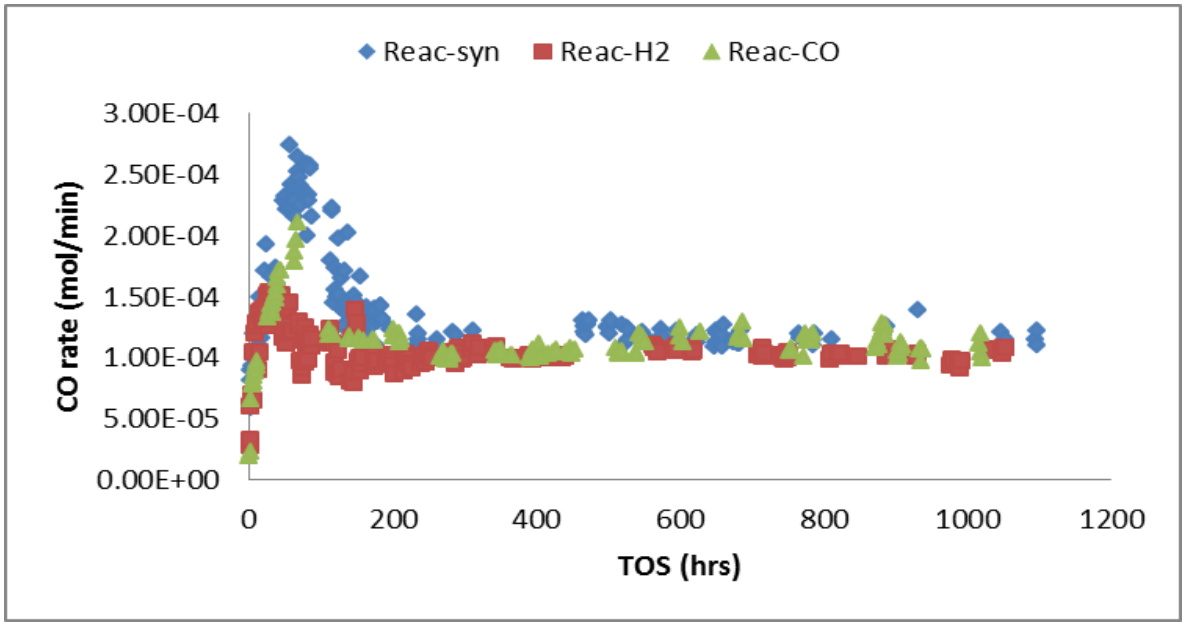

Figure 5.2: Influence of reducing gases: CO consumption rate versus time on stream at 1 bar gauge and 250 °C.

The effect of the three reducing agents in the form of syngas, hydrogen and carbon monoxide on the FT rate ($\curlyvee CO$ – $\curlyvee CO_2$) was also measured and the results are shown in Figure 5.3.

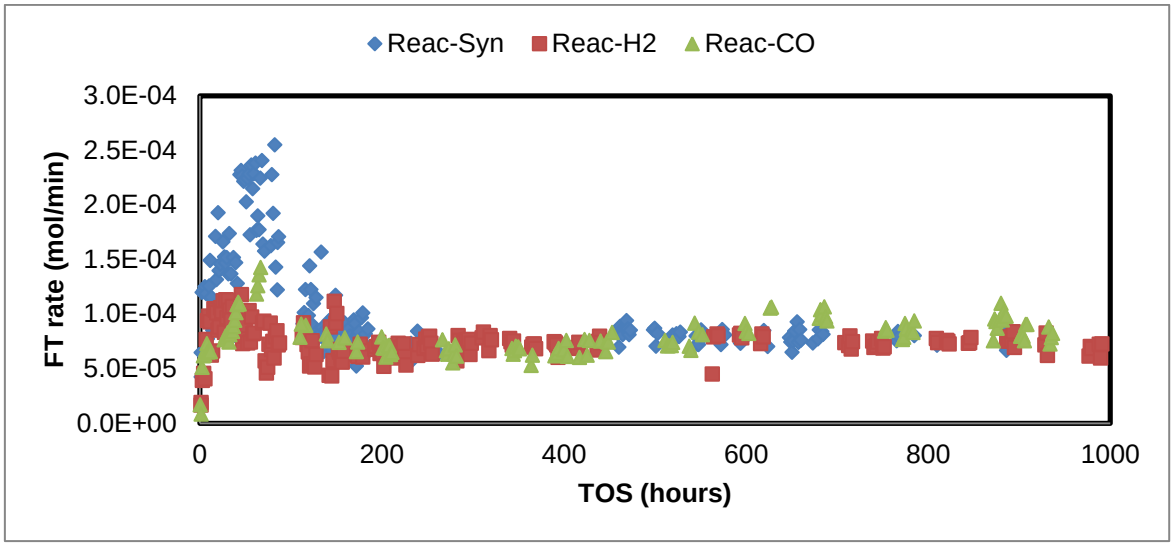

Figure 5.3: Influence of reducing gases on FT rate ($\curlyvee$CO – $\curlyvee CO_2$): FT rate versus time on stream at 1 bar gauge and 250 °C.

The FT selectivity (defined by equation 5.1) of the differently reduced catalysts recorded at steady state operation for the three reactors were approximately the same. Taking into account the experimental error of ±5%, no significant difference was observed in terms of the selectivity.

$$\text{FT selectivity} = \frac{\curlyvee CO - \curlyvee CO2}{\curlyvee CO} \qquad (5.1)$$

Where $\curlyvee CO$ is the rate of CO consumption and $\curlyvee CO2$ is the rate of CO_2 accumulation

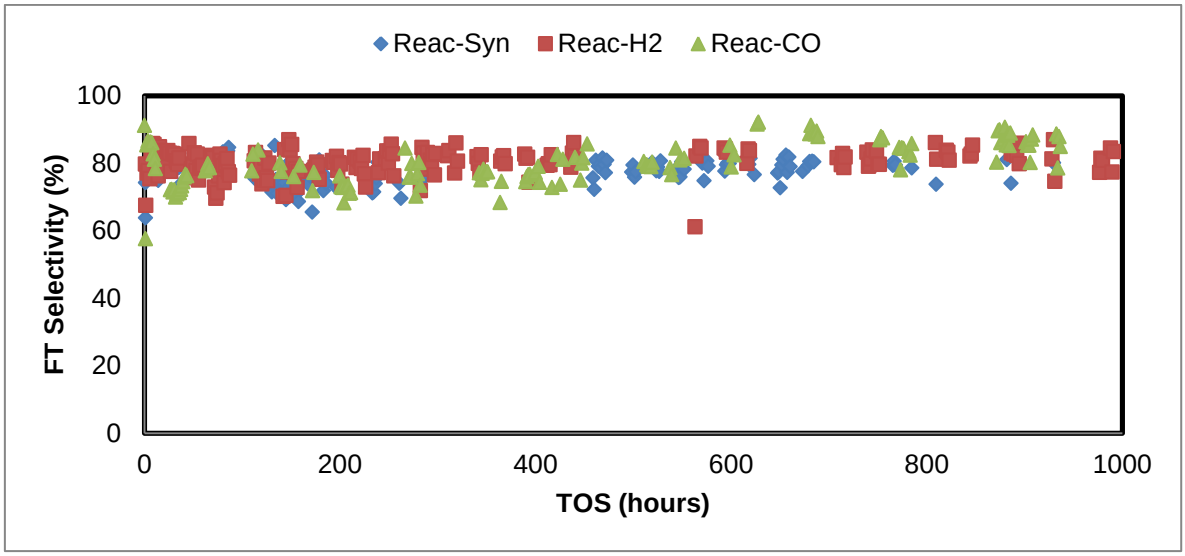

Figure 5.4: Fischer Tropsch selectivity for the three differently reduced catalysts

The FT selectivity did not show any change from the startup and from this observation it can be inferred that the ratio of $\gamma CO_2/\gamma CO$ is a constant regardless of the actual change in the overall reaction rate of CO and H_2. This suggests that when the consumption rate of the reactants spikes and decreases, both the FT reaction rate and water gas shift reaction rate respond accordingly.

5.3.2.2 Methane and carbon dioxide formation rates

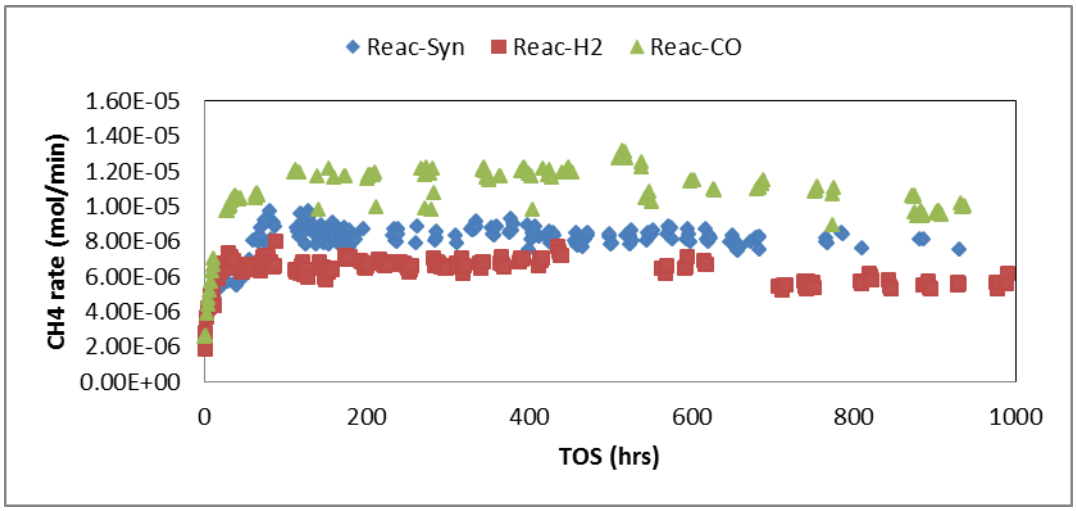

Figure 5.5: Influence of reducing agents on methane production rate (at 250 °C, 1 bar gauge, 60 (NTP)mL/min and mcat = 1 g)

Methane and carbon dioxide formation rates were calculated for the three reactors and the results are shown in **Figure 5.5** and **Figure 5.6**, respectively. It is noticeable that the Reac-CO had a higher methane production rate, followed by the Reac-syn, and lastly the React-H_2. This observed trend was maintained for long TOS and no initial spikes were observed, which is very different from the overall reaction rate as shown in **Figure 5.1**.

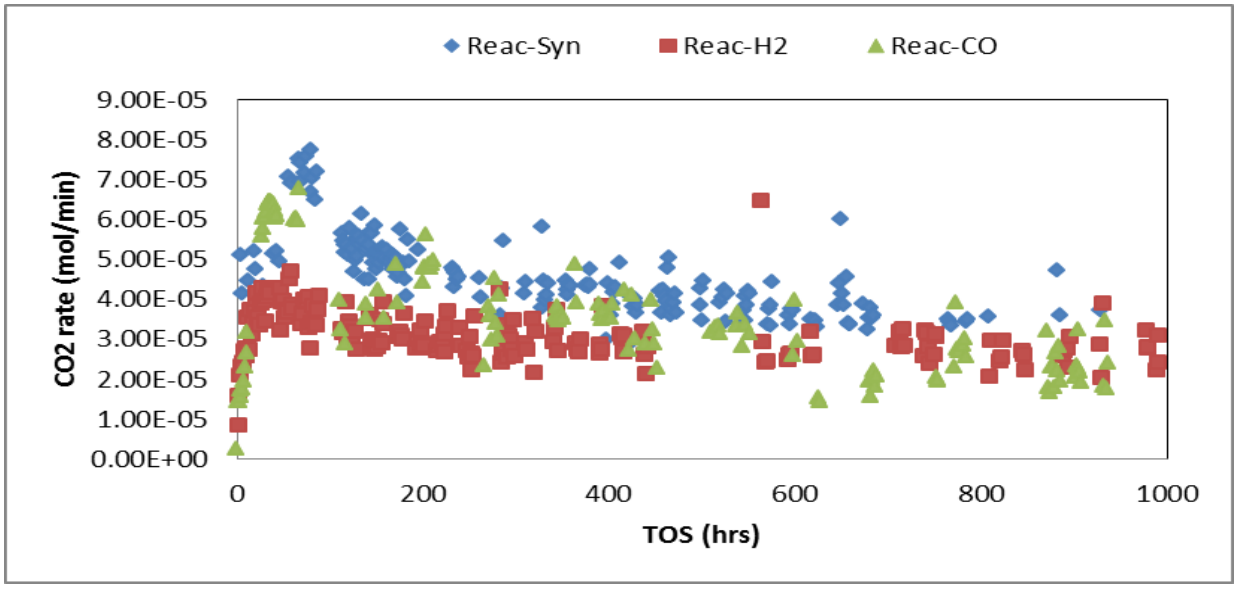

Figure 5.5: Influence of reducing agents on CO_2 production rate (at 250 °C, 1 bar gauge, 60 mL/min and mcat = 1 g)

Figure 5.6 shows the influence of reducing gases on CO_2 production rates in the first 1000 hours. It shows that reducing iron oxide with hydrogen appears to produce less carbon dioxide than syngas and carbon monoxide during startup. But the trends are not that clearly conclusive at long TOS. The γCO_2 followed a similar pattern as the γCO. This indicates that reducing gases did not to give rise to a major difference in CO_2 production rates. It is noted that the CO_2 rates showed similar spikes at early TOS, which corresponds to the overall reaction rate. When looking at the formation rates for the products reported in this work, it is clear that the high reaction rate of the reactant mainly resulted from high CO_2 formation rates and not of other products. CH_4 and CO_2 are gases which are generally undesired products in a FT synthesis process that aims to maximize the reactant conversion to valuable hydrocarbon. The results, graphed in Figures 5.5 and 5.6, indicate that reducing agents have significant influence on the production of these undesirable products under the reaction conditions implemented in this study.

5.3.2.3 Olefin formation rates

The olefin (C_2 to C_5) product formation rates were also measured to see if reducing gases affect their distribution and the results are illustrated in **Figure 5.7** (a-d).

Figure 5.7a shows the olefin (ethylene) formation rate as a function of time on stream of 1000 hours. From **Figure 5.7a**, it is shown that for all three different reducing agents, the formation rate experienced an initial spike for the first 150 hours. The ethylene formation trends were similar to the CO conversion trend observed in **Figure 5.1**, while the other olefin formation rates obtained in the experiments showed similar behavior to that of CH_4. This may suggest that the formation rates of hydrocarbons other than C_2H_4 is not linked to the overall reaction rate. The results (**Figure 5.7 a-d**) show that Reac-CO (reactor reduced with carbon monoxide) produces more olefins than Reac-Syn and Reac-H_2 throughout the experiment.

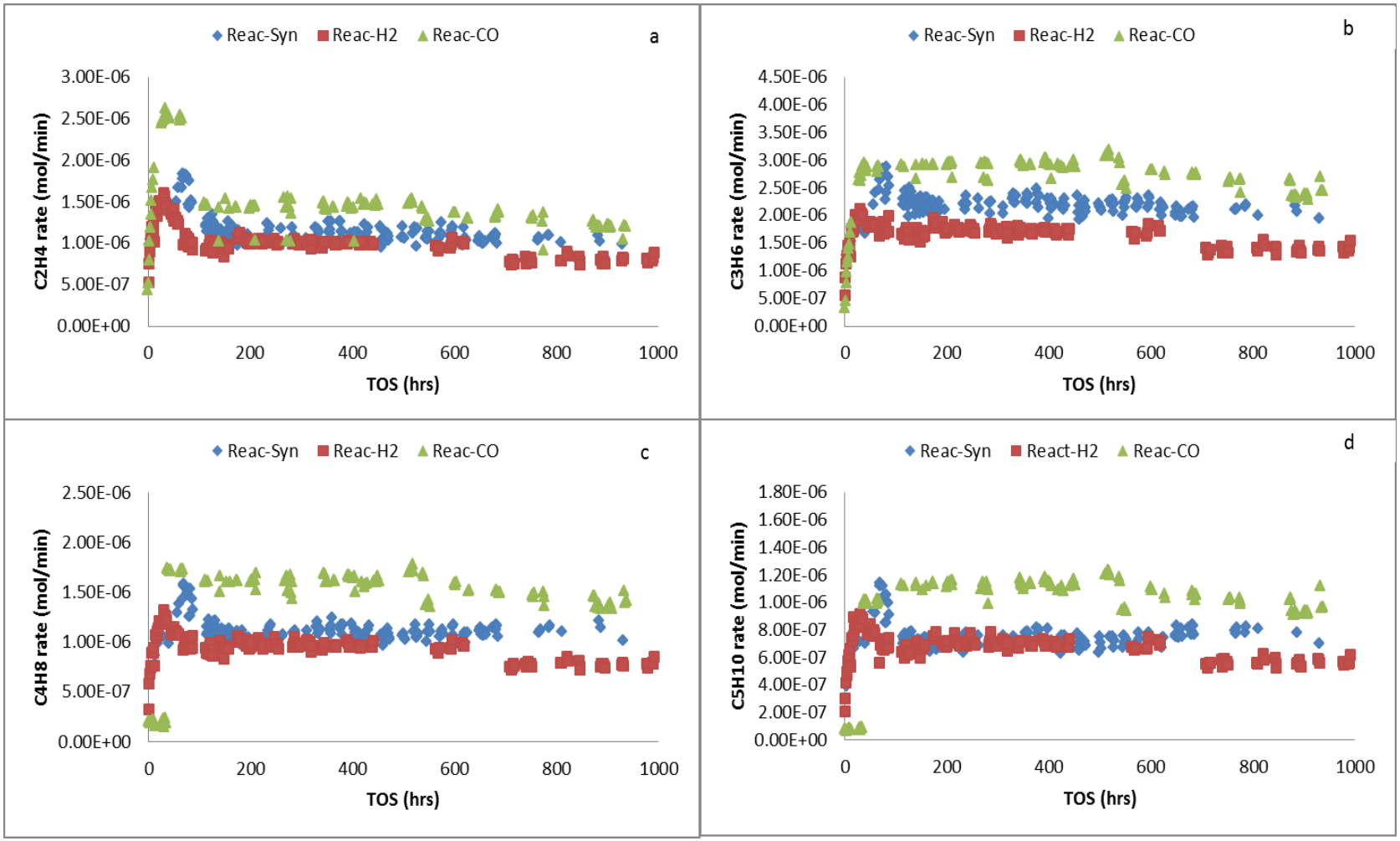

Figure 5.7: Olefin production rate against time on stream under the following conditions: 250 °C, 1 bar gauge, 60 mL(NTP)/min and mass of catalyst 1 g

The Reac-Syn and Reac-H_2 gave almost the same olefin formation rates with graphs in **Figure 5.7a-d** superimposed on each other for about 650 hours TOS. From 650 hours onwards the Reac-H_2 experienced a drop in the formation rate.

5.3.2.4 Paraffin formation rates

The paraffin (C_2 to C_5) product formation rates were also determined as a function of time on stream, and the graphs are displayed in **Figure 5.8** (a-d).

The figures show the variation of paraffin formation rates for the differently reduced reactors. The syngas reduced reactor (Reac-Syn) tends to be more inclined to the formation of paraffins. A similar trend is observed for C_2, C_3 and C_5 with an anomaly for C_4 where Reac-H_2 comparatively produced more C_4 paraffin followed by Reac-Syn and lastly Reac-CO.

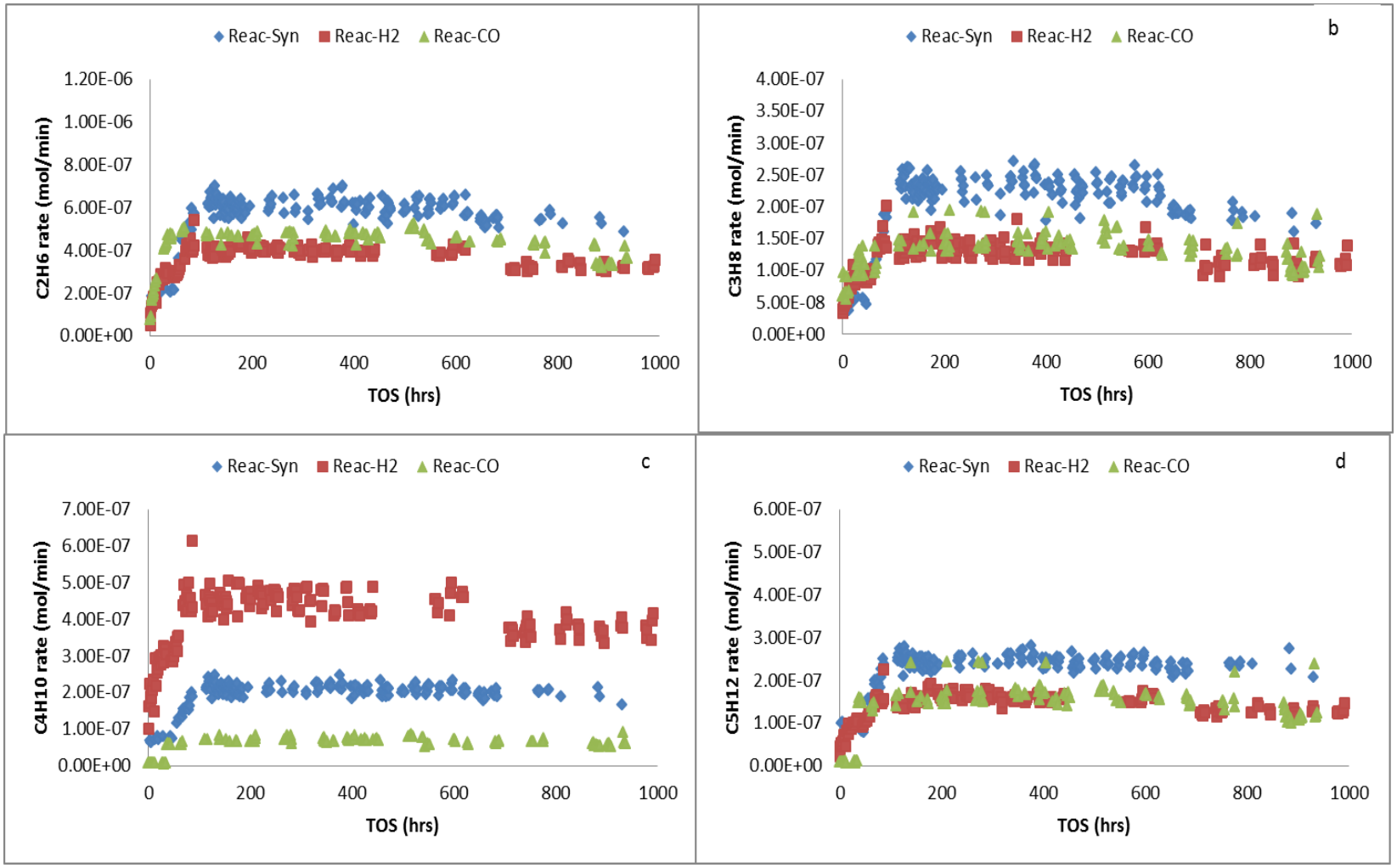

Figure 5.8: Paraffin production rate against time on stream under the following conditions: 250 °C, 1 bar gauge, 60 mL(NTP)/min and mass of catalyst 1 g

For all three reducing agents, the rate patterns increased gradually with time on stream for about 90 hours, where they attained an almost stable state for 1000 hours. However, after 90 hours of TOS, the difference in the magnitude of the formation rate of paraffins becomes more pronounced (start to differ).

The olefin formation rates (average data) as a function of carbon number were also analysed, and the results are shown in **Figure 5.9**. It is clear from Figure that Reac-CO (iron CO reduced) produced more olefins (C_2 to C_5), followed by Reac-Syn (iron syngas reduced) and Reac-H_2 (iron hydrogen reduced). In terms of the carbon number, propylene appeared to be the dominant form of olefin, followed by ethylene, butene and pentene. It is known that some of the pentene might be found in the liquid phase product, so this might explain the lesser amount recorded for pentene in the gas phase

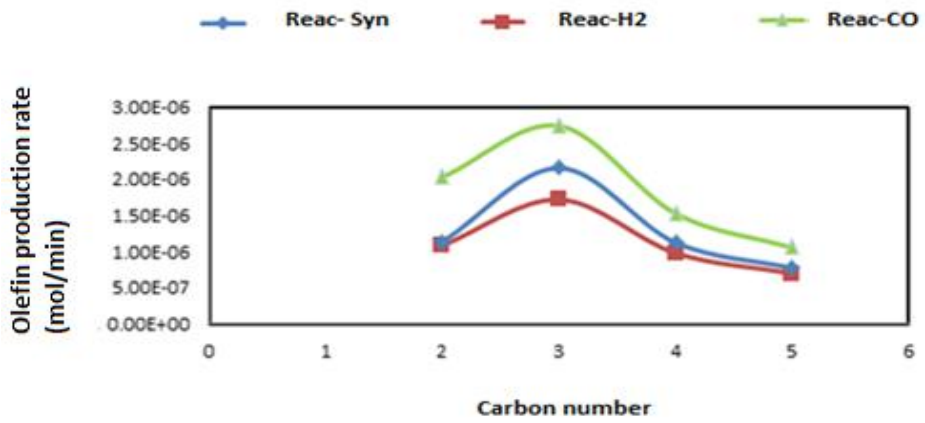

Figure 5.9: Effect of reducing agents (syngas, hydrogen and carbon monoxide) on the average steady state olefin production rate against carbon number for three differently reduced reactors (at 250 °C, 1 bar gauge, 60 (NTP)mL/min and mcat = 1 g)

In summary, the differently reduced catalyst displayed significant initial increase of the olefin (C_2 to C_5) production rate, and then decreased before reaching an almost stable formation rate. The olefin production rate was significantly higher for Reac-CO for all the hydrocarbons (from C_2-C_5), followed by the Reac-Syn and lastly the Reac-H_2. On the other hand, the production rate of the olefin increased

initially with increase in carbon number (from C_2 to C_3) and then decreased from C_3 to C_5 as shown in **Figures 5.9**. For such results, it is reported in the literature that factors such as reactivity, diffusivity and component size might cause the trend observed (Fiore et al. 2004a).

The effect of reducing agents (syngas, hydrogen and carbon monoxide) on the paraffin (C_2 to C_5) was also determined as a function of carbon number (see **Figure 5.10**), in a similar manner to the olefins. The results show that the paraffin production rate Reac-CO and Reac-syn followed a similar pattern with Reac-H_2 displaying a sigmoidal pattern. The observed trend here is the opposite of what was observed in the olefin production rates, where the rates increased from C_2 to C_3. This behaviour could be attributed to the hydrogenation extent of the olefins (Fiore et al. 2004b). An anomaly is observed in the hydrogen reduced reactor where a cyclic pattern is observed. The results are not conclusive as to which reducing agent gave rise to a high production. However, Reac-H_2 produced more butane than the other two reactors, whereas Reac-CO produced more ethylene and Reac-Syn more propane and pentane.

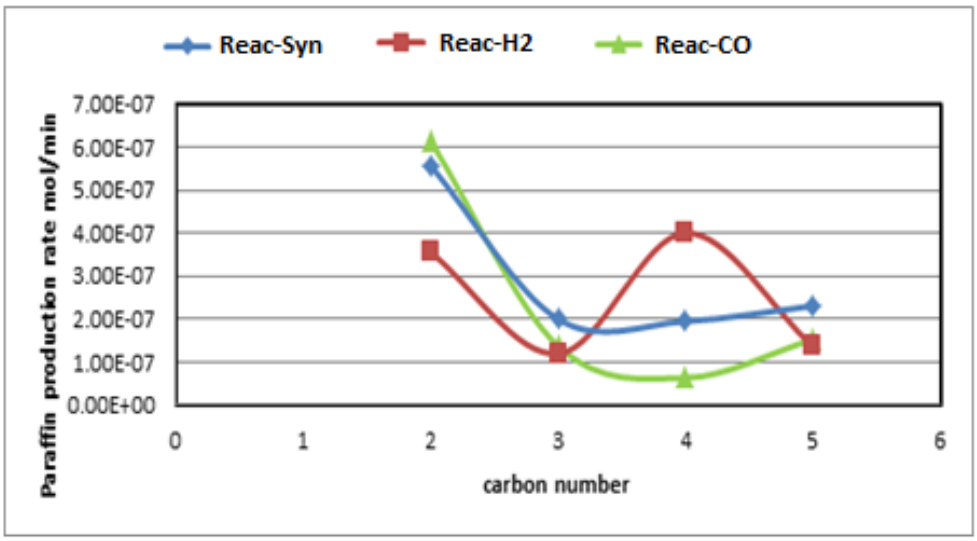

Figure 5.10: Effect of reducing agents (syngas, hydrogen and carbon monoxide) on the average steady state paraffin formation rates as a function of

carbon number under the following conditions: 250 °C, 1 bar gauge, 60 (NTP) mL/min and mass of catalyst 1 g

5.3.3 Product selectivity

The selectivities of the FT products obtained during the present experiments were calculated and are summarized in **Table 5.2**. Although the activity of FT based on the three reducing agents is similar (see **Figure 5.2**), the product formation rates are different (see **Figures 5.7** and **5.8**). From **Table 5.2** it is evident that Reac-Syn (syngas reduced reactor) reveals the lowest methane selectivity, and Reac-H_2 (hydrogen reduced) reveals the lowest selectivity to carbon dioxide. Reac-CO (which has the CO reduced catalyst), has the highest selectivity to methane, and Reac-Syn, has the highest CO_2 selectivity.

To get some insight into the product distribution, the selectivities of the differently reduced catalyst were calculated using the equation below, and the percentages are provided in **Table 5.2**.

Equation 5.2 was used for the determination of selectivity of the products.

$$Sel\ (\theta) = \frac{[nC]_\theta}{-r_{co} \times t \times m_{cat}} \qquad (5.2)$$

where:

$Sel\ (\theta)$ represents the selectivity of product θ and $[nC]_\theta$ represents the moles of carbon contained in the product θ.

Table 5.2: Selectivity to FT products for different catalyst reducing agents

Reducing agent	% Selectivity									
	CO_2	CH_4	C_2H_4	C_2H_6	C_3H_6	C_3H_8	C_4H_8	C_4H_{10}	C_5H_{10}	C_5H_{12}
Reac-Syn	21.41	7.02	1.82	0.96	5.45	0.50	3.93	0.68	3.48	1.01
Reac-H_2	19.38	6.52	1.94	0.78	5.04	0.40	3.75	1.71	3.40	0.78

Reac-CO	19.02	10.16	2.45	0.81	7.50	0.38	5.59	0.23	4.86	0.71

The results tabulated are the calculated averages at steady state under the reaction conditions (1 bar, 250 °C). The results show that product selectivity is greatly influenced by the reducing gases. Reducing with different reducing gases resulted in catalysts with different selectivities to FT products. CO_2 values are very high, and this is attributed to the WGS reaction. The syngas reduced reactor showed comparatively a higher selectivity to CO_2 than the hydrogen and carbon monoxide reduced reactor. The CO_2 selectivity is basically the amount of the carbon atoms in the feed that is converted to CO_2 as the final product.

The selectivities to CO_2 and CH_4 were found to be high in all the reactors and lower figures were obtained for C_2-C_5 hydrocarbon selectivity, and the trends observed for C_2-C_5 selectivity for the three differently reduced reactors were similar. The CO reduced reactor showed comparatively high selectivities to methane ((%CO converted to CH_4)/(%CO converted to products other than CO_2)) followed by the syngas and lastly the hydrogen reduced reactor. Methane selectivities of the three reactors showed a gradual increase (**Figure 5.5**). These data might be taken to suggest that methane selectivity is low on iron oxides, and is higher on carbided catalysts. The difference was observed in the product formation rates, as illustrated in **Figures 5.7** and **5.8.**

5.3.4 **Olefin to paraffin ratio**

The olefin to paraffin ratio (O/P ratio) as a function of time on stream (TOS) was calculated and the results are depicted in **Figure 5.11** (a-d). As a general trend, reducing with CO yielded the most active catalyst in terms of olefin production. A common and intriguing feature is that all differently reduced catalysts seemed to attain stability after about 150 hours on stream. Anomalous behaviour was observed for the CO reduced catalyst for C_4 hydrocarbons where the magnitude of the ratio was out of line with the results for the other hydrocarbons.

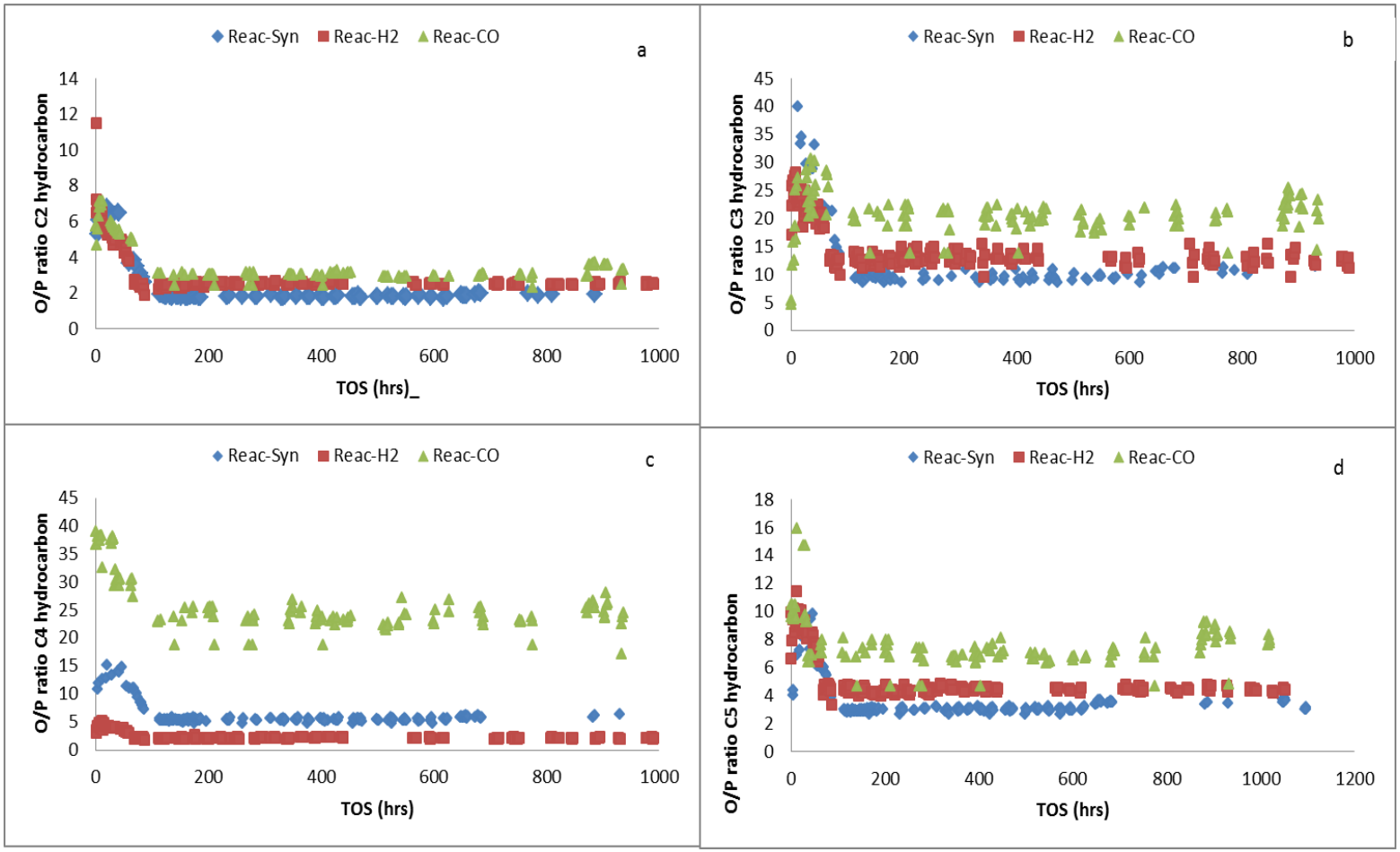

Figure 5.11: Effect of reducing agents (syngas, hydrogen and carbon monoxide) on the olefin to paraffin ratio as a function of time on stream: (a) for (O_2/P_2), (b) for (O_3/P_3), (c) for (O_4/P_4) and (d) for (O_5/P_5) under the following conditions: 250°C, 1 bar gauge, 60 mL/min and mass of catalyst 1 g. O: olefin, P: paraffin and carbon number n: 2,3,4 and 5. 5.

5.4 Discussion

The different level of activity of the catalysts was investigated in this study. From **Figure 5.1**, it is clear that the initial activities (over 150 hours) of these catalysts differ. The Reac-Syn (syngas reduced one) had the highest initial activity and the Reac-H_2 the lowest. Based on the thermodynamic analysis of the phase changes during reduction with H_2, CO, and syngas, and the results reported in the literature, the H_2 reduced Fe catalyst will in the first instance form mainly Fe_3O_4 and alpha-Fe (D. B. Bukur et al. 1995; Shroff et al. 1995; van der Kraan, Boellaard, and Crajé 1993; De Smit E. and Weckhuysen B.M. 2008). The activity of the Fe_3O_4 and α-Fe is reported lower when compared to FexCy. Therefore, a lower initial activity for the Reac-H_2 is understandable as the extent of reaction increase as the catalyst is being carburised. When syngas and CO are used during the reduction stage, FexCy will form predominantly (Rochet et al. 2011; Pham et al. 2015; Dumesic and Topsøe 1977). The presence of H_2 in the syngas tends to facilitate the formation of Fe_3O_4 due to its comparatively high diffusivity value and the carburisation of F_3O_4 by CO to iron carbides is a thermodynamically favoured process (Hallac et al. 2015; Mogalicherla and Elbashir 2011; A. Zamaniyan et al. 2013; Lualdi et al. 2011b). However, FexCy will be the main active phases for the CO and syngas reduced catalyst in this study. In this study, the high initial activity of the CO and syngas reduced catalysts can be attributed due to the FexCy formed during the reduction stage. It is also evident from the results that the activity of the CO reduced catalyst was slightly lower than the syngas reduced one. This may be attributed to two possible reasons. The first reason for the low activity may be that the number of active sites and the activity of these active sites may be different, and hence the CO reduced catalyst gave rise to a lower activity. The second possible explanation is linked to the effect of the product on the activity of the catalysts, should the intrinsic activities of these two reduced catalysts be close to each other. The FT reaction has taken place during the reduction stage when syngas was used. At this stage, presumably both long chain hydrocarbons and water built up slowly on the catalyst to form a layer or coating. A different composition of such a liquid layer could decide the overall activity of the catalyst, due to the slowing down of transportation of the reactants and the products.

Although the three catalysts presented different initial activity, the reaction rates of the three were close to each other after attaining the steady state. There are two important aspects to note for such change, firstly, the change itself, and secondly the levels where the rates are after the change. The change itself is arguably linked to the active phase change of the catalyst or the mass transfer limitation due to build-up of the products (Lu et al. 2011). Lu et al. [2011] reported that the liquid deposition decreased the reaction rate of a TiO_2 supported cobalt catalyst to a large extent. Their flushing experiments prove that once the liquid layer has been removed from the catalyst surface, the activity of the catalyst could be returned to that when the catalyst was freshly loaded (the initial activity). The different active sites could have resulted in similar reaction rates. This suggests that the limitation for the reaction rate lies in some common factor. The researcher believes this common limitation may be because of the mass transfer of the reactants.

The difference in the product selectivity supports this point of view. Although the reaction rates are similar, the product selectivities are quite different as shown in **Table 5.1**. The Reac-CO gives the highest selectivities to olefins and the Reac-H_2 gives the least. Once the operating conditions are the same and the partial pressures of the reactants are close enough, the different product selectivities are mainly caused by the different active sites of the Fe catalyst. FexCy has been reported as the most active phase in the Fe catalyst and it promotes the formation of olefins. This matches the results obtained in the present work. The Reac-CO obtained FexCy as the predominant active phase after reduction, and the Reac-H_2 obtained the least active phases. Therefore, one should expect a higher reaction rate for the Reac-CO and a lower rate for the Reac-H_2. This is true at the initial stage but not true when the initial stage has passed (as has been discussed above). This therefore suggests that the limitation for the reaction rate is because of the mass transfer limitation.

It is also noticeable that the formation rates of paraffins on these differently reduced Fe catalysts have shown an interesting behaviour. For C_2, C_3, and C_5 paraffins, the Reac-CO and Reac-syn have given similar results and the Reac-H_2 resulted in a higher rate.

This suggests that the Reac-H_2 (with Fe_3O_4 and α-Fe) promoted the hydrogenation of the primary products, olefins. For the C_4H_{10}, these three catalysts have given entirely different results when compared to the other paraffins. Although the Reac-H_2 reduced catalyst still gives the highest activity to C_4H_{10}, it is much higher than the other two catalysts. This is quite different from the other paraffins. In the meantime the syngas reduced one also gives a much higher C_4H_{10}. The researcher is not sure about these abnormal results, but they may suggest that the formation of C_4 is promoted by the combination of two C_2, especially on the H_2 reduced Fe catalyst.

When one looks at the results as a whole it appears surprising that after so long (a 1000 hours) that the three catalysts show different selectivity behaviour. We know that the syngas is active as a reducing agent and irrespective of the initial reduction method all the catalysts are in contact with this same reducing gas. Thus after the initial period (about 150 hours) when different slow solid state reactions might be taking place, the overall reaction rates become constant and one might surmise that all the solids are the same. Clearly this is not the case and one might ask why.

Now it is known (Lu et al (2011)) that a surface layer of liquid slowly builds up during a period of the order of 150 hours and because the rates are different during this period the liquid layer formed may be different in the three cases. If it is this liquid layer in contact with the solid surface that to some extent determines the solid composition one might surmise that the three systems maintain their different liquid compositions and hence different solid compositions and hence different selectivities.

It is important to note that the catalyst used in this work is a commercial catalyst with the right dimensions to be used for fixed reactors and the operation conditions chosen are to be used in the low pressure FTS in a waste to liquid processes. Therefore, the results obtained in this work are of great importance for the design of such processes.

5.5 Conclusion

When running three reactors under the same FT conditions for a 1000 h, the results obtained indicate that the initial use of different reducing agents (Syngas, CO and H_2) does not have a large impact on the long term catalyst activity but does have an impact on long term selectivity. The experimental data demonstrated that the three reactors stabilize to about the same overall conversion of CO (reactivity) after about 150 hours; however, somewhat surprisingly, the selectivities in the three reactors are not the same.

Methane selectivity showed the following trend, Carbon monoxide reduced > Syngas reduced > Hydrogen reduced. Methane selectivities of hydrogen reduced catalysts were significantly lower than those on the CO and syngas activated catalysts. Reducing with CO gives much more olefins than reducing with syngas and H_2. The paraffin production rates are much more complicated with in particular C_4 being particularly anomalous for the H_2 reduced catalyst.

Thus in conclusion while the rates after the initial period for all three reduction methods are essentially the same, the selectivity behaviour of the differently reduced catalysts are different and there does not seem to be a simple explanation for the behaviour. In some way the different initial behaviour seems to be carried over into the selectivity but not the overall rate.

References

Botes, F.G., J.W. Niemantsverdriet, and J. van de Loosdrecht. 2013. “A Comparison of Cobalt and Iron Based Slurry Phase Fischer–Tropsch Synthesis.” *Catalysis and Synthetic Fuels: State of the Art and Outlook* 215 (October): 112–20. doi:10.1016/j.cattod.2013.01.013.

Braconnier, L., E. Landrivon, I. Clémençon, C. Legens, F. Diehl, and Y. Schuurman. 2013. “How Does Activation Affect the Cobalt Crystallographic Structure? An in Situ XRD and Magnetic Study.” *Catalysis Today*, Catalysis and synthetic fuels: state of the art and outlook, 215 (October): 18–23. doi:10.1016/j.cattod.2013.02.021.

Bukur, D. B., K. Okabe, M. P. Rosynek, C. P. Li, D. J. Wang, K. R. P. M. Rao, and G. P. Huffman. 1995. “Activation Studies with a Precipitated Iron Catalyst for Fischer-Tropsch Synthesis: I. Characterization Studies.” *Journal of Catalysis* 155 (2): 353–65. doi:10.1006/jcat.1995.1217.

Bukur, D.B., S.A. Patel, and X. Lang. 1990. “Fixed Bed and Slurry Reactor Studies of Fischer-Tropsch Synthesis on Precipitated Iron Catalyst.” *Applied Catalysis* 61 (1): 329–49. doi:10.1016/S0166-9834(00)82154-5.

Bukur, Dragomir B., Manoj Koranne, Xiaosu Lang, K. R. P. M. Rao, and Gerald P. Huffman. 1995. “Pretreatment Effect Studies with a Precipitated Iron Fischer-Tropsch Catalyst.” *Applied Catalysis A: General* 126 (1): 85–113. doi:10.1016/0926-860X(95)00020-8.

Choi, G.N., S.J. Kramer, S.S. Tam, and J.M. Fox III. 1997. “Design and Economics of a Fischer-Tropsch Plant for Converting Natural Gas to Liquid Transportation Fuels.” *ACS Division of Fuel Chemistry, Preprints* 42 (2): 667–70.

Colombo, U, F Gazzarrini, and G Lanzavecchia. 1967. “Mechanisms of Iron Oxides Reduction at Temperatures below 400°C.” *Materials Science and Engineering* 2 (3): 125–35. doi:10.1016/0025-5416(67)90030-4.

De Smit E., and Weckhuysen B.M. 2008. “The Renaissance of Iron-Based Fischer-Tropsch Synthesis: On the Multifaceted Catalyst Deactivation Behaviour.” *Chemical Society Reviews* 37 (12): 2758–81. doi:10.1039/b805427d.

Ding, Mingyue, Yong Yang, Baoshan Wu, Yongwang Li, Tiejun Wang, and Longlong Ma. 2014. “Study on Reduction and Carburization Behaviors of Iron-Based Fischer-Tropsch Synthesis Catalyst.” *Energy Procedia*, International Conference on Applied Energy, ICAE2014, 61: 2267–70. doi:10.1016/j.egypro.2014.12.444.

Dinse, Arne, Max Aigner, Markus Ulbrich, Gregory R. Johnson, and Alexis T. Bell. 2012. “Effects of Mn Promotion on the Activity and Selectivity of Co/SiO2 for Fischer–Tropsch Synthesis.” *Journal of Catalysis* 288 (April): 104–14. doi:10.1016/j.jcat.2012.01.008.

Donnelly, Timothy J., and Charles N. Satterfield. 1989. “Product Distributions of the Fischer-Tropsch Synthesis on Precipitated Iron Catalysts.” *Applied Catalysis* 52 (1): 93–114. doi:10.1016/S0166-9834(00)83375-8.

Dry, M.E. 2004. “Chapter 3 - Chemical Concepts Used for Engineering Purposes.” In *Studies in Surface Science and Catalysis*, edited by André Steynberg and Mark Dry, Volume 152:196–257. Elsevier. http://www.sciencedirect.com/science/article/pii/S0167299104804609.

Dumesic, J.A., and H. Topsøe. 1977. *Mössbauer Spectroscopy Applications to Heterogeneous Catalysis*. Vol. 26. Advances in Catalysis. http://www.scopus.com/inward/record.url?eid=2-s2.0-0001279329&partnerID=40&md5=febb6d1a2d0644b67e3bedffc9d8dab5.

Farias, F. E. M., F. a. N. Fernandes, and F. G. Sales. 2010. “Effect of Operating Conditions on Fischer-Tropsch Liquid Products Produced by Unpromoted and Potassium-Promoted Iron Catalyst.” *Latin American Applied Research* 40 (2): 161–66.

Fiore, F., L. Lietti, G. Pederzani, E. Tronconi, R. Zennaro, and P. Forzatti. 2004a. “Reactivity of Paraffins, Olefins and Alcohols during Fischer-Tropsch Synthesis on a Co/Al_2O_3 Catalyst.” In *Studies in Surface Science and Catalysis*, edited by Xinhe Bao and Yide Xu, Volume 147:289–94. Elsevier. http://www.sciencedirect.com/science/article/pii/S0167299104800661.

———. 2004b. “Reactivity of Paraffins, Olefins and Alcohols during Fischer-Tropsch Synthesis on a Co/Al_2O_3 Catalyst.” In *Studies in Surface Science and Catalysis*,

edited by Xinhe Bao and Yide Xu, Volume 147:289–94. Elsevier. http://www.sciencedirect.com/science/article/pii/S0167299104800661.

Hallac, B.B., K. Keyvanloo, J.D. Hedengren, W.C. Hecker, and M.D. Argyle. 2015. “An Optimized Simulation Model for Iron-Based Fischer-Tropsch Catalyst Design: Transfer Limitations as Functions of Operating and Design Conditions.” *Chemical Engineering Journal* 263: 268–79. doi:10.1016/j.cej.2014.10.108.

Hao, Qinglan, Liang Bai, Hongwei Xiang, and Yongwang Li. 2009. “Activation Pressure Studies with an Iron-Based Catalyst for Slurry Fischer-Tropsch Synthesis.” *Journal of Natural Gas Chemistry* 18 (4): 429–35. doi:10.1016/S1003-9953(08)60134-6.

Jozwiak, W.K., E. Kaczmarek, T.P. Maniecki, W. Ignaczak, and W. Maniukiewicz. 2007. “Reduction Behavior of Iron Oxides in Hydrogen and Carbon Monoxide Atmospheres.” *Applied Catalysis A: General* 326 (1): 17–27. doi:10.1016/j.apcata.2007.03.021.

Lin, Hsin-Yu, Yu-Wen Chen, and Chiuping Li. 2003. “The Mechanism of Reduction of Iron Oxide by Hydrogen.” *Thermochimica Acta* 400 (1–2): 61–67. doi:10.1016/S0040-6031(02)00478-1.

Liu, G., E.D. Larson, R.H. Williams, and X. Guo. 2013. “Gasoline from Coal and Biomass with CCS: Performance and Cost Analysis.” In , 3:2007–17. http://www.scopus.com/inward/record.url?eid=2-s2.0-84899022582&partnerID=40&md5=df8fb686072f98b6a531c1c9671916dd.

Lualdi, M., S. Lögdberg, G. Di Carlo, S. Järås, M. Boutonnet, A.M. Venezia, E.A. Blekkan, and A. Holmen. 2011a. “Evidence for Diffusion-Controlled Hydrocarbon Selectivities in the Fischer-Tropsch Synthesis over Cobalt Supported on Ordered Mesoporous Silica.” *Topics in Catalysis* 54 (16-18): 1175–84. doi:10.1007/s11244-011-9739-1.

———. 2011b. “Evidence for Diffusion-Controlled Hydrocarbon Selectivities in the Fischer-Tropsch Synthesis over Cobalt Supported on Ordered Mesoporous Silica.” *Topics in Catalysis* 54 (16-18): 1175–84. doi:10.1007/s11244-011-9739-1.

Lu, X., X. Zhu, D. Hildebrandt, X. Liu, and D. Glasser. 2011. “A New Way to Look at Fischer-Tropsch Synthesis Using Flushing Experiments.” *Industrial and Engineering Chemistry Research* 50 (8): 4359–65. doi:10.1021/ie102095c.

Ma, W., G. Jacobs, T.K. Das, C.M. Masuku, J. Kang, V.R.R. Pendyala, B.H. Davis, J.L.S. Klettlinger, and C.H. Yen. 2014. “Fischer-Tropsch Synthesis: Kinetics and Water Effect on Methane Formation over 25%Co/γ-Al2O3 Catalyst.” *Industrial and Engineering Chemistry Research* 53 (6): 2157–66. doi:10.1021/ie402094b.

Mogalicherla, A.K., and N.O. Elbashir. 2011. “Assessment of Pore Diffusion Limitations for the near Critical and Supercritical Fischer-Tropsch Synthesis.” In . http://www.scopus.com/inward/record.url?eid=2-s2.0-84857197434&partnerID=40&md5=25530d76b6cf3743a05b9ac6b33664de.

O’Brien, R.J., L. Xu, R.L. Spicer, and B.H. Davis. 1996. “Activation Study of Precipitated Iron Fischer-Tropsch Catalysts.” *Energy and Fuels* 10 (4): 921–26.

Pham, T.H., Y. Qi, J. Yang, X. Duan, G. Qian, X. Zhou, D. Chen, and W. Yuan. 2015. “Insights into Hägg Iron-Carbide-Catalysed Fischer-Tropsch Synthesis: Suppression of CH4 Formation and Enhancement of C-C Coupling on χ-Fe5C2 (510).” *ACS Catalysis* 5 (4): 2203–8. doi:10.1021/cs501668g.

Pineau, A., N. Kanari, and I. Gaballah. 2006. “Kinetics of Reduction of Iron Oxides by H2: Part I: Low Temperature Reduction of Hematite.” *Thermochimica Acta* 447 (1): 89–100. doi:10.1016/j.tca.2005.10.004.

Rao, K.R.P.M., F.E. Huggins, G.P. Huffman, R.J. Gormley, R.J. O’Brien, and B.H. Davis. 1996. “Mössbauer Study of Iron Fischer-Tropsch Catalysts during Activation and Synthesis.” *Energy and Fuels* 10 (3): 546–51.

Rochet, A., V. Moizan, C. Pichon, F. Diehl, A. Berliet, and V. Briois. 2011. “In Situ and Operando Structural Characterisation of a Fischer-Tropsch Supported Cobalt Catalyst.” *Catalysis Today* 171 (1): 186–91. doi:10.1016/j.cattod.2011.03.079.

Rytter, E., S. Eri, T.H. Skagseth, D. Schanke, E. Bergene, R. Myrstad, and A. Lindvåg. 2007. “Catalyst Particle Size of Cobalt/rhenium on Porous Alumina and the Effect on Fischer - Tropsch Catalytic Performance.” *Industrial and Engineering Chemistry Research* 46 (26): 9032–36. doi:10.1021/ie071136+.

Shroff, M.D., D.S. Kalakkad, K.E. Coulter, S.D. Kohler, M.S. Harrington, N.B. Jackson, A.G. Sault, and A.K. Datye. 1995. “Activation of Precipitated Iron Fischer-Tropsch Synthesis Catalysts.” *Journal of Catalysis* 156 (2): 185–207. doi:10.1006/jcat.1995.1247.

Todic, Branislav, Lech Nowicki, Nikola Nikacevic, and Dragomir B. Bukur. 2016. “Fischer–Tropsch Synthesis Product Selectivity over an Industrial Iron-Based Catalyst: Effect of Process Conditions.” *Recent Advances in F-T Synthesis and Fuel Processing Catalysis* 261 (March): 28–39. doi:10.1016/j.cattod.2015.09.005.

van der Kraan, A.M., E. Boellaard, and M.W.J. Crajé. 1993. “Characterization of Catalysts by Mossbauer Spectroscopy: An Application to the Study of Fischer-Tropsch, Hydrotreating and Super Claus Catalysts.” *Nuclear Inst. and Methods in Physics Research, B* 76 (1-4): 6–12. doi:10.1016/0168-583X(93)95112-I.

Zamaniyan, Akbar, Yadollah Mortazavi, Abbas Ali Khodadadi, and Ali Nakhaei Pour. 2013. “Effect of Mass Transfer Limitations on Catalyst Performance during Reduction and Carburization of Iron Based Fischer-Tropsch Synthesis Catalysts.” *Journal of Energy Chemistry* 22 (5): 795–803. doi:10.1016/S2095-4956(13)60106-0.

Zamaniyan, A., Y. Mortazavi, A.A. Khodadadi, and A.N. Pour. 2013. “Effect of Mass Transfer Limitations on Catalyst Performance during Reduction and Carburization of Iron Based Fischer-Tropsch Synthesis Catalysts.” *Journal of Energy Chemistry* 22 (5): 795–803. doi:10.1016/S2095-4956(13)60106-0.

CHAPTER 6

RESPONSE OF GAS PHASE FT PRODUCTS OF DIFFERENTLY REDUCED CATALYSTS TO CHANGES IN OPERATING CONDITIONS

The data contained in this chapter are written in a paper format and the manuscript is ready for submission

Abstract

The effect of operating conditions on Fischer Tropsch synthesis (FTS) on product selectivity of Gas Phase products was investigated in a fixed bed reactor with an industrial iron-based catalyst $FeCuKSiO_2$ under reaction times on stream (TOS) representative of industrial practice. The study followed the experimental plan discussed in Chapter 4 and the results were analysed based on how the three differently reduced catalysts responded to pressure and gas flow rate changes. This chapter focuses on the response to changes in process conditions of the Fe-based catalyst initially reduced with different reducing gases. The responses were compared in terms of the conversion, the product selectivities and the ratios of main products (Olefin/paraffin ratio). Experiments were performed over a range of different reaction conditions, vis a vis three gas flow rates of 60, 30 and 15 mL/min, and three pressure ranges of 1, 10, and 20 bar based on one synthesis gas feed composition ($H_2/CO = 2$) and temperature of 250 °C.

These changes have an impact on the design of the small-scale biomass/waste to liquid process. When such a process is designed to run at low pressure (such as 1 bar(gauge) in this study), a higher conversion is desired to utilise the feedstock as much as it can. Therefore, a low flow rate needs be implemented. However, the experimental results obtained in this work suggest that the combination of a high conversion with low flow rate actually hinders the production of liquid products, therefore the carbon efficiency for the process will be very low. This will have a great impact on the economic viability for the biomass/waste to liquid projects that could be run at low pressure

6.1 Introduction

Fischer Tropsch synthesis (FTS) is a well-known chemical reaction in which synthesis gas is converted to liquid fuels over a metal catalyst (Dry 1983; Maitlis & de Klerk 2013). Several transition metals, such as cobalt, iron, nickel and ruthenium, can be used in the FT process (Muleja et al. 2016). FTS plays a vital and central role in addressing the need for transportation fuels, and the technology has found industrial applications in most parts of the world including Germany, South Africa, China and the Netherlands.

FT products are mainly linear hydrocarbons, predominately alkenes and alkanes (Maitlis & de Klerk 2013). The hydrocarbons are distributed between the vapour and liquid phases, with the lighter components preferentially concentrating in the vapour while the heavy oils and waxes preferentially concentrate in the liquid phase (Muleja et al. 2016). Various products such as methane (C_1), petroleum gas (C_2- C_4), gasoline (C_5- C_{11}), diesel (C_{12}- C_{20}), and wax (C_{21+}) are formed from the process. The wax can be further processed by cracking to produce gasoline and diesel (Rauch et al. 2013).

Generally, the operating conditions of the FT process tend to influence these product distributions (Farias, Sales & Fernandes 2008a). For instance, pressure, flow rate and temperature are the main factors affecting the product selectivity and the CO conversion in FT synthesis. Recently, several publications have dealt in detail with the influences of these operating conditions on FT activity and selectivity (Atashi et al. 2015; Farias et al. 2008a, 2008b; Todic et al. 2016). Furthermore, studies on the effects of pressure and flow rate have also shown that total pressure has a positive effect on FTS product distribution (Dalai & Davis 2008; Todic et al. 2016a).

The concept of varying parameters in FT is not new. In early studies, researchers have periodically reported noticeable beneficial effects of varying operating condition to yield a preferred product distribution (Atashi et al. 2015; Dinse et al. 2012; Farias et al. 2008; Farias et al. 2007). Studies on cobalt based catalyst (Co/SiO_2) also revealed that the product distributions formed during FTS depend on the reaction pressure and promotors such as manganese (Dinse et al. 2012).

Bukur and Lang (1999) investigated the effect of both pressure and gas space velocity in a stirred tank slurry reactor using precipitated iron catalyst ($FeCuKSiO_2$), and reported that catalyst productivity was increased by operating at higher synthesis pressure while maintaining a constant contact time in the reactor. In the same study, Bukur and Lang (1999 tested the catalyst at 15 bar (1.5 MPa) and obtained syngas conversion of 76–80%, while further increase in pressure to 22 bar (2.2 Mpa) resulted in the decrease in syngas conversion down to 68%. Generally, most of the FT operations reported in the literature are carried out between 5 and 50 days in lab-scale reactors, and therefore may only address short-term effects of these parameter changes on the response of the catalyst. The pressure and/or the gas flow rate can be altered in order to counteract the effect of catalyst deactivation, which tends to reduce the FT product yield. In industrial operations catalyst deactivation, which happens during the first 6–18 months of operation, can cause 30–60% loss in catalyst activity in low-temperature Fischer Tropsch synthesis (LTFTS) (Rytter and Holmen 2015).

On the other hand, large amounts of money and time are usually consumed during spent catalyst replacement in an FT operation plant. Such disturbances are inevitable during operation since the catalyst deactivates, and ways to maintain the yield at reasonable cost to enable the plant run continuously for a long time may be required. The prolonged operation ensures that maximum achievable profit can be obtained. A systematic control system can be used by altering the operating parameters to maintain the conversion (product formation). The choice of the right parameters, either individual or in combinations could maintain the yield, and the need to replace the catalyst can be delayed. Fortunately, it appears possible to reactivate the catalyst to approach the level (in terms of activity) of a freshly equilibrated catalyst by changing the parameters. In this study, the FTS reaction was studied over a long period of time (more than 19 months), during which a number of operating condition changes were made and catalyst deactivation was observed. The need for the above mentioned properties has led to this research to ascertain how differently reduced catalysts after operating for an extended period respond to operational condition changes.

6.2 Experimental work

The experimental conditions selected consisted of reducing the catalyst ($FeCuKSiO_2$) at low temperature (250 ^oC) and atmospheric pressure. The FT operating conditions were initially kept mild, reactor pressure of 1 bar gauge, temperature of 250 ^oC and syngas gas flow rate of 60 mL(NTP)/min for about 4000 hours of time on stream. For this lengthy run the catalyst showed a significant decrease in conversion. Thereafter various changes were made to the FT reactor parameters, such as pressure, gas flow rate and catalyst deactivation. These variations in operating conditions had an effect on the conversion. The operating conditions implemented at different time on streams (TOS) for three differently reduced reactors are depicted in **Table 6.1**.

Table 6.1: Operating conditions implemented at different time on streams (TOS) for three differently reduced reactors

Reac-Syn			Range TOS (hrs)	
Flowrate (NTP)mL/min	Pressure (bar)	Temperature (°C)	From	TO
60	1	250	0.00	1100.00
60	1	250	5791.72	6061.57
30	1	250	6089.66	6277.58
15	1	250	6284.49	6816.84
60	10	250	13676.04	13982.51
60	20	250	13987.08	14340.29
Reac-H2			Range TOS (hrs)	
Flowrate (NTP)mL/min	Pressure (bar)	Temperature (°C)	From	TO
60	1	250	0.00	1143.66
60	1	250	5195.29	5889.17
30	1	250	5901.12	6051.85
15	1	250	6113.13	6630.27
60	10	250	13724.55	13979.95
60	20	250	13984.70	14132.18
Reac-CO			Range TOS (hrs)	
Flowrate (NTP)mL/min	Pressure (bar)	Temperature (°C)	From	TO
60	1	250	0.00	1019.00
60	1	250	5138.57	5355.36
30	1	250	5402.24	5567.91
15	1	250	5577.81	6084.79
60	10	250	13112.81	13382.26
60	20	250	13399.95	13636.04

Typically, the three differently reduced catalysts were subjected to a series of parameter variations to enable the investigator to compare the catalyst response after a long time on stream. A series of long-term FTS runs (about 14 200 hours) were conducted. At various times as indicated in **Table 6.1** flow rates from 15 mL(NTP)/min to 30 mL(NTP)/min and 60 mL(NTP)/min and then pressures from 1 to 10 and finally 20 bar gauge were tested. The aim was to test the responses of the catalyst initially reduced with different gases, to changes in the operating conditions. The results were part of a series of tests meant to identify the best reducing agent in terms of long term catalyst activity, stability and resistance to deactivation.

6.3 Results

6.3.1 Effect of flow rate on the CO conversion

The effect of varying syngas flow rate on FTS catalytic activity was investigated. The CO conversion was plotted against time on stream (TOS) for different gas flow rates, namely 15, 30 and 60 mL(NTP)/min at a constant pressure of 1 bar gauge. The results are presented in **Figure 6.1**. The data show that the CO conversion increases with decreasing syngas flow rate from 60, 30 and 15 mL(NTP)/min at a constant reactor temperature of 250 ºC and pressure of 1 bar gauge.

The three differently reduced catalysts responded positively to the effect of reducing flow rate. However, the responses were of different magnitudes, with Reac-Syn showing a highest, a 2.31-fold increase from 60 to 30 mL(NTP)/min, followed by Reac-H_2 with a 1.77-fold increase, and lastly Reac-CO with a 1.69-fold increase in terms of conversion. A further halving in flow rate did not yield quite as much difference in the conversion (see **Figure 6.1** and **Table 6.2**). From 30 to 15 mL(NTP)/min the conversion of Reac-Syn (the syngas reduced catalyst) increased from 9.86% to 17.20% (which is a 1.74-fold increase), Reac-H_2 (hydrogen reduced) increased from 12.35% to 20.97 % (a 1.70-fold increase) and lastly Reac-CO (carbon monoxide reduced) increased from 7.34% to 10.18 % (which is a 1.39-fold increase).

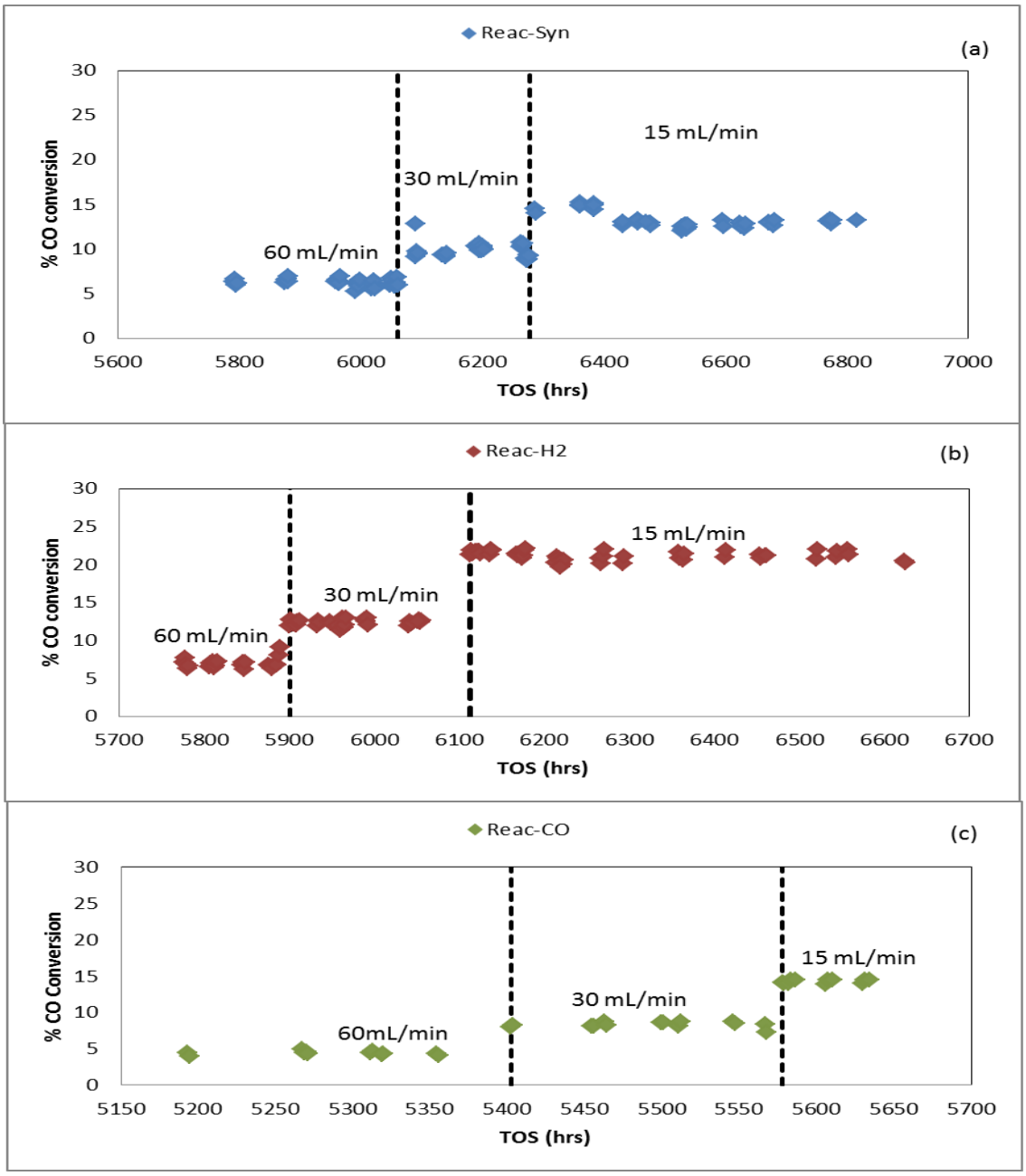

Figure 6.1: Conversions of differently reduced reactors with changing flow rate: (a) for syngas reduced (Reac-Syn); (b) for hydrogen reduced (Reac-H_2) and (c) carbon monoxide reduced (Reac-CO). Reactor temperature was kept at 250 °C and reactor pressure at 1 bar gauge.

Table 6.2: Conversion averages for the three reactors at different flow rates

Flow Rate (mL/min	CO conversion (%)		
	Reac-Syn	Reac-H_2	Reac-CO
60	6.03	6.99	4.36
30	9.86	12.35	7.34
15	17.20	20.97	10.18

The results listed in **Table 6.2** were obtained after 5 000 hours TOS, compared with the reaction rates presented in chapter 5 (for TOS of 1000 hours) where the CO consumption rates were higher for Reac-Syn and Reac-CO. It can be seen that the Reac-H_2 has shown the highest reaction rate when the catalyst has been used for a long time (for more than 5000 hours in this study). This could be due to the different deactivation behaviour for the different active phases contained in these three catalysts caused by the reduction conditions (Collett & McGregor 2016; Sartipi et al. 2014).

Thus one can see that the performance of the Reac-Syn reactor in terms of conversion is better than the Reac-CO but worse than the Reac-H_2 as shown in **Table 6.1**. For long time synthesis run, the activity of the Reac-H_2 is comparatively better in terms of performance. This suggests that H_2 in the syngas has helped the catalyst to maintain a higher activity when compared to the catalyst initially reduced by CO only.

The CO consumption rates of differently reduced reactors with changing flow rate: (a) for syngas reduced (Reac-Syn); (b) for hydrogen reduced (Reac-H_2) and (c) carbon monoxide reduced (Reac-CO) are depicted in **Figure 6.2**. It can be seen that when the conversion is less than about 10% the reaction rates remain approximately the same as the flow rate is decreased from 60 to 30 mL(NTP)/min, but once the conversion gets above 10% the further decrease in flow rate from 30 to 15 mL(NTP)/min has a more

significant effect on the conversion. This is possibly because the average reactant gas composition in the reactor is now effectively smaller.

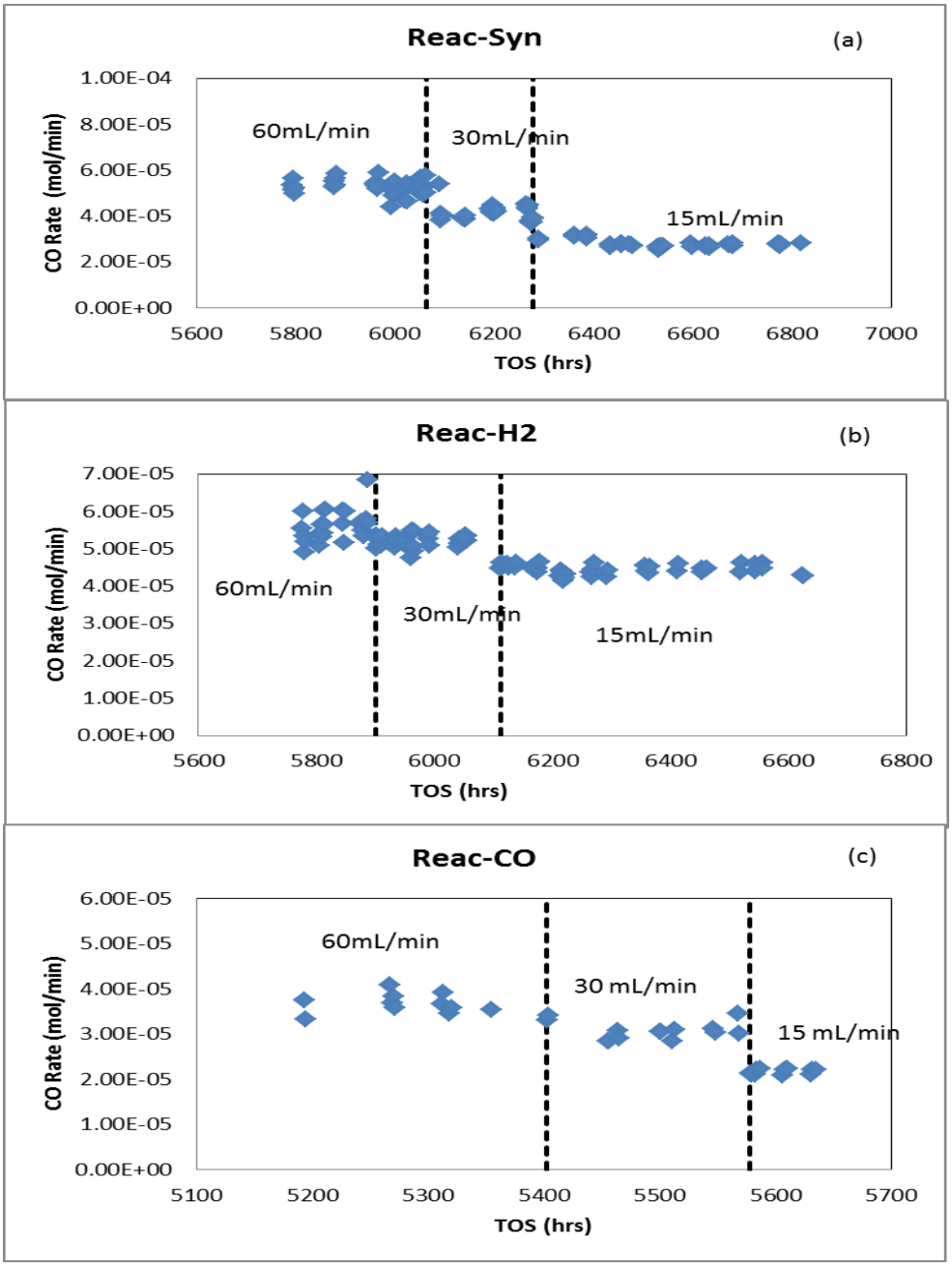

Figure 6.2: CO consumption rates of differently reduced reactors with changing flow rate: (a) for syngas reduced (Reac-Syn); (b) for hydrogen reduced (Reac-H_2) and (c) carbon monoxide reduced (Reac-CO). Reactor temperature was kept at 250 °C and reactor pressure at 1 bar gauge.

6.3.2 **Effect of flow rate on the selectivity to the products**

The effect of flow rate on the selectivity to the FT hydrocarbons was determined and the results are shown in **Table 6.3** (a-c) for the light olefins, light paraffins and for both the light hydrocarbons and the heavy hydrocarbons for all three reactors: Reac-Syn (reduced with syngas), Reac-H_2 (reduced with hydrogen) and Reac-CO (reduced with carbon monoxide). These results are only shown as averages in the tables rather than graphs as in **Figures 6.1** and **6.2**, as it can be seen that the averages are a simple and very good indicator of the results.

The selectivity to paraffins was observed to increase with the decrease in flow rate, while the selectivity towards olefins followed the same pattern except for the dicreapancies of C_2 olefin for Reac-Syn and Reac-H_2. In general, the lighter hydrocarbons increased in selectivity with decrease in the flow rate whereas the selectivity towards C_{5+} (heavy hydrocarbons) decreased with decreasing flow rates (see **Tables 6.3**). As with the conversion results for the flowrates from 60 to 30 mL(NTP)/min the change was relatively small compared to when the flowrates changed from 30 to 15 mL(NTP)/min. Therefore, the lower the syngas flow for the lower amount of the higher than C_{5+} products formed. Clearly residence time, possibly because of changes in conversion, has an effect on the product selectivity. The results of the effect of flow rate on the the selectivity to C_{5+} for all three reactors are plotted in **Figure 6.3**.

It is worthwile to point out that the selectivity to the C_{5+} products dropped sharply when the the gas flow rate decreased to low values (from 30 to 15 mL(NTP)/min). This potentially has a big impact on the design of the small-scale biomass/waste to liquid process. When such a process is designed to run at low pressure (such as 1 bar(gauge) in this study), a higher conversion is desired to utilise the feedstock as much as . Therefore, a low flow rate needs be implemented. However, the experimental results obtained in this work suggest that the combination of a high conversion with low flow rate actually hinders the production of liquid products, therefore the carbon efficiency for the process will be very low. This could have a large impact on the economic viablity of the biomass/waste to liquid projects that is run at low pressure.

Table 6.3: Component selectivities at different flow rates (a) Olefin Selectivity (b) Paraffin Selectivity (c) Olefin + Paraffin and C_{5+} Selectivity

(a)	Olefin Selectivity (%)											
Component	C_2H_4			C_3H_6			C_4H_8			C_5H_{10}		
Reactor	Reac-Syn	Reac-H_2	Reac-CO	Reac-Syn	Reac-H_2	Reac-CO	Reac-Syn	Reac-H_2	Reac-CO	Reac-Syn	Reac-H_2	Reac-CO
60 mL/min	4.92	4.23	5.03	9.84	6.87	6.52	7.69	6.09	5.03	6.51	5.14	3.81
30 mL/min	3.78	4.25	5.64	9.82	8.16	8.36	7.50	7.15	6.30	6.57	6.28	4.75
15 mL/min	3.20	3.47	6.59	10.14	9.28	11.69	7.34	7.40	8.44	6.47	6.46	6.45

(b)	Paraffin Selectivity (%)											
Component	C_2H_6			C_3H_8			C_4H_{10}			C_5H_{12}		
Reactor	Reac-Syn	Reac-H_2	Reac-CO	Reac-Syn	Reac-H_2	Reac-CO	Reac-Syn	Reac-H_2	Reac-CO	Reac-Syn	Reac-H_2	Reac-CO
60 mL/min	1.15	0.45	0.41	0.51	0.24	0.18	0.42	0.76	0.18	0.83	0.33	0.22
30 mL/min	1.43	0.75	0.72	0.59	0.32	0.31	0.48	0.99	0.23	1.17	0.59	0.34
15 mL/min	1.68	1.29	1.47	0.75	0.51	0.45	0.56	1.39	0.34	1.71	1.15	0.78

(c)	Hydrocarbons Selectivity (%)														
Component	C2			C3			C4			C5			C5+		
Reactor	Reac-Syn	Reac-H2	Reac-CO	Reac-Syn	Reac-H2	Reac-CO	Reac-Syn	Reac-H2	Reac-CO	Reac-Syn	Reac-H2	Reac-CO	Reac-Syn	Reac-H2	Reac-CO
60 mL/min	6.07	4.68	5.45	10.35	7.11	6.70	8.11	6.85	5.21	7.33	5.48	4.03	42.05	59.77	57.82
30 mL/min	5.22	5.00	6.36	10.41	8.48	8.67	7.98	8.13	6.53	7.74	6.87	5.08	34.15	45.38	43.39
15 mL/min	4.88	4.76	8.06	10.89	9.79	12.14	7.91	8.79	8.78	8.18	7.61	7.23	20.84	29.35	7.66

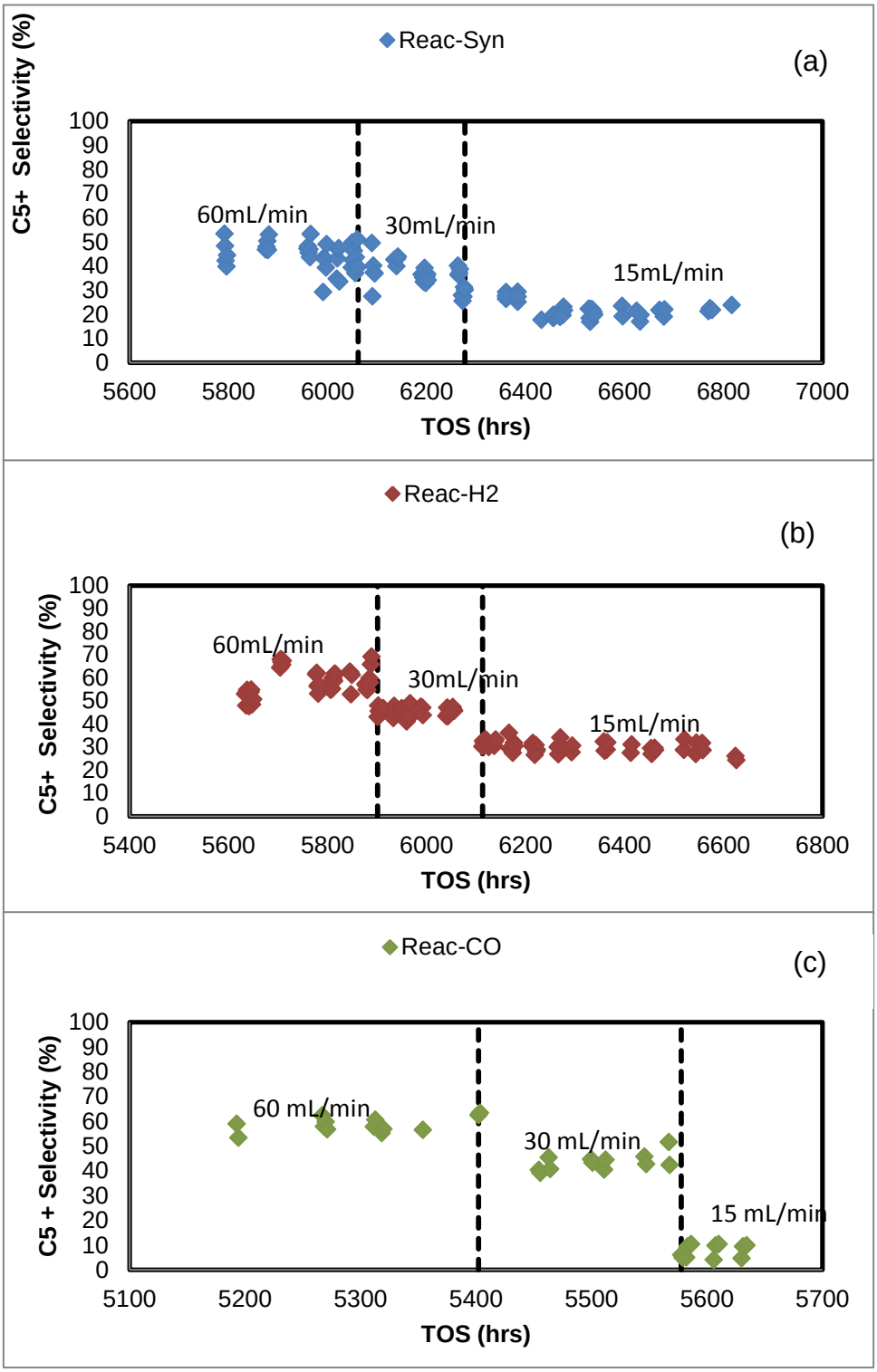

Figure 6.3: Selectivity to heavy hydrocarbons (C_{5+}) for (a) Reac-Syn (syngas reduced, (b) Reac-H_2 (hydrogen reduced), and (c) Reac-CO (Carbon monoxide reduced) under FT operating conditions: 250 °C, 1 bar gauge and various flow rates (15, 30 and 60 mL(NTP)/min)

The effect of flow rate on the selectivity to carbon dioxide and methane was also determined for all three reactors. The data are plotted against TOS and presented in **Figure 6.4** (a) for Reac-Syn (syngas reduced), (b) for Reac-H_2 (hydrogen reduced), and (c) for Reac-CO (carbon monoxide reduced reactor). The results show that the selectivity to CO_2 was observed to increase with decrease in flow rate, while the selectivity towards methane remained virtually unchanged.

The CO_2 selectivity for the syngas and CO reduced catalysts increased to around 65% when the flow rate was decreased from 30 to 15 mL(NTP)/min, and that of Reac-H_2 was increased to around 40%. The Reac-H_2 reduced Fe has shown a lower selectivity to CO_2 when compared to the Reac-Syn and Reac-CO reactors. More importantly, when the operating pressure is low (1 bar(gauge) in this study), the CO_2 selectivity would increase to unacceptable levels if there was an attempt to increase the conversion of the reactants by operating the reactor at a low flow rate. This result and the result above in the selectivity to C_{5+} products, strongly suggest that a combination of low pressure, low flow rate and a higher conversion is definitely not the design region for the biomass/waste to liquid processes.

What might be happening as the residence time is increased (flowrate is lowered) is that the reaction extent to FT increases but this means more water and thus the WGS reaction increases even more than the the FT reaction and the main product is now CO_2. This is clearly undesireable as we are turning feed carbon into a very undesireable product. If this assumption is correct then as one wants a high conversion of the CO to useful product it would probably be best to have a few reactors in series with intermediate knockout of the water. This should keep the average water concentration in the reactors lower and thus minimise the overall extent of the Water Gas Shift reaction.

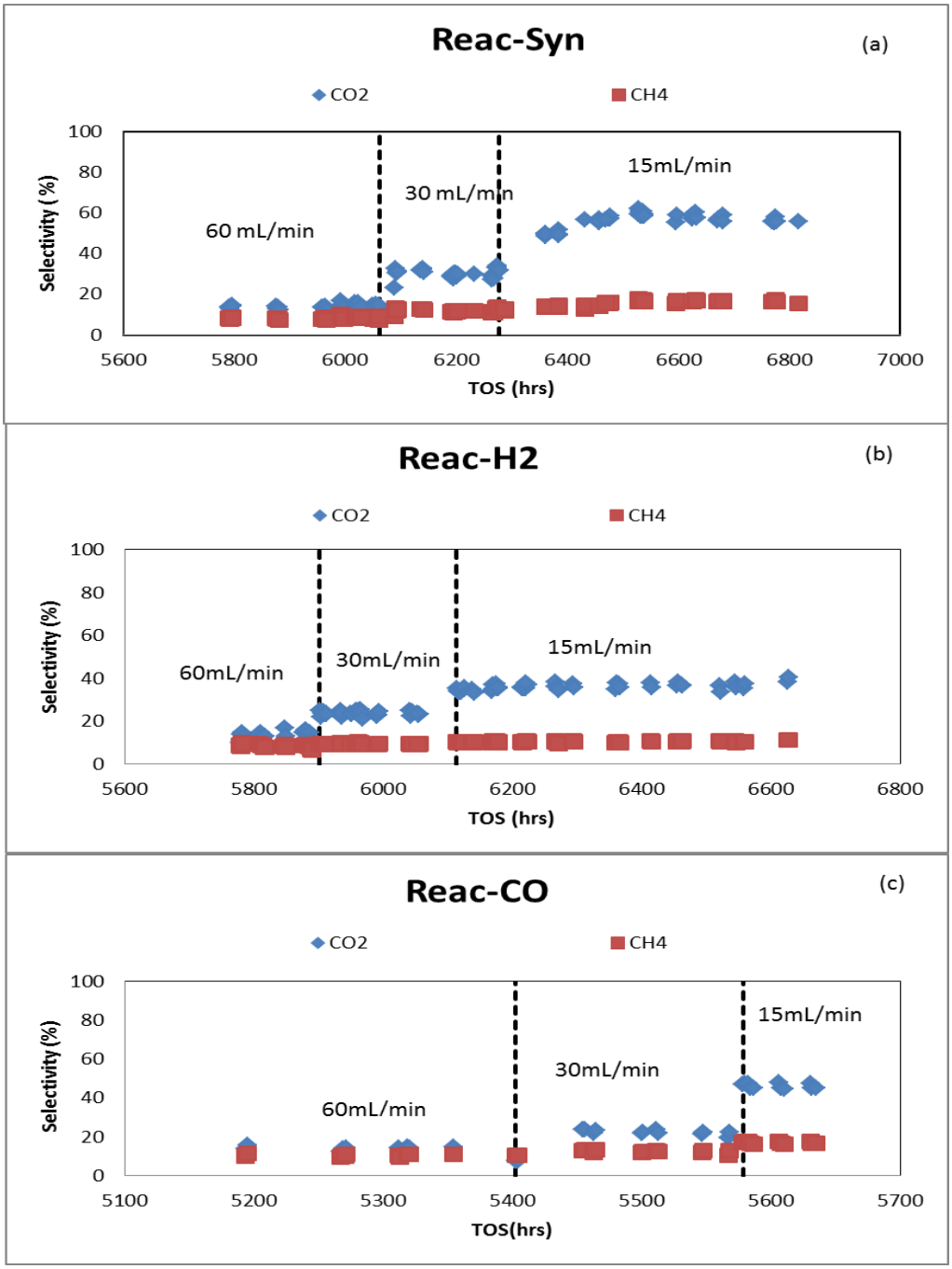

Figure 6.4: Effect of flow rate on the selectivity to CO_2 and CH_4 under FT conditions of 250 ^{o}C, 1 bar gauge and various flow rate values of 15, 30 and 60 mL(NTP)/min

6.3.3 **Effect of flow rate on the olefin to paraffin ratios**

The olefin and paraffin ratios for the light hydrocarbons (C_2 to C_5) are plotted as a function of TOS in **Figure 6.5** (a) to (c) for the Reac-Syn, Reac-H_2 and Reac-CO reactors, respectively. The O/P ratio decreases with carbon number in all the systems, and this trend is also consistent with findings in the literature (Shi & Davis, 2005). The probability of a secondary reaction for olefins is said to increase with carbon number (Kuipers et al. 1996) and this could possibly explain the result. As said before, it is clear from these ratios that the CO reduced catalyst makes more olefin and has a much higher O/P than the others. Clearly changing the flow rate does not have a big effect on the O/P ratios for all the catalysts using the different reduction methods.

For reasons that are not clear, the C_4 O/P remains anomalously low for the hydrogen reduced catalyst. This is a very strange result and may bear further scrutiny at a later stage as it may give clues to what is happening on FT catalysts. Perhaps feeding in some n-butene possibly deuterated, might be a useful experiment to perform?

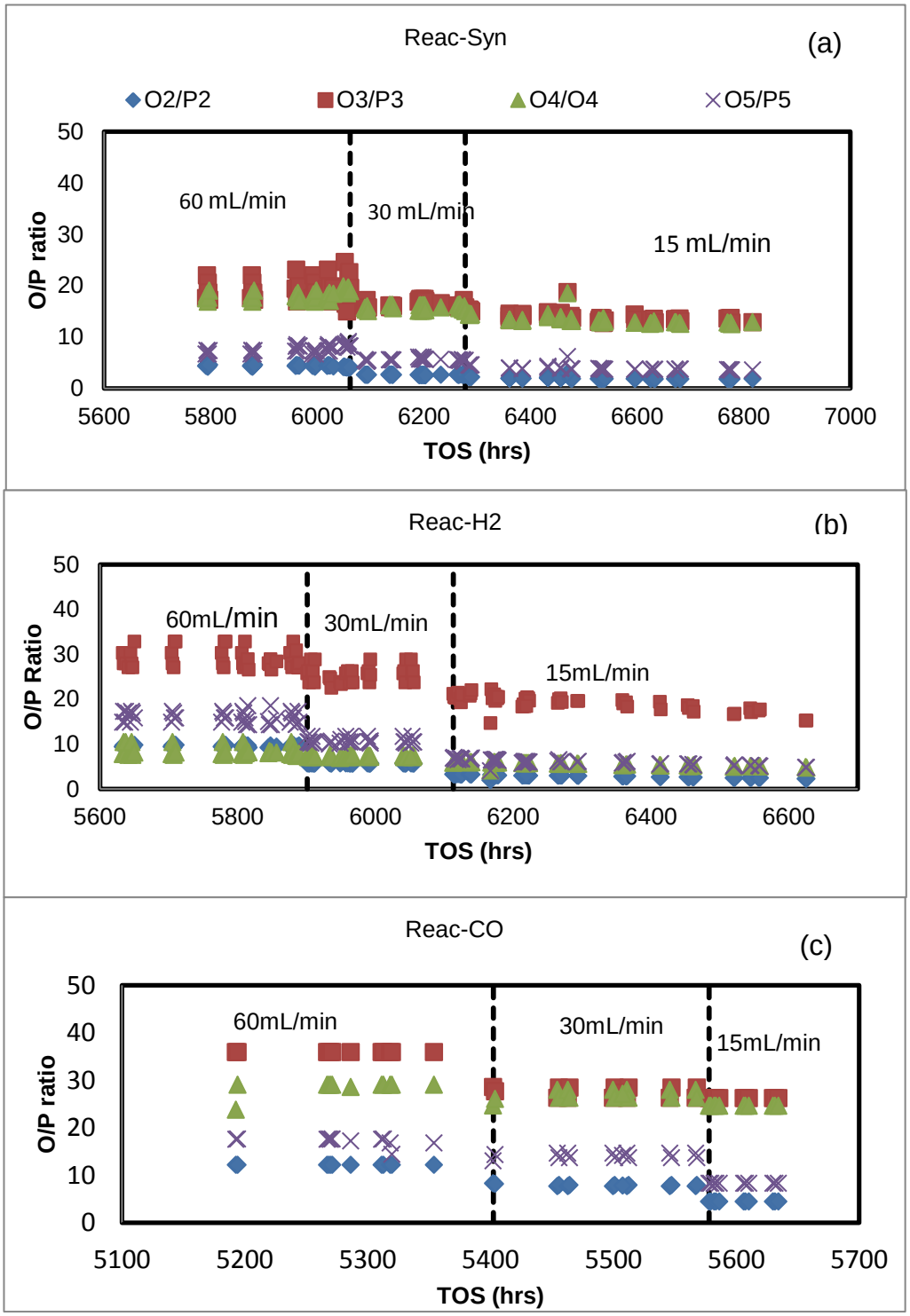

Figure 6.5: Effects of changing flow rates to olefin to paraffin ratio for (a) Reac-Syn, (b) for Reac-H_2, and (c) for Reac-CO under FT conditions of 250 ^{o}C, 1 bar gauge and various flow rate values 15, 30 and 60 mL(NTP)/min.

6.3.4 **Effect of pressure on the CO conversion**

The CO conversion was measured as a function of time on stream (TOS) at different reactor operating pressures (1, 10 and 20 bar (gauge)) while keeping the flow rate (60 mL(NTP)/min) and temperature (250 ^{o}C) constant. The results are presented in **Figure 6.6** (a) for the Reac-Syn, **Figure 6.6** (b) for the Reac-H_2 and **Figure 6.6** (c) for the Reac-CO. **Figure 6.6** shows that upon increasing the total pressure from 1 bar to 10 bar, the CO conversion of the three catalysts, syngas reduced (Reac-Syn), hydrogen reduced (Reac-H_2), and carbon monoxide reduced (in Reac-CO), increased 2.54-fold, 3.81-fold and 5.39-fold, respectively. When the reactor pressure was further increased from 10 to 20 bar (gauge), the CO conversion increased 2.17-fold, 1.56-fold and 1.75-fold for the syngas, hydrogen and carbon monoxide reduced reactors, respectively (see **Table 6.4**).

These data are interesting because the iron catalyst was loaded in these reactors (Reac-Syn, Reac-H_2 and Reac-CO) and FT was carried out for over 12 000 hours under essentially similar conditions before the effect of pressure was tested. By this time after various experimental changes were made to the FT reactors the catalyst was already deactivated by more than 50% from the initial activity. The results in **Figure 6.6** are useful as the catalyst activity still after more than 500 days seemed to be correlated to the reducing gas which was initially used in the catalyst reduction. The performance in terms of activity followed these trends: Reac-Syn > Reac-CO > Reac-H_2. This seems to suggest that the different methods of initial reduction gave rise to permanent changes to the catalysts that were not affected by subsequent FT reaction conditions.

Table 6.4: Summary of averaged conversions for a given TOS range

Reac-Syn			Range TOS (hrs)		
Flowrate (NTP)mL/min	Pressure (bar)	Temperature (°C)	From	TO	% Conversion
60	1	250	12168.03	12377.32	10.00
60	10	250	13676.04	13982.51	25.39
60	20	250	13987.08	14340.29	55.07
Reac-H2			Range TOS (hrs)		
Flowrate (NTP)mL/min	Pressure (bar)	Temperature (°C)	From	TO	% Conversion
60	1	250	12861.45	13116.80	9.31
60	10	250	13724.55	13979.95	35.42
60	20	250	13984.70	14132.18	55.24
Reac-CO			Range TOS (hrs)		
Flowrate (NTP)mL/min	Pressure (bar)	Temperature (°C)	From	TO	% Conversion
60	1	250	11908.21	11965.41	4.285
60	10	250	13112.81	13382.26	23.09
60	20	250	13399.95	13636.04	40.40

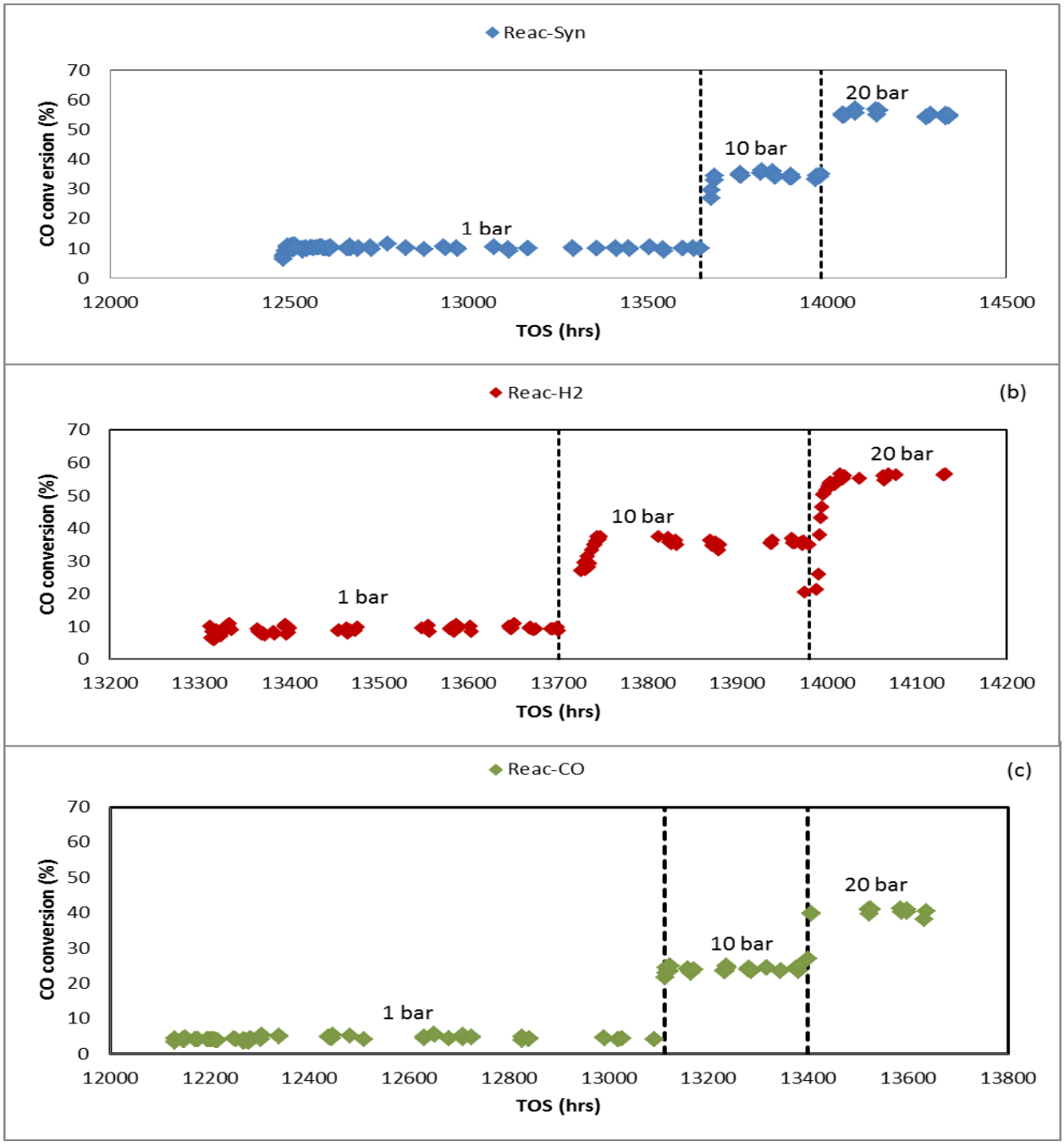

Figure 6.6: Effect of pressure on the CO conversion at various pressures: 1, 10 and 20 bar gauge while keeping the temperature at 250 ^{o}C, flow rate at 60 mL(NTP)/min, feed ratio H_2/CO = 2 and 1 g mass of the iron catalyst loaded in different reactors; (a) for Reac-Syn , (b) for Reac-H_2 and (c) for Reac-CO for TOS between 12000- 13 800 hours

The CO conversion increased with increasing pressure for all the differently reduced catalysts although the magnitude of increase was different. Most notably,

the increase in CO conversion from 1 to 10 bar had a comparatively higher magnitude than the increase from 10 to 20 bar. As shown by averaged values in **Table 6.4**, the CO conversion increased 2.54-fold, 3.81-fold and 5.34-fold for Reac-Syn, Reac-H_2 and Reac-CO reduced reactors respectively from 1 to 10 bar gauge. From 10 to 20 bar the Reac-Syn had the largest increase of 2.17-fold followed by the Reac-CO reduced with a 1.75-fold and lastly Reac-H_2 with a 1.56-fold increase.

The graphs of rates in **Figure 6.7** depict the same pattern as the conversion, the rate of CO consumption increased with pressure.

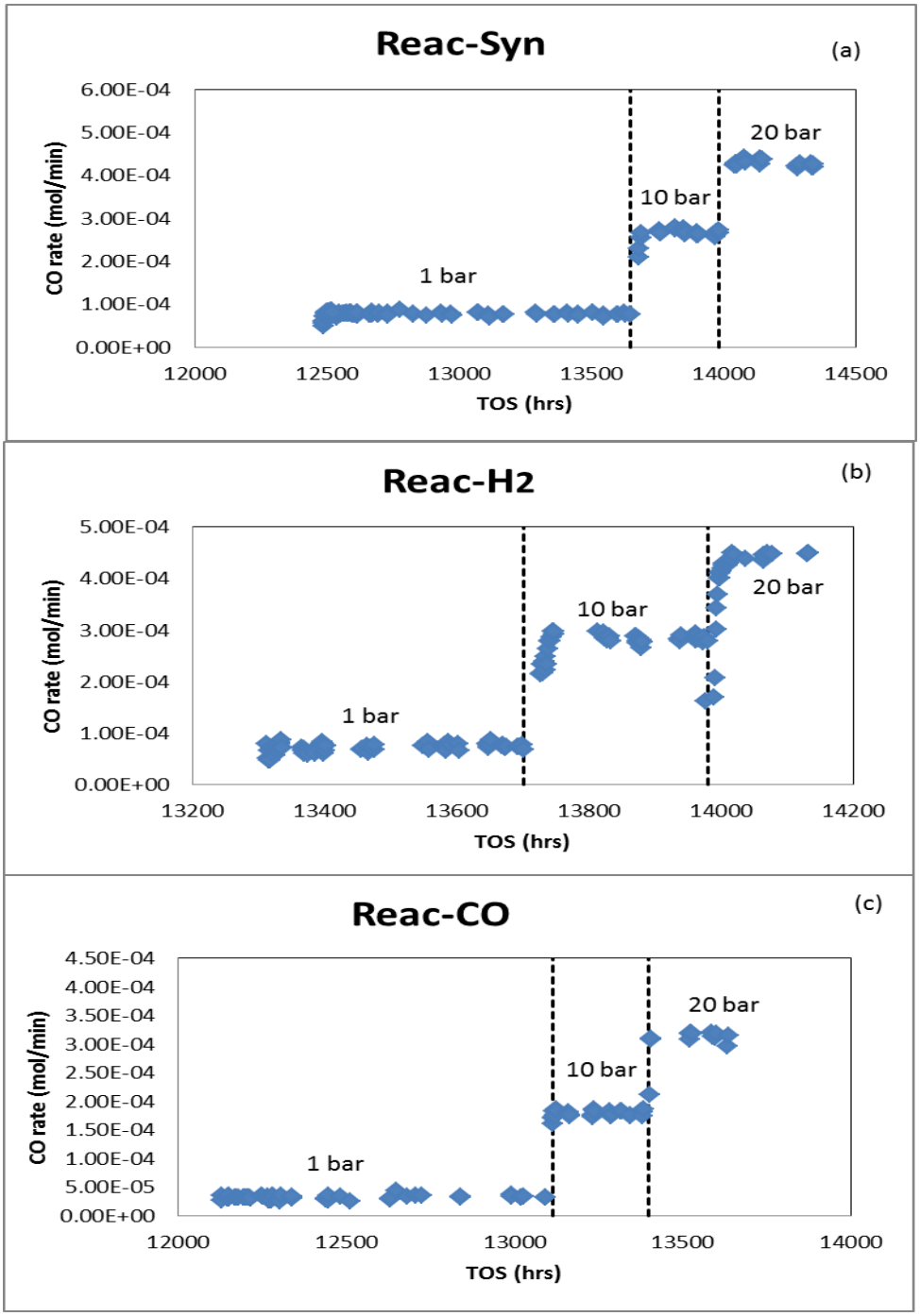

Figure 6.7: Effect of pressure on the CO rates at various pressures: 1, 10 and 20 bar gauge while keeping the temperature at 250 ^{o}C, flow rate at 60 mL(NTP)/min, feed ratio H_2/CO = 2 and 1 g mass of the iron catalyst loaded in different reactors; (a) for Reac-Syn , (b) for Reac-H_2 and (c) for Reac-CO for TOS between 12000- 13 800 hours

The effect of increasing pressure may be used to counteract the effect of catalyst deactivation by increasing the conversion, thus reducing the frequency of expensive regeneration of the catalyst. When the catalyst is reduced with different gases, the pathway of reduction may differ. Therefore, the kinetics of an Fe catalyst seems to depend on this initial treatment which possibly results in different active phases (Hallac et al. 2015; Mousavi et al. 2015; Nakhaei Pour et al. 2014; Okeson et al. 2016).

6.3.5 Effect of pressure on the selectivity to the products

The effect of pressure on the selectivity to the light products (C_2 to C_5) was determined, and the results are depicted in **Figure 6.8** (a) for carbon number 2, **Figure 6.8** (b) for carbon number 3, **Figure 6.8** (c) for carbon number 4 and Figure 6.11 (d) for carbon number 5 for all three reactors: Reac-Syn reduced with syngas, Reac-H_2 reduced with hydrogen and Reac-CO reduced with carbon monoxide.

Figure 6.8 (a) shows that the selectivity to C_2 olefins decreased with the increase in the FT reactor pressure from 1 bar (gauge) to 10 bar (gauge) and from 10 bar (gauge) to 20 bar gauge for all three reactors, whereas the selectivity to C_2 paraffins increased with rise in the pressure. In **Figure 6.8** (b), similar trends were observed for the selectivity to carbon number 3 hydrocarbons, with the exception noticed at 1 bar for the hydrogen reduced which yielded low C_3 olefin selectivity. For the C_3 paraffins, the selectivity increased with increasing pressure for all the differently reduced catalysts.

Figure 6.8 (c) shows the selectivity to butene and butane. Upon increasing the total pressure from 1 bar to 10 bar, the syngas reduced and the hydrogen reduced showed an increase in the C_4 olefin selectivity (from 4.30% to 5.74% and 2.73% to 4.63%, respectively) with further increase of pressure to 20 bar gauge resulting in a noticeable decrease in selectivity to 3.94 % and 4.27 %, respectively. The C_4 paraffin selectivity maintained the incremental trend as with the C_3 and C_2 paraffins.

In **Figure 6.8** (d), the trends of the olefin selectivity observed for the syngas and hydrogen reduced reactors for C_5 were similar to those for the individual C_4, and C_3 hydrogen reduced. For both reactors, the selectivity to C_5 increased when the reactor pressure was adjusted from 1 bar to 10 bar and then decreased when pressure was further increased to 20 bar, whereas the selectivity to paraffins increased with increasing total pressure.

For all the light hydrocarbons reported in this chapter, the Reac-CO reactor when compared to the Reac-Syn and Reac-H_2 reactors, always showed a larger scale change in terms of selectivity to olefins and paraffins when the operating pressure was changed, . This may be due to the difference in the active phases in these three differently reduced catalysts. The CO reduced as the thermodynamics suggests is believed to have more iron carbides when compared to the other two (Sault & Datye 1993; Soled et al. 1990) (see also thermodynamic predictions in Chapter 3). It should also be noted that the selectivity to ethane is particularly high and to some extent for propane not for butane and a little bit for pentane for the syngas reduced catalyst. It is not at all obvious why this might be happening.

The behaviour noticed was that the selectivity to olefins (C_2 and C_3) decreasing at the highest reactor pressure, while the selectivity to paraffins (C_2 and C_3) increasing with increasing reactor pressure could be attributed to the hydrogenation of olefins to paraffins (Todic et al. 2016b; Yan et al. 2014). In general, the results confirm that when the FT reactor pressure is increased, the product selectivity is more towards paraffinic products. Paraffinic product means more wax product, and this finding agrees with findings proposed by Farias et al. (2008b) where it is reported that high pressures (25 to 30 atm) favoured the production of waxes, while moderate pressure such as 20 atm showed selectivity towards the diesel.

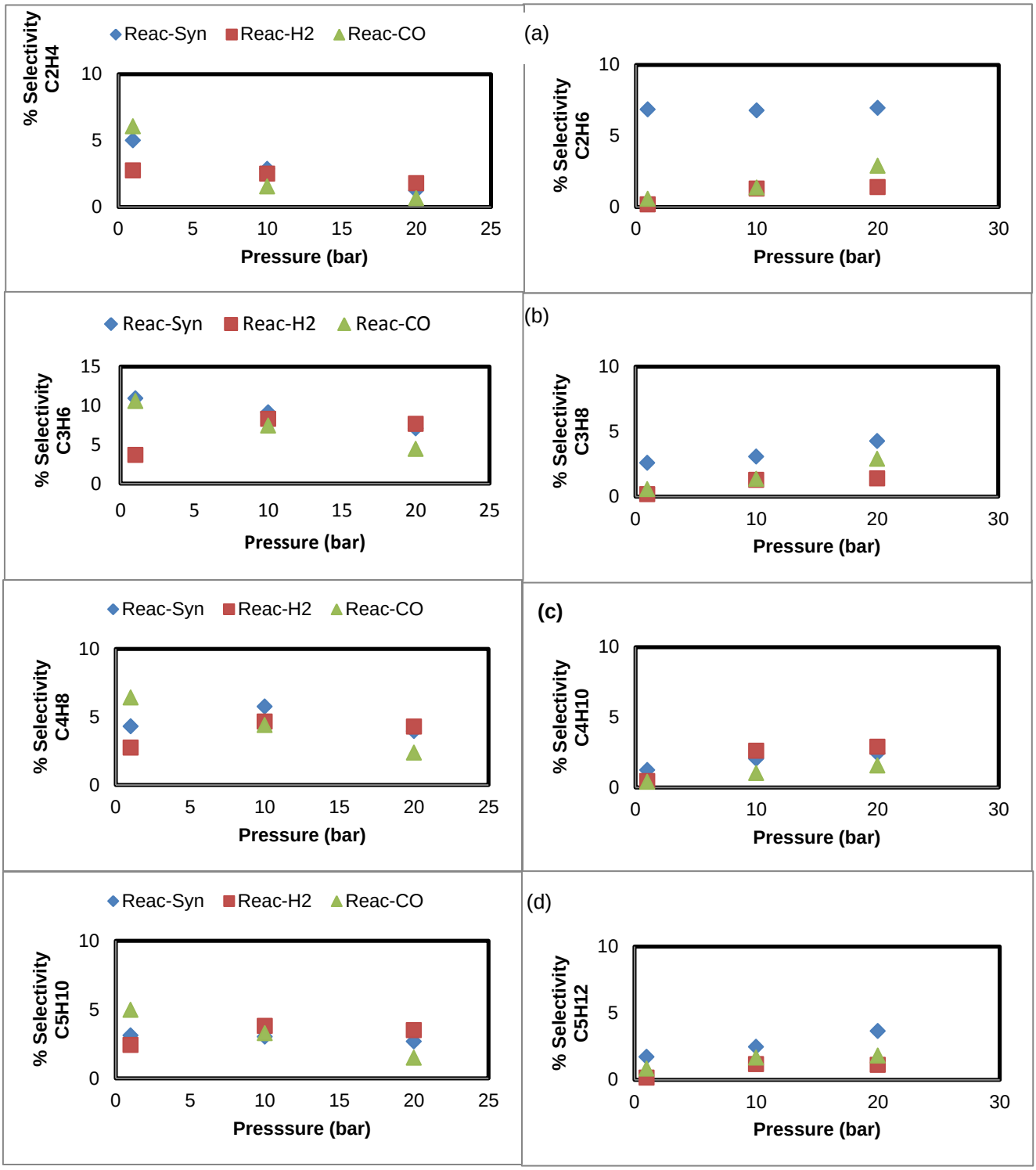

Figure 6.8: Comparison of the selectivities to olefins and paraffins at different pressures

6.3.6 **Effect of pressure on the olefin to paraffin (O/P) ratio**

The olefin and paraffin ratios for the light hydrocarbons (C_2 to C_5) are plotted as a function of TOS in **Figure 6.9** (a) to (c) for the syngas (Reac-Syn), hydrogen (Reac-H_2) and carbon monoxide (Reac-CO) reduced reactors, respectively. The results show that for all three differently reduced reactors, when the reaction pressure was increased, the O/P ratios decreased. However, the extent to which this change occurred was more pronounced when the pressure was increased from 1 to 10 bars, whereas from 10 to 20 bar the magnitude of the differences was not that high.

The product (O/P) ratios are affected by the increase of the reaction pressure or conversion for the three reactors with differently reduced catalysts (Yan et al. 2014). **Figure 6.9** (a) to (c) reveal that at low pressure (1 bar gauge), the product distribution is most olefinic. From **Figure 6.6** shows that the CO conversion was lowest at low pressure (1 bar gauge). It is generally known that at low conversion, the FT products are mostly olefinic (Muleja et al. 2016). These results could suggest that olefins are the primary product of the FTS in all three systems. On the other hand, with increasing pressure (high conversion), the selectivity to paraffins increased and the fraction of olefins decreased, but the extent to which this change occurred varied. When pressure is increased, the selectivity to olefins decreases whereas selectivity to paraffins increases (see **Figure 6.8** (a) to (d)).

When the pressure was at 1 bar(gauge), the H_2 and CO reduced catalyst gave much higher O/P ratios than the syngas reduced one. Although the syngas reduced catalyst gave low O/P ratios, similar to the CO reduced one, both C_3 and C_4 O/P ratios were higher. However, when the operating pressure was increased from 1 bar to 10 bar, the O/P ratios for all three reactors decreased. When the pressure was increased further to 20 bar(gauge), the O/P ratio levels for the H_2 reduced one remained almost unchanged, whereas the syngas and CO reduced ones dropped further, and after dropping the levels were very comparable. These results observed in this work have not previously been noted. These differences could presumably be attributed to the different active phases in these three

different catalysts, as suggested in Chapter 3. Although the catalysts had been under the same operating conditions for more than 10000 hours, the selectivity to light hydrocarbons was still influenced by the condition of different reducing gases applied during the reduction. Dinse et al. (2012) have reported similar findings, that is, the O/P ratio of the products decreased with increasing pressure. However, in the current study, the data show that the original reducing gases tend to influence the O/P ratios at any given pressure.

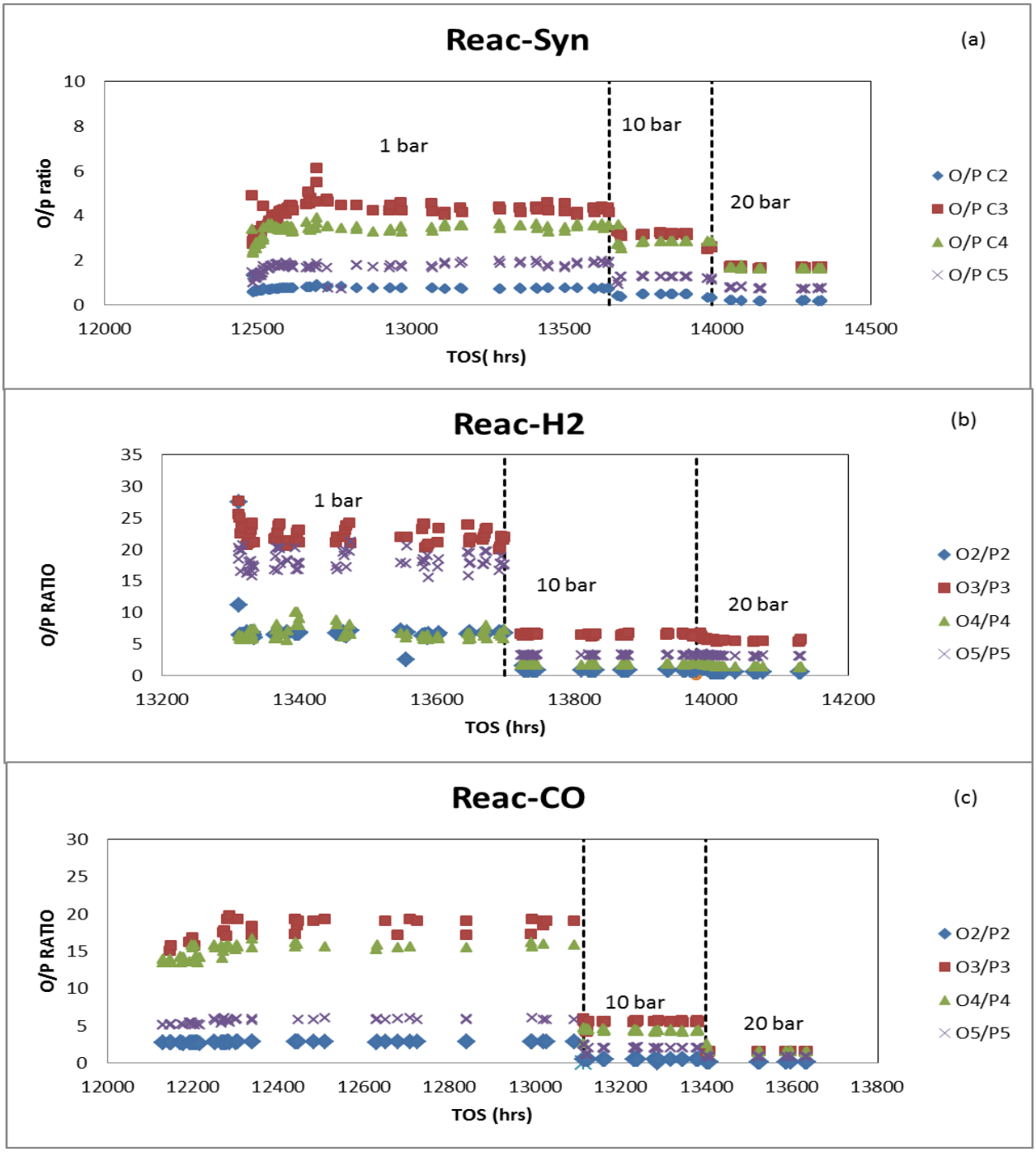

Figure 6.9: Variation of olefin to paraffin ratio with pressure for syngas reduced catalyst: (a) to (c) for the syngas, hydrogen and carbon monoxide reduced catalysts, respectively

6.3.7 **Methane and CO_2 production**

The effect of pressure on the selectivity to methane and carbon dioxide was also measured for all three reactors. The results are displayed in **Figure 6.10** (a) for Reac-Syn, **Figure 6.10** (b) for Reac-H_2 and Figure 6.13 (c) Reac-CO. The data show that with increasing pressure, CO_2 selectivity increases slightly while the CH_4 selectivity remains almost the same, and alkane selectivity increases, while the olefin selectivity decreases overall. Statistical models based on experimental data by Atashi et al. (2015) are also in agreement with these patterns.

The CO_2 selectivity is a function of the extent of the water gas shift (WGS) reaction, and increasing pressure from 1 to 10 bar gave a slight but obvious increase in selectivity, whereas from 10 to 20 the magnitude of increase was insignificant. The CO_2 selectivity increases slightly with pressure for all the reactors. Reac-H_2 (reduced with hydrogen) showed a slight increase in selectivity from 1 to 10 bar gauge from 15.76% to 20.54%, a 1.30-fold increase. And Reac-CO gave a 1.23-fold increase in selectivity from 16.89% to 20.70% at the same pressure increase. Reac-Syn gave the lowest increase, of a 1.12-fold increase (from 16.25% to 18.19%).

In the previous section on flowrate change, where there was a large increase in CO_2 selectivity with residence time, it was surmised that this might be due to the presence of increased water (increased conversion) and hence more WGS activity. However these pressure results do not directly bear this out as there is large increase in conversion with increase in pressure and not the same increase in CO_2 selectivity. It should however be further noted that as the pressure is increased the mean residence time is actually decreased. If the WGS activity is to some extent equilibrium limited then its activity could be somewhat independent of pressure whereas the FT activity could be strongly pressure dependent. This might help to explain the apparent discrepancy between the flowrate and the pressure results.

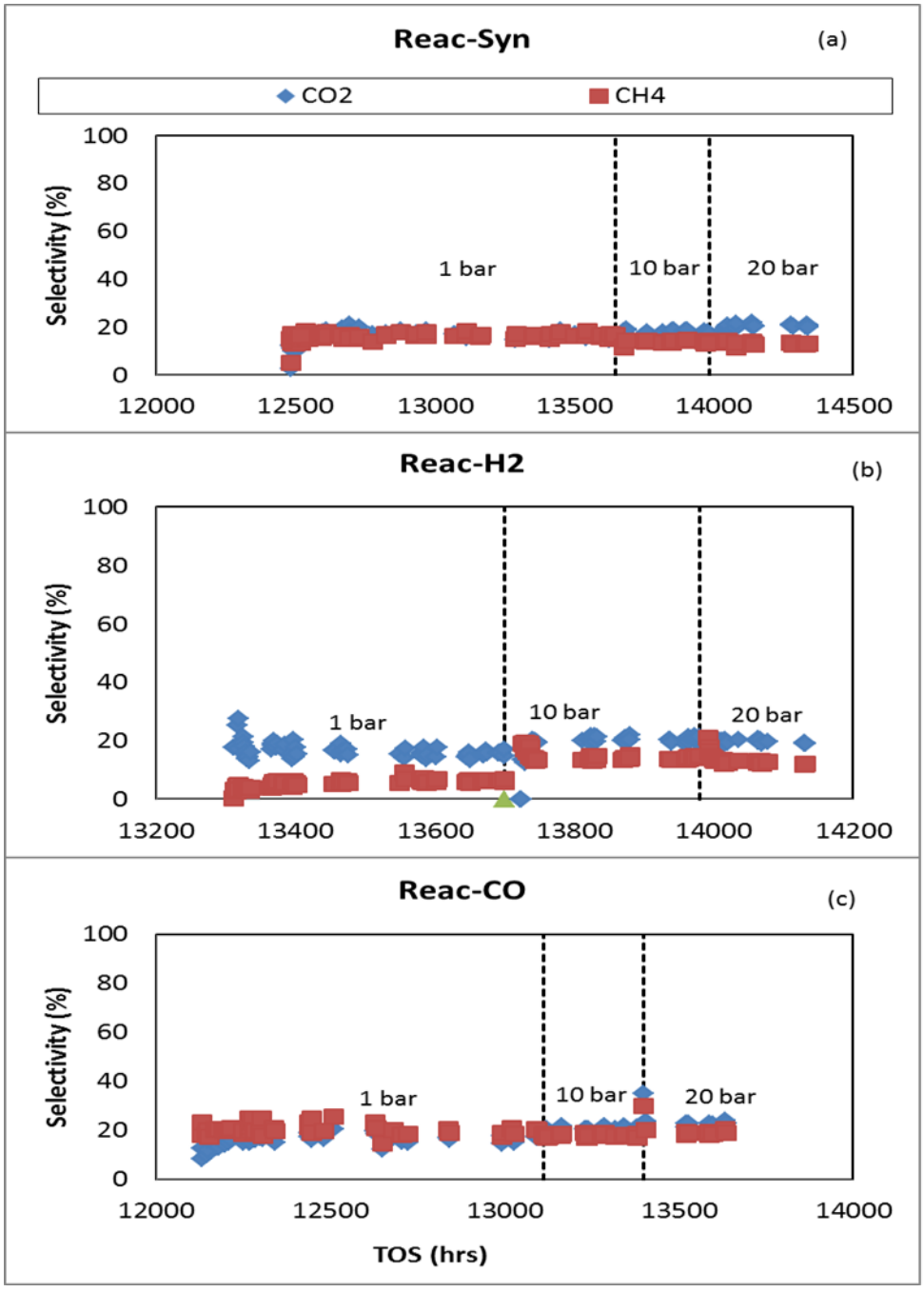

Figure 6.10: The effect of pressure on CO_2 and CH_4 selectivity for (a) Reac-Syn (syngas reduced), (b) Reac-H_2 (hydrogen reduced) and (c) Reac-CO (carbon monoxide reduced) under FT conditions: 60 mL(NTP)/mL, 250 ^{o}C pressure from 1 to 10 bar gauge and 10 to 20 bar gauge

Changes in methane selectivity with pressure are shown in **Figure 6.10**. Methane selectivity was quite high in all reactors (~ 20 %). As shown in **Figure 6.10**, methane selectivity was to some extent governed by the reducing gases, hydrogen reduction giving the lowest percentage selectivity, followed by syngas, and lastly carbon monoxide reduced giving highest selectivity. When the pressure was increased to 10 and then to 20 bar (gauge), the same selectivity to methane for the syngas and hydrogen reduced catalysts was obtained. The Reac-CO reactor was more selective to methane throughout the run, demonstrating that pretreatment procedure results in significant difference in the catalyst response to. This suggests that the iron carbides favoured the formation of methane (Huo et al. 2009; Pérez De Berti et al. 2016). This prediction is supported based on the calculated reaction energies and effective barriers by Huo et al. (2009) using spin-polarized density functional theory calculations that CH_4 formation is more favorable on Fe_5C_2 and Fe_2C. Studies done by Pérez De Berti et al. (2016) support this observation, those researchers showing clearly that activation with pure H_2 leads to a catalyst more active and less selective to methane than that activated with syngas, and this they attributed to different active phases formed with different reduction steps.

6.4 Discussion

The effect of pressure on the FT process with iron catalyst reduced with syngas, hydrogen and carbon monoxide show that increasing total pressure from 1 bar to 10 bar and to 20 bar led to an overall decrease in the formation of olefins and an increase in the formation of paraffins. The syngas reduced catalyst recorded the highest selectivities to C_2, C_3 and C_5 paraffins. The trends observed support the assumption of olefins to undergo secondary hydrogenation to paraffins increases with increasing pressure (Farias et al. 2008b). The olefin and paraffin selectivities were also analysed individually, as illustrated in **Figure 6.2**. It can be seen that at low pressure which results in low CO conversion (due to low reactants partial pressures), the selectivity to olefins was higher for all the reactors and the paraffin selectivities were lower.

On the other hand, the effect of flow rate on the catalyst performance in the FT process is discussed below. The product selectivity (either olefinic or paraffinic) is a function of the process conditions, such as flow rate, temperature and pressure. Decrease in flow rate results in shifts towards the products that are saturated (paraffinic products). Several previous authors have described the effect of these parameters on the yield and selectivity of the FT process (Atashi et al. 2015; Denny & Twigg 1980; Farias et al. 2010; Farias et al. 2007).

The influence of the flow rate of the synthesis gas on the selectivity has been investigated by Dinse et al. (2012), who observed a decrease in the olefin to paraffin ratio with increasing conversion. The CO conversion increases with decreasing flow rates due to increased residence time. These findings are consistent with what is in the literature. The general assumption is that the readsorption chances of the α-olefins increase with contact time inside the pores (Kuipers et al., 1995). Kuiper et al. (1995) have also shown that paraffin selectivity decreases with increasing flow rate. This conclusion was reached after investigating four different flow rates (5, 10, 15 and 20 NmL/min). These findings support the statement that the olefin/paraffin ratio is not affected by the transport limitation only flow rate plays a significant role. The formed paraffins cannot undergo a secondary reaction under FT conditions of operation, whereas the olefins will undergo hydrogenation or be reinserted into the growing chain, hence the decrease in the olefin/paraffin ratio with increased residence time.

6.5 Conclusion

Effects of process conditions (reaction pressure and flow rate) on reactant consumption and product distribution were studied in a fixed-bed reactor during conventional FTS. It was found that olefin content decreased and paraffin increased with either increased pressure or decreasing flow rate, whereas methane selectivities were essentially independent of reaction conditions. Reduction in residence time retarded the secondary reaction that is paraffin formation, and reduction in the reactor pressure has the same effect.

There were still significant differences in the selectivities of the catalysts reduced in different ways after more than 12000 hours of similar operations. This suggests that the original reductions of the catalyst caused permanent changes in the catalysts. What these might be, are difficult to imagine.

References

Atashi, H., Razmjooei, S., Khorashadizadeh, M., Shiva, M., Tabrizi, F. F., & Mousavi, S. A. H. S. (2015). Effects of operating conditions on selectivity of Fe-Co-Mn/MgO at high temperature CO hydrogenation. *Journal of the Taiwan Institute of Chemical Engineers*, *54*, 83–90. http://doi.org/10.1016/j.jtice.2015.03.017

Atashi, H., Razmjooei, S., Khorashadizadeh, M., Shiva, M., Tabrizi, F. F., & Mousavi, S. A. H. S. (2015). Effects of operating conditions on selectivity of Fe–Co–Mn/MgO at high temperature CO hydrogenation. *Journal of the Taiwan Institute of Chemical Engineers*, *54*, 83–90. http://doi.org/10.1016/j.jtice.2015.03.017

Bukur, D. B., & Lang, X. (1999). Highly active and stable iron Fischer-Tropsch catalyst for synthesis gas conversion to liquid fuels. *Industrial and Engineering Chemistry Research*, *38*(9), 3270–3275.

Collett, C. H., & McGregor, J. (2016). Things go better with coke: The beneficial role of carbonaceous deposits in heterogeneous catalysis. *Catalysis Science and Technology*, *6*(2), 363–378. http://doi.org/10.1039/c5cy01236h

Dalai, A. K., & Davis, B. H. (2008). Fischer-Tropsch synthesis: A review of water effects on the performances of unsupported and supported Co catalysts. *Applied Catalysis A: General*, *348*(1), 1–15. http://doi.org/10.1016/j.apcata.2008.06.021

de Klerk, A., & Maitlis, P. M. (2013). What Can We Do with Fischer-Tropsch Products? In *Greener Fischer-Tropsch Processes for Fuels and Feedstocks* (pp. 81–105). Retrieved from http://www.scopus.com/inward/record.url?eid=2-s2.0-84886325490&partnerID=40&md5=42789a81c56c1d4da204e95afa7e3632

Denny, P. J., & Twigg, M. V. (1980). *Factors Determining the Life of Industrial Heterogeneous Catalysts* (Vol. 6). Retrieved from http://www.scopus.com/inward/record.url?eid=2-s2.0-0019227790&partnerID=40&md5=4b61b3e9d99a15399f437b6c02ffc731

Dinse, A., Aigner, M., Ulbrich, M., Johnson, G. R., & Bell, A. T. (2012). Effects of Mn promotion on the activity and selectivity of Co/SiO 2 for Fischer-Tropsch Synthesis. *Journal of Catalysis*, *288*, 104–114. http://doi.org/10.1016/j.jcat.2012.01.008

Dry, M. E. (1983). *SASOL FISCHER - TROPSCH PROCESSES.* (Vol. 2). Retrieved from http://www.scopus.com/inward/record.url?eid=2-s2.0-0020863666&partnerID=40&md5=48a768eaada5ef6e07f30b9ea0e66687

Farias, F. E. M., Fernandes, F. a. N., & Sales, F. G. (2010). Effect of operating conditions on Fischer-Tropsch liquid products produced by unpromoted and potassium-promoted iron catalyst. *Latin American Applied Research*, *40*(2), 161–166.

Farias, F. E. M., Sales, F. G., & Fernandes, F. A. N. (2008a). Effect of operating conditions and potassium content on Fischer-Tropsch liquid products produced by potassium-promoted iron catalysts. *Journal of Natural Gas Chemistry*, *17*(2), 175–178. http://doi.org/10.1016/S1003-9953(08)60047-X

Farias, F. E. M., Sales, F. G., & Fernandes, F. A. N. (2008b). Effect of operating conditions and potassium content on Fischer-Tropsch liquid products produced by potassium-promoted iron catalysts. *Journal of Natural Gas Chemistry*, *17*(2), 175–178. http://doi.org/10.1016/S1003-9953(08)60047-X

Farias, F. E. M., Silva, F. R. C., Cartaxo, S. J. M., Fernandes, F. A. N., & Sales, F. G. (2007). Effect of operating conditions on Fischer-Tropsch liquid products. *Latin American Applied Research*, *37*(4), 283–287.

Hallac, B. B., Keyvanloo, K., Hedengren, J. D., Hecker, W. C., & Argyle, M. D. (2015). An optimized simulation model for iron-based Fischer-Tropsch catalyst design: Transfer limitations as functions of operating and design conditions. *Chemical Engineering Journal*, *263*, 268–279. http://doi.org/10.1016/j.cej.2014.10.108

Huo, C.-F., Li, Y.-W., Jianguo, W., & Haijun, J. (2009). Insight into CH4 formation in iron-Catalysed Fischer-Tropsch synthesis. *Journal of the American Chemical Society*, *131*(41), 14713–14721. http://doi.org/10.1021/ja9021864

Kuipers, E. W., Scheper, C., Wilson, J. H., Vinkenburg, I. H., & Oosterbeek, H. (1996). Non-ASF Product Distributions Due to Secondary Reactions during

Fischer–Tropsch Synthesis. *Journal of Catalysis*, *158*(1), 288–300. http://doi.org/10.1006/jcat.1996.0028

Kuipers, E. W., Vinkenburg, I. H., & Oosterbeek, H. (1995). Chain Length Dependence of α-Olefin Readsorption in Fischer-Tropsch Synthesis. *Journal of Catalysis*, *152*(1), 137–146. http://doi.org/10.1006/jcat.1995.1068

Maitlis, P. M., & de Klerk, A. (2013). *Greener Fischer-Tropsch Processes for Fuels and Feedstocks*. Retrieved from http://www.scopus.com/inward/record.url?eid=2-s2.0-84891585298&partnerID=40&md5=bb8fe751c73e28307e8a7191396f1118

Mousavi, S., Zamaniyan, A., Irani, M., & Rashidzadeh, M. (2015). Generalized kinetic model for iron and cobalt based Fischer-Tropsch synthesis catalysts: Review and model evaluation. *Applied Catalysis A: General*, *506*, 57–66. http://doi.org/10.1016/j.apcata.2015.08.020

Muleja, A. A., Yao, Y., Glasser, D., & Hildebrandt, D. (2016). A study of Fischer-Tropsch synthesis: Product distribution of the light hydrocarbons. *Applied Catalysis A: General*, *517*, 217–226. http://doi.org/10.1016/j.apcata.2016.03.015

Muleja, A. A., Yao, Y., Glasser, D., & Hildebrandt, D. (2016). Effect of feeding nitrogen to a fixed bed Fischer-Tropsch reactor while keeping the partial pressures of reactants the same. *Chemical Engineering Journal*, *293*, 151–160. http://doi.org/10.1016/j.cej.2016.02.059

Nakhaei Pour, A., Khodabandeh, H., Izadyar, M., & Housaindokht, M. R. (2014). Detailed kinetics of Fischer-Tropsch synthesis on a precipitated iron catalyst. *Reaction Kinetics, Mechanisms and Catalysis*, *111*(1), 29–44. http://doi.org/10.1007/s11144-013-0640-8

Okeson, T. J., Keyvanloo, K., Lawson, J. S., Argyle, M. D., & Hecker, W. C. (2016). On the kinetics and mechanism of Fischer-Tropsch synthesis on a highly active iron catalyst supported on silica-stabilized alumina. *Catalysis Today*, *261*, 67–74. http://doi.org/10.1016/j.cattod.2015.08.054

Pérez De Berti, I. O., Bengoa, J. F., Stewart, S. J., Cagnoli, M. V., Pecchi, G., & Marchetti, S. G. (2016). Effect of activation atmosphere in the Fischer-Tropsch Synthesis using a “quasi-model” catalyst of γ-Fe2O3 nanoparticles

supported on SBA-15. *Journal of Catalysis*, *335*, 36–46. http://doi.org/10.1016/j.jcat.2015.12.004

Rauch, R., Kiennemann, A., & Sauciuc, A. (2013). Fischer-Tropsch Synthesis to Biofuels (BtL Process). In *The Role of Catalysis for the Sustainable Production of Bio-Fuels and Bio-Chemicals* (pp. 397–443). Retrieved from http://www.scopus.com/inward/record.url?eid=2-s2.0-84926448805&partnerID=40&md5=6295e204b170e53d9a691dbaa5e2d70c

Sartipi, S., Makkee, M., Kapteijn, F., & Gascon, J. (2014). Catalysis engineering of bifunctional solids for the one-step synthesis of liquid fuels from syngas: A review. *Catalysis Science and Technology*, *4*(4), 893–907. http://doi.org/10.1039/c3cy01021j

Sault, A. G., & Datye, A. K. (1993). An Auger Electron Spectroscopy Study of the Activation of Iron Fischer-Tropsch Catalysts. II. Carbon Monoxide Activation. *Journal of Catalysis*, *140*(1), 136–149. http://doi.org/10.1006/jcat.1993.1073

Shi, B., & Davis, B. H. (2005). Fischer–Tropsch synthesis: The paraffin to olefin ratio as a function of carbon number. *International Conference on Gas-Fuel 05International Conference on Gas-Fuel 05International Conference on Gas-Fuel 05*, *106*(1–4), 129–131. http://doi.org/10.1016/j.cattod.2005.07.159

Soled, S., Iglesia, E., & Fiato, R. A. (1990). Activity and selectivity control in iron Catalysed Fischer-Tropsch synthesis - The influence of iron catalyst phase on slurry Fischer-Tropsch reaction pathways; Selective synthesis of alpha-olefins. *Catalysis Letters*, *7*(1-4), 271–280. http://doi.org/10.1007/BF00764508

Todic, B., Nowicki, L., Nikacevic, N., & Bukur, D. B. (2016a). Fischer-Tropsch synthesis product selectivity over an industrial iron-based catalyst: Effect of process conditions. *Catalysis Today*, *261*, 28–39. http://doi.org/10.1016/j.cattod.2015.09.005

Todic, B., Nowicki, L., Nikacevic, N., & Bukur, D. B. (2016b). Fischer-Tropsch synthesis product selectivity over an industrial iron-based catalyst: Effect of process conditions. *Catalysis Today*, *261*, 28–39. http://doi.org/10.1016/j.cattod.2015.09.005

Yan, F., Qian, W., Sun, Q., Zhang, H., Ying, W., & Fang, D. (2014). Product distributions and olefin-to-paraffin ratio over an iron-based catalyst for Fischer–Tropsch synthesis. *Reaction Kinetics, Mechanisms and Catalysis*, *113*(2), 471–485. http://doi.org/10.1007/s11144-014-0746-7

CHAPTER 7

GAS PHASE PRODUCTS FROM FISCHER TROPSCH EXPERIMENTS AFTER OXIDATIVE REGENERATION OF IRON BASED CATALYSTS

The material in this chapter has been written in a paper format for submission to the Journal of Catalysis.

Abstract

This chapter reports on the regeneration of iron based catalysts used to convert synthesis gas (syngas) to hydrocarbons in a fixed bed reactor operated at a low pressure. As described in Chapter 4, the iron catalyst was loaded into three separate reactors, and then reduced using three different reducing agents, namely, syngas (in Reac-Syn), hydrogen (in Reac-H_2) and carbon monoxide (in Reac-CO). The conditions in the reactors were kept at a constant temperature of 250 $^{\circ}$C, a flow rate of 60 mL(NTP)/min and a pressure of 1 atm for a period of 48 hrs. The Fischer Tropsch reactions were then carried out using the reduced catalysts and under the same conditions of temperature and gas flow rate, but increasing the operating pressure to 1 bar. The activity, selectivity and degree of conversion by the catalysts were then measured and compared at different time intervals until the catalyst was deactivated. The spent catalysts were then regenerated in all the three reactors using syngas as the only reducing agent. After the regeneration step, Fischer Tropsch runs were conducted under similar conditions as those used before regeneration, and the activity, selectivity of the gas phase products and conversion were measured again and compared to the performance of the catalyst prior to regeneration. The objective was to investigate whether oxidative regeneration restored the catalyst performance to levels achieved prior to regeneration.

7.1 Introduction

Fischer Tropsch synthesis (FTS) is a catalysed reaction that converts synthesis gas (syngas) to linear hydrocarbons, predominantly alkanes and alkenes. Cobalt and iron are the most used metal based catalyst in FTS reactors (Van de Loosdrecht et al. 2013; Rauch, Kiennemann, and Sauciuc 2013; de Klerk, Li, and Zennaro 2013; Lappas and Heracleous 2010; Van Ommen and Grievink 2014). Catalyst deactivation in the Fischer Tropsch reaction has been a topic of industrial and academic interest for many years (Polinski et al. 1984; Bartholomew 1984; Butt 1984; Moulijn et al. 2001; Istadi et al. 2011a; Hegedus and McCabe 1980; Butt 1982; Marafi et al. 2010a). In many cases it is difficult to trace the origin of catalyst deactivation. Bartholomew (1984) and Hegedus and McCabe (1980) reported that catalyst deactivation is a complex problem where several mechanisms contribute to the loss of activity and/or selectivity.

In Fischer Tropsch synthesis, the progressive deactivation of catalysts is of major economic concern, and understanding the stability of catalysts has become as essential as controlling their activity and selectivity (Ahn and Bae 2015; Meshkani and Rezaei 2015; Brunner et al. 2015; Zheng et al. 2015). For these reasons, it is important to understand the catalyst deactivation or loss in selectivity, and to investigate possible efficient regenerative solutions. It appears that catalyst deactivation is an inevitable phenomenon in the Fischer Tropsch process and the results of this mechanism can be delayed and/or reversed during the regeneration (Marafi et al. 2010; Van Loosdrecht et al. 2008; Windawi and Katzer 1980).

The literature on catalyst deactivation categorizes the deactivation process according to different types, such as chemical, thermal, and mechanical deactivation, and by mechanism, such as poisoning, fouling, thermal degradation, vapour formation, vapour–solid and solid–solid reactions, and attrition/crushing (Argyle and Bartholomew 2015a).

The science of catalyst deactivation has received considerable interest from scientists, and extensive studies have been published in the form of books, (Butt

1984; Raje et al. 1997; Bogdan et al. 1988; Denny and Twigg 1980; Zhang et al. 2001), comprehensive reviews on the subject (Bartholomew 1984; Argyle and Bartholomew 2015b; Ferdous and Demirel 2010), and journal articles (Moulijn et al. 2001; Hegedus and McCabe 1980; Butt 1982; Raje et al. 1997). Argyle and Bartholomew (2015b) reported with a more detailed description of the methods for renewing deactivated catalysts, that is, cleaning, rejuvenating, and regenerating (Argyle and Bartholomew 2015b). However, the focus of this chapter is to investigate the regenerability of the iron based catalysts. Argyle and Bartholomew (2015b) defined regeneration as a complete restoration of the catalytically active materials to bring the catalyst to its original state, or even achieving a higher catalytic activity through a series of relatively sophisticated treatments.

In situ oxidative regenerations of the spent catalyst could be performed after a significant decrease in activity. For example, Pennline and Pollack (1986) reported on the deactivation and regeneration of FT catalysts *in situ* using an oxidative method. The authors observed that the oxidative regeneration did not succeed in returning the catalyst to its initial synthesis activity. Pour and Housaindokht (2013) also used the oxidative regeneration of an iron based catalyst with 10% (v/v) O_2/N_2 gas mixture, and reported that although the method was effective, the catalyst activity was different from the initial activity of the catalyst. Mikhailova et al. (2010) studied the *in situ* regeneration of 20% Co/Hβ cobalt-zeolite FT catalyst, and proposed that the regeneration with hydrogen was most effective at 400 °C, even though the regenerated catalytic levels were lower than the initial values.

Amongst the different deactivating modes, deactivation by coking seems to be the main cause, and has been extensively studied in the literature (Istadi et al. 2011b; Vogelaar et al. 2007; Meng et al. 2007; Lin et al. 2007; Taufiqurrahmi et al. 2010; Nogueira et al. 2011). This mode is an important technological and economic problem in FT and other petrochemical industries. Studies have shown that remedies to counteract catalyst deactivation by coking can be achieved by modifying catalyst surface composition, such as the use of polymetallic catalysts and/or by manipulation of the reaction environment (Whaley and Veser 2010;

Jiménez-García et al. 2010). When the catalyst activity reaches unacceptable limits, the regeneration by oxidative burning off carbon residues in the presence of a medium containing oxygen gas is usually carried out (Li and Wu 2014). However, Li and Wu pointed out that the burn-off must be carefully controlled to avoid overheating which may cause the catalyst to sinter. Therefore, dilution of the oxygen with inert gases such as nitrogen or argon may be more appropriate. Regeneration has been conducted both *in situ* and *ex situ*, and the operation proved to be effective even done for multiple cycles (Van Loosdrecht et al. 2008; Windawi and Katzer 1980).

The rate of carbonaceous material removal from the spent catalysts during medium temperature oxidation was investigated by Lucchini et al. (2016) and Xianghai et al. (2001). From the temperature programmed burn-off, the major reactions occurring during burn-off are proposed to yield CO_2, CO and H_2O (Yoshimura and Furimsky 1986b). Reactions (7.1) to (7.3) represent the non-catalytic burn-off, which has been used as a basis for development of models predicting temperature rise during early stages of burn-off of spent cracking catalysts.

$$C_{(s)} + O_{2(g)} = CO_{2(g)} \qquad (7.1)$$

$$C_{(s)} + \frac{1}{2} O_{2(g)} = CO_{(g)} \qquad (7.2)$$

$$H_{2(g)} + \frac{1}{2} O_{2(g)} = H_2O_{(g)} \qquad (7.3)$$

The probability of burn-off increases with increasing surface area, that is, the greater the loss of surface area due to coke deposition, the slower the burn-off. The rate of deposit removal during burn-off depends on their surface area, and the loss of surface area due to coke deposition was observed to reduce the rate of the burn-off (Yoshimura and Furimsky 1986a). Massoth and Menon (1969) measured the yield of H_2O and carbon oxides produced during burn-off experiments, and observed that the removal of hydrogen from deposits was more rapid than that of

carbon, and the part of deposits that had a high H/C ratio were removed during the very first contact with oxygen. It is believed that in the coke distributed on outer parts of catalyst particles is converted to oxides first, followed by the coke deposited in pores or before the coke deposited in catalyst pores is removed (Yoshimura and Furimsky 1986b). Yoshimura and Furimsky (1986b) proposed that the availability of oxygen in the pores may be affected by mass transfer.

Unfortunately, there is not much information available on the long-term performance (≥ 8760 hours or 12 months) of iron catalyst at low pressure and its regeneration . Furthermore, most of the literature revealed that the *in situ* oxidative experiments were carried out at high pressure (≥ 10 bar) and temperature (≥ 300 ^{o}C). Therefore, the aim of this chapter is to apply an oxidation-reduction method to regenerate the spent iron catalyst, evaluate the regeneration techniques, and suggest their applicability as methods of the regenerating an iron catalyst used over a long period of time. In addition, this chapter evaluates the *in situ* regeneration of commercial iron based catalysts which had operated for 13 000 hrs' time on stream (TOS) at low pressure (1 bar gauge) and medium temperature (250 ^{o}C) in a fixed bed reactor.

7.2 Materials and methods

The iron catalyst was acquired commercially, and contained Fe, Cu and K supported on silica. The catalyst was characterized for physical properties, and the results are depicted in **Table 7.1**.

Table 7.1: BET results of the iron catalyst

Surface Area	**Values**
Single point surface area at P/Po = 0.199:	148.404 m^2/g
BET Surface Area:	153.521 m^2/g
BJH Adsorption cumulative surface area of pores between 1.7 nm and 300.0 nm diameter:	160.259 m^2/g
BJH Desorption cumulative surface area of pores between 1.7 nm and 300.0 nm diameter:	192.719 m^2/g
Pore Volume	
Single point adsorption total pore volume of pores less than 447.83 nm diameter at P/Po = 0.996:	0.416 cm^3/g
BJH Adsorption cumulative volume of pores between 1.7000 nm and 300.0000 nm diameter:	0.437 cm^3/g
BJH Desorption cumulative volume of pores between 1.7 nm and 300.0 nm diameter:	0.454 cm^3/g
Pore Size	
Adsorption average pore width (4V/A by BET):	10.828 nm
BJH Adsorption average pore diameter (4V/A):	10.918 nm
BJH Desorption average pore diameter (4V/A):	9.4310 nm

7.3 Fischer Tropsch synthesis

Fischer Tropsch synthesis experiments were conducted according to the experimental procedure of Chapter 4. Three fixed bed reactors were each loaded (in the middle of the reactor) with 1 gram of a commercial iron catalyst. The catalyst was reduced with syngas for Reactor 1(names Reac-Syn), hydrogen for Reactor 2(Reac-H_2), and carbon monoxide for Reactor 3(Reac-CO), at 250 $^{\circ}$C, and gas flowrate of 60 mL(NTP)/min, for 48 hours at ambient pressure. The reactor pressure for the syngas reduced reactor (Reac-Syn) was adjusted to 1 bar gauge and the FT runs started. For Reac-H_2, (H_2 reduced) and Reac-CO (CO reduced), the flows for the H_2 and CO were stopped after 48 hours and replaced with the syngas at 1 bar gauge and 60 mL(NTP)/min. The FT runs were performed for 1000 hours under the above mentioned operating conditions, and thereafter several other alternative conditions were applied until 12 000 hours of time on stream. When the catalyst showed a decrease in the activity of more than 50% in all the three reactors, *in situ* regeneration was initiated. The regeneration process comprized passing oxygen gas from a premixed cylinder of composition 4.9% O_2 in 94.1% helium through the catalyst. This cylinder was connected to the system and arranged such that flow during oxidation could be varied to the desired parameters.

The procedure adopted was a modified oxidative regeneration process which has been applied in different systems (Saib et al. 2010; Pennline and Pollack 1986). The same regeneration steps were conducted for all the three reactors at a different time on stream (TOS) starting with Reac-Syn followed by Reac-CO and lastly Reac-H_2 (the sequence of regeneration was arbitrary). The following steps were followed:

- The flow of syngas to the reactor, which was set at 60 mL(NTP)/min, was stopped and nitrogen gas was introduced into the system at the same flow rate.

- The back pressure regulator was fully opened to allow the system to be at atmospheric pressure.

- The temperature was increased from 250 to 270 °C at a ramping rate of 1 °C/min.

- The reactor was then left under the flow of nitrogen at 60 mL(NTP)/min, at atmospheric pressure, and at 270 °C for 12 hrs .

- Then the temperature was decreased from 270 to 100 °C and a mixture gas of 4.9% O_2 in 94.1% helium was introduced to the reactor at a flow rate of 30 mL(NTP)/min, whilst the flow of N_2 (60 mL(NTP)/min) was maintained through the reactor. This was continued overnight.

- After that, the temperature of the reactor was increased to 180 °C at a ramping rate of 20 °C in 10 mins and maintained there for one hour, then increased another 20 °C in 10 mins until 200 °C.

- While the temperature was still at 200 °C, the flow of N_2 was stopped and that of O_2/He remained at 30 mL(NTP)/min overnight.

- N_2 was then re-introduced at 60 mL(NTP)/min whilst the flow of O_2/He was slowly reduced to zero; this marked the end of catalyst oxygenation.

The catalyst oxidation process was then followed by the reduction pathway. The temperature was reduced to 120 °C and kept there for 2 hours in order to dry the moisture from the reactor. This was followed by the reduction of the catalyst under the same conditions (250 °C, 60 mL(NTP)/min at atmospheric pressure for 48 hours) as done previously, but this time syngas was used as the reducing agent for all the reactors. This marked the end of regeneration. After regeneration, the researcher reverted to normal FT runs where the reactor pressure was increased to 1 bar gauge and the flow rate maintained at 60 mL(NTP)/min at a temperature at 250 °C. Throughout the FT runs the tail gas from the rig was monitored with a DANI GC fitted with a flame ionisation detector (FID) and two thermal conductivity

detectors (TCD A and TCD B). The monitoring was conducted in order to analyse both the inorganic and hydrocarbon gases in the gas phase. The data obtained after the regeneration were compared with the data obtained prior to regeneration.

7.4 Results and discussion

The catalyst activity measured by CO consumption rates and as a function of time on stream (TOS) during the steady-state period before regeneration, during reduction, and after regeneration for the three differently reduced reactors, is shown in **Figures 7.1** (a), (b) and (c). Although the regeneration procedure employed was the same for all the reactors, the Reac-Syn (syngas reduced reactor) comparatively showed a significant increase in activity by 53.40% after regeneration (when compared to the activity before regeneration), whereas the Reac-H_2 (hydrogen reduced reactor) increased by 1.18% and the Reac-CO (Carbon monoxide reduced reactor) by 6.25% on average. The underlying reasons for such a difference in the magnitude in percentage increase observed are not yet understood. The activity and stability during the post regeneration catalytic tests remained stable.

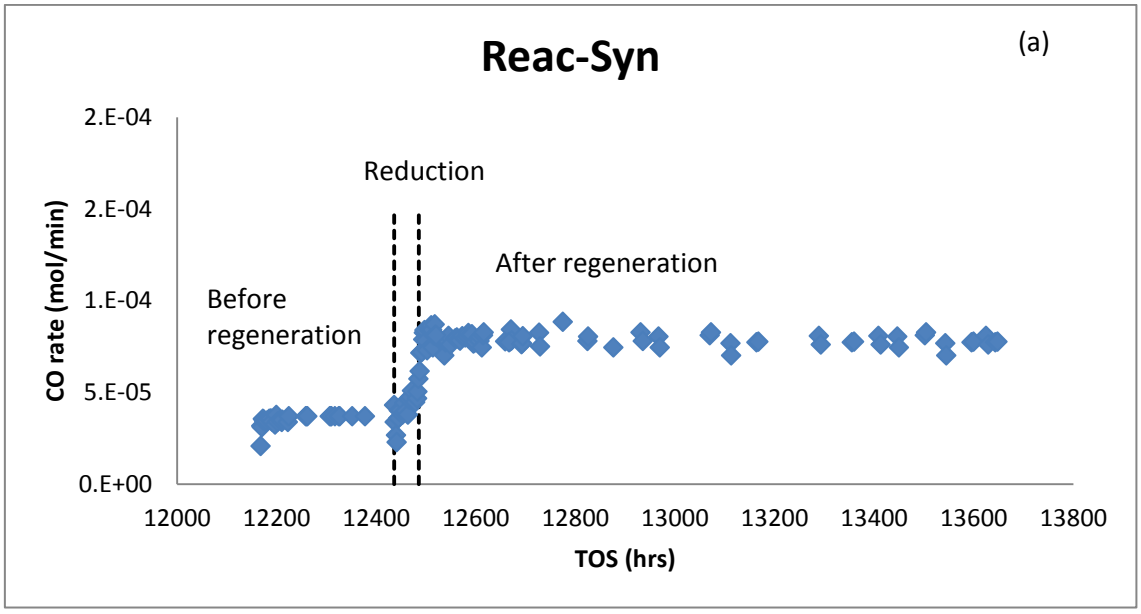
Reac-Syn
(a)
2.E-04
2.E-04
1.E-04
5.E-05
0.E+00
CO rate (mol/min)
Reduction
After regeneration
Before
regeneration
12000
12200
12400
12600
12800
13000
13200
13400
13600
13800
TOS (hrs)

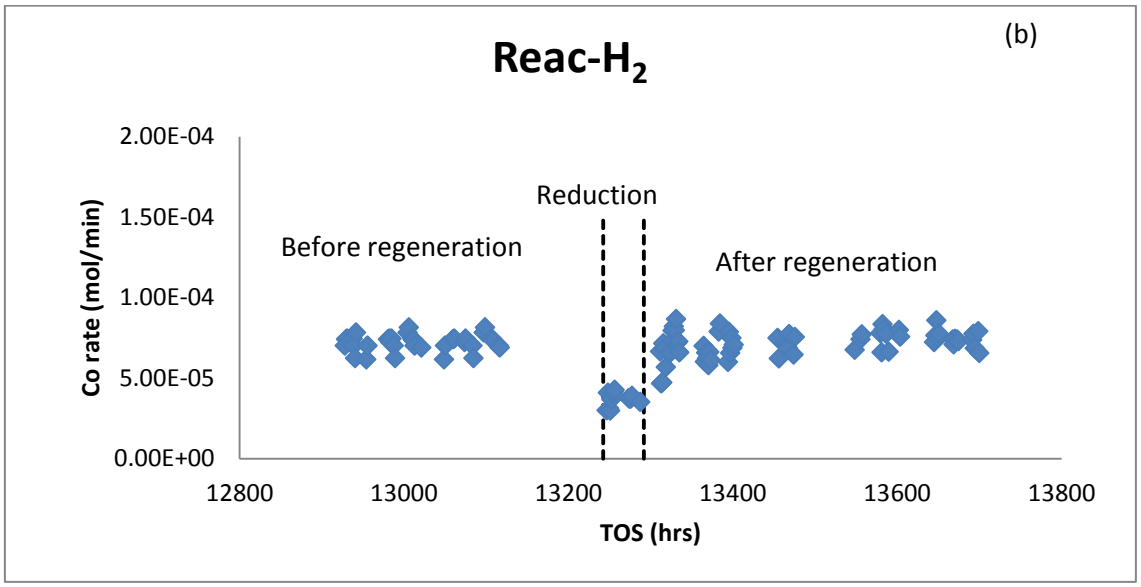
Reac-H2
(b)
2.00E-04
1.50E-04
1.00E-04
5.00E-05
0.00E+00
Co rate (mol/min)
Reduction
Before regeneration
After regeneration
12800
13000
13200
13400
13600
13800
TOS (hrs)

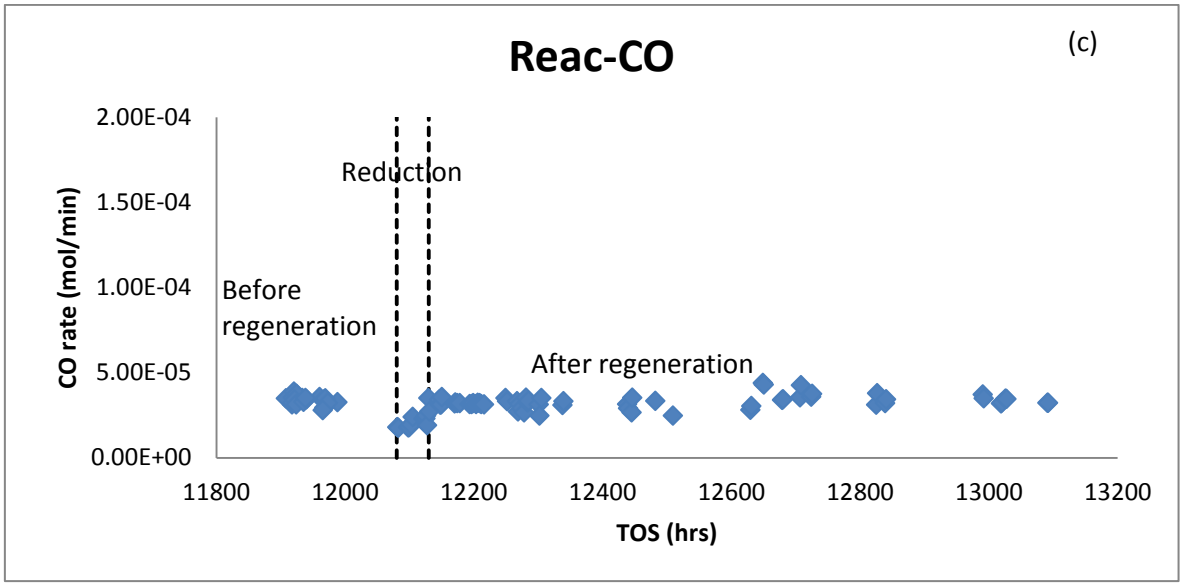

Figure 7.1: CO consumption rate before, during and after the regeneration under operating conditions: 250 ^{o}C, 60 mL(NTP)/min at 1 bar(gauge) for (a) Reac-Syn (syngas reduced), (b) Reac-H_2 (hydrogen reduced) and (c) Reac-CO (carbon monoxide reduced reactors).

Figures 7.2 (a – c) show the WGS which is the ratio of CO_2 production to total CO consumption. FT selectivity was measured as a function of the CO converted to hydrocarbons and the CO conversion. The three graphed parameters showed an appreciable change after the regeneration procedure. The WGS reactions for all the differently reduced reactors show an increase of 78.26% for Reac-H_2, 77.06% for Reac-CO and 74.29% for Reac-Syn reduced. Surprisingly although the overall CO reaction rates are different, all three catalysts have shown similar increase in the CO_2 selectivity. However, the differences among these three reactors is almost negligible. The FT selectivity values decline with an increase in WGS selectivity since these two reactions are antagonistic. The said selectivities did not vary much with time on stream or with the activation route.

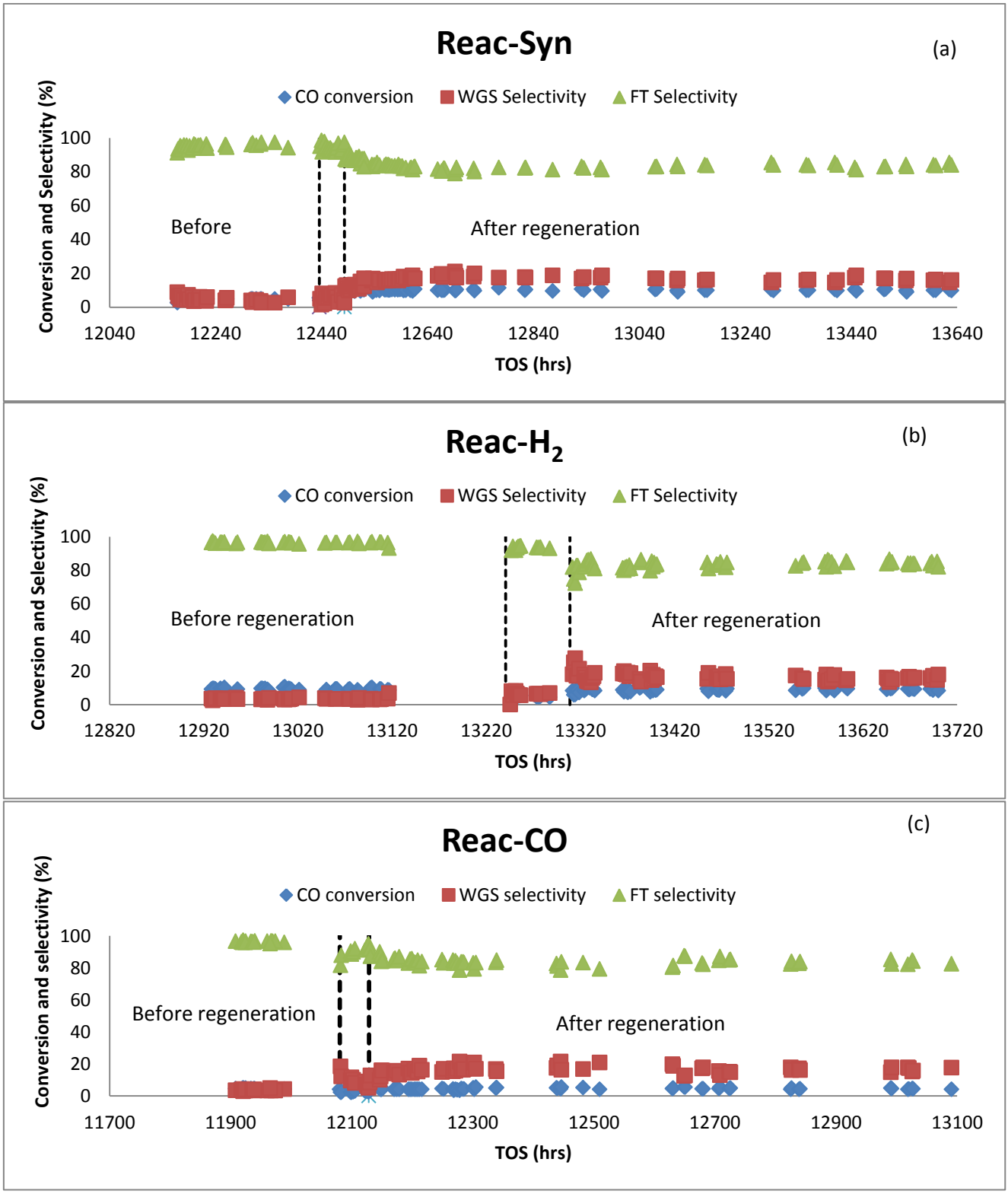

Figure 7.2: CO conversion and FT selectivity before, during and after regeneration under operating conditions: 250 °C, 60 mL(NTP)/min at 1 bar gauge for (a) Reac-Syn, (b) Reac-H_2 and (c) Reac-CO reactors. Regeneration period is indicated by dotted lines

During the regeneration procedure, the catalysts in the reactors were activated, as evidenced by an increase in the CO conversion and also a shift in the product distribution. **Figure 7.3** (a) and (b) depict olefinic and paraffinic product selectivities before and after regeneration, respectively. The general trend observed on the olefinic products is that the selectivities increase in all the differently reduced reactors, though the increases are of different magnitudes. The least observed increase was exhibited by the Reac-H_2 originally reduced catalyst for C_2 and C_3 olefins with percentage increases of 11.85% and 4.38%, respectively. The highly activated catalyst is the one which was originally reduced with CO (Reac-CO) which showed highest increase in the olefinic products C_2 (47.39%), C_3 (70.74%), C_4 (76.34%) and C_5 (79.60%).

The initially syngas reduced reactor after regeneration was more selective to the paraffinic products. **Figure 7.3** (b) depicts changes observed before and after the oxidative regeneration to product selectivities. Reac-Syn and Reac-CO show a selectivity increase for all the components (both olefins and paraffins), whereas the hydrogen reduced exhibit a decrease in the paraffinic selectivities. The syngas reduced showed an average selectivity of 80.53% for C_2–C_5 paraffins. The hydrogen reduced exhibited a decrease in paraffin selectivity. This particular catalyst did not change significantly.

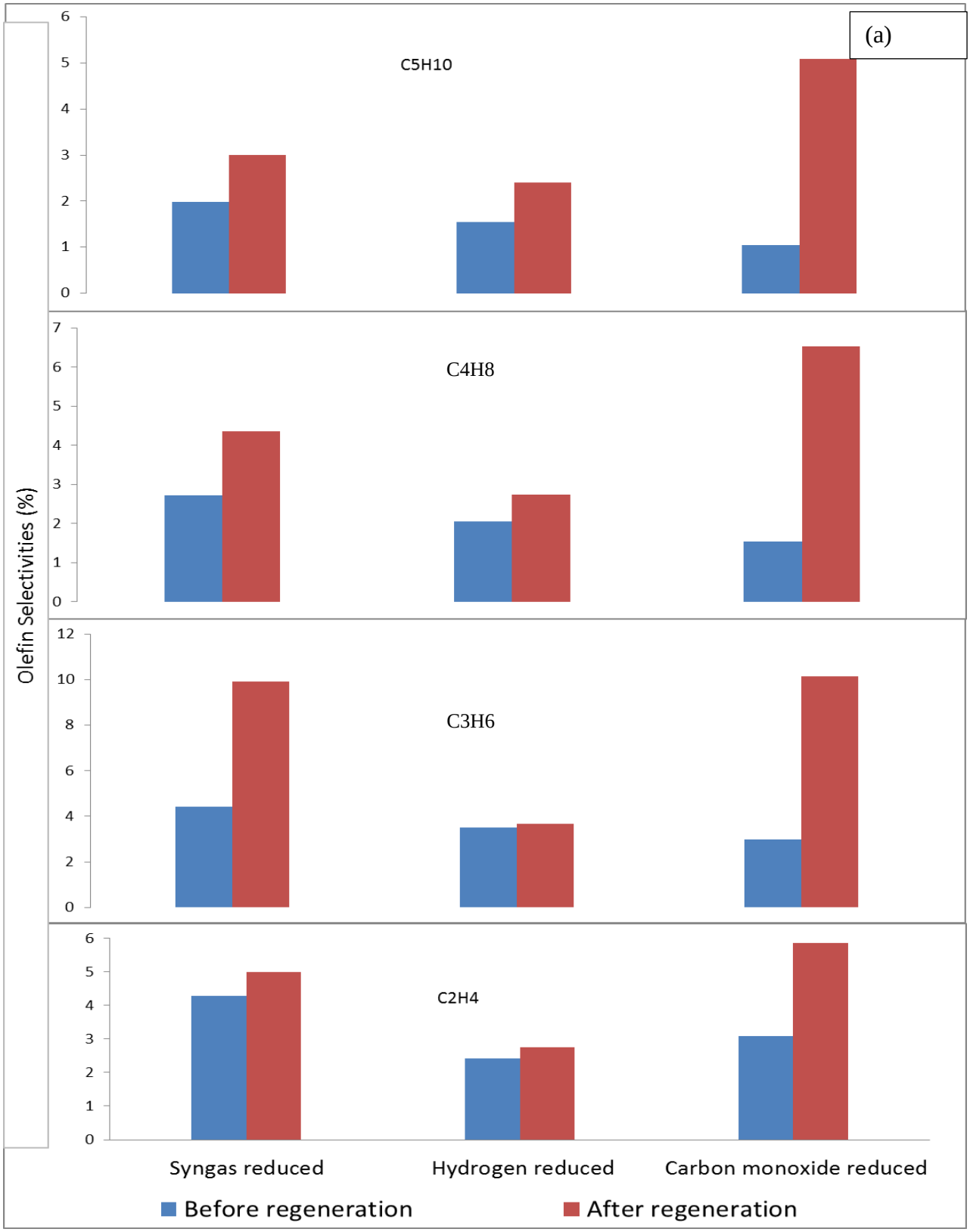
(a)
C5H10
C4H8
C3H6
C2H4
Olefin Selectivities (%)
Syngas reduced
Hydrogen reduced
Carbon monoxide reduced
Before regeneration
After regeneration

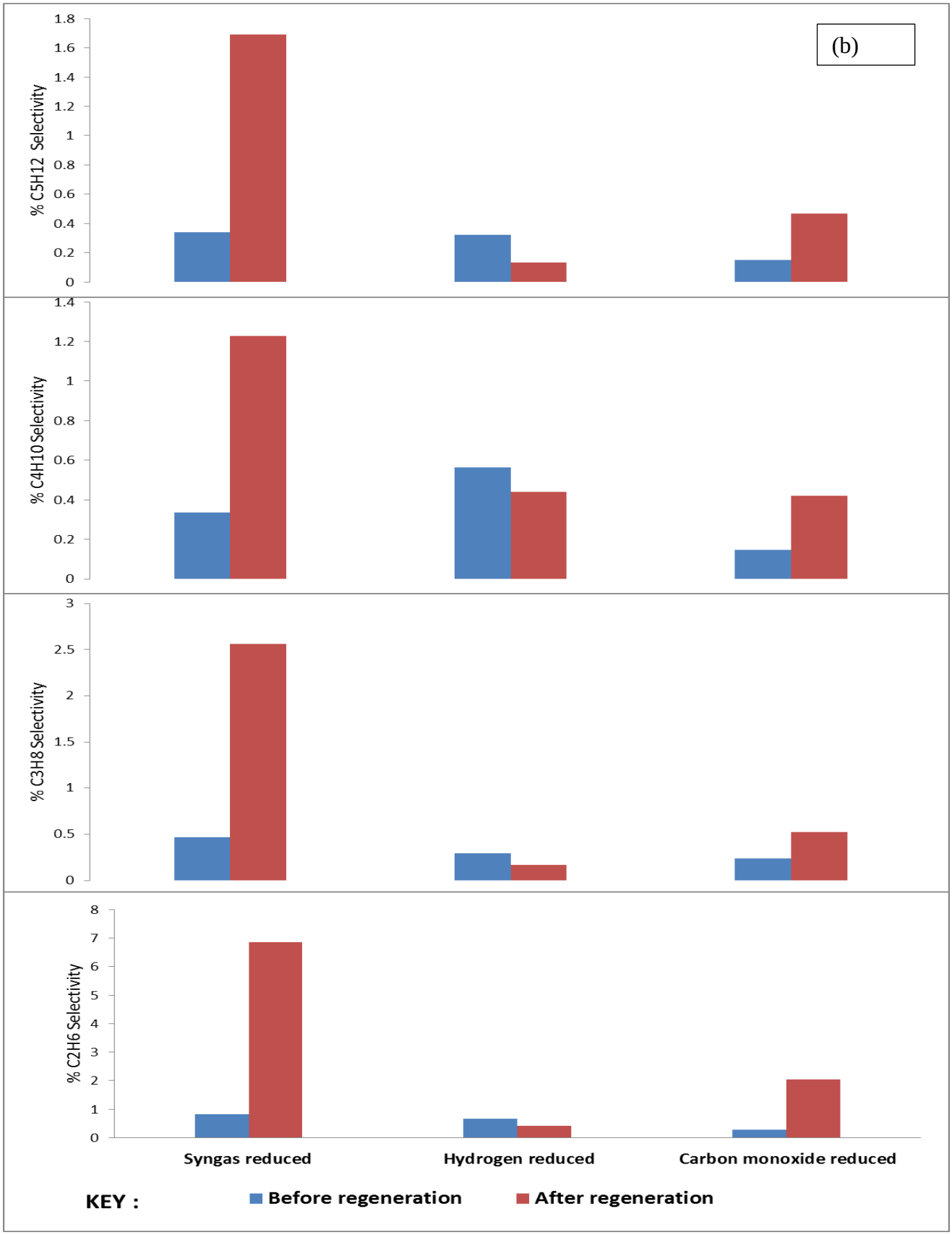
(b)
% C5H12 Selectivity
1.8
1.6
1.4
1.2
1
0.8
0.6
0.4
0.2
0
% C4H10 Selectivity
1.4
1.2
1
0.8
0.6
0.4
0.2
0
% C3H8 Selectivity
3
2.5
2
1.5
1
0.5
0
% C2H6 Selectivity
8
7
6
5
4
3
2
1
0
Syngas reduced
Hydrogen reduced
Carbon monoxide reduced
KEY :
Before regeneration
After regeneration

Figure 7.3: Selectivity to the light hydrocarbons before and after regeneration under operating conditions: 250 °C, 60 mL(NTP)/min at 1 bar gauge for average data (a) olefin, (b) paraffin for different reducing agents/reactors.

Figure 7.4 depicts the selectivity to the carbon dioxide, methane and heavy hydrocarbon (C_{5+}) as a function of reducing agent. The regeneration resulted in hydrocarbon distribution shifting to a lighter fraction, as noted by the decrease in the C_{5+} selectivity in all reactors. The methane selectivity increased for the syngas reduced by 50.37%, 71.53% for the CO reduced and the hydrogen reduced experienced a decrease of 5.91%. The WGS selectivity for all the reactors increased by almost the same magnitude of about 76.54%.

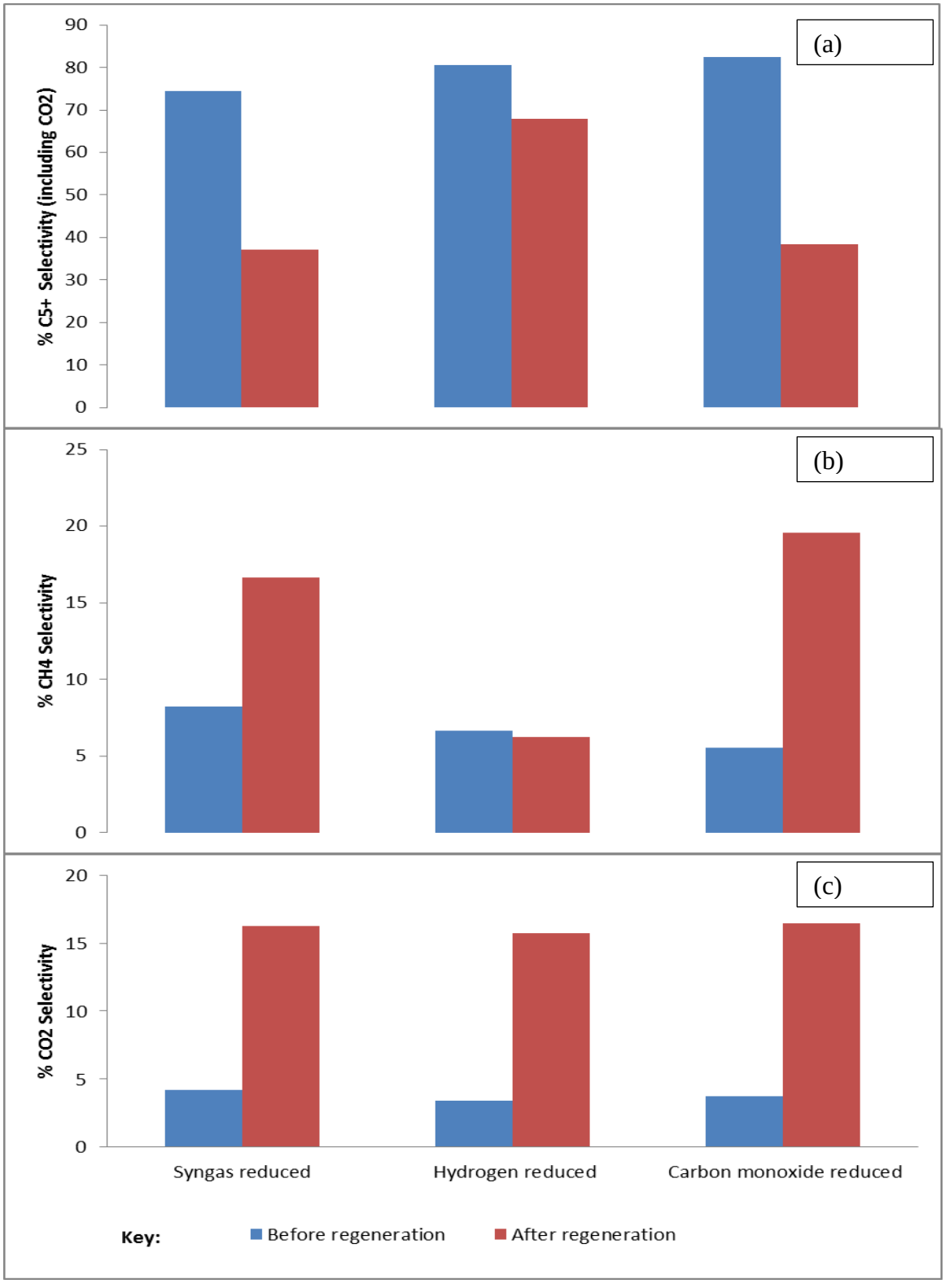

Figure 7.4: Selectivity to CO_2, CH_4 and C_{5+} before and after regeneration under operating conditions: 250 ^{o}C, 60 mL(NTP)/min at 1 bar gauge for average data (a) CO_2, (b) CH_4 and (c) C_{5+} for different reducing agents/reactors.

In an endeavour to account for these differences, the fresh catalyst together with the spent catalyst from the three different reactors was subjected to HRTEM imaging.

The catalyst samples (from the three reactors) were prepared by drop-coating one drop of specimen solution onto a holey carbon coated nickel grid. This was then dried under a Xenon lamp for about 10 minutes, where after the sample coated grids were analysed under the microscope. Transmission electron micrographs were collected using an FEI Tecnai G2 20 field-emission gun (FEG) TEM, operated in bright field mode at an accelerating voltage of 200 kV. Energy dispersive x-ray spectra were collected using an EDAX liquid nitrogen cooled Lithium doped Silicon detector.

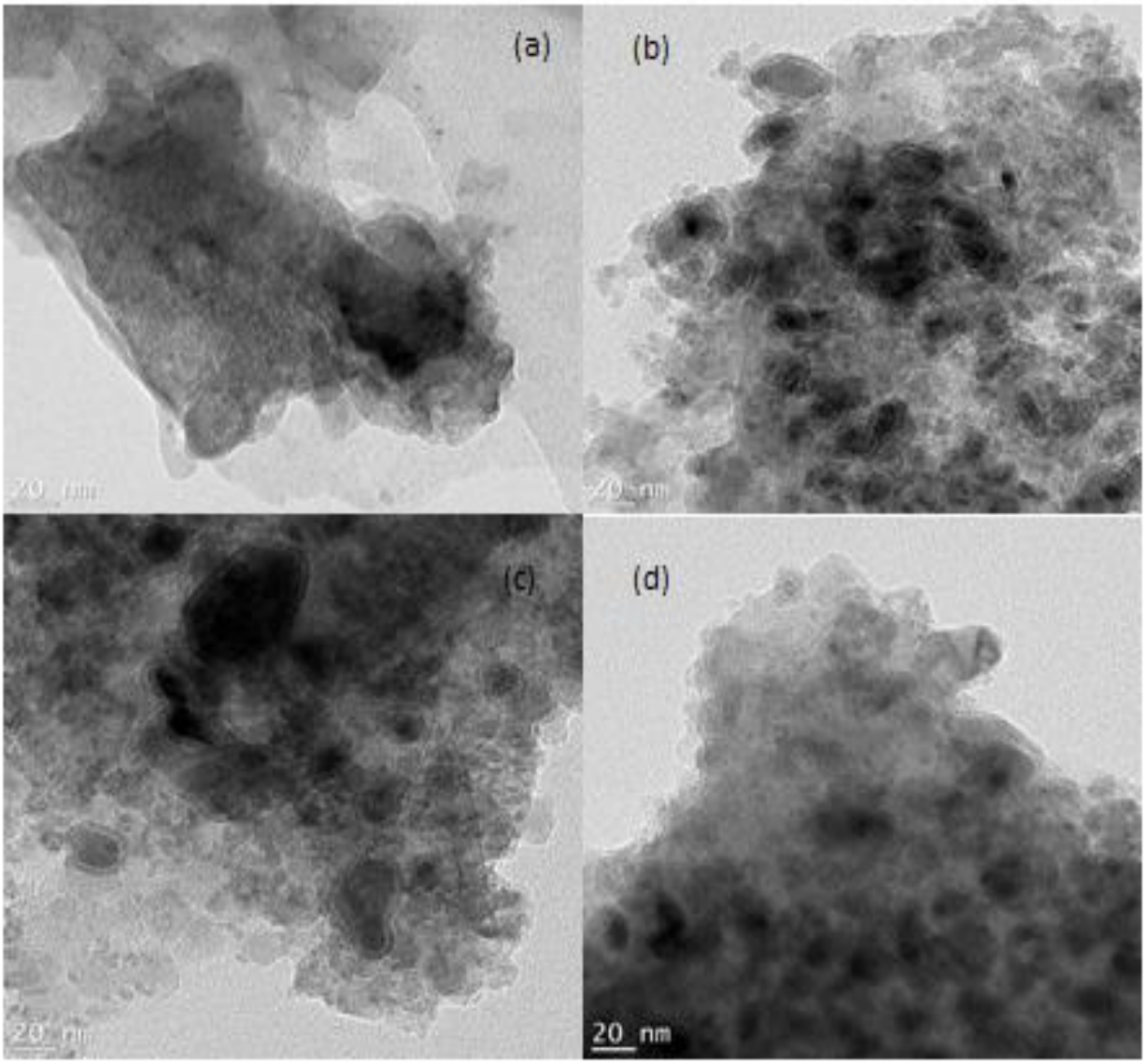

Figure 7.5: HRTEM image of (a) fresh catalyst (b) Reac-Syn spent catalyst (c) Reac-H_2 spent catalyst (d) Reac-CO spent catalyst

The morphological differences of the supported iron catalyst reduced with different reducing agents were confirmed with HRTEM. **Figure 7.5** shows the distribution of the iron particles on silica support after a long TOS of 14 000 hours. The corresponding electronic diffractograms is depicted.

In all the cases, the growth of catalyst particles during the Fischer Tropsch reaction is evident. Hence, it can be inferred that the catalyst particle grows during

the synthesis. However the nature of this growth (chemical and morphological nature) is not understood and more studies are required.

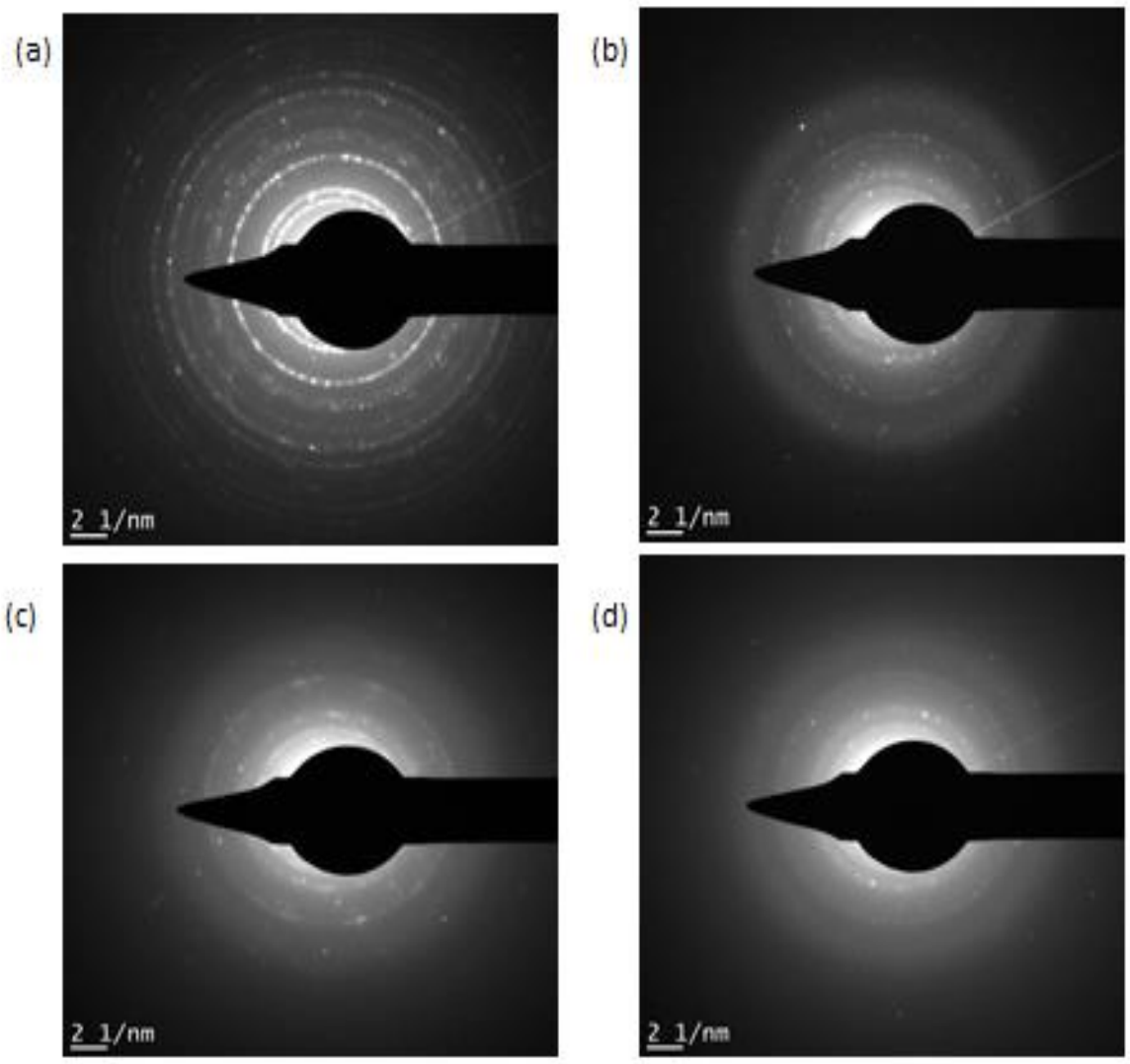

Figure 7.6: The corresponding electron diffractograms of the HRTEM images depicted in Figure 7.5 (a) fresh catalyst (b) Reac-Syn spent catalyst (c) Reac-H_2 spent catalyst (d) Reac-CO spent catalyst

Figure 7.6 shows the difference in the diffraction pattern, this is evident of the presence of different phases. The XRD spectra in **Figure 7.7** show the differences in the phases and crystallographic planes existing in different catalyst. The fresh catalyst gave only one peak whereas the used catalyst indicated the presence of several phases hence several peaks.

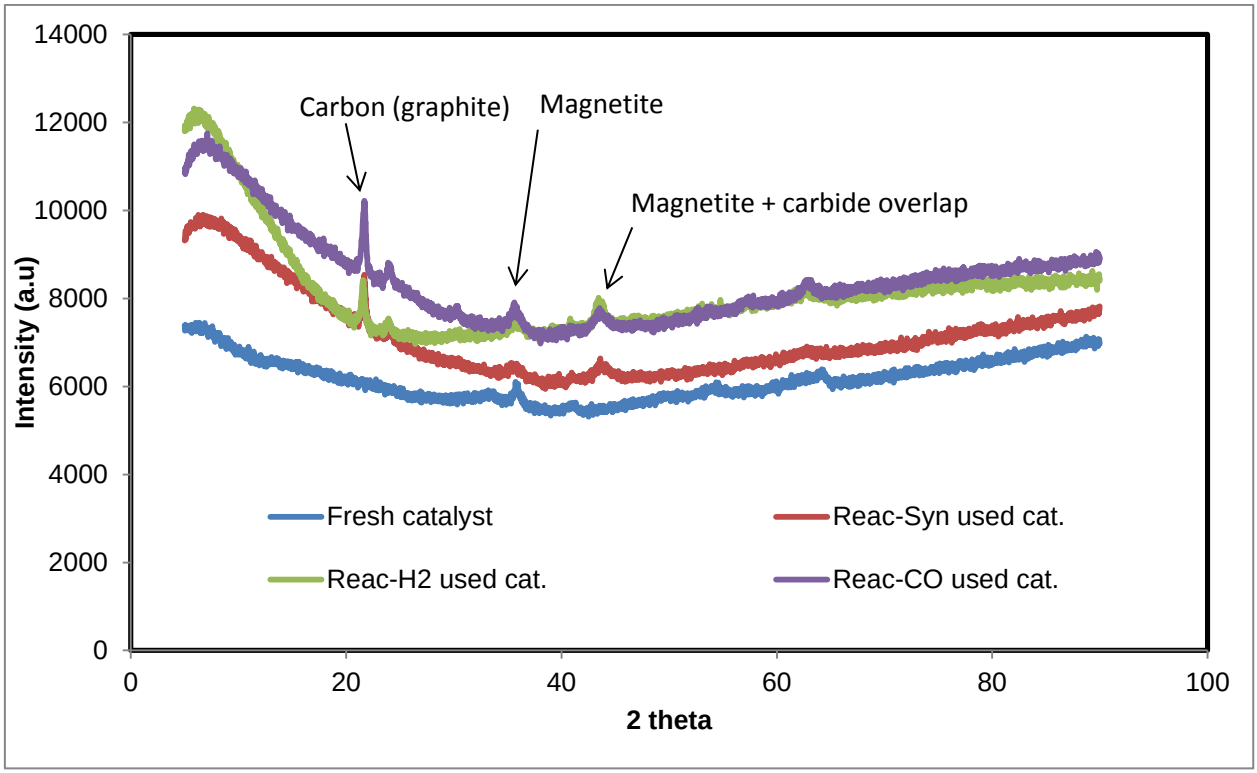

Figure 7.6: XRD spectra of the fresh catalyst and the used ones from different reactors (After 14 000 hours TOS)

7.5 Discussion

The results obtained for the catalysts after regeneration are a great puzzle. The overall observation is that the success of regeneration really depends on the path(s) that the catalyst undergoes before the regeneration. As the catalysts have been originally reduced with three different gases, the active phases and composition of these active phases were different. Therefore, these three catalysts would go through different deactivation paths although the operation conditions were the same during reaction. The literature has reported that oxidation, sintering, and carbon deposition are the main reasons given for the deactivation of Fe catalysts in FTS. Under the operation conditions applied here, sintering and oxidation are the plausible reasons for the deactivation as no carbon deposition would be expected. Carbon deposition will cause a rapid deactivation of the catalyst, which was not observed during the experiments. It is understandable that Fe oxides, especially Fe_3O_4, exist during the reaction, as metallic Fe and FexCy could be oxidized in the presence of product H_2O. Both the literature and the

present thermodynamic calculations support this point of view. However, the oxidation of FexCy to Fe_3O_4 depends on the partial pressure or the H_2O/H_2 ratio. A low H_2O/H_2 ratio will favour the presence of FexCy and suppress the formation of Fe_3O_4. The results reported in Chapter 6 and **Figures 7.4** (a), (b) and (c) suggest that the CO_2 selectivities were low before the regeneration of the catalysts, and this agrees with the low conversion of the reactants. Therefore, it seems that the deactivation of the catalyst is mainly due to the loss of the active sites but not due to the conversion of FexCy to Fe_3O_4. The characterization results show that the available active sites were limited before the catalysts were regenerated. The regeneration did bring back more active sites, especially the catalyst that was reduced by syngas originally. However, it also seems that the regeneration treatment did not increase the active sites by much for the two that were originally reduced by H_2 and CO. The reason is that the way the catalyst loses its activity is mainly decided by the path of operation before the regeneration.

Another important observation here is that the CO_2 selectivities of all the catalysts have increased and the percentages are similar. Before regeneration, the CO_2 selectivities of three catalysts were actually at a low level, around 4-5%. After regeneration, the CO_2 selectivity increased to around 17%. A low CO_2 selectivity may suggest a low content of Fe oxide available in the catalysts. The data, after regeneration, suggest that both active Fe_3O_4 and FexCy were increased for the catalyst originally reduced by syngas, but those two originally reduced by CO and H_2 only have Fe_3O_4 increased and that some of the FexCy was also converted to Fe oxide. It seems that the oxidation stage managed to convert FexCy to Fe oxides but the reduction did not manage to reduce the Fe oxides much.

The third important observation here is the increase of olefin selectivity for all three catalysts. This result is contradictory, at a first glance, with the CO_2 selectivity change discussed above. It is suggested that the regeneration of catalysts resulted a higher content of Fe oxide by converting some of the FexCy. This change of the active sites would actually suppress the formation of olefins. However, the results obtained in the present experiments were that the olefins increased. This may be linked with the availability of the promoter, K. In Chapter 5,

the CO reduced catalyst was observed to give the most olefins, and that was linked to the possible availability of the K. The regeneration treatment, especially the oxidation stage, may have caused the migration of K, and then the ratio of K and active sites may consequently have been altered. As reported in the literature, a higher K content in a precipitated Fe catalyst helps the selectivity to olefins, and the change of K/active sites ratio will result a change to the olefin selectivity.

One would expect that the regeneration of a catalyst would increase active sites on the catalyst, in line with the results reported in the literature (Marafi, Stanislaus, and Furimsky 2010b; Yoshimura and Furimsky 1986a; Windawi and Katzer 1980); however, the results reported in this work suggest that it is not that straight forward. It depends on the availability of the reducible Fe oxides but not the overall amount of Fe oxides. In the meantime, the availability of the reducible Fe oxides is actually decided by the amount of Fe or Fe oxide that could be accessed by oxygen during the oxidation stage, and by reducing gas (CO and H_2) during the reduction stage. It seems that the Fe oxide might have sintered for the two that were originally reduced by CO and $H_{2,}$ and the regeneration process did not manage to break such sintered particles. This could be because the regeneration only had an effect on the Fe compounds on the outer layer of the particles.

7.6 Conclusion

An oxidative regeneration process was adopted with the intent of hypothetically removing carbon deposition on the catalyst. The oxidative regeneration of differently reduced catalysts exerted a considerable effect on the subsequent catalytic selectivity. In this case, the regenerated samples exhibited an increase in the catalytic activity and a selectivity change. Regeneration with the syngas reduced was most effective: the conversion of the system in this case increased from 4.66% to 10.00%, which is a 53.40% increase. However, the researcher failed to obtain a high increase in conversions for the hydrogen reduced with the maximum of 1.18% and the CO reduced 6.25% after regeneration.

The results show that the activity was restored for the reactor which was initially reduced with syngas by 53.40% (CO conversion 4.65 to 9.99%), whereas the H_2 and CO reduced show little increase in conversion. Although the oxidative regeneration did not restore the catalytic activity to the initial CO conversion of 16%, it is proven that the technique employed can be successfully used for regenerating the catalyst even after more than 1 year. The results could be useful for industrial application as industrial FT processes have required long time experiments. Consequently, the oxidative regeneration of the catalyst is possible, and conditions should be further optimized.

References

Ahn, C.-I., and J.W. Bae. 2015. “Fischer-Tropsch Synthesis on the Al2O3-Modified Ordered Mesoporous Co3O4 with an Enhanced Catalytic Activity and Stability.” Article in Press. Scopus. http://www.scopus.com/inward/record.url?eid=2-s2.0-84951748154&partnerID=40&md5=08c7d87290e3376c5007a3679dfc8c7a.

Argyle, M.D., and C.H. Bartholomew. 2015a. “Heterogeneous Catalyst Deactivation and Regeneration: A Review.” *Catalysts* 5 (1): 145–269. doi:10.3390/catal5010145.

———. 2015b. “Heterogeneous Catalyst Deactivation and Regeneration: A Review.” *Catalysts* 5 (1): 145–269. doi:10.3390/catal5010145.

Bartholomew, Calvin H. 1984. “Catalyst deactivation.” *Chemical Engineering (New York)* 91 (23): 96–112.

Bogdan, C.E., J.G. Nunan, J.G. Santiesteban, R.G. Herman, and K. Klier. 1988. *Deactivation Studies of the Cs/Cu/ZnO and alkali/MoS2 Alcohol Synthesis Catalysts*. Vol. 38. Studies in Surface Science and Catalysis. http://www.scopus.com/inward/record.url?eid=2-s2.0-79957471473&partnerID=40&md5=4eff06ece2c8ac9c50ef57bb5897c751.

Brunner, K.M., B. Huang, B.F. Woodfield, and W.C. Hecker. 2015. “Iron Fischer-Tropsch Catalysts Prepared by Solvent-Deficient Precipitation (SDP): Effects of Washing, Promoter Addition Step, and Drying Temperature.” *Catalysts* 5 (3): 1352–74. doi:10.3390/catal5031352.

Butt, John B. 1982. “Catalyst poisoning and chemical process dynamincs.” In , 153–208. http://www.scopus.com/inward/record.url?eid=2-s2.0-0020275607&partnerID=40&md5=2b76edd249a448a940a19cd94418fd68.

———. 1984. *Catalyst deactivation and regeneration.* Vol. 6. Catalysis: Science and Technology. http://www.scopus.com/inward/record.url?eid=2-s2.0-0021595034&partnerID=40&md5=66178b1d44bb6108e18744ec38eec899.

de Klerk, A., Y.-W. Li, and R. Zennaro. 2013. “Fischer-Tropsch Technology.” In *Greener Fischer-Tropsch Processes for Fuels and Feedstocks*, 53–79. http://www.scopus.com/inward/record.url?eid=2-s2.0-84886342123&partnerID=40&md5=e93de2acaa5be7d6ad57d9bdfc0287d4.

Denny, P.J., and M.V. Twigg. 1980. “Factors Determining the Life of Industrial Heterogeneous Catalysts.” In *Studies in Surface Science and Catalysis*, edited by B. Delmon and G.F. Froment, Volume 6:577–99. Elsevier. http://www.sciencedirect.com/science/article/pii/S0167299108652581.

Ferdous, D., and B. Demirel. 2010. “Deactivation of Iron Based Fischer-Tropsch Catalyst: A Critical Problem.” In , 2:1266–72. http://www.scopus.com/inward/record.url?eid=2-s2.0-84877608658&partnerID=40&md5=9304941a3ed5dd765a3311bfae95a6aa

Hegedus, L.L., and R.W. McCabe. 1980. “Catalyst poisoning.” *Studies in Surface Science and Catalysis* 6: 471–505.

Istadi, I., D.D. Anggoro, N.A.S. Amin, and D.H.W. Ling. 2011a. “Catalyst Deactivation Simulation through Carbon Deposition in Carbon Dioxide Reforming over Ni/cao-Al 2o 3 Catalyst.” *Bulletin of Chemical Reaction Engineering and Catalysis* 6 (2): 129–36.

——. 2011b. “Catalyst Deactivation Simulation through Carbon Deposition in Carbon Dioxide Reforming over Ni/cao-Al 2o 3 Catalyst.” *Bulletin of Chemical Reaction Engineering and Catalysis* 6 (2): 129–36.

Jiménez-García, G., R. Quintana-Solórzano, R. Aguilar-López, and R. Maya-Yescas. 2010. “Modelling Catalyst Deactivation by External Coke Deposition during Fluid Catalytic Cracking.” *International Journal of Chemical Reactor Engineering* 8. http://www.scopus.com/inward/record.url?eid=2-s2.0-77649334770&partnerID=40&md5=7f12d69d13a783ae966fa076bf642297.

Lappas, A., and E. Heracleous. 2010. “Production of Biofuels via Fischer-Tropsch Synthesis: Biomass-to-Liquids.” In *Handbook of Biofuels Production: Processes and Technologies*, 493–529.

http://www.scopus.com/inward/record.url?eid=2-s2.0-84869086429&partnerID=40&md5=9647400344ea06fd2366cb787430e07e.

Lin, X., Y. Fan, G. Shi, H. Liu, and X. Bao. 2007. “Coking and Deactivation Behavior of HZSM-5 Zeolite-Based FCC Gasoline Hydro-Upgrading Catalyst.” *Energy and Fuels* 21 (5): 2517–24. doi:10.1021/ef0700634.

Li, Y., and Z. Wu. 2014. “Deactivation and Burning Regeneration of Coked Acid Catalysts in Catalytic Cracking Process of Biomass Tar.” *Zhongguo Dianji Gongcheng Xuebao/Proceedings of the Chinese Society of Electrical Engineering* 34 (8): 1297–1303. doi:10.13334/j.0258-8013.pcsee.

Lucchini, M.A., A. Testino, A. Kambolis, C. Proff, and C. Ludwig. 2016. “Sintering and Coking Resistant Core-Shell Microporous Silica-Nickel Nanoparticles for CO Methanation: Towards Advanced Catalysts Production.” *Applied Catalysis B: Environmental* 182: 94–101. doi:10.1016/j.apcatb.2015.09.012.

Marafi, Meena, Antony Stanislaus, and Edward Furimsky. 2010a. “Chapter 4 - Catalyst Deactivation.” In *Handbook of Spent Hydroprocessing Catalysts*, 51–92. Amsterdam: Elsevier. http://www.sciencedirect.com/science/article/pii/B9780444535566000045.

———. 2010b. “Chapter 6 - Regeneration.” In *Handbook of Spent Hydroprocessing Catalysts*, 121–90. Amsterdam: Elsevier. http://www.sciencedirect.com/science/article/pii/B9780444535566000069.

———. 2010c. “Chapter 7 - Rejuvenation.” In *Handbook of Spent Hydroprocessing Catalysts*, 191–226. Amsterdam: Elsevier. http://www.sciencedirect.com/science/article/pii/B9780444535566000070.

Massoth Fe and Menon PG. 1969. “Active species on coked silica-Alumina Catalyst” 8 (3): 383–85.

Meng, Xianghai, Chunming Xu, and Jinsen Gao. 2007. “Coking Behavior and Catalyst Deactivation for Catalytic Pyrolysis of Heavy Oil.” *Fuel* 86 (12–13): 1720–26. doi:10.1016/j.fuel.2006.12.023.

Meng, X., C. Xu, and J. Gao. 2007. “Coking Behavior and Catalyst Deactivation for Catalytic Pyrolysis of Heavy Oil.” *Fuel* 86 (12-13): 1720–26. doi:10.1016/j.fuel.2006.12.023.

Meshkani, F., and M. Rezaei. 2015. “Hydrogen Production by High Temperature Water Gas Shift Reaction over Highly Active and Stable Chromium Free Fe-Al-Ni Catalysts.” *International Journal of Hydrogen Energy* 40 (34): 10867–75. doi:10.1016/j.ijhydene.2015.06.170.

Mikhailova, Ya.V., S.N. Potapova, and S.A. Sviderskii. 2010. “Effect of the Regeneration Conditions of a Cobalt - Zeolite Catalyst on Its Properties in the Synthesis of Hydrocarbons from CO and H2.” *Solid Fuel Chemistry* 44 (2): 127–32. doi:10.3103/S0361521910020102.

Moulijn, J.A, A.E van Diepen, and F Kapteijn. 2001. “Catalyst Deactivation: Is It Predictable?: What to Do?” *Catalyst Deactivation* 212 (1–2): 3–16. doi:10.1016/S0926-860X(00)00842-5.

Nakhaei Pour, A., and M.R. Housaindokht. 2013. “Fischer-Tropsch Synthesis on Iron Catalyst Promoted with HZSM-5 Zeolite: Regeneration Studies of Catalyst.” *Journal of Natural Gas Science and Engineering* 14: 49–54. doi:10.1016/j.jngse.2013.05.004.

Nogueira, I.M., G.Q. Sabadia, A.A. Moreira, J.M. Filho, and A.C. Oliveira. 2011. “Investigation of the Deactivation of Iron Nanocomposites by Coking in the Dehydrogenation of Ethylbenzene.” *Journal of Molecular Catalysis A: Chemical* 351: 81–92. doi:10.1016/j.molcata.2011.09.020.

Pennline, H.W., and S.S. Pollack. 1986. “Deactivation and Regeneration of a Promoted Transition-Metal-Zeolite Catalyst.” *Industrial & Engineering Chemistry Fundamentals* 25 (1): 11–14.

Polinski, Leon M., V.Udaya S. Rao, and John M. Stencel. 1984. *Catalysis and catalytic deactivation.* Sci and Technol of Coal and Coal Util.

Raje, A.P., R.J. O’Brien, L. Xu, and B.H. Davis. 1997. *Deactivation of Iron-Based Catalysts for Slurry Phase Fischer-Tropsch Synthesis*. Vol. 111. Studies in

Surface Science and Catalysis. http://www.scopus.com/inward/record.url?eid=2-s2.0-37849185752&partnerID=40&md5=10b705486c4a634526e3208e5e395b13

Rauch, R., A. Kiennemann, and A. Sauciuc. 2013. “Fischer-Tropsch Synthesis to Biofuels (BtL Process).” In *The Role of Catalysis for the Sustainable Production of Bio-Fuels and Bio-Chemicals*, 397–443. http://www.scopus.com/inward/record.url?eid=2-s2.0-84926448805&partnerID=40&md5=6295e204b170e53d9a691dbaa5e2d70c

Saib, A.M., D.J. Moodley, I.M. Ciobîc, M.M. Hauman, B.H. Sigwebela, C.J. Weststrate, J.W. Niemantsverdriet, and J. Van De Loosdrecht. 2010. “Fundamental Understanding of Deactivation and Regeneration of Cobalt Fischer-Tropsch Synthesis Catalysts.” *Catalysis Today* 154 (3-4): 271–82. doi:10.1016/j.cattod.2010.02.008.

Taufiqurrahmi, N., A.R. Mohamed, and S. Bhatia. 2010. “Deactivation and Coke Combustion Studies of Nanocrystalline Zeolite Beta in Catalytic Cracking of Used Palm Oil.” *Chemical Engineering Journal* 163 (3): 413–21. doi:10.1016/j.cej.2010.07.049.

Van de Loosdrecht, J., F.G. Botes, I.M. Ciobica, A. Ferreira, P. Gibson, D.J. Moodley, A.M. Saib, J.L. Visagie, C.J. Weststrate, and J.W. Niemantsverdriet. 2013. “Fischer-Tropsch Synthesis: Catalysts and Chemistry.” In *Comprehensive Inorganic Chemistry II (Second Edition): From Elements to Applications*, 7:525–57. http://www.scopus.com/inward/record.url?eid=2-s2.0-84902559789&partnerID=40&md5=bf301f4c6f75c09906975ae6e8ae11a9.

Van Loosdrecht, J.D., M.M. Hauman, D.J. Moodley, S.D. Nthute, A.M. Saib, and B.H. Sigwebela. 2008. “Regeneration of Cobalt Based Fischer-Tropsch Synthesis Catalysts.” In .

Van Ommen, J.R., and J. Grievink. 2014. “Synthesis Gas Utilization for Transportation Fuel Production.” In *Biomass as a Sustainable Energy Source for the Future: Fundamentals of Conversion Processes*, 525–46.

http://www.scopus.com/inward/record.url?eid=2-s2.0-84926397752&partnerID=40&md5=bb1c612e3f077d1cdc74d932564e946a.

Vogelaar, B.M., J. Gast, E.M. Douma, A.D. Van Langeveld, S. Eijsbouts, and J.A. Moulijn. 2007. “Coke Deposition Profiles during Artificial Aging of Hydroprocessing Catalysts.” *Industrial and Engineering Chemistry Research* 46 (2): 421–29. doi:10.1021/ie060870a.

Whaley, L.Z., and G. Veser. 2010. “Coking Resistant, High-Temperature Stable Ni@SiO2 Core-Shell Catalysts.” In . http://www.scopus.com/inward/record.url?eid=2-s2.0-79251497053&partnerID=40&md5=ec842dfb9e0f96d8d9bf6d21d1dff8fb.

Windawi, H., and J.R. Katzer. 1980. “Regeneration of metallic catalysts.” *American Chemical Society, Division of Petroleum Chemistry, Preprints* 25 (2): 324–31.

Yoshimura, Y., and E. Furimsky. 1986a. “Oxidative Regeneration of Hydrotreating Catalysts.” *Applied Catalysis* 23 (1): 157–71. doi:10.1016/S0166-9834(00)81459-1.

———. 1986b. “Funcat Cogas ’86: The International symposiumRemoval of Carbonaceous Deposits from the Surface of Cobalt-Molybdate Catalyst via Oxidative Regeneration.” *Fuel* 65 (10): 1388–91. doi:10.1016/0016-2361(86)90110-9.

Zhang, Y., N. Sirimanothan, R.J. O’Brien, H.H. Hamdeh, and B.H. Davis. 2001. *Study of Deactivation of Iron-Based Fischer-Tropsch Synthesis Catalysts*. Vol. 139. Studies in Surface Science and Catalysis. http://www.scopus.com/inward/record.url?eid=2-s2.0-0035787138&partnerID=40&md5=fd5bdc1d5853a6f916e90e1da14a319d.

Zheng, S., J. Sun, D. Song, Z. Chen, and J. Chen. 2015. “The Facile Fabrication of Magnetite Nanoparticles and Their Enhanced Catalytic Performance in Fischer-Tropsch Synthesis.” *Chemical Communications* 51 (55): 11123–25. doi:10.1039/c5cc03336e.

CHAPTER 8

FURTHER ANALYSIS OF THE GAS PHASE FT EXPERIMENTAL DATA: P/O RATIOS, LU PLOTS AND YAO PLOTS

The data contained in this chapter have been written in a paper format.

Abstract

Fischer Tropsch synthesis (FTS) is a catalysed chemical reaction in which synthesis gas (H_2 + CO) is converted to clean fuels and chemicals. The main products are paraffin and olefins. The paraffin to olefin ratio is an important factor which reflects the product distribution of FTS. In this study, two new approaches to FT product distribution are presented and compared using the experimental data obtained in three fixed bed reactors (each loaded with 1 gram of the same iron based catalyst, and reduced with syngas (CO/H_2), H_2 and CO, respectively) over a wide range of FT reaction conditions.

In the first approach, the researcher plotted $P_{(n+1)}/O_{(n+1)}$ versus P_n/O_n with carbon number n = 2-5, which is called Yao's plot. The results showed that although the P/O ratios are strongly dependent on the process conditions, such as reduction agents, flow rate and pressures etc., the plots of $P_{(n+1)}/O_{(n+1)}$ against $P_{(n)}/O_{(n)}$ yielded a nearly linear relationship though with different gradients for all the three reactors; these results indicate that the olefin and paraffin distributions are not independent. The current data, including the effect of the reducing agents on the catalyst performance, widen the range of the application of the Yao plot. Just like the classical Anderson-Schulz-Flory distribution model, this model has some deviations especially for n = 2. The second plot, referred to as the Lu plot, depicts the relationship between normalized mole fractions of O_n, O_{n+1} and P_n. These plots show how the equilibrium points migrate with changes in the experimental conditions. These equilibrium point migrations seem to be due to changes in the conversion.

8.1 Introduction

Fischer Tropsch synthesis (FTS) yields a plethora of products, with straight chain olefins and paraffins being the dominant products. FTS products display a clear inter-relationship between the various products, whether gases, liquids or in wax form. These inter-relationships are mainly attributed to the step-wise growth nature of the FT mechanism (Biloen, Helle, & Sachtler, 1979; Carter, 2001). The chain growth mechanism still remains a bone of contention, but with many researchers agreeing on the proposed step-wise growth mechanism.

Different models have been developed to compare and predict the hydrocarbon product distributions from Fischer-Tropsch synthesis. The Anderson-Schulz-Flory (ASF) model has been used by many researchers to describe the product distribution of hydrocarbons in FTS (Hillestad, 2015; Förtsch, Pabst, & Groß-Hardt, 2015; Liu, Hamasaki, Honma, & Tokunaga, 2011; Ma, Ding, Luo, Lin, & Lin, 2001; Van Santen, Ghouri, Markvoort, & Hensen, 2014; Zhang et al., 2012).

The ASF plot and model predictions are given by equation 8.1:

$$W_n/n=(1-\alpha)^2\alpha^{(n-1)} \qquad (8.1)$$

where *Wn* is the mass fraction of a hydrocarbon, n is the number of carbon atoms in the molecule and α is the growth probability factor which is assumed to be constant.

In this model α signifies the probability of the molecules to continue reacting to form longer chains. Thus, a plot of the logarithm of W_n/n versus *n* gives a straight line plot with the gradient giving the α value (as seen in **Figure 8.1**). This distribution model has been used by many researchers to explain the product distribution; however, some significant deviations from this ideal distribution have been observed. These deviations are observed regardless of the nature of the catalyst; both iron and cobalt catalysts have showed this deviation.

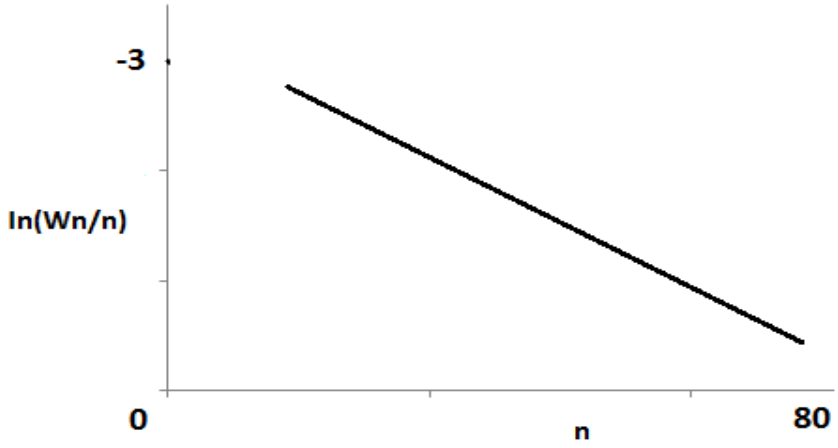

Figure 8.1: Typical ASF hydrocarbon product distribution plot (Bao, El-Halwagi, & Elbashir, 2010)

A plethora of models have been developed in the past in an endeavor to describe the distribution of the products obtained in FT processes. Several researchers have modelled the influences of diffusion limitation (Becker, Güttel, & Turek, 2015; Hallac, Keyvanloo, Hedengren, Hecker, & Argyle, 2015; Zamaniyan, Mortazavi, Khodadadi, & Pour, 2013; Zohdi-Fasaei, Atashi, Farshchi Tabrizi, & Mirzaei, 2016) and this phenomenon has been reported to have an impact on the product distribution. It has been suggested that the olefin to paraffin ratio (O/P) is governed by the rate of diffusion which enhances the olefin readsorption, leading to secondary reaction (Iglesia, Reyes, & Madon, 1991).

The patterns observed in the literature show that the P/O ratio increases much more slowly with carbon number (Y.-J. Lu, Zhang, & Zhou, 1999; Madon & Iglesia, 1993; Muleja, Yao, Glasser, & Hildebrandt, 2016). Moreover, most of the authors agreed that diffusion limitations for the olefin products and their subsequent re-incorporation as chain initiators do not make a major impact on the product distribution (Shi & Davis, 2005; Wang, Hu, Rector, & Liu, 2007).

Recently, the present researchers have seen the introduction of novel ways of plotting FT data, referred to as Yao plots and Lu Plots (Muleja, Yao, Glasser, & Hildebrandt,

2016). The Yao plots were developed by Yao, Liu, Hildebrandt, & Glasser (2012) while the Lu plots were developed by X. Lu, Hildebrandt, Liu, & Glasser (2012a). The plots are basically graphical techniques for representing the relationship between two FT products, for example olefin and paraffin. These graphs are a visual representation of the relationship between immediate neighboring carbon numbers of olefin/paraffin and lower olefin and higher olefin and/or lower paraffin and higher paraffin. These plots were designed in an endeavour to come up with a model that is relatively easy to use and gives better precision of the product distributions behaviour for a given set of process conditions.

Yao plots show a linear relationship between $P_{(n+1)}/O_{(n+1)}$ and $P_{(n)}/O_{(n)}$ and this relationship holds regardless of the type of reactor used, the composition of the syngas, reaction conditions and the kind of catalyst (Yao, 2012). The relationship between $P_{(n+1)}/O_{(n+1)}$ and $P_{(n)}/O_{(n)}$ are shown in equation 8.2 for n > 2 and equation 8.3 for n = 2.

$$\left.\frac{P_{(n+1)}/O_{(n+1)}}{P_n/O_n}\right|_{n>2} \approx \xi_{n>2} \tag{8.2}$$

$$\left.\frac{P_3/O_3}{P_2/O_2}\right|_{n=2} \approx \xi_{n=2} \tag{8.3}$$

For n > 2, the ξ values are always greater than 1 with small gradient variations caused by the type of catalysts, reactor types and operating conditions, whereas, for n = 2, the ξ values are always in the range between 1 and 0 .

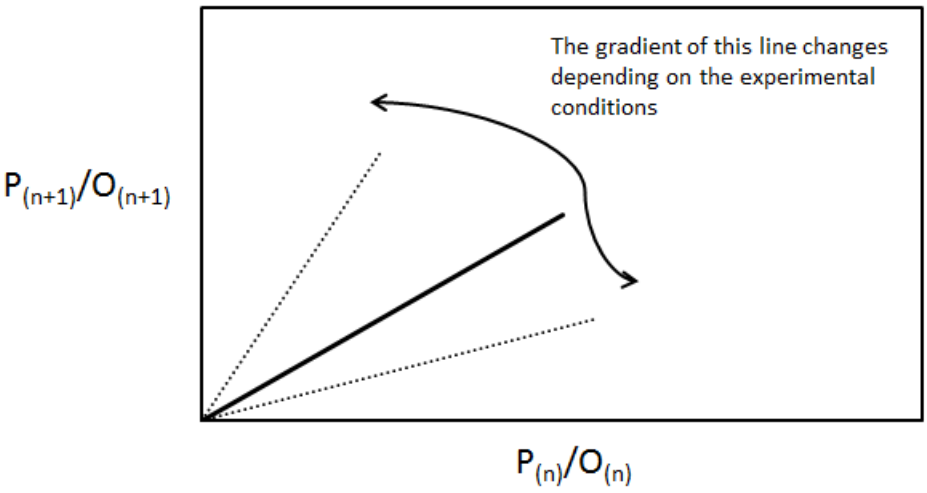

Figure 8.2: The plot of the ratio of $P_{(n+1)}/O_{(n+1)}$ as a function of the ratio of $P_{(n)}/O_{(n)}$ for Fischer-Tropsch synthesis

In the Yao plots, researchers developed two simple models: one is based on the assumption of vapour liquid equilibrium (VLE) and the other is based on quasi-reaction equilibrium to explain this unique experimental observation. This model showed a good ability to predict product distributions. Muleja et al. (2016) used the same plots and obtained similar patterns and mentioned that the linear phenomenon might be due to the combination of quasi reaction equilibrium and VLE.

A Lu plot is a triangular diagram inspired by Residue Curve Maps in distillation and reactive distillation (Muleja, 2016) which displays the proportion of three variables that sum to a constant 1 (X. Lu, Hildebrandt, Liu, & Glasser, 2012b). This plot depicts the relationship between the olefin and paraffin products in an FT reaction as shown in **Figure 8.3**. The normalized molar amounts of O_n, P_n and O_{n+1} are made to add up to the constant value of unity and n can assume any number from 2 onwards. Every point on a triangular plot represents a different composition of the three components.

Note that the pure components are at coordinates (0; 0) for pure P_n and pure O_n is at (1;0) and pure O_{n+1} at coordinates (0;1) as Lu (2012b) has elaborated.

The chain growth and hydrogenation of C_nH_{2n} can be simply written as follows:

$$C_nH_{2n} + CO + 2H_2 \rightarrow C_{n+1}H_{2(n+1)} + H_2O \quad 8.4$$

$$C_nH_{2n} + H_2 \rightarrow C_nH_{2n\,2} \quad 8.5$$

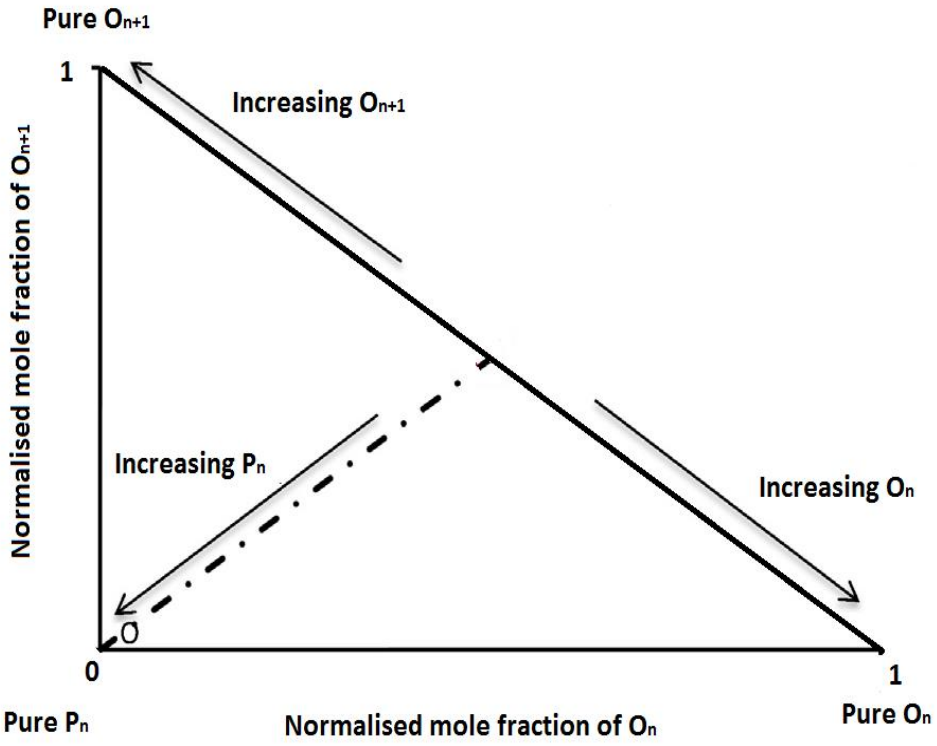

Figure 8.3: The Lu plot: A plot of the normalised mole fractions O_{n+1} versus O_n

Olefins and paraffins behave differently depending on their reactivities in FTS, with olefins more prone to secondary reactions. They also behave differently due to the difference in their solubility and diffusivity coefficients (Naghsh et al, 2012; Staudt-Bickel & Koros, 2000). The olefin to paraffin ratio has been reported to vary with catalyst particle size in FTS. Nakhaei & Housaindokht (2013) showed that the olefin/paraffin ratio decreased with decreasing the catalyst particle size. The O/P ratio also depended on the impact of the solubility of the produced hydrocarbons (vapour–liquid equilibrium). The variation of paraffin to olefin ratio as a function of carbon number has also been

studied by many researchers and all showed that the P/O ratio increases much more slowly with carbon number (Buchang Shi & Davis, 2005; Fu, Jiang, Lv, & Li, 2013; X. Lu, Hildebrandt, Liu, & Glasser, 2012c; A. Nakhaei Pour & Housaindokht, 2013; Nawaz, Baksh, Zhu, & Wei, 2013; Schon, Lau, Min, Thomas, & Wu, 2013; Todic, Olewski, Nikacevic, & Bukur, 2013).

8.2 Experimental work

The experimental procedure employed in this chapter is similar to the methods presented in previous chapters. It is briefly explained. Three fixed bed reactors (FBR), each loaded with 1 gram of the same iron based catalyst ($Fe/Cu/K/SiO_2$), were set in parallel and reduced, with syngas (CO/H_2) for reactor one (Reac-Syn), H_2 for reactor two (Reac H_2) and CO for reactor three (Reac-CO), respectively, for 48 hrs at 250 ^oC, at atmospheric pressure and a flow rate of 60 mL(NTP)/min. Then, the temperatures of Reac-H_2 and Reac-CO were cooled to temperatures below 100 ^oC. Next, the same syngas used in Reac-Syn was introduced to Reac-H_2 and Reac-CO. Then, the temperature for Reac-H_2 and Reac-CO was gradually increased back to 250 ^oC. Thereafter, the three different reactors were subjected to a series of parameter variations to enable the investigator to compare the catalyst response after a long time on stream for FT reactions. Various changes were made to the FT reactor parameters, such as pressure and gas flow rate, to get different conversions.

A series of long-term FTS runs (about 14 200 hours) were conducted, starting with a low pressure (1 bar gauge), and altering both the pressure, from 1 to 10 and finally to 20 bar gauge, and the flow rate, from 15 mL(NTP)/min to 30 mL(NTP)/mL/min and 60 mL(NTP)/min. The aim was to test the responses of the catalyst, initially reduced with different gases, to changes in the operating conditions. The FT reaction conditions for the three reactors are summarised in **Table 8.1**.

Table 8.1: Summary of the FT reaction conditions for the three reactors

Reac-Syn			Range TOS (hrs)	
Flowrate mL(NTP)/min	Pressure (bar)	Temperature (°C)	From	TO
60	1	250	0.00	1100.00
60	1	250	5791.72	6061.57
30	1	250	6089.66	6277.58
15	1	250	6284.49	6816.84
60	10	250	13676.04	13982.51
60	20	250	13987.08	14340.29

Reac-H2			Range TOS (hrs)	
Flowrate mL(NTP)/min	Pressure (bar)	Temperature (°C)	From	TO
60	1	250	0.00	1143.66
60	1	250	5195.29	5889.17
30	1	250	5901.12	6051.85
15	1	250	6113.13	6630.27
60	10	250	13724.55	13979.95
60	20	250	13984.70	14132.18

Reac-CO			Range TOS (hrs)	
Flowrate mL(NTP)/min	Pressure (bar)	Temperature (°C)	From	TO
60	1	250	0.00	1019.00
60	1	250	5138.57	5355.36
30	1	250	5402.24	5567.91
15	1	250	5577.81	6084.79
60	10	250	13112.81	13382.26
60	20	250	13399.95	13636.04

8.3 Results

8.3.1 The olefin to paraffin ratio

Figure 8.4 depicts the P/O ratio for gaseous components (C_2 to C_5) for the three differently reduced reactors under reaction conditions shown in **Table 8.1**. **Table 8.2** displays the P/O ratio for the average data of gaseous components (C_2 to C_5) for all three differently reduced reactors. It also shows the average for the CO conversion under the experimental conditions summarized in **Table 8.1**. Although the effects of the

reducing agents on the O/P ratios were different, the O/P ratio increased with decreasing flowrate from 60 through 30 to 15 mL(NTP) /min for all the three reactors (see **Table 8.2)**. The decrease in flowrate resulted in the increase in conversion as well.

Increasing pressure had the same effect on the P/O ratio. Generally the response of P/O ratio is consistent with what is in the literature (Ali Nakhaei Pour & Housaindokht, 2013b). It is worth noting that the different P/O ratios were obtained even with the same reaction conditions but at different times on stream for all the three reactors (see the results at 60 mL(NTP) /min, 1 bar and 250 ^{o}C in **Table 8.2**). In addition, with different reduction agents, the P/O ratios differ and the following trend was obtained Reac-Syn > Reac-H_2 > Reac-CO reduced catalyst under most of the FT reaction conditions conducted, excluding P_4/O_4 (P_4/O_4 is much higher for Reac-H_2 than that for Reac-Syn and Reac-CO).

Table 8.2: Paraffin to Olefin ratios (P/O) at different conditions

Reac-Syn			Range TOS (hrs)			Averaged P/O ratios			
Flowrate mL(NTP)/min	Pressure (bar)	Temperature (°C)	From	TO	% Conversion	C_2	C_3	C_4	C_5
60	1	250	0.00	1100.00	15.23	0.523	0.092	0.175	0.289
60	1	250	5791.72	6061.57	4.27	0.234	0.052	0.054	0.126
30	1	250	6089.66	6277.58	9.86	0.379	0.060	0.063	0.178
15	1	250	6284.49	6816.84	17.20	0.527	0.074	0.076	0.264
60	10	250	13676.04	13982.51	34.50	2.391	0.335	0.354	0.813
60	20	250	13987.08	14340.29	55.07	5.705	0.600	0.616	1.369
Reac-H2			Range TOS (hrs)			Averaged P/O ratios			
Flowrate mL(NTP)/min	Pressure (bar)	Temperature (°C)	From	TO	% Conversion	C_2	C_3	C_4	C_5
60	1	250	0.00	1143.66	13.07	0.398	0.078	0.364	0.230
60	1	250	5195.29	5889.17	6.99	0.107	0.035	0.125	0.065
30	1	250	5901.12	6051.85	12.35	0.176	0.040	0.138	0.094
15	1	250	6113.13	6630.27	20.97	0.371	0.055	0.188	0.178
60	10	250	13724.55	13979.95	35.42	1.048	0.153	0.561	0.303
60	20	250	13984.70	14132.18	55.24	1.514	0.180	0.675	0.316
Reac-CO			Range TOS (hrs)			Averaged P/O ratios			
Flowrate mL(NTP)/min	Pressure (bar)	Temperature (°C)	From	TO	% Conversion	C_2	C_3	C_4	C_5
60	1	250	0.00	1019.00	13.94	0.329	0.050	0.042	0.145
60	1	250	5138.57	5355.36	4.36	0.082	0.028	0.035	0.058
30	1	250	5402.24	5567.91	7.34	0.128	0.037	0.037	0.071
15	1	250	5577.81	6084.79	10.18	0.224	0.038	0.041	0.121
60	10	250	13112.81	13382.26	23.09	2.175	0.181	0.232	0.503
60	20	250	13399.95	13636.04	40.40	6.297	0.651	0.657	1.198

8.4 Yao Plots

Table 8.2 shows that the P/O ratios for FTS are strongly dependent on the operation conditions, such as flowrate, pressure, time on stream and the catalyst activation agents. Most often, the trend of the O/P ratio is not easy to summarize and predict. The author now used a new way which may show some interesting behaviour that is not apparent from the typical way in which data is presented.

As mentioned in the introduction section, a graph of $P_{(n+1)}/O_{(n+1)}$ against $P_{(n)}/O_{(n)}$ is called the Yao plot in this chapter. In order to investigate the relationship among O/P ratios with different chain lengths, Yao plots are plotted with the carbon number n = 2-5 for the three reactors. **Figure 8.4** shows that the plots of $P_{(n+1)}/O_{(n+1)}$ against $P_{(n)}/O_{(n)}$ yielded a nearly linear relationship, though with different gradients for all three reactors.

In particular, the data used in **Figure 8.4** cover the effect of reduction agents, flowrate, pressure, and reaction time. From the graphs depicted in **Figure 8.4**, the gradients are tabulated in **Table 8.3**. For n = 2 the values for Reactors 1, 2 and 3 are far less than 1 (<<<1). These values are similar to the values obtained by Yali (2012) ranging from 0.04 – 0.181 for different reaction conditions, and Muleja (2016) reported a value of 0.0698.

In order to obtain a clear image of all the data and for comparison, the data for each reactor with the same chain length have been plotted as one set of data, and the results from the ratios are presented graphically in **Figure 8.5**. Similar slopes were obtained for the plots P_3/O_3 vs P_2/O_2 for the three differently reduced catalysts (**Figure 8.5** (a)). Based on these graphs in **Figure 8.5**, one can argue that the gradient for n = 2 is a constant which is not affected by the reduction agents, flowrate, pressure and reaction time. With n = 3–5, the gradient values are similar and greater than 1 for Reac-Syn and Reac-CO. However, an essentially linear relationship for $P_{(n+1)}/O_{(n+1)}$ against $P_{(n)}/O_{(n)}$ were obtained for each of the carbon numbers (**Figure 8.4**), but the gradients for Reac-H_2 are far from Reac-Syn

and Reac-CO as shown in **Figure 8.5**, which is due to the P_4/O_4 for Reac-H_2 being far higher than for Reac-Syn and Reac-CO (see **Table 8.2**).

The trends demonstrated in the current work are consistent with the previous findings by Yao et al. (2012). However, the gradients with different carbon numbers are slightly different; for instance, Yao found that when n > 2, the slopes with different n were quite similar, with an average slope of 1.39. Muleja et al. (2016) used the same plots and obtained similar patterns to this work (straight lines with different gradients). Yao et al. introduced two models, one based on quasi-reaction equilibrium and the other based on vapour liquid equilibrium (VLE) to explain the linear relationship. Muleja et al. (2016) also mentioned that the linear phenomenon might be due to the combination of quasi reaction equilibrium and VLE. Although the Yao's and Muleja's data covered a wide range of reaction conditions, the catalysts were only reduced by H_2. The current data includes the effect of the reducing agents on the catalyst performance; thus it enlarges the range of the application of the Yao's plot.

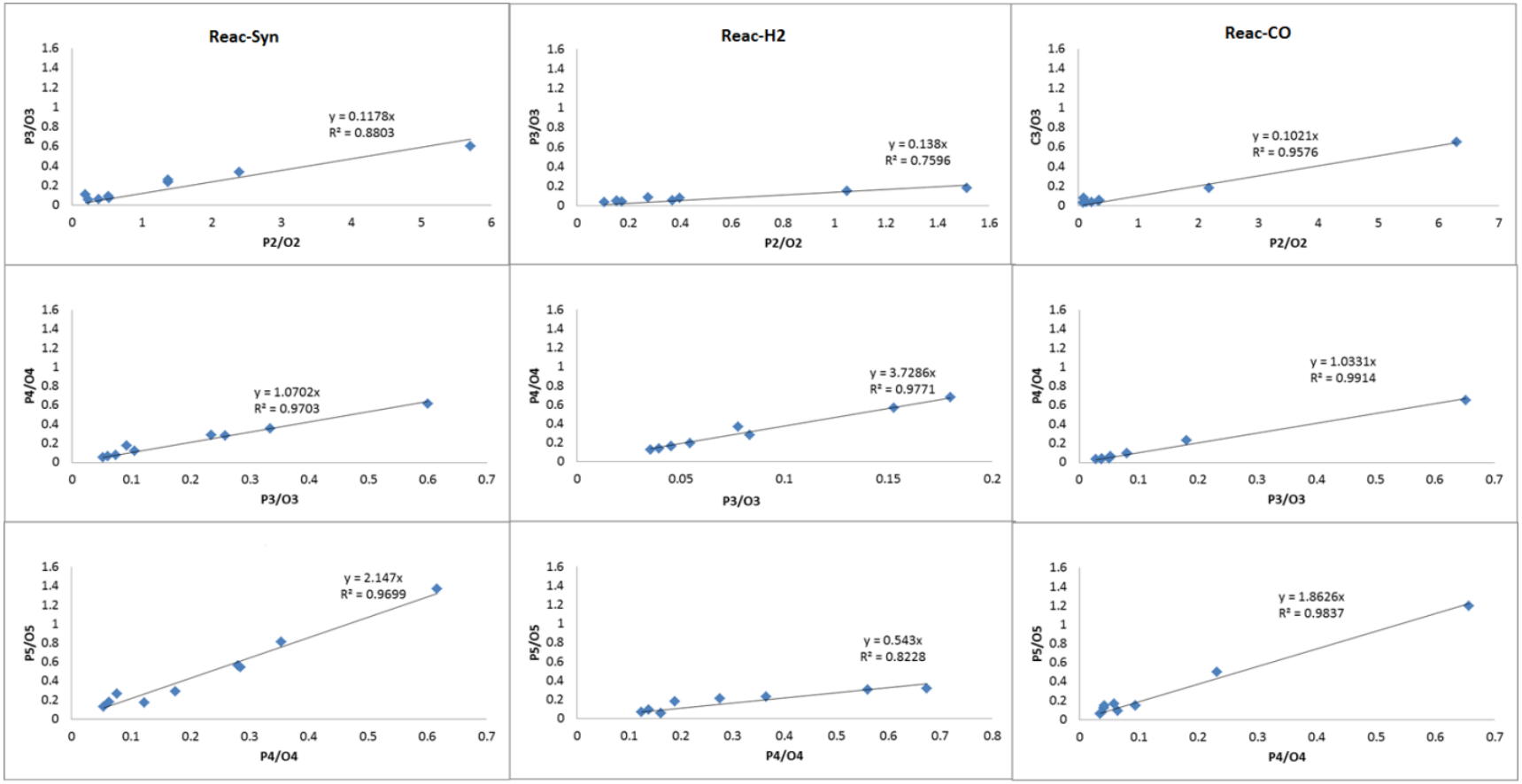

Figure 8.4: The paraffin to olefin ratio $P_{(n+1)}/O_{(n+1)}$ as a function of P_n/O_n for FTS over iron based catalysts. Reac-Syn (reduced by syngas), Reac-H_2 (reduced by H_2) and Reac-CO (reduced by CO) and the reaction condition as shown in Table 8.1.

Table 8.3: Gradients obtained at different n values

Carbon number (n)	Reac-Syn	Reac-H_2	Reac-CO
2	0.118	0.138	0.102
3	1.070	3.729	1.033
4	2.147	0.543	1.863

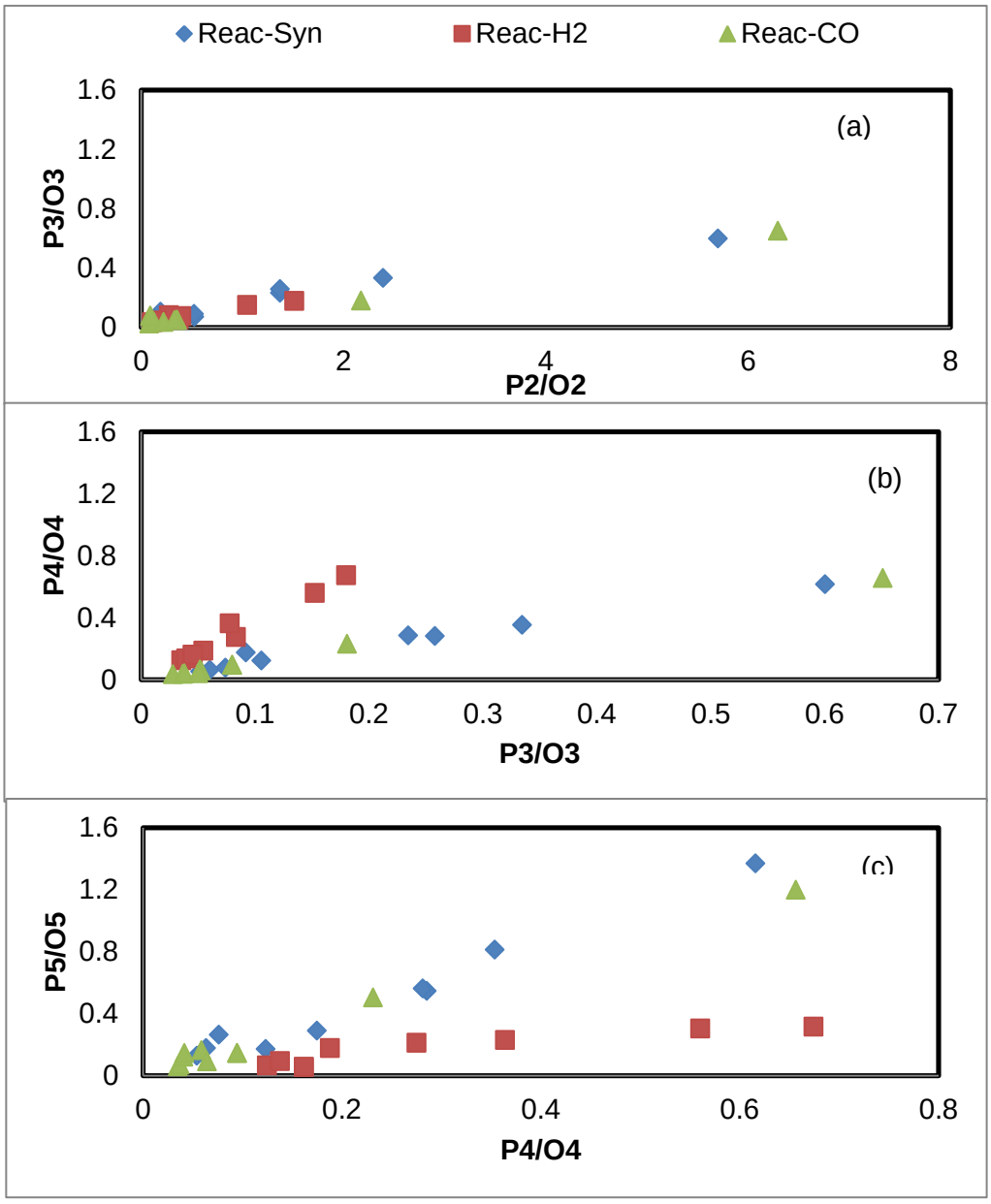

Figure 8.5: The paraffin to olefin ratio $P_{(n+1)}/O_{(n+1)}$ as a function of P_n/O_n for FTS over the iron based catalyst: (a) n = 2, (b) n = 3 and (c) n = 4 for differently reduced reactors (Reac-Syn, Reac-H_2 and Reac-CO)

8.5 Lu Plots

These plots indicate the existence of “equilibrium” points where reactant conversion rate as well as the product formation rate are at a steady state. Any perturbation to the system is believed to change/move this “equilibrium” (Muleja, 2016) as the conversion rates are changed. This phenomenon if presented on Lu plots is analagous to a reactive distillation map with a stable point. From the plots hereunder (**Figure 8.6**) unlike the results of Lu the steady state (“equilibrium points”) points migrate as the system is perturbed by varying reaction parameters to yield high conversions. This migration of steady state points is towards lower olefins moving from O_{n+1} to O_n. This kind of migration presumably means more O_n hydrogenation to P_n (equation 8.5) and suppression of formation of the immediate higher olefin by -CH_2- insertion (equation 8.4). **Figure 8.6** clearly depicts this migration of the so-called “equilibrium” points and this varies with increase in conversions.

This study was limited to the light hydrocarbons, due to analysis limitations (accuracy of the online GC). The normalized mole fractions for C_nH_{2n}, C_nH_{2n+2}, and $C_{n+1}H_{2(n+1)}$ when n = 2,3 and 4 are plotted in **Figures 8.6–8.8** using the averaged steady state values obtained at different conditions.

In the Lu experiments, the data points migrated as a function of time. For instance, in the C_3H_6 ,C_3H_8, C_4H_8 and C_4H_8 ,C_4H_{10}, C_5H_{10} scenario, he observed that at the beginning of the experimental run, the data points were situated far from the point (0,0), which means the paraffin fractions were low and the olefin fractions were high. As the reaction time increased the paraffin (C_3H_8, C_4H_{10}) fractions increased, as could be seen from the data points, which approached the pure paraffin point (0, 0) in both plots. As explained above, the closer the data are to point (0,0), the higher the paraffin fraction.

In the present study, variation in the experimental conditions resulted in data point migration in the Lu Plots. These variations resulted in the data migration being a function of conversion. What is of interest is that all the differently reduced reactors

showed a similar kind of trend. The direction of arrows indicates the direction of decrease in conversion. For n = 2 a clear trend is observed (see **Figure 8.6**); for these results the steady state points migrated towards C_2H_4 as the conversion decreased. This observed trend is similar in all the reactors (Reac-Syn, H_2, CO).

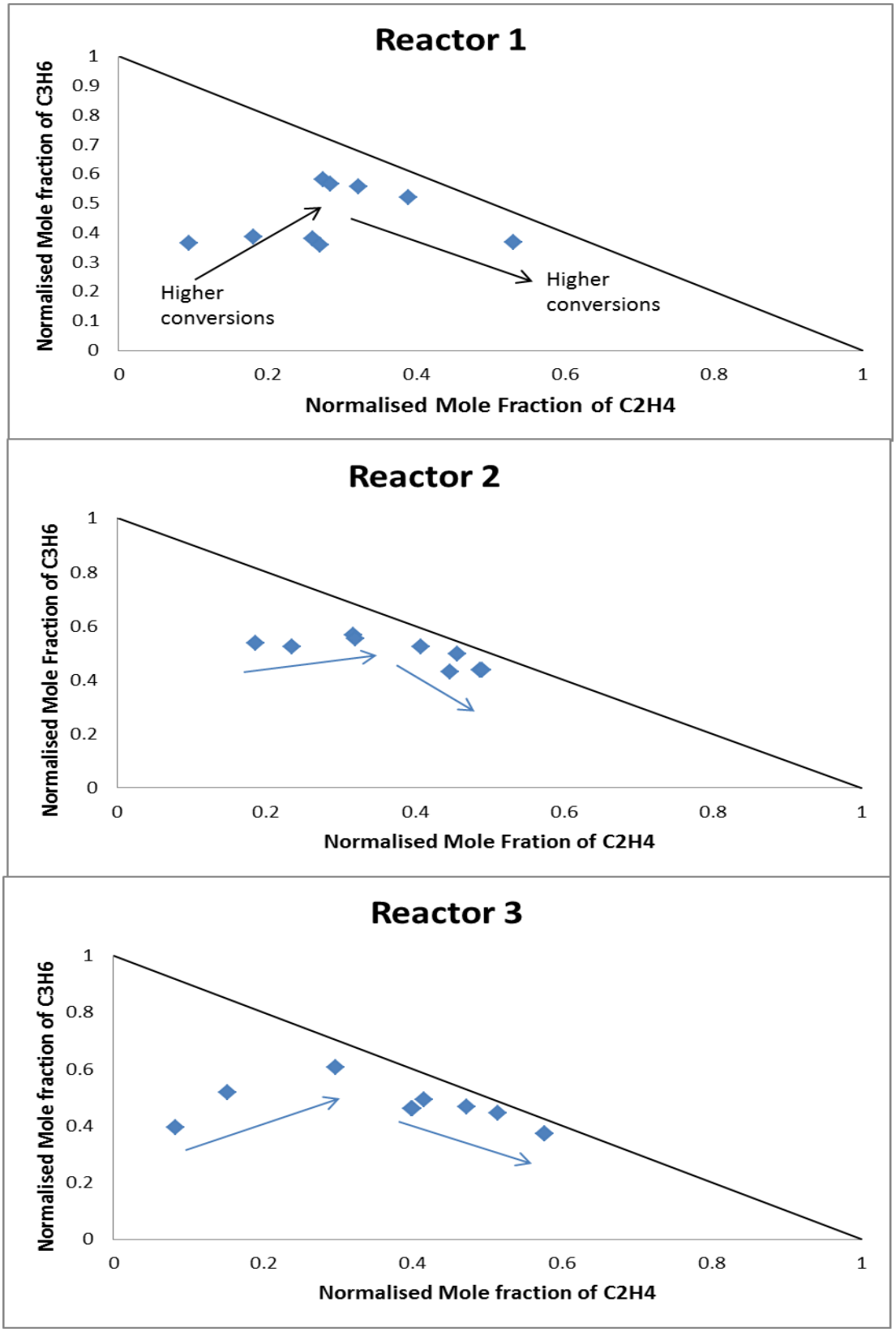

Figure 8.6: Normalized mole fraction for C_2H_4, C_2H_6, and C_3H_6 for the three differently reduced reactors

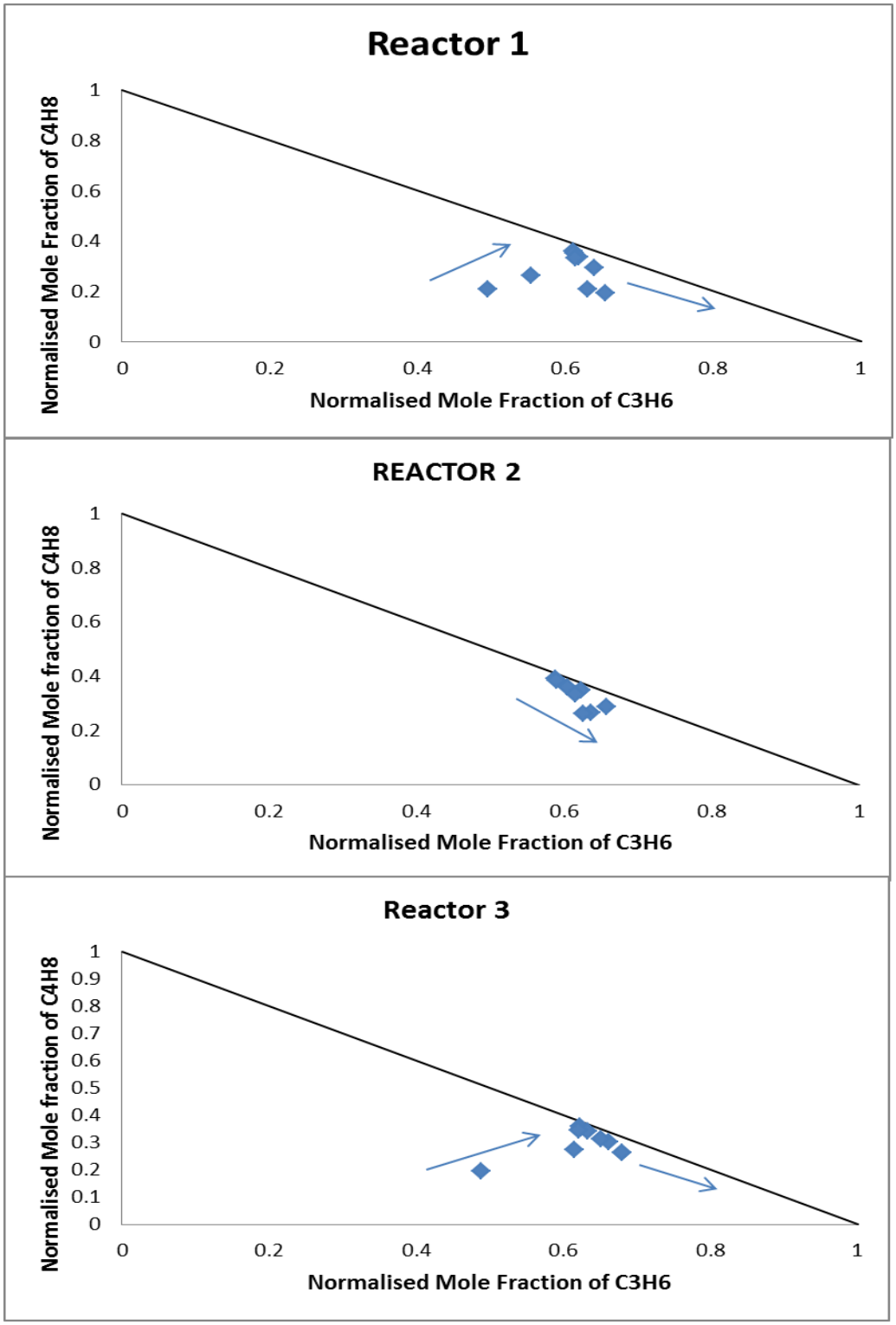

Figure 8.7: Normalized mole fraction for C_3H_6, C_3H_8, and C_4H_8 for the three differently reduced reactors

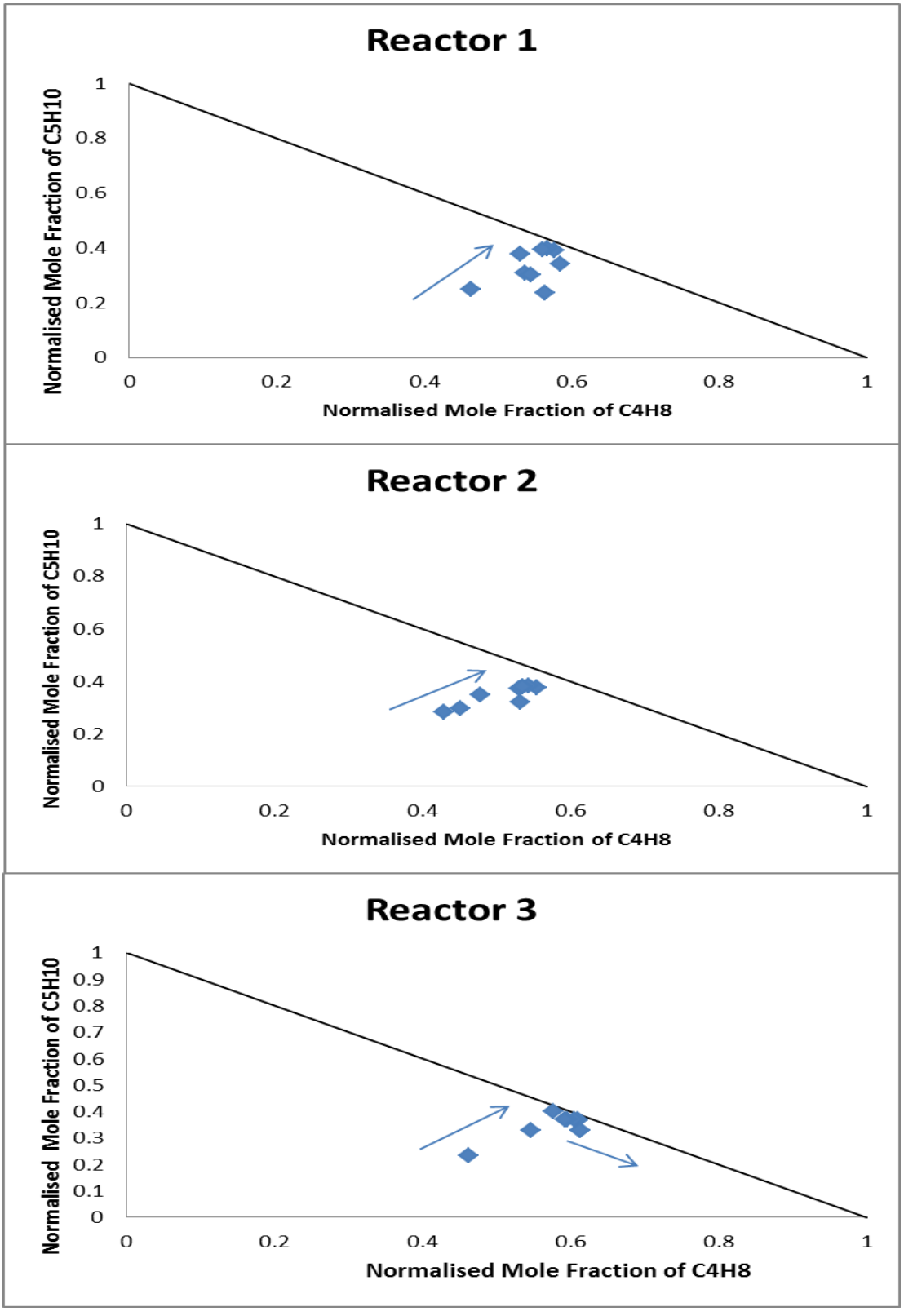

Figure 8.8: Normalized mole fraction for C_4H_8, C_4H_{10}, and C_5H_{10} for the three differently reduced reactors

Using the same normalized mole fraction concept, novel plots of C_nH_{2n+1}, C_nH_{2n}, and $C_{n+1}H_{2(n+1)}$, that is paraffin n, olefin n and paraffin n+1, when n = 2, 3 and 4, are plotted and depicted in **Figures 8.9** to **8.11**. It is intriguing to note that a linear trend is also observed, which mostly runs towards the olefinic corner. The direction of the arrow shows the steady state point migration with increase in conversion. The slope of the lines for the differently reduced catalysts is somewhat different. This observed phenomenon is in agreement with the P/O ratios observed in **Table 8.1** which shows an increase in the ratio with conversion.

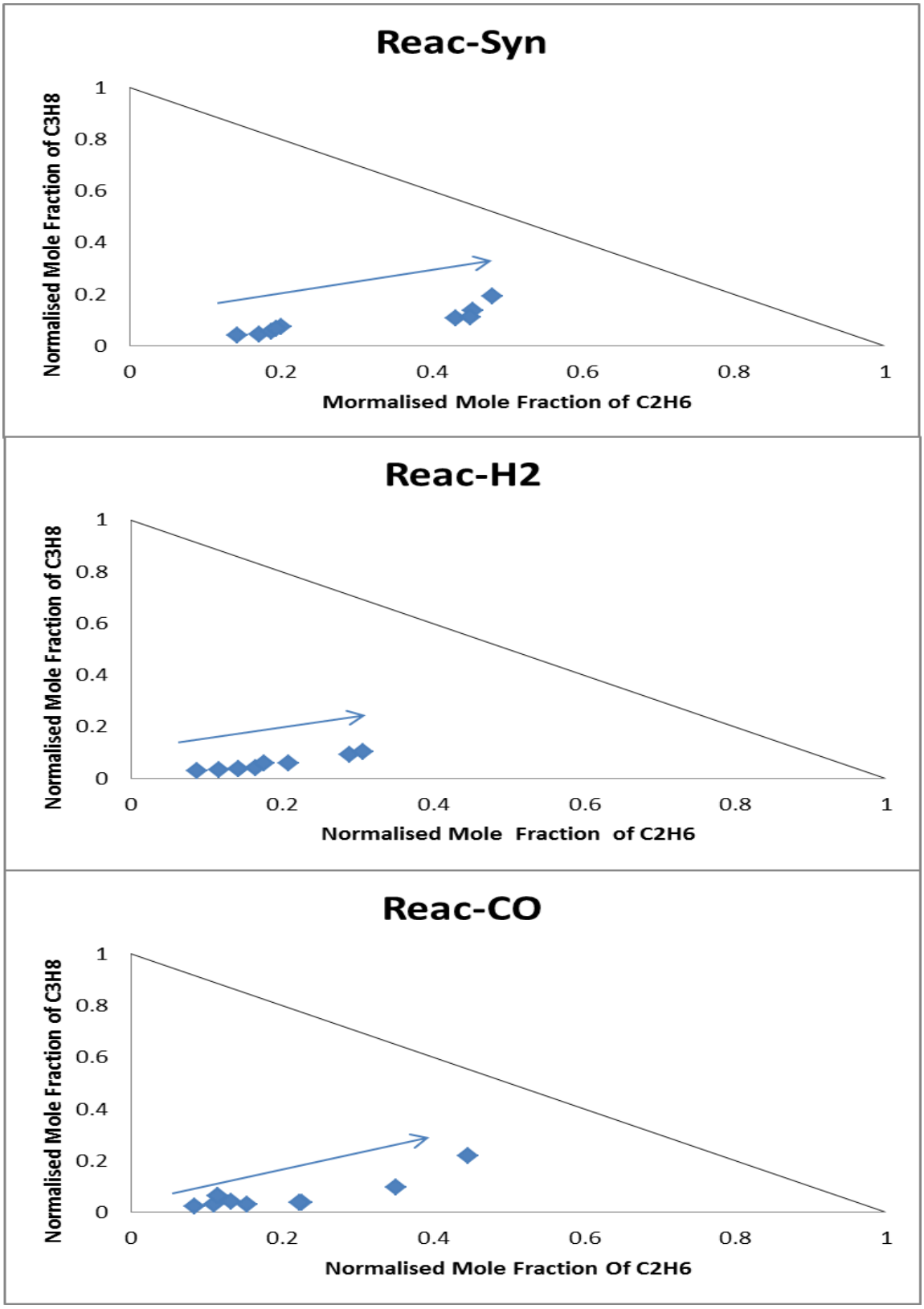

Figure 8.9: Normalized mole fraction for C_2H_6, C_3H_6, and C_3H_8 for the three differently reduced reactors

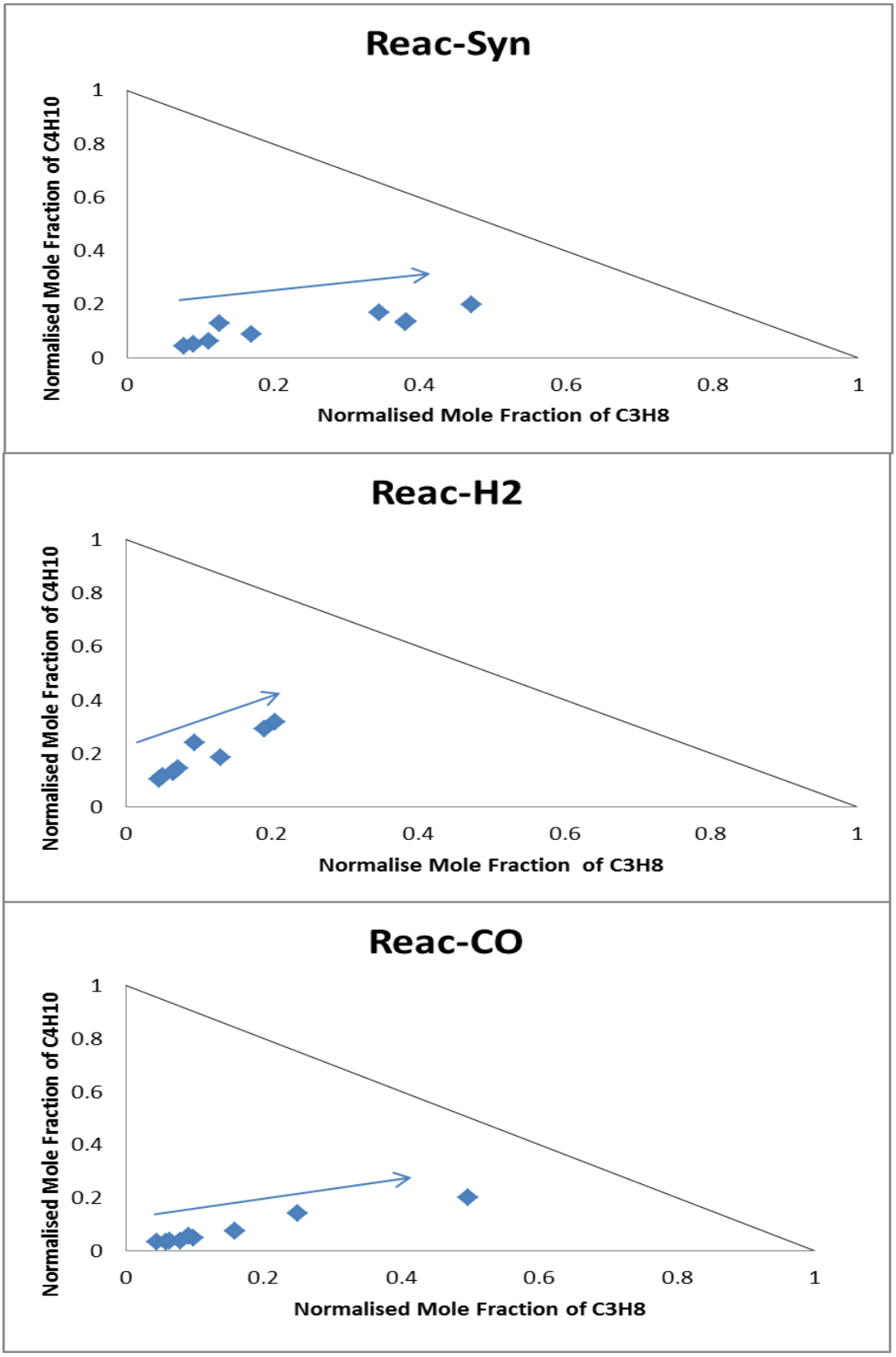

Figure 8.10: Normalized mole fractions for C_3H_8, C_4H_8, and C_4H_{10} for the three differently reduced reactors

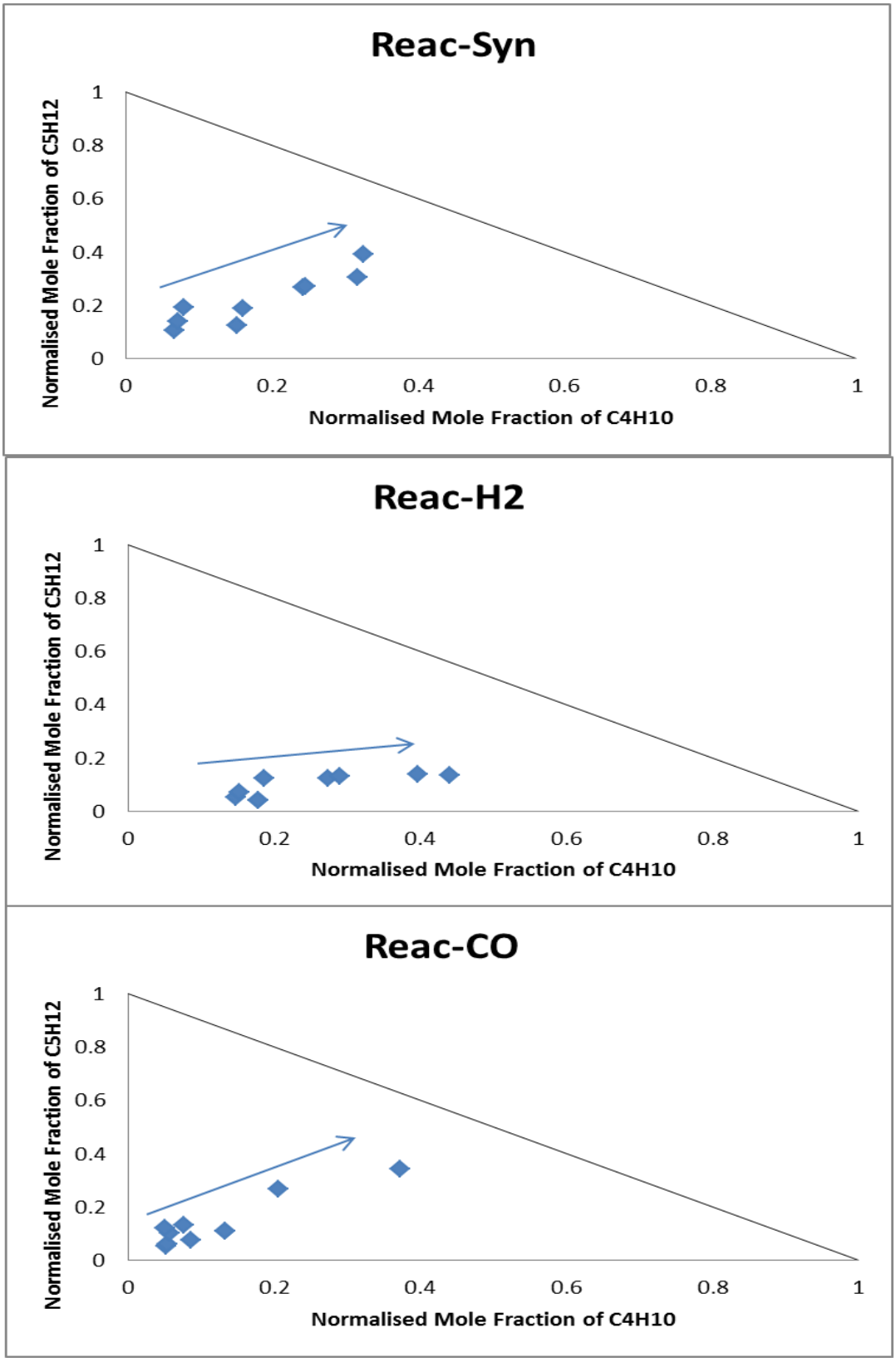

Figure 8.11: Normalized mole fractions for C_4H_{10}, C_5H_{10}, and C_5H_{12} for the three differently reduced reactors

8.6 The olefin to paraffin ratio as a function of CO conversion

As the previous results suggest the O/P ratio may be determined by the conversion it is useful to plot the results as a function of conversion. The dependence of the olefins to paraffins ratio on conversion is depicted in **Figures 8.12**. All differently reduced catalysts displayed the same exponential decrease in the O/P ratio with increase in conversion. This decreasing trend could be attributed to an increased olefin secondary reaction with increasing conversion. The CO conversion is increased by decreasing the flow rate and increasing the reaction pressure. Decreasing flow rate increases the reactant, intermediate product residence time, hence allowing olefins to undergo hydrogenation, which is a secondary reaction. Increasing pressure increases the partial pressure of hydrogen since the percentage composition of this component in the feed was 60%, hence more hydrogen for secondary reaction, since the number of catalyst active sites remained the same.

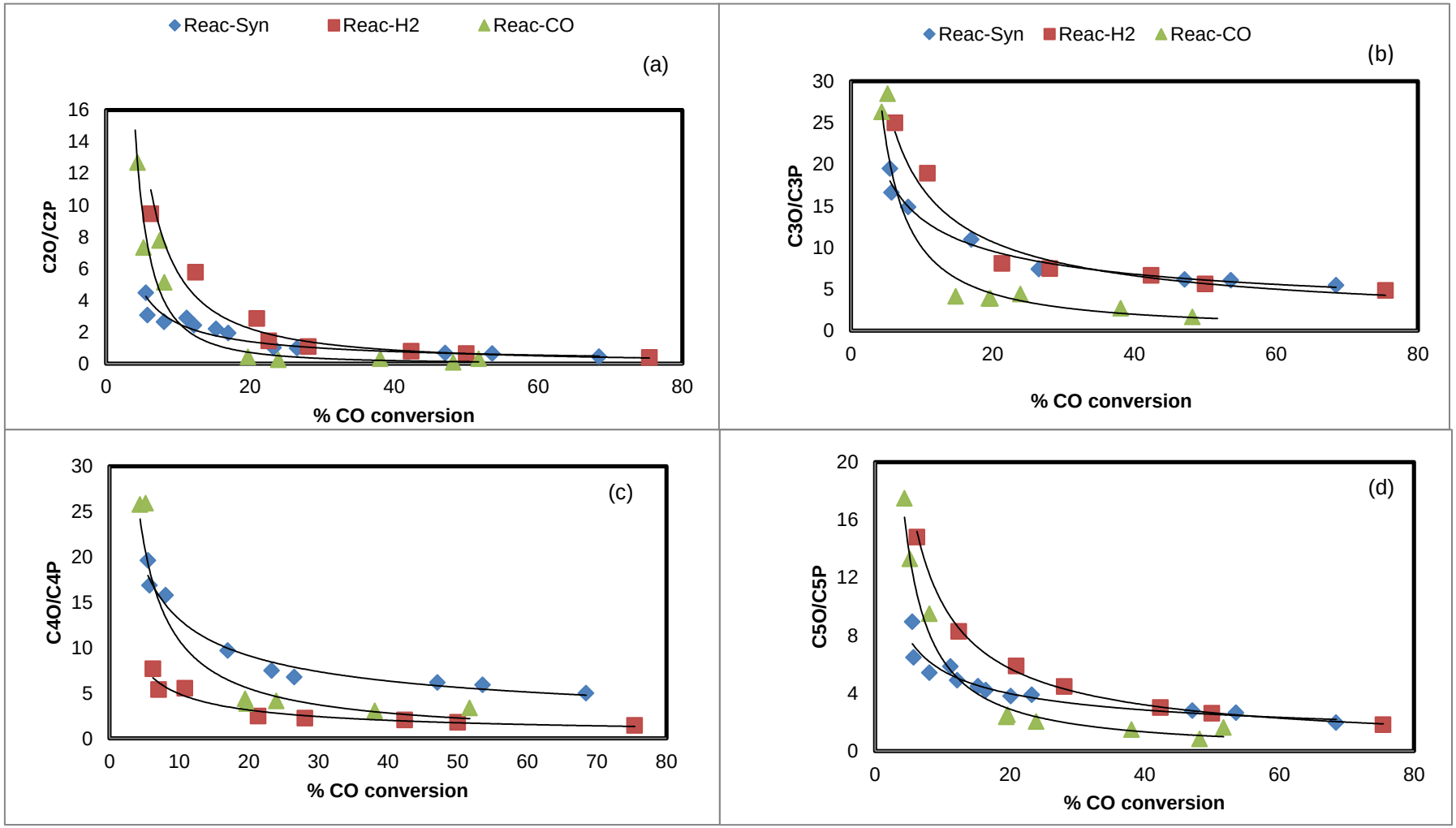

Figure 8.12: Olefin/Paraffin ratio as a function of conversion for all differently reduced reactors

8.7 Conclusion

With the aim of investigating the effect of the reducing agents and reaction conditions on the product distribution, three fixed bed reactors, each loaded with 1 gram of the same iron based catalyst, were used in parallel, and they were reduced with syngas (CO/H_2), H_2 and CO, respectively. Then a series of Fischer Tropsch experiments were performed at 250 ^oC, pressures of 1, 10 and 20 bar (gauge) and flowrates of 15, 30 and 60 mL(NTP) /min for a total time on stream (TOS) of 15 000 hrs.

The experimental results show that the olefin to Paraffin (O/P) ratios were strongly dependent on the catalyst activation agents, reaction conditions and the time on stream of the reaction. (1) With different reduction agents, the P/O ratios differ, and the following trend was obtained: Reac-Syn > Reac-H_2 > Reac-CO reduced reactors under most of the FT reaction conditions which were conducted; (2) higher P/O ratios were measured for lower flow rate and higher pressure; (3) under the same reaction conditions but at different times on stream, the P/O ratios were also changed, which was difficult to summarize for the trend for all three reactors.

In order to make sense of the data, two new ways were used to plot the data. Firstly, the researcher used the Yao plot; this is a plot introduced by a member of the research group: it is a plot of P_{n+1}/O_{n+1} versus P_n/O_n where n is a carbon number from n = 2–5. The results show that although the P/O ratios changed with different reaction conditions, the linear relationship between $P_{(n+1)}/O_{(n+1)}$ and $P_{(n)}/O_{(n)}$ holds for a large number of experiments, which indicates that the olefin and paraffin distributions are related to each other. Compared with the previous research by Yao et al. (2012) and Muleja et al. (2016), the current phenomenon could reveal that the product distribution might be determined by quasi reaction equilibrium or vapour liquid equilibrium, or by a combination of the two factors.

The significance of using different models to yield different graphical plots in FT is discussed, and these models are seen to support each other. The Lu plots clearly

show the movement of steady state points with conversion. Thus, the classical ASF model can be augmented with the newly introduced Lu and Yao Plots to aid in explaining the product distribution. The performance of three differently reduced catalysts confirmed the usefulness of these kinds of plots, though there were some deviations that are not easy to explain.

The Lu type plots strongly suggested that the olefin to paraffin ratios were mainly determined by conversion and plots of these ratios versus conversion confirmed this hypothesis. The importance of this for practical purposes cannot be overemphasised as it strongly suggests that in order to get mainly olefinic products one needs low conversions and to get mainly paraffinic products one needs high conversions. Thus for instance making fuels one does not want olefins and so one should use reactors with high conversions.

Also the constancy of the slopes in the Yao plots suggests that the paraffin to olefin ratios are not independent of each other but are determined by some sort of equilibrium type process between the species. Again a result of some practical importance.

References

Bao, B., El-Halwagi, M. M., & Elbashir, N. O. (2010). Simulation, integration, and economic analysis of gas-to-liquid processes. *Fuel Processing Technology*, *91*(7), 703–713. http://doi.org/10.1016/j.fuprc.2010.02.001

Becker, H., Güttel, R., & Turek, T. (2015). Enhancing internal mass transport in Fischer-Tropsch catalyst layers utilizing transport pores. *Catalysis Science and Technology*, *6*(1), 275–287. http://doi.org/10.1039/c5cy00957j

Biloen, P., Helle, J. N., & Sachtler, W. M. H. (1979). Incorporation of surface carbon into hydrocarbons during Fischer-Tropsch synthesis: Mechanistic implications. *Journal of Catalysis*, *58*(1), 95–107. http://doi.org/10.1016/0021-9517(79)90248-3

Carter, M. K. (2001). A molecular mechanism for Fischer-Tropsch catalysis. *Journal of Molecular Catalysis A: Chemical*, *172*(1-2), 193–206. http://doi.org/10.1016/S1381-1169(01)00080-2

Förtsch, D., Pabst, K., & Groß-Hardt, E. (2015). The product distribution in Fischer-Tropsch synthesis: An extension of the ASF model to describe common deviations. *Chemical Engineering Science*, *138*, 333–346. http://doi.org/10.1016/j.ces.2015.07.005

Fu, T., Jiang, Y., Lv, J., & Li, Z. (2013). Effect of carbon support on Fischer-Tropsch synthesis activity and product distribution over Co-based catalysts. *Fuel Processing Technology*, *110*, 141–149. http://doi.org/10.1016/j.fuproc.2012.12.006

Hallac, B. B., Keyvanloo, K., Hedengren, J. D., Hecker, W. C., & Argyle, M. D. (2015). An optimized simulation model for iron-based Fischer-Tropsch catalyst design: Transfer limitations as functions of operating and design conditions. *Chemical Engineering Journal*, *263*, 268–279. http://doi.org/10.1016/j.cej.2014.10.108

Hillestad, M. (2015). Modeling the Fischer-Tropsch Product Distribution and Model Implementation. *Chemical Product and Process Modeling*, *10*(3), 147–159. http://doi.org/10.1515/cppm-2014-0031

Iglesia, E., Reyes, S. C., & Madon, R. J. (1991). Transport-enhanced α-olefin readsorption pathways in Ru-Catalysed hydrocarbon synthesis. *Journal of Catalysis*, *129*(1), 238–256. http://doi.org/10.1016/0021-9517(91)90027-2

Liu, X., Hamasaki, A., Honma, T., & Tokunaga, M. (2011). Anti-ASF distribution in Fischer-Tropsch synthesis over unsupported cobalt catalysts in a batch slurry phase reactor. *Catalysis Today*, *175*(1), 494–503. http://doi.org/10.1016/j.cattod.2011.03.030

Lu, X., Hildebrandt, D., Liu, X., & Glasser, D. (2012a). A thermodynamic approach to olefin product distribution in fischer-tropsch synthesis. *Industrial and Engineering Chemistry Research*, *51*(51), 16544–16551. http://doi.org/10.1021/ie3000453

Lu, X., Hildebrandt, D., Liu, X., & Glasser, D. (2012b). A thermodynamic approach to olefin product distribution in fischer-tropsch synthesis. *Industrial and Engineering Chemistry Research*, *51*(51), 16544–16551. http://doi.org/10.1021/ie3000453

Lu, X., Hildebrandt, D., Liu, X., & Glasser, D. (2012c). A thermodynamic approach to olefin product distribution in fischer-tropsch synthesis. *Industrial and Engineering Chemistry Research*, *51*(51), 16544–16551. http://doi.org/10.1021/ie3000453

Lu, Y.-J., Zhang, Z.-X., & Zhou, J.-L. (1999). Carbon number distribution and selectivity of slurry F-T product over Raney Fe. *Journal of Natural Gas Chemistry*, *8*(4), 294–304.

Madon, R. J., & Iglesia, E. (1993). The Importance of Olefin Readsorption and H2/CO Reactant Ratio for Hydrocarbon Chain Growth on Ruthenium Catalysts. *Journal of Catalysis*, *139*(2), 576–590. http://doi.org/10.1006/jcat.1993.1051

Ma, W., Ding, Y., Luo, H., Lin, P., & Lin, L. (2001). Non-anderson-schulz-flory product distribution of fischer-tropsch synthesis over iron/activated charcoal catalyst. *Chinese Journal of Catalysis*, *22*(3), 279–282.

Muleja, A. A., Yao, Y., Glasser, D., & Hildebrandt, D. (2016). A study of Fischer-Tropsch synthesis: Product distribution of the light hydrocarbons. *Applied Catalysis A: General*, *517*, 217–226. http://doi.org/10.1016/j.apcata.2016.03.015

Naghsh, M., Sadeghi, M., Moheb, A., Chenar, M. P., & Mohagheghian, M. (2012). Separation of ethylene/ethane and propylene/propane by cellulose acetate-silica nanocomposite membranes. *Journal of Membrane Science*, *423-424*, 97–106. http://doi.org/10.1016/j.memsci.2012.07.032

Nakhaei Pour, A., & Housaindokht, M. R. (2013a). The olefin to paraffin ratio as a function of catalyst particle size in Fischer–Tropsch synthesis by iron catalyst. *Journal of Natural Gas Science and Engineering*, *14*, 204–210. http://doi.org/10.1016/j.jngse.2013.06.007

Nakhaei Pour, A., & Housaindokht, M. R. (2013). The olefin to paraffin ratio as a function of catalyst particle size in Fischer-Tropsch synthesis by iron catalyst. *Journal of Natural Gas Science and Engineering*, *14*, 204–210. http://doi.org/10.1016/j.jngse.2013.06.007

Nakhaei Pour, A., & Housaindokht, M. R. (2013b). The olefin to paraffin ratio as a function of catalyst particle size in Fischer–Tropsch synthesis by iron catalyst. *Journal of Natural Gas Science and Engineering*, *14*, 204–210. http://doi.org/10.1016/j.jngse.2013.06.007

Nawaz, Z., Baksh, F., Zhu, J., & Wei, F. (2013). Dehydrogenation of C3-C4 paraffin's to corresponding olefins over slit-SAPO-34 supported Pt-Sn-based novel catalyst. *Journal of Industrial and Engineering Chemistry*, *19*(2), 540–546. http://doi.org/10.1016/j.jiec.2012.09.024

Schon, S. G., Lau, H. K., Min, A. A., Thomas, M., & Wu, L. (2013). Olefin-paraffin separation by reversible reactive distillation (RRD). Presented at the AIChE Annual Meeting, Conference Proceedings. Retrieved from https://www.scopus.com/inward/record.uri?eid=2-s2.0-84881326301&partnerID=40&md5=621e0a6fbc89b58f1a11b4fa66432d1a

Shi, B., & Davis, B. H. (2005). Fischer-Tropsch synthesis: The paraffin to olefin ratio as a function of carbon number. *Catalysis Today*, *106*(1-4), 129–131. http://doi.org/10.1016/j.cattod.2005.07.159

Staudt-Bickel, C., & Koros, W. J. (2000). Olefin/paraffin gas separations with 6FDA-based polyimide membranes. *Journal of Membrane Science*, *170*(2), 205–214. http://doi.org/10.1016/S0376-7388(99)00351-8

Todic, B., Olewski, T., Nikacevic, N., & Bukur, D. B. (2013). *Modeling of fischer-tropsch product distribution over Fe-based catalyst* (Vol. 32). Retrieved from

https://www.scopus.com/inward/record.uri?eid=2-s2.0-84879222957&partnerID=40&md5=db61104f2829f6d9bea81dba703a65da

Van Santen, R. A., Ghouri, M. M., Markvoort, A. J., & Hensen, E. J. M. (2014). The Molecular Kinetics of the Fischer-Tropsch Reaction. In *Bridging Heterogeneous and Homogeneous Catalysis: Concepts, Strategies, and Applications* (pp. 553–606). Retrieved from https://www.scopus.com/inward/record.uri?eid=2-s2.0-84927075939&partnerID=40&md5=beb988c65d4cef624a7a6c821c9fa4d2

Wang, Y., Hu, J., Rector, D., & Liu, W. (2007). Tailored fischer-tropsch product distributions using a microstructured reactor (Vol. 3, pp. 1824–1832). Presented at the 24th Annual International Pittsburgh Coal Conference 2007, PCC 2007. Retrieved from https://www.scopus.com/inward/record.uri?eid=2-s2.0-84877646535&partnerID=40&md5=b9e9eb02abe3fdfb278a0f9c6ef42c5c

Yao, Y., Liu, X., Hildebrandt, D., & Glasser, D. (2012). Fischer–Tropsch synthesis using H2/CO/CO2 syngas mixtures: A comparison of paraffin to olefin ratios for iron and cobalt based catalysts. *Applied Catalysis A: General*, *433–434*, 58–68. http://doi.org/10.1016/j.apcata.2012.04.041

Zamaniyan, A., Mortazavi, Y., Khodadadi, A. A., & Pour, A. N. (2013). Effect of mass transfer limitations on catalyst performance during reduction and carburization of iron based Fischer-Tropsch synthesis catalysts. *Journal of Energy Chemistry*, *22*(5), 795–803. http://doi.org/10.1016/S2095-4956(13)60106-0

Zhang, X., Liu, Y., Liu, G., Tao, K., Jin, Q., Meng, F., … Tsubaki, N. (2012). Product distributions including hydrocarbon and oxygenates of Fischer-Tropsch synthesis over mesoporous MnO2-supported Fe catalyst. *Fuel*, *92*(1), 122–129. http://doi.org/10.1016/j.fuel.2011.07.041

Zohdi-Fasaei, H., Atashi, H., Farshchi Tabrizi, F., & Mirzaei, A. A. (2016). Effects of mass transfer on Fischer-Tropsch kinetics over mesoporous silica-supported Co-Mn-Ce nano catalysts in a fixed-bed reactor. *Journal of Natural Gas Science and Engineering*, *32*, 262–272. http://doi.org/10.1016/j.jngse.2016.03.090

CHAPTER 9

CONCLUSIONS AND RECOMMENDATIONS

9.1 Conclusions

The primary objective of the research undertaken for this thesis was to utilize the experimental findings to advance knowledge on the possibilities of simplifying the FT process, to validate the operating conditions, to reactivate the activity once the catalyst starts to deactivate, and to explore the possibilities of regenerating the catalyst in situ. Based on the results and discussions presented in the previous chapters (Chapters 3, 5-8), the major results and observations arising from the studies undertaken are summarized in this chapter.

Substantial progress has been made in this thesis towards generating detailed knowledge on the effects of producing hydrocarbons at low pressure of 1 bar gauge for a very long time on stream of approximately 14 350 hours. Experimental investigations were performed at laboratory scale using an industrial iron catalyst at various pressures (1, 10 and 20 bar), and flow-rates (15, 30 and 60 mL(NTP)/min) conditions and fixed reactor temperature of 250 ^{o}C, where invaluable data were successfully collected and analysed. Useful insights were acquired regarding the long term behaviour of the catalyst to parameter changes and long term response.

The experimental work proved the possibility of reducing the iron based catalyst using different reducing agents (namely, H_2, syngas, and CO), and operating the FT synthesis reaction at low pressure (1 bar) conditions. The experimental set-up was arranged in such a way that the syngas was fed in all three reactors from the same source while all other conditions were kept constant. The data obtained were analysed both qualitatively and quantitatively, in order to: (1) assess any emerging trends in the product distribution at low pressure, (2) assess new trends associated with changes in operating conditions, and (3) assess the trends before

and after the catalyst regeneration. The knowledge obtained by varying the experimental conditions could make available new possibilities for the effective use of FT process parameter changes to tailor the product distribution and to reduce the effect of catalyst deactivation during service. Based on the results and discussions presented in the previous chapters (Chapters 3, 5-8), the main conclusions can be drawn as follows.

9.1.1 Use of stability diagrams to predict catalyst speciation during activation

The use of stability diagrams was adopted in an endeavour to explain iron catalyst speciation during reduction. The speciation was shown at different partial pressures of the reducing gases.

The thermodynamic study revealed the presence of certain stable phases only during reduction, but not during FT synthesis using an iron catalyst. . For instance, a review by De Smit and Weckhuysen (2008) reported on the formation of Fe_7C_3, χ-Fe_5C_2, Θ-Fe_3C and ἐ-$Fe_{2.2}C$ phases while the catalyst is functioning. While these results appear to give some valuable insights into the behaviour of the catalyst, their direct value is somewhat limited, mainly because the thermodynamic data in the analysis is limited to only some of the major compounds for iron.

Unfortunately, the thermodynamic data available thus far is insufficient to include all these phases in the analysis. Under these circumstances, while the analytic methods highlighted in Chapter 4 could prove very useful in appreciating the differences in the starting catalyst phases, the thermodynamic analysis results do not explain in detail on what is actually happening in the operating catalyst at this stage. However, the ratio of the partial pressures in the tail gas could be used to predict the phase of the catalyst in operation.

9.1.2 Low pressure FT runs

The experimental results obtained at low pressure conditions from the three differently reduced catalysts indicate that the use of different reducing agents does

not have a significant impact on the catalyst activity, but does have an obvious impact on the product selectivity. The experimental data obtained demonstrated that all the reactors reached a steady state in terms of conversion after about 150 hours. Furthermore, methane selectivity shows the following trend, Reac-CO > Reac-H_2 > Reac-Syn reduced. The methane selectivity of the hydrogen reduced catalysts was significantly lower than those on the CO and syngas activated catalysts, which could indicate the possible effects of different carbide phases. In other words, the selectivity to methane is lower on the catalyst which contains significant amounts of bulk iron oxides than on the partially carbided catalyst. The paraffin production rates were much more complicated, with the reduction with CO being observed to give much more olefins than the reduction using syngas and H_2.

9.1.3 **Effects of operating conditions**

The response of the three differently reduced catalysts to variation of the FTS operating conditions (pressure: from 1 bar to 10 bar and then 20 bar gauge; Flow Rate: from 60 mL(NTP)/min to 30 and 15 mL(NTP)/min; and constant T: 250 °C) during a long TOS approximately 14 350 hours was also analysed. The results revealed that olefin content decreased with increasing pressure for all the reactors, with a significant decrease being observed from 1 bar to 10 bar while the decrease from 10 to 20 bar was of a lesser magnitude. This means the paraffin content increased with increasing pressure. The effect of decreasing flowrate resulted in the increase in the paraffin content (decrease in the olefin content). Thus, increasing pressure has got a synergistic effect to a decrease in the flowrate. On the other hand, the selectivity to methane was essentially independent of the reaction conditions.

9.1.4 **Oxidative regeneration of the almost deactivated catalyst**

An in-situ oxidative regeneration pathway of the catalyst was developed and tested using syngas as the reducing gas for all three reactors. The regeneration resulted in an increase in the catalytic activity and a selectivity change. Regeneration with the syngas reduced was most effective: the conversion of the

system in this case increased from 4.66% to 10.00%, which is a 53.40% increase. However, the researcher failed to obtain a high increase in conversions for the hydrogen reduced with the maximum of 1.18% and the CO reduced 6.25% after regeneration.

9.1.5 Use of plots to depict product distributions

It has been demonstrated that the use of models and/or plots including olefin to paraffin ratios is a promising approach for displaying product distribution in the FT process. The experimental results show that the paraffin to olefin (P/O) ratios were strongly dependent on the catalyst activation agents, reaction conditions, and the time on stream of the reaction: (1) With different reduction agents, the P/O ratios differ, and the following trend was obtained: Reac-Syn > Reac-H_2 > Reac-CO reduced reactors under most of the FT reaction conditions which were conducted; (2) higher P/O ratios were measured for lower flow rate and higher pressure; (3) under the same reaction conditions but at different times on stream, the P/O ratios were also changed, with no observable or generalizable trend.

The significance of using different models to yield different graphical plots such as Yao plots (Yao et al. 2012) and Lu plots (Lu et al, 2012; Xiaojun Lu, 2012) in FT was investigated, and these models are seen to support each other. The Lu plots clearly show the movement of steady state points with conversion. Thus, the classical ASF model can be augmented with the newly introduced Lu and Yao plots to aid in explaining the product distribution. The performance of three differently reduced catalysts confirmed the value of these kinds of plots, though there were some deviations. In this case/ study, the Yao plots and the Lu plots were applied to predict the product distribution behaviour. Based on the present laboratory data these plots (Yao and Lu) could be used to give reasonable predictions. This operational knowledge can be a valuable tool that would aid FT operators and process engineers in making timely decisions with regard to control and performance optimization of the FT process. The data collected in this project, though quite useful, remains valid only to the fixed bed type of reactors investigated. However, it is hoped that the project has given some impetus for

further research, and where the analysis is inconclusive, it provokes further thinking for improvements. Thus, this thesis is a contribution to the understanding of the FT process at low pressure and long term runs using an industrial iron based catalyst.

9.2 Recommendations

The research findings presented in this thesis has made significant progress in terms of low pressure FT runs and the possibility of reducing the FT catalyst with the syngas that will be used for reaction. Different reducing agents did not show much difference in terms of catalyst activity, and also showed negligible deactivation for long TOS of about 1000 hours. Based on the thermodynamic data, the formation of metallic iron on reduction with hydrogen is not likely at the reduction temperature used in this work, although the literature has reported its presence.

In order to have an in-depth understanding of the catalyst speciation during reduction and reaction, and the catalyst response to low pressure runs and in-situ regenerability, the following recommendations for further work/research are suggested.

1) There is need to develop probes that can be used to carry out in-situ catalyst characterization and to extract information on catalyst speciation pathways in realistic environments. In this case, the probes would give the catalyst phases at any particular instance.
2) Perform rigorous low pressure tests of the method in different reactor types (such as fluidized bed type reactors) and compare against historical data acquired or available before scaling up to pilot studies. This would help to understand the applicability of low pressure conditions in different reactor types.

3) While it has been demonstrated clearly that oxidative regeneration is effective for only the one reactor, there is need to gather more data to justify

whether the syngas reduction only results in these findings. A positive result in this regard would enhance the confidence required to use syngas as a reducing agent.

References

De Smit, E., & Weckhuysen, B. M. (2008). The renaissance of iron-based Fischer-Tropsch synthesis: On the multifaceted catalyst deactivation behaviour. *Chemical Society Reviews*, *37*(12), 2758–2781. http://doi.org/10.1039/b805427d

Lu, X. (2012). *Fischer-Tropsch Synthesis: Towards understanding.* Retrieved from http://mobile.wiredspace.wits.ac.za/handle/10539/11175

Lu, X., Hildebrandt, D., Liu, X., & Glasser, D. (2012). A thermodynamic approach to olefin product distribution in fischer-tropsch synthesis. *Industrial and Engineering Chemistry Research*, *51*(51), 16544–16551. http://doi.org/10.1021/ie3000453

Yao, Y., Liu, X., Hildebrandt, D., & Glasser, D. (2012). Fischer–Tropsch synthesis using H2/CO/CO2 syngas mixtures: A comparison of paraffin to olefin ratios for iron and cobalt based catalysts. *Applied Catalysis A: General*, *433–434*, 58–68. http://doi.org/10.1016/j.apcata.2012.04.041